JOURNAL OF FLUID MECHANICS

VOLUME 11 PART 2

SEPTEMBER 1961

PUBLISHED BY

CAMBRIDGE UNIVERSITY PRESS

BENTLEY HOUSE, 200 EUSTON ROAD, LONDON, N.W.1

AMERICAN BRANCH: 32 EAST 57TH STREET, NEW YORK 22, N.Y.

Price 30*s.* (*U.S.A.* $5.00)

The JOURNAL OF FLUID MECHANICS exists for the publication of theoretical and experimental investigations of all aspects of the mechanics of fluids, and is issued in four parts per volume.

EDITORS

DR G. K. BATCHELOR, DR T. BROOKE BENJAMIN

Department of Applied Mathematics and Theoretical Physics, University of Cambridge, Free School Lane, Cambridge, England

ASSISTANT EDITORS

DR J. R. A. PEARSON, DR O. M. PHILLIPS

ASSOCIATE EDITORS

PROF. G. F. CARRIER

Pierce Hall, Harvard University, Cambridge 38, *Massachusetts, U.S.A.*

DR W. C. GRIFFITH

Lockheed Missiles and Space Division, Palo Alto, California, U.S.A.

M. J. LIGHTHILL

Royal Aircraft Establishment, Farnborough, Hampshire, England

PROF. R. R. LONG

School of Engineering, The Johns Hopkins University, Baltimore 18, *Maryland, U.S.A.*

DR P. G. SAFFMAN

Department of Mathematics, King's College, London, W.C. 2, *England*

Authors wishing to have papers published in the JOURNAL should communicate them to any one of the persons named above, choosing one in their own country where possible.

Authors are urged to ensure that their papers are written clearly and attractively, in order that their work will be readily accessible to readers.

Manuscripts should be typed in double spacing on one side of the paper only, with references listed at the end in alphabetical order of authors. Drawings should be done on a large scale in Indian ink on tracing cloth or drawing paper, the lettering being shown clearly in pencil for reproduction by the printer; the list of captions should be typed at the end of the manuscript. Proofs of papers from overseas will usually be despatched to authors by airmail. There is no charge for publication. Authors are entitled to receive 50 offprints of a paper in the JOURNAL free of charge, and additional offprints can be purchased if ordered in advance.

SUBSCRIPTIONS

The subscription price for a volume of four parts is £5. 10*s*. net, post free, payable in advance; separate parts 30*s*. net, plus postage. Subscriptions may be sent to any bookseller, or to the Cambridge University Press, Bentley House, 200 Euston Road, London, N.W.1.

Subscribers in the United States should send their orders to the Cambridge University Press, American Branch, 32 East 57th Street, New York 22, N.Y. The subscription price per volume is $18.50, post free, payable in advance; separate parts $5.00, plus postage.

Quotations for available back volumes and parts may be obtained on application to the Cambridge University Press.

A sol
unde
direc
oil te
oil vi
small
Th
briefl

1. I

Th
flow
layer
The t
and s
devel
oils a
(Wint
tunne
1952)
It i
and a
ing of
unifo
The
in the
for al
been
layer,
relate
The
but th
in §6.

The motion of a thin oil sheet under the steady boundary layer on a body

By L. C. SQUIRE
Royal Aircraft Establishment, Bedford

(Received 10 March 1961)

A solution is obtained for the motion of a thin oil sheet, of non-uniform thickness, under a boundary layer. The following points are deduced: (*a*) The oil flows in the direction of the boundary-layer skin-friction, except near separation, where the oil tends to indicate separation too early. These conclusions are independent of oil viscosity. (*b*) The effect of the oil flow on the boundary-layer motion is very small.

The application of the results to the interpretation of oil-flow patterns is briefly considered.

1. Introduction

The oil-flow technique is nowadays widely used for visualization of the surface flow on wind-tunnel models. In this technique the model is coated with a thin layer of oil and the oil pattern is observed during, and at the end of, a tunnel run The types of oil used vary widely. Heavy gear oil is used in continuous transonic and supersonic tunnels, and times of up to a quarter of an hour are needed to develop the full flow pattern (Stanbrook 1957). On the other hand, very light oils are used in intermittent tunnels where the total running time is 10–20 sec (Winter, Scott-Wilson & Davies 1954). Paraffin is often used in low-speed wind tunnels (Black 1952), and heavy oils are used in low-speed water tunnels (Prandtl 1952).

It is of interest to know to what extent the presence of the oil affects the flow, and also what the oil-flow pattern represents. As a basic step in the understanding of the oil-flow technique, the theoretical motion of a thin oil sheet, of non-uniform thickness, on a surface under a boundary layer is studied here.

The main parameter in the problem is the ratio of the viscosity of the fluid in the boundary layer to the viscosity of the oil. The solutions obtained are valid for all values of this ratio likely to be found in practice. Numerical results have been produced for infinite wings with velocity distributions, outside the boundary layer, of the form $U = ax$ or $U = \beta_0 - \beta_1 x$. The parameters a, β_0 and β_1 have been related to typical pressure distributions and are calculated in Appendix 1.

The numerical methods apply to incompressible laminar boundary layers, but the extension of the results to compressible and turbulent layers is discussed in § 6.

2. Equations governing the motion of a thin oil sheet

2.1. *Equations for the oil-flow direction*

The thickness h of the oil sheet is a function of surface position and time. It is generally not greater than about 0·05 in., and in the following analysis will be assumed to be of the same order as the boundary-layer thickness. Then the motion of the oil is governed by the equations of slow viscous motion:

$$\frac{\partial u_2}{\partial t} = \nu_2 \nabla^2 u_2 - \frac{1}{\rho_2}\frac{\partial p_2}{\partial x}, \tag{1}$$

$$\frac{\partial v_2}{\partial t} = \nu_2 \nabla^2 v_2 - \frac{1}{\rho_2}\frac{\partial p_2}{\partial y}, \tag{2}$$

$$\frac{\partial w_2}{\partial t} = \nu_2 \nabla^2 w_2 - \frac{1}{\rho_2}\frac{\partial p_2}{\partial z}, \tag{3}$$

together with the continuity equation

$$\frac{\partial u}{\partial x} + \frac{\partial v}{\partial y} + \frac{\partial w}{\partial z} = 0. \tag{4}$$

The co-ordinate system, and velocity components are defined in figure 1. The suffix 2 refers to motion in the oil and suffixes 0 and 1 refer to free-stream and boundary-layer flow, respectively. The boundary conditions are (i) that the oil velocities are equal to those in the boundary layer at the surface of the oil, (ii) that the viscous stresses in the oil and the air are also equal at the oil/air surface, and (iii) that at the body surface the oil is stationary. These conditions may be written

$$\left.\begin{aligned} &u_1 = u_2, \quad v_1 = v_2, \quad w_1 = w_2 \quad \text{at} \quad z = h, \\ &u_2 = v_2 = w_2 = 0 \quad \text{at} \quad z = 0; \end{aligned}\right\} \tag{5}$$

$$\mu_1 \frac{\partial u_1}{\partial z} = \mu_2 \frac{\partial u_2}{\partial z}, \quad \mu_1 \frac{\partial v_1}{\partial z} = \mu_2 \frac{\partial v_2}{\partial z} \quad \text{at} \quad z = h. \tag{6}$$

(For the derivation of (6), see Appendix 2.)

Equations (1) to (3) will now be simplified by order-of-magnitude considerations, taking account of two small quantities, the boundary-layer thickness δ and the ratio of the viscosities of air and oil $\mu_1/\mu_2 (= \lambda$, say). (For the range of oils used in wind tunnels, λ lies in the range 10^{-2} to 10^{-4}.)

According to standard boundary-layer theory, $\partial u_1/\partial z$ and $\partial v_1/\partial z$ are $O(1/\delta)$. Thus, by equation (6), $\partial u_2/\partial z$ and $\partial v_2/\partial z$ are $O(\lambda/\delta)$. At $z = 0$, u_2 and v_2 are zero. Thus, within the oil, u_2 and v_2 are $O(\lambda)$; their derivatives with respect to x and y are also of the same order of magnitude.

From the continuity equation, it then follows that $\partial w/\partial z$ is $O(\lambda)$ and, since $w_2 = 0$, at $z = 0$, that w_2 is $O(\lambda\delta)$. Differentiation of the continuity equation with respect to z then shows that $\partial^2 w_2/\partial z^2$ is $O(\lambda/\delta)$.

The order of the terms $\partial u_2/\partial t$, $\partial v_2/\partial t$ will now be considered. It has already been shown that u_2 and v_2 are $O(\lambda)$, and so their influence on the boundary layer will be small. In this case, equations (1) to (6) represent the motion of an oil sheet under

a steady boundary layer, in which the only variation with time enters through the boundary conditions (5) and (6), since h is a function of time. Therefore the derivatives under consideration may be written

$$\frac{\partial u_2}{\partial t} = \frac{\partial u_2}{\partial h}\frac{dh}{dt}, \quad \frac{\partial v_2}{\partial t} = \frac{\partial v_2}{\partial h}\frac{dh}{dt}.$$

At the edge of the layer, $w_2 = dh/dt$; thus dh/dt is $O(\delta\lambda)$ while $\partial u_2/\partial h$ and $\partial v_2/\partial h$ have the same order of magnitude as $\partial u_2/\partial z$ and $\partial v_2/\partial z$, namely $O(\lambda/\delta)$. Thus the time derivatives of u_2 and v_2 are $O(\lambda^2)$. Similarly, the derivative $\partial w_2/\partial t$ is $O(\lambda^2\delta)$.

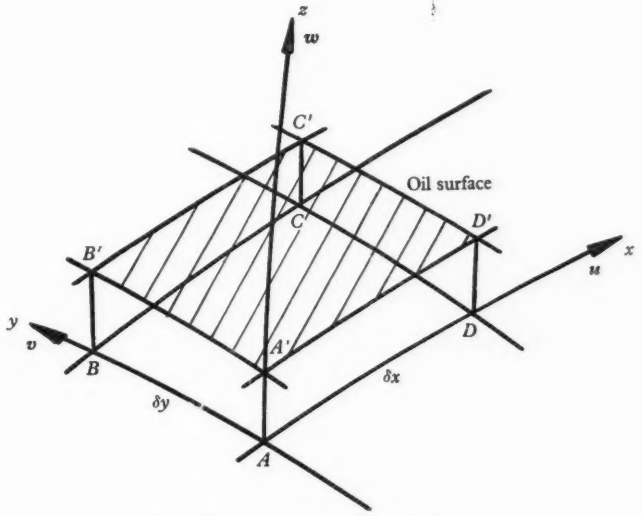

FIGURE 1. The co-ordinate system.

When the order of magnitude of the terms in equation (3) are considered, it is found that the pressure change through the oil layer is $O(\lambda\delta)$. Thus the pressure may be regarded as constant through the oil layer; and since by standard boundary-layer theory $p_0(x, y) = p_1(x, y)$, then

$$p_2(x, y) = p_1(x, y) = p_0(x, y). \tag{7}$$

If equations (1) and (2) are now divided by ν_2, the pressure terms may be written (with $\rho_0 = \rho_1$)

$$\frac{1}{\mu_2}\frac{\partial p_2}{\partial x} = \frac{\lambda}{\mu_1}\frac{\partial p_0}{\partial x} = \frac{\lambda}{\nu_1}\frac{1}{\rho_0}\frac{\partial p_0}{\partial x}, \tag{8}$$

$$\frac{1}{\mu_2}\frac{\partial p_2}{\partial y} = \frac{\lambda}{\mu_1}\frac{\partial p_0}{\partial y} = \frac{\lambda}{\nu_1}\frac{1}{\rho_0}\frac{\partial p_0}{\partial y}. \tag{9}$$

By boundary-layer theory, δ is $O(\nu_1^{\frac{1}{2}})$, while by Bernoulli's equation $\rho_0^{-1}\partial p_0/\partial x$ and $\rho^{-1}\partial p_0/\partial y$ are $O(1)$. Thus the pressure terms in equations (8) and (9) are

$O(\lambda/\delta^2)$. Equations (1) and (2) may now be simplified by retaining terms of the highest order only, whereupon they become

$$\nu_2 \frac{\partial^2 u_2}{\partial z^2} = \frac{1}{\rho_2}\frac{\partial p_0}{\partial x}, \tag{10}$$

$$\nu_2 \frac{\partial^2 v_2}{\partial z^2} = \frac{1}{\rho_2}\frac{\partial p_0}{\partial y}. \tag{11}$$

In equations (10) and (11) the pressure terms are known from the external flow, so that the equations are ordinary second-order equations for u_2 and v_2. These equations must be solved, in conjunction with the boundary-layer equations

$$\left.\begin{aligned} u_1\frac{\partial u_1}{\partial x}+v_1\frac{\partial u_1}{\partial y}+w_1\frac{\partial u_1}{\partial z} &= -\frac{1}{\rho_1}\frac{\partial p}{\partial x}+\nu_1\frac{\partial^2 u_1}{\partial z^2}, \\ u_1\frac{\partial v_1}{\partial x}+v_1\frac{\partial v_1}{\partial y}+w_1\frac{\partial v_1}{\partial z} &= -\frac{1}{\rho_1}\frac{\partial p}{\partial y}+\nu_1\frac{\partial^2 v_1}{\partial z^2}, \end{aligned}\right\} \tag{12}$$

$$\frac{\partial u_1}{\partial x}+\frac{\partial v_1}{\partial y}+\frac{\partial w_1}{\partial z} = 0, \tag{13}$$

to satisfy the boundary conditions (5) and (6). [Equations (12) and (13) strictly apply only to a flat surface, but they may be used for slightly curved surfaces. On more highly curved surfaces the full equations must be used (see, for example, Squire 1956).]

A simple iterative approach, to be used here, is to find solutions of equations (10) and (11) satisfying the conditions $u_2 = v_2 = 0$ at $z = 0$, and $\mu_1(\partial u_1/\partial z) = \mu_2(\partial u_2/\partial z)$, $\mu_1(\partial v_1/\partial z) = \mu_2(\partial v_2/\partial z)$ at $z = h$. The third condition is then satisfied by finding a solution of the boundary-layer equations such that at $z = h$, $u_1 = (u_2)_{z=h}$, $v_1 = (v_2)_{z=h}$, where $(u_2)_{z=h}$, and $(v_2)_{z=h}$ are found from the solution of the oil-flow equations. (The boundary condition $w_2 = w_1$ should also be applied but as w_2 is $O(\lambda, \delta)$ this condition is replaced by $w_1 = 0$ at $z = h$.) This process is iterative since $(\partial u_1/\partial z)_{z=h}$ and $(\partial v_1/\partial z)_{z=h}$ depend on $(u_2)_{z=h}$ and $(v_2)_{z=h}$. However, since these velocities are $O(\lambda)$, the changes in $(\partial u_1/\partial z)_{z=h}$ and $(\partial v_1/\partial z)_{z=h}$ are also small and so the process should converge quickly.

By direct integration of equations (10) and (11), solutions which satisfy the two boundary conditions are found to be

$$\left.\begin{aligned} u_2 &= \lambda\left\{\left(\frac{1}{\mu_1}\frac{\partial p}{\partial x}\right)\left(\frac{z^2}{2}-hz\right)+\left(\frac{\partial u_1}{\partial z}\right)_{z=h} z\right\}, \\ v_2 &= \lambda\left\{\left(\frac{1}{\mu_1}\frac{\partial p}{\partial y}\right)\left(\frac{z^2}{2}-hz\right)+\left(\frac{\partial v_1}{\partial z}\right)_{z=h} z\right\}. \end{aligned}\right\} \tag{14}$$

At the oil surface, $z = h$, these solutions give

$$\left.\begin{aligned} (u_2)_{z=h} &= \lambda\left\{-\frac{h^2}{2}\left(\frac{1}{\mu_1}\frac{\partial p}{\partial x}\right)+h\left(\frac{\partial u_1}{\partial z}\right)_{z=h}\right\}, \\ (v_2)_{z=h} &= \lambda\left\{-\frac{h^2}{2}\left(\frac{1}{\mu_1}\frac{\partial p}{\partial y}\right)+h\left(\frac{\partial v_1}{\partial z}\right)_{z=h}\right\}, \end{aligned}\right\} \tag{15}$$

which are the velocities needed in the solution of the boundary-layer equations.

The investigation of the boundary layer with the boundary conditions $u_1 = u_2$, $v_1 = v_2$ is carried out in §§3 and 4, where it is shown that the change in the boundary-layer skin friction is small.

It should be noted that the oil film, in addition to giving the boundary layer a non-zero velocity at the oil surface, also effectively changes the body shape, and hence the external flow. The latter effect, however, is small for thin oil films and is ignored. Then the boundary-layer equations can be solved for the original pressure distribution with the non-zero velocity condition transferred to the body surface, that is $u_1 = (u_2)_h$, $v_1 = (v_2)_h$ at $z = 0$.

It is advisable at this point to consider the range of validity of the order-of-magnitude analysis made in this section. Goldstein (1948) has shown that the approximations of boundary-layer theory break down in the immediate neighbourhood of separation; consequently, the equations for this oil flow, which are based on this theory, will also be invalid in this condition. As the main interest is to determine the position of separation, it is important to know how close to separation the simplified equations hold. A numerical study of the boundary-layer solution for a linearly retarded main-stream has shown that the equations are valid for 99·5 % of the distance to separation. It is reasonable to assume that the simplified oil-flow equations are also valid in the same region.

2.2. *Equation governing the thickness of the oil sheet*

So far the oil thickness h has been regarded as an arbitrary function of surface position and time. The equation satisfied by this function will now be determined. Consider the area $ABCD$ in figure 1; then in time δt the increase in height multiplied by the area $\delta x\,\delta y$ is equal to the amount of oil which has moved on to the base $ABCD$ less the amount which has moved off this area. In the infinitesimal limit, the equation for h becomes

$$\frac{\partial h}{\partial t} = -\frac{\partial}{\partial x}\int_0^h u_2\,dz - \frac{\partial}{\partial y}\int_0^h v_2\,dz. \tag{16}$$

On the substitution for u_2 and v_2 from equation (14), this becomes

$$\begin{aligned}\frac{1}{\lambda}\frac{\partial h}{\partial t} = &-\frac{\partial}{\partial x}\left\{\left(\frac{\partial u_1}{\partial z}\right)_{z=h}\frac{h^2}{2} - \frac{1}{\mu_1}\frac{\partial p}{\partial x}\frac{h^3}{3}\right\}\\ &-\frac{\partial}{\partial y}\left\{\left(\frac{\partial v_1}{\partial z}\right)_{z=h}\frac{h^2}{2} - \frac{1}{\mu_1}\frac{\partial p}{\partial y}\frac{h^3}{3}\right\}.\end{aligned} \tag{17}$$

Equation (17) is a non-linear partial differential equation where the coefficients $(\partial u_1/\partial z)_{z=h}$ and $\partial p/\partial x$, $\partial p/\partial y$ are, in general, known only in numerical form. Thus solutions will usually have to be found by numerical methods. However, one simple solution has been found corresponding to flow near a stagnation point in two-dimensional flow. This solution is described in §3; the result of a direct numerical integration of equation (17) will be described in §4.2.

3. Oil motion near a stagnation point in two-dimensional flow

Near a two-dimensional stagnation point, the velocity distribution in the streamwise direction outside the boundary layer is of the simple form $u = ax$; the oil flow in this case is of special interest because both the modified boundary-

layer equations and equation (17) can be solved. Making, as in standard boundary-layer theory, the transformation $u_1 = axf'(\eta)$, where $\eta = (a/\nu_1)^{\frac{1}{2}} z$ and the accent denotes differentiation with respect to η, we find that the two-dimensional boundary-layer equations (i.e. (12) and (13) with $v_1 = 0$) reduce to

$$f'''(\eta) + f''(\eta) f(\eta) = \{f'(\eta)\}^2 - 1 \tag{18}$$

(cf. Goldstein 1938, p. 139).

At the wall, $z = 0$, we have $f'(0) = (u_2)_h/ax$, instead, of the more usual value $f'(0) = 0$. The other boundary conditions remain the same, i.e. $f(0) = 0, f'(\infty) \to 1$. The value of $(u_2)_h$ can be found from equation (15) to be

$$(u_2)_h = \lambda \left\{ \frac{a^2}{\nu_1} \frac{h^2}{2} + \left(\frac{a^3}{\nu_1}\right)^{\frac{1}{2}} h f''(0) \right\} x, \tag{19}$$

so that

$$f'(0) = \lambda \left\{ \frac{a}{\nu_1} \frac{h^2}{2} + \left(\frac{a}{\nu_1}\right)^{\frac{1}{2}} h f''(0) \right\} = \gamma, \quad \text{say.} \tag{20}$$

In practice equations (18) and (20) must be solved by iteration, but before this is possible it is necessary to find h, which (by substitution of equation (19) in equation (17)) is given as the solution of the equation

$$\begin{aligned} \frac{\partial h}{\partial t} &= -\lambda \frac{\partial}{\partial x} \left\{ \left(\frac{a^3}{\nu_1}\right)^{\frac{1}{2}} f''(0) \frac{h^2}{2} + \frac{a^2}{\nu_1} \frac{h^3}{3} \right\} x \\ &= -\lambda \left\{ \left(\frac{a^3}{\nu_1}\right)^{\frac{1}{2}} f''(0) \frac{h^2}{2} + \frac{a^2}{\nu_1} \frac{h^3}{3} \right\} = -Ah^2 - Bh^3, \quad \text{say,} \end{aligned} \tag{21}$$

provided h is independent of x, which is true if h is constant at time $t = 0$.

Equations (18), (20) and (21) now depend on the three parameters γ, A and B, where γ and A are functions of $f''(0)$. Equations (18) and (21) can, however, be solved for arbitrary values of these parameters, and the solutions can be combined iteratively with equation (20) to find the solution of any particular problem.

First consider equation (18). As $(u_1)_h$ is $O(\lambda)$, this equation can be linearized by putting $f'(\eta) = f_0'(\eta) + \gamma g'(\eta)$, where $f_0'(\eta)$ is the standard two-dimensional solution and where $g'(0) = 1$, $g(0) = 0, g'(\infty) \to 0$. Then $g'(\eta)$ satisfies the equation

$$g'''(\eta) + f_0(\eta) g''(\eta) + f_0''(\eta) g(\eta) - 2f_0'(\eta) g'(\eta) = 0. \tag{22}$$

This equation has been solved by standard numerical techniques to give the solution tabulated in table 1.

The solution of equation (21) is readily obtained as

$$At = \frac{1}{h} - \frac{1}{h_z} + \frac{B}{A} \log \frac{h}{h_z} \left\{ \frac{A + Bh_z}{A + Bh} \right\}, \tag{23}$$

or

$$Ah_z t = \left(\frac{1}{K} - 1\right) + C \log K \left\{ \frac{1 + C}{1 + CK} \right\}, \tag{24}$$

where $C = h_z(B/A)$, $K = h/h_z$ and h_z is the oil height at $t = 0$. K is plotted against $Ah_z t$ in figure 2 for various values of C.

These solutions for $f(\eta)$ and h_z can now be combined to find the oil and boundary-layer flow in the following particular case. The initial oil thickness is assumed to

be 0·018 in. with $\lambda = 1 \times 10^{-4}$, and the kinematic viscosity of air to be 2×10^{-4} ft./sec. The external velocity is assumed to be of the form $U = 10^4 x$ ft./sec (i.e. $a = 10^4\,\mathrm{sec}^{-1}$). This corresponds, for example, to an aerofoil in an airstream of 120 ft./sec with the flow outside the boundary layer attaining the main-stream velocity at 0·144 in. behind the stagnation point.

η	$g'(\eta)$	η	$g'(\eta)$
0	1·000	2·0	0·053
0·2	0·840	2·2	0·034
0·4	0·686	2·4	0·021
0·6	0·547	2·6	0·012
0·8	0·425	2·8	0·007
1·0	0·322	3·0	0·004
1·2	0·238	3·2	0·002
1·4	0·171	3·4	0·001
1·6	0·119	3·6	0·000
1·8	0·081		

$$g''(0) = -0{\cdot}810.$$

TABLE 1

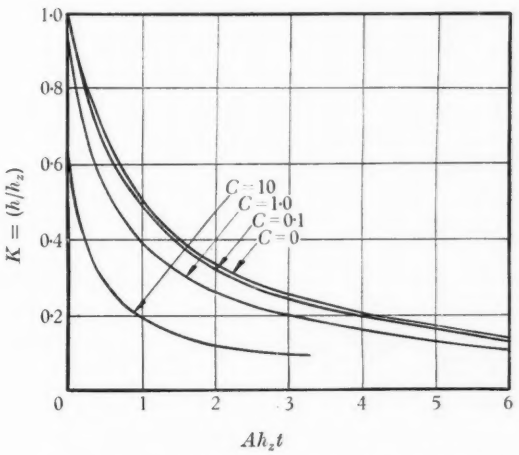

FIGURE 2. Variation of the thickness of the oil sheet at a stagnation point.

Consider the oil flow at the start of the motion. In the first stage of the iteration, use is made of the standard two-dimensional solution for $f_0''(0)$, from which $f''(0) = f_0''(0) = 1{\cdot}232$ and so $\gamma = 4{\cdot}3 \times 10^{-3}$ (equation (20)). With this value the second approximation for $f''(0)$ becomes 1·228, and there is no change in γ. Thus, in this case, with a rather thick oil layer, the skin friction (which is proportional to $f''(0)$) is reduced by less than $\frac{1}{2}\%$.

Now consider the motion after 10 sec. Using $f''(0) = 1{\cdot}230$ and the above values of h_z and a, it follows that $C = 5{\cdot}8$ and $Ah_z t = 65$, so that from equation (24) K is approximately 0·015 and the oil thickness has been reduced to less than one-

sixtieth of its original value. This example, although of little practical interest, is of value from two points of view. In the first place the numerical results can be used to check the magnitude of the terms ignored in equations (1), (2) and (3). Also, the change in oil thickness is quite rapid in this case, so that it is possible that the unsteady boundary-layer equations should have been used. However, in the 10 sec considered, γ changes from $4{\cdot}3\times10^{-3}$ to almost zero. Thus, $d\gamma/dt \doteqdot 4{\cdot}3\times10^{-4}\,\mathrm{sec}^{-1}$ and, since $u_1 = ax\{f'(\eta)+\gamma g'(\eta)\}$, $du_1/dt \doteqdot ax\times4{\cdot}3\times10^{-4}$. In equation (12) the dominant terms near $z=0$ are $\rho_1^{-1}\partial p/\partial x$ and $\nu_1\partial^2 u_1/\partial z^2$, and $\rho_1^{-1}\partial p/\partial x = -a^2x$. Thus the ratio of the unsteady term $\partial u_1/\partial t$ compared with the dominant terms is $a^{-1}\times10^{-4}$ or $O(10^{-8})$, which confirms that use of the steady equation is justified.

4. General solutions of the equations of §2

4.1. *Effect of the oil on a two-dimensional boundary layer with an arbitrary pressure gradient*

In this section the effect of the oil on two-dimensional boundary layers is considered. The extension to three-dimensional boundary layers would involve considerable numerical work, which has not been carried out since the analysis of the present section suggests that the effect of the oil is extremely small for cases which are likely to arise in practice. The method is based on the momentum equation; it is first shown that this equation is unaltered by the changed inner boundary condition,† and then that the velocity can be represented by a modified Pohlhausen profile.

By integration of the two-dimensional form of the boundary-layer equations (12) and (13) with respect to z, the following equation is obtained

$$\int_0^\delta u_1\frac{\partial u_1}{\partial z}dz+\int_0^\delta w_1\frac{du_1}{\partial z}dz=\int_0^\delta u_0\frac{\partial u_0}{\partial x}dz-\nu_1\left[\frac{\partial u_1}{\partial z}\right]_0, \tag{25}$$

where $\rho_1^{-1}\partial p/\partial x$ has been replaced by $u_0(\partial u_0/\partial x)$. Using the continuity equation, we reduce the second term of the left-hand side by writing

$$\begin{aligned}\int_0^\delta w_1\frac{\partial u_1}{\partial z}dz &= [w_1u_1]_0^\delta-\int_0^\delta u_1\frac{\partial w_1}{\partial z}dz\\ &= [w_1u_1]_0^\delta+\int_0^\delta u_1\frac{\partial u_1}{\partial x}dz.\end{aligned} \tag{26}$$

The lower limit of the term in square brackets is 0, since at $z=0$ we have $w_1=0$ (this is true although $u_1\neq0$); at $z=\delta$ we have

$$w_1=\int_0^\delta\frac{\partial w}{\partial z}dz=-\int_0^\delta\frac{\partial u_1}{\partial x}dz.$$

Thus equation (25) becomes

$$2\int_0^\delta u_1\frac{\partial u_1}{\partial x}dz-u_0\int_0^\delta\frac{\partial u_1}{\partial x}dz-\int_0^\delta u_0\frac{\partial u_0}{\partial x}dz=-\nu_1\left[\frac{\partial u_1}{\partial z}\right]_{z=0}. \tag{27}$$

† For convenience the inner boundary condition will be applied at $z'=0$ rather than $z=h$, and the dash dropped in the remainder of the paper.

This equation is exactly the same as the standard two-dimensional equation, and will be written

$$\frac{\partial\theta^2}{\partial x} = 2\frac{\theta^2}{u_0}\frac{\partial u_0}{\partial x}(2+H) - \frac{2\nu_1 l}{u_0}, \tag{28}$$

where

$$\theta = \int_0^\delta \left(1-\frac{u_1}{u_0}\right)\frac{u_1}{u_0}dz; \quad \delta_1 = \int_0^\delta \left(1-\frac{u_1}{u_0}\right)dz,$$

$$H = \delta_1/\theta, \quad l = \frac{\theta}{u_0}\left(\frac{\partial u_1}{\partial z}\right)_{z=0}.$$

Equation (28) may be solved in the usual manner by regarding u_1/u_0 as a polynominal function of z/δ, satisfying certain boundary conditions. These conditions will now be considered. At the edge of the boundary layer, u_1 tends smoothly to u_0. Thus, as in the standard method,

$$\frac{u_1}{u_0} = 1, \quad \frac{\partial}{\partial z}\left(\frac{u_1}{u_0}\right) = 0, \quad \frac{\partial^2}{\partial z^2}\left(\frac{u_1}{u_0}\right) = 0 \quad \text{at} \quad z = \delta.$$

At $z = 0$, we have $u_1 = (u_2)_h$ (i.e. the oil velocity). Thus, $u_1/u_0 = (u_2)_h/u_0 = \gamma$, where γ may be a function of x. At $z = 0$, we also have $w_1 = 0$; thus, in equation (12),

$$\nu_1\left(\frac{\partial^2 u_1}{\partial z^2}\right)_{z=0} = (u_2)_h\frac{\partial(u_2)_h}{\partial x} - u_0\frac{\partial u_0}{\partial x}.$$

But

$$\nu_1\frac{\partial^2 u_1}{\partial z^2} = \nu_1\frac{u_0}{\delta^2}\frac{\partial^2(u_1/u_0)}{\partial(z/\delta)^2},$$

and therefore

$$\left[\frac{\partial^2(u_1/u_0)}{\partial(z/\delta)^2}\right]_{z=0} = \frac{\delta^2}{\nu_1}\left\{\gamma\frac{\partial(u_2)_h}{\partial x} - \frac{\partial u_0}{\partial x}\right\} = \Lambda, \quad \text{say.} \tag{29}$$

A Pohlhausen profile modified to satisfy these boundary conditions is

$$\frac{u_1}{u_0} = \gamma + (1-\gamma)\left\{2\left(\frac{z}{\delta}\right) - 2\left(\frac{z}{\delta}\right)^3 + \left(\frac{z}{\delta}\right)^4\right\} + \frac{\Lambda}{6}\left\{1-\left(\frac{z}{\delta}\right)^3\right\}\left(\frac{z}{\delta}\right). \tag{30}$$

Then, by integration of this function, it is found that

$$\theta = \frac{\delta}{315}\{(1-\gamma)(37+\tfrac{115}{2}\gamma) - \tfrac{1}{3}\Lambda(1+\tfrac{55}{8}\gamma) - \tfrac{5}{144}\Lambda^2\}, \tag{31}$$

$$\delta_1 = \frac{\delta}{120}\{36(1-\gamma) - \Lambda\}, \tag{32}$$

$$\left(\frac{\partial u_1}{\partial z}\right)_{z=0} = \frac{1}{\delta}\left\{2(1-\gamma) + \frac{\Lambda}{6}\right\}. \tag{33}$$

These values could be substituted into equation (28) to give an equation for Λ. Instead, a slightly different approach is used which leads to less numerical work. In this approach, H and l are regarded as functions of the parameters

$$(\theta^2/u_0)(\partial^2 u_1/\partial z^2)_{z=0} \quad [= (\theta^2/\delta^2)\Lambda = \alpha, \text{say}]$$

and γ. These functions, obtained from equations (31) and (32), are plotted in figures 3 and 4.

The method has been used to study the boundary layer developed by an external velocity of the form $u_0 = \beta_0 - \beta_1 x$. The following cases have been assumed: $\gamma = 0$, $\pm 0{\cdot}05$, and γ varying linearly from $+0{\cdot}05$ at the leading edge to $-0{\cdot}05$ at the trailing edge.† The resulting skin-friction curves are plotted in figure 5. From comparison with the curve in the absence of oil ($\gamma = 0$), it will be

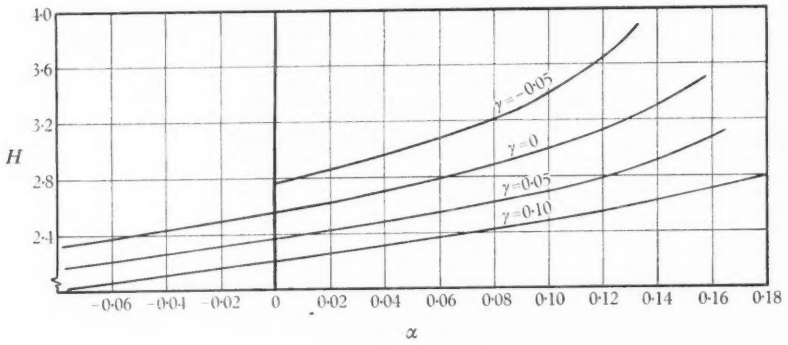

FIGURE 3. The function $H(\alpha, \gamma)$.

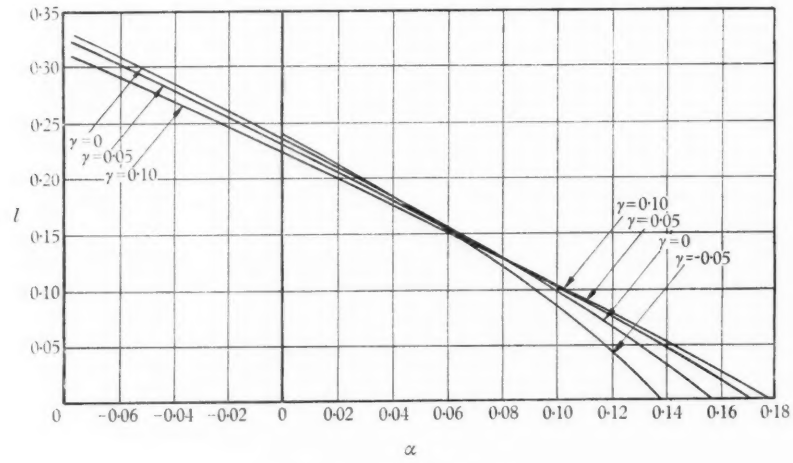

FIGURE 4. The function $l(\alpha, \gamma)$.

seen that the major effect of the oil is where the skin friction approaches zero, that is in the vicinity of separation; the distance to separation is changed by at most 9 %. In Appendix 1 values of γ likely to be found in practice are investigated, and it is found that maximum values of γ are of the order of 0·01. Thus, in general, the oil will only have a small influence on the boundary layer, changing

† Too many parameters enter a practical case for it to be tractable to use an actual distribution of γ. However, in all cases γ is positive at the leading edge and negative at separation.

the distance to separation by at most 2%. It should be noted that γ increases as the oil viscosity decreases, and thus the influence of the oil on the boundary layer increases with a decrease in oil viscosity.

The accuracy of the present analysis for the boundary layer on a moving surface, as compared with the accuracy of the Pohlhausen method for a stationary

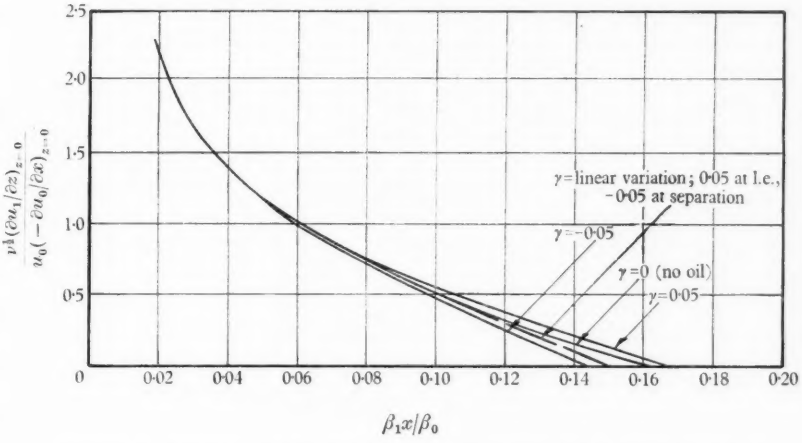

FIGURE 5. Variation of the skin-friction on a surface for different values of the parameter γ.

surface has been investigated briefly. For the case of zero-pressure gradient the skin friction as given by equations (28) and (30) has been compared with an exact solution of the problem (Squire 1956). The skin-friction values given by the two methods are in close agreement for all values of γ between 0 and 1. With an adverse pressure gradient, the accuracy is more difficult to estimate; however, it has been found that for the velocity distributions $u = \beta_0 - \beta_1 x$ and $\gamma \geqslant 0{\cdot}15$, the separation point begins to move towards the leading edge as γ is increased, thus reversing the trend shown in figure 5 for $\gamma < 0{\cdot}05$. This forward movement of the separation point is contrary to the expected physical action of the moving surface and suggests that the Pohlhausen method becomes less accurate for large values of γ.

4.2. *Variation of the thickness of the oil sheet with time*

The variation of the oil thickness h with time and position is determined by the solution of equation (17). Only one solution of this equation has been found, and this for the rather restricted case of the two-dimensional stagnation point. From the form of the equation it can be seen that in two dimensions a steady oil state is impossible, for in the steady state $\partial h/\partial t = 0$, and this would imply that

$$\frac{\partial}{\partial x}\int_0^h u_2 dz = 0 \quad \text{or} \quad \int_0^h u_2 dz = \text{const.} \tag{34}$$

It would then follow that the amount of oil passing any point is constant, but since at the leading edge u_2 is zero, no oil passes that point and the constant in equation (34) is zero. Thus, by equation (17), it appears that

$$\tfrac{1}{2}h^2\left(\frac{\partial u_1}{\partial z}\right)_0 - \frac{h^3}{3}\frac{1}{\mu_1}\frac{\partial p}{\partial x} = 0,$$

so that either $$h = 0 \quad \text{or} \quad h = \frac{3}{2}\left(\frac{\partial u_1}{\partial z}\right)_0 \Big/ \frac{1}{\mu_1}\frac{\partial p}{\partial x}. \tag{35}$$

The non-zero form of h is infinite at the pressure minimum, and so there is no steady form of h except $h = 0$. (This result is also true on infinite yawed wings, since in this case the y-derivative of the integral of v_2 over the thickness h is zero.)

In general, then, h is a variable function of time. No approximate method has been found to determine h, and it would appear that the only method is the direct numerical integration of equation (17). (Expansion in powers of t was found to be only slowly convergent, even for very small values of t.)

A numerical integration of equation (17) has been carried out for the oil thickness under a two-dimensional boundary layer with an external velocity distribution of the form $u_0 = \beta_0 - \beta_1 x$. In this case equation (17) may be written

$$\frac{\partial h'}{\partial(t/\lambda\beta_1)} = -\frac{\partial}{\partial\xi}\{(1-\xi)[\tfrac{1}{2}(h')^2 f(\xi) - \tfrac{1}{3}(h')^3]\}, \tag{36}$$

where $\xi = (\beta_1/\beta_0)x$, $h' = (\beta_1/\nu_1)^{\frac{1}{2}}h$ and $f(\xi)$ is the non-dimensional skin friction given by Howarth (1938). The boundary condition was $h' = 0{\cdot}5$, for all ξ, at $t = 0$.

The numerical integration of equation (36) is very long and laborious, and so only coarse steps have been used to determine the trends of the solution. In general the oil leaves the leading edge very quickly and flows downstream. Over the rear half of the region between the leading edge and the boundary-layer separation, the oil thickness is almost uniform, but increases steadily with time. The indication from this rough calculation is that the actual amount of oil on the surface appears to increase, suggesting that there may be an inflow of oil from downstream of separation.

5. Oil streamline directions

In this section the oil-flow direction on a general surface is considered. From the oil velocities given in equation (14), the oil streamline direction is

$$\frac{dy}{dx} = \frac{(\partial v_1/\partial z)_{z=0} + (\nu_1\rho_1)^{-1}(\partial p/\partial y)\{\frac{1}{2}z - h\}}{(\partial u_1/\partial z)_{z=0} + (\nu_1\rho_1)^{-1}(\partial p/\partial x)\{\frac{1}{2}z - h\}}. \tag{37}$$

This direction varies between

$$\frac{(\partial v_1/\partial z)_{z=0} - (h/\nu_1\rho_1)\,\partial p/\partial y}{(\partial u_1/\partial z)_{z=0} - (h/\nu_1\rho_1)\,\partial p/\partial x}$$

at the wall, and

$$\frac{(\partial v_1/\partial z)_{z=0} - (h/2\nu_1\rho_1)\,\partial p/\partial y}{(\partial u_1/\partial z)_{z=0} - (h/2\nu_1\rho_1)\,\partial p/\partial x}$$

at the oil surface.

The direction of the boundary-layer surface streamlines in the absence of the oil is

$$\left(\frac{\partial v_1}{\partial z}\right)_{z=0} \Big/ \left(\frac{\partial u_1}{\partial z}\right)_{z=0}.$$

In general the pressure term is small compared with the skin-friction term, and so has only a small influence on the oil direction except near points of small skin

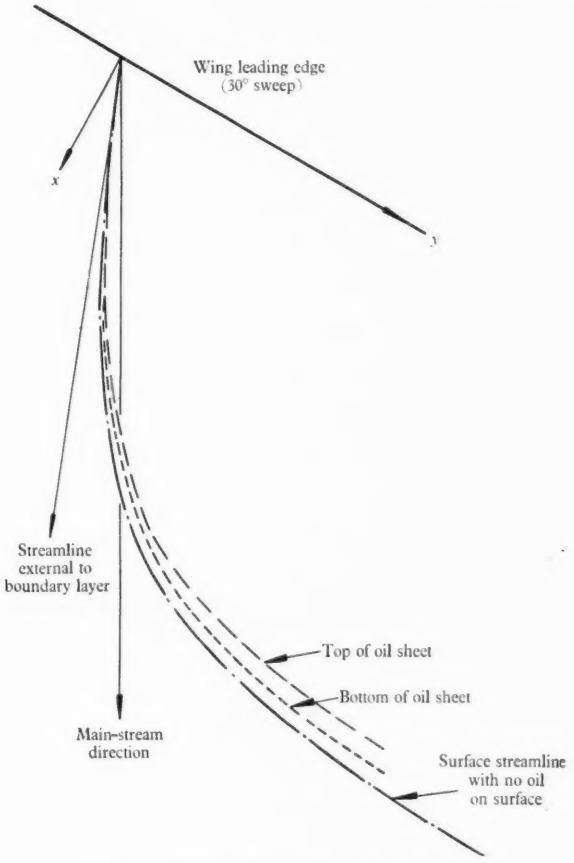

FIGURE 6. Oil streamline pattern on a yawed wing.

friction—for example, near separation. In figure 6 the oil streamlines at the wing surface and at the oil surface on an infinite swept wing are drawn. The chord-wise velocity on this wing was assumed to be of the form† $u_0 = \beta_0 - \beta_1 x$; the skin friction was then found from the power-series solution (Howarth 1938) and the cross-flow by an approximate method (Squire 1956). The oil streamlines were considered

† The constants β_0 and β_1 are related to the velocity of an R.A.E. 104 aerofoil; details are given in Appendix 1.

for a stage when the oil height varied linearly from zero at the leading edge to twice its original height at the separation point (starting from an initial uniform height of 0·001 in.). (The oil thickness at other conditions, i.e. with a non-linear variation along the surface, did not greatly affect the results as plotted.) It will be seen in figure 6 that the two oil streamlines closely follow the surface streamline with no oil on the surface, except that the oil streamlines become parallel to the leading edge before the surface streamline.

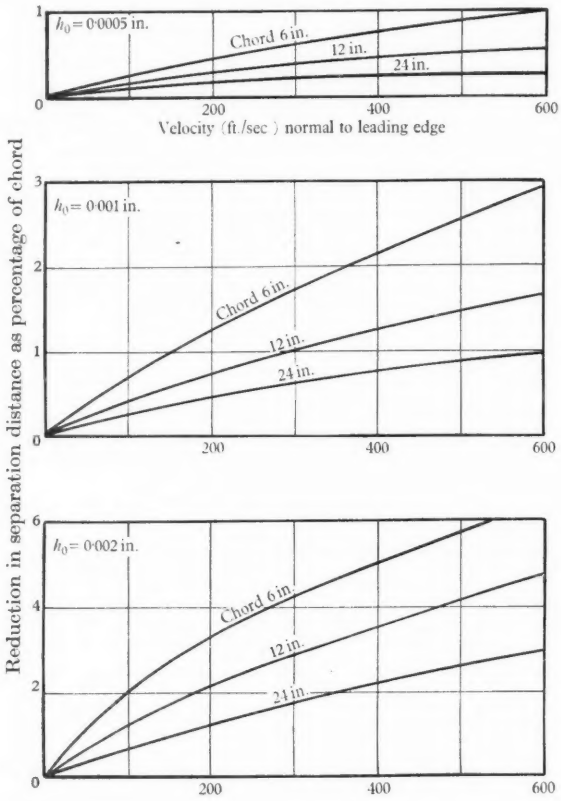

FIGURE 7. Percentage reduction in apparent separation distance for different oil-sheet thicknesses and aerofoil chords with speed.

Eichelbrenner & Oudart (1955) have shown that on a general surface the surface streamlines form an envelope at the separation line, and an envelope of the oil streamlines is usually taken as indicating separation. On a yawed infinite wing, the envelope is parallel to the leading edge. Thus, in figure 6, the oil tends to indicate separation too early.

Changes in oil thicknesses, forward speeds, and velocity distributions do not affect the shape of the curves but merely the relative position at which the

curves become parallel to the leading edge; the actual positions are given by the two points at which

$$\left(\frac{\partial u_1}{\partial z}\right)_0 - \frac{h}{\nu_1 \rho_1}\frac{\partial p}{\partial x} = 0$$

and

$$\left(\frac{\partial u_1}{\partial z}\right)_0 - \frac{h}{2\nu_1 \rho_1}\frac{\partial p}{\partial x} = 0.$$

With the mean of these two points taken as the separation point indicated by the oil, the reduction in separation distance, as a percentage of the chord, for various speeds and model sizes is plotted in figure 7.

These curves, which are independent of the oil viscosity, are useful as guides to the thickness of oil which should be used. For example, with a velocity normal to the leading edge of 600 ft./sec and a chord of 6 in., an oil height of less than 0·0005 in. must be used to keep the separation line indicated by oil within 1 % of the true separation line. For a chord of 24 in. and the same velocity, the oil thickness can be doubled while still giving results of the same accuracy.

6. Extension of the results to turbulent and compressible boundary layers

6.1. *Turbulent boundary layers*

So far the analysis has been confined to laminar layers since the calculation of the boundary layer in this case is relatively simple. In this section the flow under a turbulent boundary layer is studied in a qualitative manner. Within the oil layer the equations of motion, and the boundary conditions, are unaltered, provided that the boundary condition defining equality of stress is written

$$\mu_2 \partial u_2/\partial z = (\tau_x)_1, \quad \mu_2 \partial v_2/\partial z = (\tau_y)_1, \tag{38}$$

where $(\tau_x)_1$ and $(\tau_y)_1$ are the x- and y-components of the mean skin friction (i.e. mean with respect to time) in the turbulent boundary layer. With this form of boundary condition the oil-velocity components become

$$u_2 = \frac{1}{\mu_2}\left\{\frac{\partial p}{\partial x}\left(\frac{z^2}{2} - hz\right) + (\tau_x)_1 z\right\}, \tag{39}$$

$$v_2 = \frac{1}{\mu_2}\left\{\frac{\partial p}{\partial y}\left(\frac{z^2}{2} - hz\right) + (\tau_y)_1 z\right\}, \tag{40}$$

with corresponding forms for the streamlines.

To make use of these equations would involve the calculation of $(\tau_x)_1$ and $(\tau_y)_1$, and so far no method is available for such a calculation in the general case. Even for the case of the infinite yawed wing, experimental results show that the chordwise flow is not sufficiently independent of the cross-flow to be found by two-dimensional methods. Thus, even in this simple case, two-dimensional values may not strictly be used in equation (39) to determine the apparent separation line. However, such results are probably adequate to indicate the order of the distance between apparent and actual separation. For this purpose experimental

results quoted by Goldstein (1938) for a cylinder and an aerofoil ($t/c = 15\,\%$) are used in equations (39) and (40). These experimental results give values of the skin friction and the pressure distributions on a cylinder of 5·89 in. diameter at Reynolds numbers between 1×10^5 and $2{\cdot}5 \times 10^5$. Similar measurements are given for the aerofoil at various incidences.

From the results quoted for the aerofoil (and the cylinder at the higher Reynolds numbers), it is found, for oil thicknesses of 0·005 in. and less, that the change in the separation point as indicated by the oil is of the same order as in laminar flows. Since on the wing the flow is now attached over most of the surface, the ratio of apparent attached flow to actual attached flow will be closer to unity for turbulent boundary layers than for laminar flows.

The flow on the cylinder is initially laminar, but becomes turbulent before separation. The skin friction on the cylinder increases with distance from the stagnation point, reaches a maximum near the minimum pressure point, and then decreases again. At transition the turbulence causes the skin friction to increase again, before it finally becomes zero at the separation point. At the lower Reynolds numbers the skin friction at transition is quite low, whereas the pressure gradient is quite large, and substitution of the quoted values in equation (39) shows that u_2 could be zero at the transition point for an oil thickness of about 0·005 in. So, on a yawed cylinder, the oil streamlines could form an envelope at the transition line. In the absence of any other information, this pattern could be erroneously interpreted as a laminar separation followed possibly by a turbulent reattachment.

6.2. *Boundary layers in compressible flow*

In § 2 it has been shown that the velocity is very much smaller in the oil than in the external flow; thus, even in cases where the external flow is supersonic, the flow is still governed by the equations of slow viscous motion, and the solution is as in equation (14). It therefore seems probable that the oil pattern will be similar to that discussed in § 5 for incompressible flows. However, the flow may now be complicated by the presence of shock waves. The pressure rise through a shock may be sufficient to separate the boundary layer, and the inferences made in § 5 about the oil motion in the region of separation will also apply to such shock-induced separations. In § 5 it was shown that near separation the oil velocity becomes zero before the boundary-layer skin friction is zero, and in this case also the oil may be expected to indicate an earlier separation. For a linear adverse pressure gradient, it has been shown that the oil indication underestimates the distance to separation by, at most, 5 %. As the upstream influence of the shock wave in the boundary layer is of the order of 100 boundary-layer thicknesses, it would appear that the error in indicated separation will be of the order of 5 boundary-layer thicknesses.

Another effect at higher speeds is that of aerodynamic heating, and heat transfer. In general the heating will change the oil viscosity and so the ratio λ will become a variable depending on the state of the boundary layer. However, provided this change in λ is not too great, the main effect on the oil pattern will be small since, as shown in § 5, the actual pattern is independent of oil viscosity.

7. Application of the results obtained to the interpretation of wind-tunnel oil-flow patterns

In this paper the motion of a thin oil sheet has been studied, as the first stage in the understanding of the oil-flow patterns obtained in model testing. If the oil actually moved as a sheet, the resultant oil pattern would supply only limited indication of the oil motion: the only features to be seen would be separation, where the oil would accumulate upstream, and regions of high skin friction, such as under a vortex, where the surface would be cleared of oil. Generally in practice, the oil, although applied as a sheet, moves in filaments, which provide more detailed information on the direction of the oil motion. The motion of these filaments depends on a different set of equations to those considered in this paper. However, the mechanism of the motion is probably similar; that is, the resultant force acting on the oil is a balance between the pressure gradient outside the boundary layer and the stress due to the boundary-layer skin friction. Thus it may reasonably be supposed that the description of the oil-film motion also applies qualitatively to the motion of the filaments, and that the orders of magnitude of the changes in separation point are similar in both cases. Stalker (1955) has studied the mechanism which results in the formation of the filaments, and by order-of-magnitude considerations shows that these filaments do in fact follow the surface streamlines except near separation.

8. Conclusions

A solution has been obtained for the motion of a thin oil sheet moving on a surface under the influence of a boundary layer. The following deductions are made from the analysis.

(*a*) *The motion of the oil relative to the boundary layer.* The oil follows the boundary-layer surface streamlines except near separation where it tends to form an envelope upstream of the true separation envelope. This early indication of separation is expected to occur for both compressible and incompressible flow; it is less marked for turbulent than laminar layers. The distance by which separation is apparently altered depends on the oil thickness, and the model size, but it is independent of the oil viscosity (provided this viscosity is much greater than the viscosity of the fluid of the boundary layer).

(*b*) *The effect of the oil flow on the motion of the boundary layer.* This effect is very small in most practical cases but increases as the oil viscosity decreases.

(*c*) *Interpretation of the oil pattern at low Reynolds number.* Results at low Reynolds number should be treated with caution as transition could be erroneously interpreted as separation.

Appendix 1. Values of the constants β_0, β_1, (§§ 4, 5) and the constant γ (equation (20))

In most of the boundary-layer problems in this paper, the velocity outside the boundary layer has been assumed to have linear variation along the chord of the form $u_0 = \beta_0 - \beta_1 x$. The constants can be related to the velocity distributions on

the upper surface of the R.A.E. aerofoil sections (Pankhurst & Squire 1950), if it is assumed that the velocity varies linearly from the value at the maximum suction point to the value at the trailing edge. For all sections with lift coefficients in the range $0{\cdot}2 \leqslant C_L \leqslant 0{\cdot}6$ it has been found that $1{\cdot}2u_0 \leqslant \beta_0 \leqslant 1{\cdot}8u_0$ and

$$0{\cdot}3u_0/C \leqslant \beta_1 \leqslant 0{\cdot}9u_0/C.$$

All calculations have been carried out with the typical values, $\beta_0 = 1{\cdot}5u_0$, $\beta_1 = 0{\cdot}6u_0/C$.

The constant γ (equation (20)) may be evaluated for the external flow $u_0 = \beta_0 - \beta_1 x$. Using the skin friction $f(\xi)$ quoted by Goldstein (1938), the oil velocity at the oil surface (equation (15)) becomes

$$\lambda\left\{\beta_0(1-\xi)\frac{\beta_1^{\frac{1}{2}}}{\nu_1^{\frac{1}{2}}}f(\xi)\,h - \frac{1}{\nu_1}\beta_0\beta_1(1-\xi)\,h^2\right\}, \tag{41}$$

where

$$\xi = (\beta_1/\beta_0)\,x.$$

Then γ, the ratio of the oil velocity to the mainstream velocity, becomes

$$\gamma = \lambda\left\{\frac{\beta_1^{\frac{1}{2}}}{\nu_1^{\frac{1}{2}}}f(\xi)\,h - \frac{\beta_1}{\nu_1}h^2\right\}. \tag{42}$$

This parameter has been used in the calculation of the effect of the oil on the boundary-layer flow, and a maximum value of this parameter is required. It is not possible to find the maximum by standard methods since the variation of h with ξ (or x) is not known. However, with practical oil thicknesses and $\beta_1 = 0{\cdot}6u_0/C$, it is found that $(h^2\beta_1/\nu_1)$ is at most 1. Also $f(\xi)$ is $O(1)$, except close to the leading edge. Thus the maximum value of γ is $O(\lambda)$. The maximum value of λ found in practice is 0·02 for paraffin in a wind tunnel; for the type of heavy oil used in high-speed tunnels, λ and hence γ are $O(10^{-4})$.

Appendix 2. The equality of viscous stress at the air/oil interface

Equation (6) states the conditions that the viscous stresses shall be equal across the air/oil face. The condition given is strictly valid only for an oil surface parallel to the body surface, i.e. $z = \text{const.}$ However, this paper is concerned with oil layers with thicknesses varying with position, that is, the oil surface is given by $z = f(x, y)$. The purpose of this Appendix is to show that equation (6) is valid for such surfaces provided $\partial z/\partial x$, $\partial z/\partial y$ are $o(1/\delta)$.

The proof will be given for a surface $z = f(x)$. At a point on this surface direction cosines to the surface normal, in the plane $y = \text{const.}$, are l and n, and the velocity along the surface in this plane is

$$ul - wn. \tag{43}$$

The derivative of this velocity along the surface normal is

$$l^2\frac{\partial u}{\partial z} + ln\left(\frac{\partial u}{\partial x} - \frac{\partial w}{\partial z}\right) - n^2\frac{\partial w}{\partial x}. \tag{44}$$

Thus the strict boundary condition at the interface is

$$\mu_1\left\{l^2\frac{\partial u_1}{\partial z} + ln\left(\frac{\partial u_1}{\partial x} - \frac{\partial w_1}{\partial z}\right) - n^2\frac{\partial w_1}{\partial x}\right\} = \mu_2\left\{l^2\frac{\partial u_2}{\partial z} + ln\left(\frac{\partial u_2}{\partial x} - \frac{\partial w_2}{\partial z}\right) - n^2\frac{\partial w_2}{\partial x}\right\}. \tag{45}$$

In the boundary layer $\partial u_1/\partial z$ is $O(1/\delta)$, $\partial u_1/\partial x, \partial w_1/\partial z$ are $O(1)$ and $\partial w_1/\partial x$ are $O(\delta)$. Thus, provided n/l is $o(1/\delta)$, the dominant term on the left-hand side of equation (45) is $\mu_1 l^2 \partial u_1/\partial z$. In the oil flow, $\partial w_2/\partial z$, $\partial u_2/\partial x$ are of the same order of magnitude, by the continuity equation, and $u_1 = u_2$, $w_1 = w_2$ at the oil surface. Thus we might expect the terms on the right-hand side of equation (45) to have a similar relationship to each other. In this case equation (45) reduces to equation (6). The use of equation (6) in § 2 gives a solution which confirms that the terms in equation (45) can be dropped. Thus equation (6) holds for the surface $z = f(x)$ provided the ratio of n/l, or $\partial z/\partial x$, is $o(1/\delta)$. A similar result holds for $z = f(x, y)$.

The analysis of this Appendix again breaks down in the vicinity of the separation point. However, the region affected is the same as that for the analysis of § 2 so that the region of validity is not reduced further.

REFERENCES

Black, J. 1952 *J. Roy. Aero. Soc.* **56**, 279.

Eichelbrenner, E. A. & Oudart, A. 1955 *La Recherche Aeronautique*, **47**, 11.

Goldstein, S. (Ed.) 1938 *Modern Developments in Fluid Dynamics.* Oxford University Press.

Goldstein, S. 1948 *Quart. J. Mech. Appl. Math.* **1**, 43.

Howarth, L. 1938 *Proc. Roy. Soc.* A, **164**, 547.

Pankhurst, R. C. & Squire, H. B. 1950 *Aero. Res. Counc., Lond., Curr. Pap.* 80.

Prandtl, L. 1952. *Essentials of Fluid Dynamics.* London: Blackie.

Squire, L. C. 1956 Ph.D. Thesis, University of Bristol.

Stalker, R. J. 1955 *Australian A.R.L. Report* A 96.

Stanbrook, A. 1957 *Aero. Res. Counc., Lond., Rep. & Mem.* 3114.

Winter, K. G., Scott-Wilson, J. B. & Davies, F. V. 1954 *Aero. Res. Counc., Lond., Curr. Pap.* 212.

The motion of a shock-wave through a region of non-uniform density

By G. A. BIRD

Department of Aeronautical Engineering, The University of Sydney, Sydney, Australia

(Received 24 February 1961)

The method of characteristics is used to calculate numerical solutions for the one-dimensional motion of a plane shock-wave through a stationary gas which contains a region of non-uniform density. These solutions are compared with those given by the Chisnell–Whitham approach which ignores the effects on the shock-wave of the disturbances which are generated in the flow behind it, and also with the asymptotic solution given by the simple theory which regards the non-uniform region as a contact-surface discontinuity. It is concluded that the results of the simplified theories must be applied with caution.

1. Introduction

Consider the one-dimensional unsteady flow in which a plane shock-wave propagates into a stationary gas which contains a stratum from $x = 0$ to $x = 1$ in which the density changes from a value ρ_0 which is constant for $x < 0$ to another value ρ_1 which remains constant for $x > 1$. Figure 1 is a representation of the resulting flow in the distance-time (x, t) plane.

The shock-wave is represented by the line OAB and, before it meets the region of non-uniform density, it has a constant shock Mach number* M_{s_0} and the flow behind it is uniform. The shock strength changes in the non-uniform region between O and A and reflected waves are produced. As these reflected waves pass through the non-isentropic region OBC between the shock and the particle path through O, further waves (which will be called re-reflected waves) are produced which travel in the same direction as the shock and eventually overtake it. These re-reflected waves influence the rate of variation of shock strength between O and A and they also cause the shock to continue to alter in strength after it has passed through the non-uniform region at A. To the left of OC, the reflected waves form a simple wave system—unless, of course, they are compression waves, in which case another shock and further re-reflected waves are eventually formed.

Chisnell (1955) obtained an expression for the change in strength of a shock-wave at an infinitesimal density discontinuity. He then integrated this expression to obtain a relationship between shock strength and density. This approach, which had previously been applied by Moeckel (1952) to the corresponding interaction in two-dimensional steady flow, ignores the influence of the re-reflected

* The shock Mach number is defined as the ratio of the speed of the shock-wave to the speed of sound in the gas in front of it.

waves. Chisnell (1957) used a similar method to treat the interaction of a shock-wave with a non-uniformity in area, and the approach was further generalized by Whitham (1958) who applied it to a large number of non-uniform shock-wave propagation problems. The results of this approach will be referred to as Chisnell–Whitham solutions.

When the density change is discontinuous, the non-uniform region reduces to a contact surface and the solution is easily obtained (Paterson 1948). As noted by Chisnell, this solution must give correctly the ultimate strength of the transmitted and reflected waves. The results of this approach will, therefore, be referred to as the asymptotic solution.

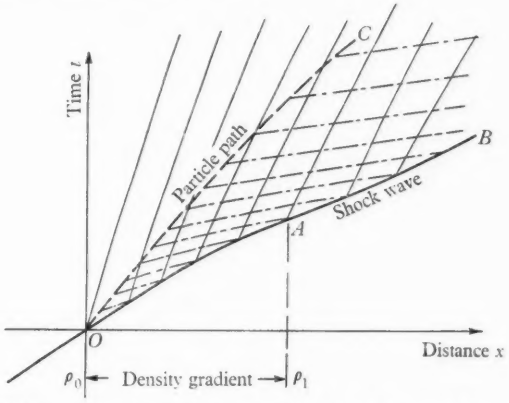

FIGURE 1. Distance–time diagram for motion of shock-wave through region of non-uniform density. ——, Reflected waves; —·—·, re-reflected waves.

The Chisnell–Whitham approach gives a gradual change in shock Mach number or strength between O and A and then a constant value beyond A. In general, there is a considerable discrepancy between this value and that given by the asymptotic solution, and little is known about the rate at which the asymptotic state is reached. However, the advent of high-speed electronic computers has made it possible to obtain complete numerical solutions by the method of characteristics on a sufficiently extensive scale to enable a realistic assessment to be made of the value of the Chisnell–Whitham approach. The object of this note is to present such an assessment for this particular shock-wave interaction problem.

2. Description of method

The appropriate characteristics relationships and boundary conditions (e.g. Rudinger 1955) were set up in a form suitable for automatic computation and were programmed, using a simplified coding scheme, for the SILLIAC digital computer in the University of Sydney. The calculations were made for a perfect gas.

The programme specified the (x) mesh length along the shock-wave. This was reduced where there was a large gradient in shock strength and was made

particularly small near the discontinuity in density gradient at A. Table 1 shows a typical effect of mesh size on the accuracy of the calculation. The shock Mach number quoted is that at A ($x = 1$) for $M_{s_0} = 4$, with the density varying linearly from $\rho_0 = 1$ to $\rho_1 = 0{\cdot}125$ and a specific-heat ratio $\gamma = \frac{7}{5}$.

Sufficient accuracy was obtained here for an average mesh length at the shock of less than 0·05. The solution eventually oscillated about the result given by the asymptotic solution; for reasonably small mesh sizes the amplitude of these oscillations was of the order of one-tenth of 1 % of the asymptotic shock Mach number. A typical calculation involved a total of about 500 mesh points and required about 30 min. computing time. The Chisnell–Whitham and the asymptotic solutions were also programmed for automatic computation.

Average mesh length at shock	Shock Mach number at $x = 1$
0·2	2·553
0·1	2·506
0·05	2·500
0·025	2·499

TABLE 1. Influence of mesh size.

3. Results and discussion

The accuracy of the Chisnell–Whitham approach was found to depend on the shock Mach number, the specific-heat ratio of the gas, the shape of the density profile and the magnitude of the density change.

Figure 2 shows an example (for $M_{s_0} = 1{\cdot}1$, $\rho_0 = 1$, $\rho_1 = 0{\cdot}125$ and $\gamma = \frac{7}{5}$) in which the Chisnell–Whitham solution provides an excellent description of the flow. The shock Mach number given by the characteristics solution is indistinguishable from that given by the Chisnell–Whitham solution up to the end of the non-uniform region and it then tends very slowly to the asymptotic solution —at $x = 10$ it has changed by only one-tenth of the difference. On the other hand, figure 3 (for $M_{s_0} = 4$, $\rho_0 = 1$, $\rho_1 = 32$ and $\gamma = \frac{7}{5}$) is an example in which the Chisnell–Whitham solution gives little more than the initial slope of the curve of shock Mach number against distance. At $x = 1$, the characteristics solution gives $M_s = 7{\cdot}963$ compared with $M_s = 9{\cdot}985$ by the Chisnell–Whitham method and $M_s = 7{\cdot}582$ by the asymptotic solution. If the pressure ratio across the shock were used as the measure of shock strength, the corresponding figures would be 74·98, 116·2 and 68·07. The asymptotic shock Mach number is, in fact, effectively reached by $x = 1{\cdot}5$, or in a distance beyond the end of the non-uniform layer which is much less than the thickness of the layer. This asymptotic shock strength is calculated on the assumption that the reflected waves do not form a shock-wave. However, as noted in the introduction, this is not always true but, even in this extreme example, the asymptotic shock strength would be altered by only 1·5 % to $M_s = 7{\cdot}492$. This adjustment would take place over a distance which is very large in comparison with the thickness of the non-uniform layer.

Part of the contrast between the performances of the Chisnell–Whitham approach in these two examples can be attributed to the fact that in the first

the density decreases whilst in the second it increases. (Unless otherwise stated, the density variation with distance in all these examples is linear.) This effect is illustrated in figure 4 which is for $M_{s_0} = 4$, $\rho_0 = 1$, $\rho_1 = 8$ or 0·125, and

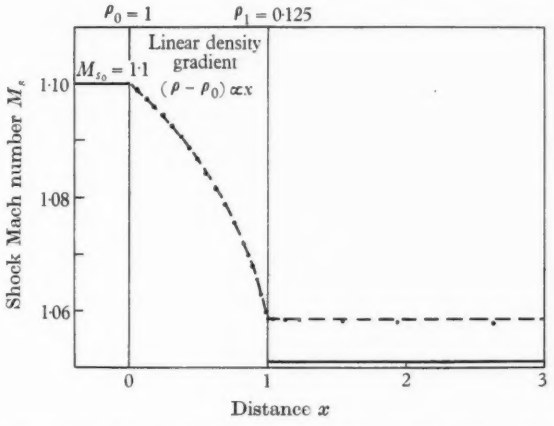

FIGURE 2. Example of good performance by Chisnell–Whitham solution. $\gamma = \frac{7}{5}$. ----, Chisnell–Whitham; ——, asymptotic; ....., characteristics.

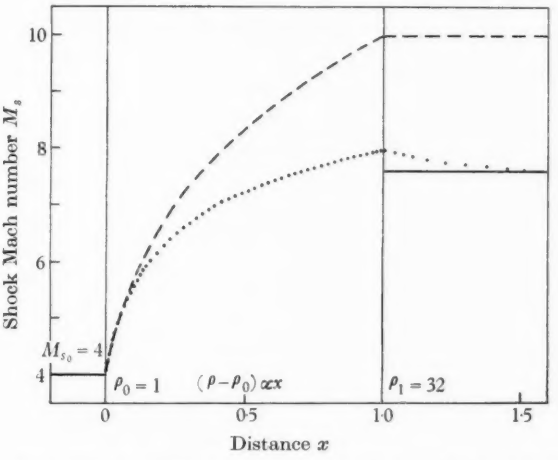

FIGURE 3. Example of poor performance by Chisnell–Whitham solution. $\gamma = \frac{7}{5}$. ----, Chisnell–Whitham; ——, asymptotic; ....., characteristics.

$\gamma = \frac{7}{5}$. For the positive density gradient, the shock Mach number at A ($x = 1$) has made up 73% of the difference between the Chisnell–Whitham solution and the asymptotic solution, and the latter is effectively reached at $x = 1{\cdot}75$. However, when the density decreases the corresponding figures are 19 % and $x = 5{\cdot}5$. It is noticeable that for the increasing density the major part of the increase in shock strength occurs near $x = 0$ so that the re-reflected waves have a considerable influence on the shock before it reaches $x = 1$. Opposite considerations apply

for the decreasing density and the re-reflected waves do not overtake the shock for a considerable distance. This suggested dependence on the shape of the density profile is confirmed in figure 5 which is for $M_{s_0} = 4$, $\rho_0 = 1$, $\rho_1 = 8$, $\gamma = \frac{7}{5}$

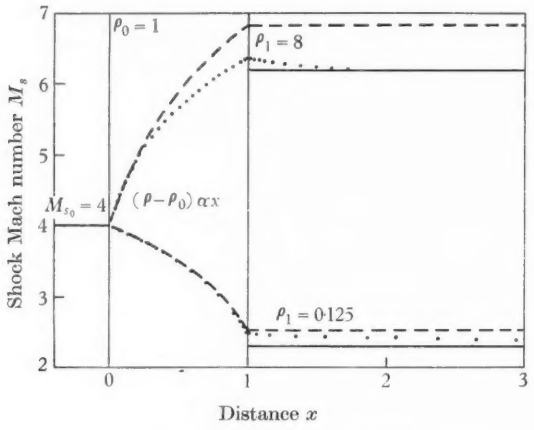

FIGURE 4. Influence of density gradient. $\gamma = \frac{7}{5}$.
----, Chisnell–Whitham; ——, asymptotic; ....., characteristics.

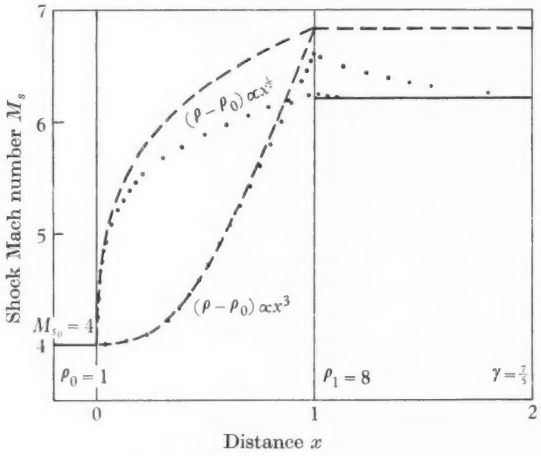

FIGURE 5. Influence of density profile. $\gamma = \frac{7}{5}$.
----, Chisnell–Whitham; ——, asymptotic; ....., characteristics.

and a density proportional to $x^{\frac{1}{2}}$ or x^3. The performance of the Chisnell–Whitham solution is far better when the major changes occur near the end of the layer.

Apart from this dependence on the density profile, the rate at which the asymptotic solution is approached for a given specific-heat ratio is largely a function of the shock Mach number. This is illustrated in figure 6 which shows M_s/M_{s_0} as a function of distance for $\rho_0 = 1$, $\rho_1 = 8$, $\gamma = \frac{7}{5}$ and $M_{s_0} = 1{\cdot}1$, 2 and 16.

Note that, for the increasing density, the characteristics solution is well below the Chisnell–Whitham solution even for an initial shock Mach number as low as 1·1.

Figure 7 (for $M_{s_0} = 4$, $\rho_0 = 1$, $\rho_1 = 8$ and $\gamma = \frac{5}{3}$ or $\frac{19}{17}$) illustrates the effect of specific-heat ratio. For the lower value of specific-heat ratio, the asymptotic shock Mach number is approached far more quickly than for the higher value.

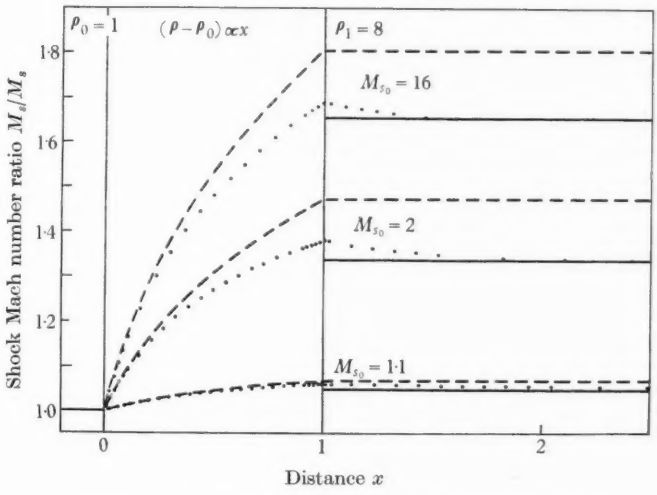

FIGURE 6. Influence of initial shock Mach number. $\gamma = \frac{7}{5}$.
----, Chisnell–Whitham; ——, asymptotic; ....., characteristics.

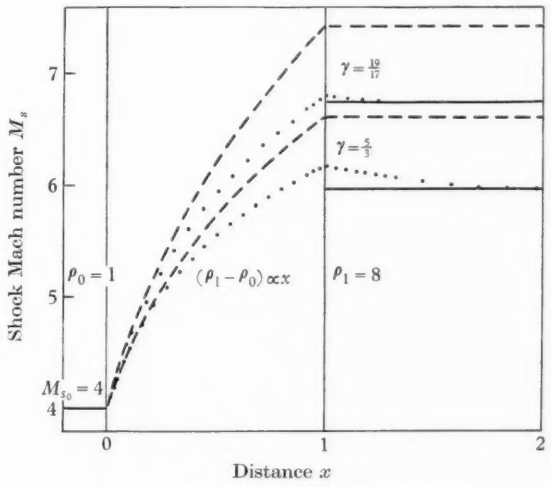

FIGURE 7. Influence of specific-heat ratio.
----, Chisnell–Whitham; ——, asymptotic; ....., characteristics.

The magnitude of the over-all change in density does not have any profound effect on the comparisons between the solutions. A large over-all change merely serves to magnify the differences and vice versa.

It is clear from these results that, given a combination of a weak shock-wave, a favourable density profile and a gas with a high ratio of specific heats, the Chisnell–Whitham approach can furnish an excellent quantitative description of the flow. However, for strong shock-waves in gases with low ratios of specific heats, the results given by the simple contact surface discontinuity theory can be more meaningful. If a detailed solution is required in a general case, there does not seem to be any real substitute for a full numerical analysis.

REFERENCES

CHISNELL, R. F. 1955 *Proc. Roy. Soc.* A, **223**, 350.

CHISNELL, R. F. 1957 *J. Fluid Mech.* **2**, 286.

MOECKEL, W. E. 1952 *Nat. Adv. Comm. Aero. Tech. Note* no. 2725.

PATERSON, S. 1948 *Proc. Phys. Soc.* **61**, 119.

RUDINGER, G. 1955 *Wave Diagrams for Non-Steady Flow in Ducts.* New York: Van Nostrand.

WHITHAM, G. B. 1958 *J. Fluid Mech.* **4**, 337.

Cavity flow past a slender pointed hydrofoil

By E. CUMBERBATCH AND T. Y. WU
California Institute of Technology, Pasadena, California

(Received 1 July 1960 and in revised form 3 April 1961)

A slender-body theory for the flow past a slender, pointed hydrofoil held at a small angle of attack to the flow, with a cavity on the upper surface, has been worked out. The approximate solution valid near the body is seen to be the sum of two components. The first consists of a distribution of two-dimensional sources located along the centroid line of the cavity to represent the variation of the cross-sectional area of the cavity. The second component represents the cross-flow perpendicular to the centroid line. It is found that over the cavity boundary which envelops a constant pressure region, the magnitude of the cross-flow velocity is not constant, but varies to a moderate extent. With this variation neglected only in the neighbourhood of the hydrofoil, the cross-flow is solved by adopting the Riabouchinsky model for the two-dimensional flow. The lift is then calculated by integrating the pressure along the chord; the dependence of the lift on cavitation number and angle of attack is shown for a specific case of the triangular plan form.

1. Introduction

In the operation of propellers, pumps and high-speed water-craft, cavitation occurs when the effect of high speed or low ambient pressure is sufficient to reduce the local fluid pressure to the vapour pressure. The latter cause, of low ambient pressure, often results from the operation of a hydrofoil near a free surface, sometimes with the cavity being ventilated by the atmosphere. It may seem desirable from several practical viewpoints that a hydrofoil boat should be supported by hydrofoils of small aspect ratio. With this and other applications in mind, an analysis of the problem of cavity flow over a slender hydrofoil is presented in this paper.

Only one attempt on a problem of similar type has come to the notice of the authors. This work is due to Tulin (1959) who considered fully cavitating flow past a pointed delta wing at a small angle of attack. Conical flow was assumed and it was shown that such a régime of flow was in evidence over most of the wing only when the total apex angle of the delta wing was at least 30°. Also only flows having long trailing cavities (i.e. flows operating at zero cavitation number) were considered. Some results for flows operating at small cavitation numbers were inferred using formulae valid for two-dimensional theory. It is evident that the model treated by Tulin does not satisfy the slenderness conditions of the present paper and hence there exists no common range of validity for any comparison of results of these two cases.

The problem, formally presented in § 2 below, is that of the cavitating flow over a pointed hydrofoil placed at a small angle of attack in an otherwise uniform stream. The flow, separating from the sharp side and trailing edges of the hydrofoil, forms a cavity which envelops the entire upper surface and is assumed to close at some position downstream of the trailing edge. The system of the hydrofoil and the cavity is assumed to be slender. This means that the maximum lateral dimension of the system is small compared with the total length of the cavity. The flow is assumed to be inviscid, irrotational and incompressible. A velocity potential therefore exists for the flow outside the cavity, and will satisfy the Laplace equation in three dimensions. Appropriate boundary conditions (apart from the condition of uniform flow far upstream) on the velocity potential are applied at the wetted side of the hydrofoil and at the cavity boundary; these are the following. The kinematic condition on a stationary surface is that the flow velocity must be tangential to the boundary. This condition is applied both on the cavity and hydrofoil boundaries. The dynamic condition, that the pressure in the cavity is a constant, must also be applied on the cavity boundary. It is to be noted that the position of the cavity boundary is not known *a priori*, but is determined by the flow conditions. Hence the boundary conditions on the cavity are applied on an undetermined surface; the problem is thus essentially non-linear. This is a general feature complicating most free-surface flow problems. In this analysis the gravity effects are neglected (a very reasonable approximation for high speed).

The method of investigation of the problem of supersonic flow past a slender body of general cross-section, developed by Ward (1949) is adaptable to subsonic flow with slight modifications. The Laplace equation for the incompressible flow indicates that a Fourier, instead of a Laplace, transformation may be made to this equation. The analysis and results obtained by Ward then follow in similar fashion for the incompressible case. For completeness, this modified analysis for the incompressible case is presented in brief form in § 2. A solution is obtained there in terms of an infinite series of Bessel functions. This solution is expanded for use near the body, where the boundary conditions may be used to estimate the size of the terms in this region. The result, obtained by Ward for the supersonic case, that the perturbation velocity in the downstream direction is of smaller order than the perturbation velocities in the lateral directions is shown to remain valid in the present case of incompressible flow past a slender cavity-hydrofoil system, since the same kinematic boundary condition holds on the free-cavity boundary as on the solid hydrofoil boundary.

The approximate solution valid near the body is seen to be the sum of two components. The first consists of a distribution in the downstream direction of functions representing two-dimensional sources in planes perpendicular to the downstream direction. The source strength varies with distance downstream in such a way as to represent the effect of the variation of the cross-sectional area of the body. The second component is the component of the total flow in planes perpendicular to the downstream direction and is called the cross-flow. In the flow past a slender solid body (cf. Ward 1949, and Sacks 1954), the best approximation may be obtained when the cross-flow planes are chosen perpendicular to the line

of centroids of the cross-sections of the body. Since only bodies of small camber are considered, this line may be approximated by a mean straight line. The axial source-like component of the flow is then assumed to satisfy the kinematic boundary condition on the body. Physically this means that in the interpretation within the framework of the slender-body approximation, the cross-flow is set up in such a way that the flow at moderate and large distances from the body axis senses only the mean location of the centroids of the body cross-sections and the variation of the cross-sectional area, and is not affected by the local geometric details of the surface of the body. The cross-flow at a particular station downstream has then to satisfy zero normal-flow conditions on the body and hence represents the two-dimensional flow past a body whose shape is given by the cross-sectional shape of the body at the station chosen. The solution of this flow is then obtained by the usual potential-flow methods. It is to be noted that the cross-flow is a two-dimensional problem only when the boundary conditions do not involve flow derivatives in the axial direction, as in the case of the flow past a solid body without separation or cavitation.

In the present case of the cavity flow over a slender hydrofoil, the problem has certain additional complexities. A complicating factor, again arising from the fact that the shape of the cavity is not known *a priori*, is that the centroid line of the cavity-hydrofoil cross-sections is also unknown. In other words, this centroid line is to be determined as a part of the problem. As a result, the direction of the centroid line of the cavity-hydrofoil cross-sections (and hence also the direction of the cross-flow) must be considered as an unknown parameter, which is to be determined subsequently by the analysis of the flow. With this in mind then, the approximate solution valid near the cavity-hydrofoil system may be separated as explained above into components along, and perpendicular to, the axis of the centroids. The axial component represents the variation of the area of the cavity-hydrofoil cross-sections, which are also to be determined subsequently. The axial flow is again assumed to satisfy the kinematic boundary condition on the cavity and on the hydrofoil. The cross-flow is then the component of the total flow in planes perpendicular to the axial direction and must satisfy zero normal-velocity boundary conditions on the cavity and on the hydrofoil. The cross-flow in this case is the potential flow in a plane past a plate set normal to the stream, where the plate is the shape of the hydrofoil at the section chosen. The flow separates from the edges of the plate to form a cavity on the rear side. However, the pressure condition on the cavity connects velocity components in the cross-flow directions with the velocity component in the axial direction. The downstream co-ordinate therefore enters the problem in more than the parametric fashion of the non-separating solid-body case. To reduce the problem to a tractable form, it is assumed that the axial velocity component has a constant value over the cavity. It is deduced in the subsequent analysis that in fact this velocity component over the cavity differs only slightly from a constant, the value of which is also determined. With this assumption then, the cross-flow reduces to a two-dimensional cavity-flow problem. The solution to this flow problem may be deduced using a variety of models for the flow; for discussion of these models, see Wu (1956). It is found convenient to use the Riabouchinsky model, in which an

image plate is introduced downstream of the real plate. This model provides a good description of the flow near the real plate and estimates the force on the plate fairly accurately. The cross-flow solution is derived in this manner in § 3.

The lift on the plate is determined in § 4 by integration of the normal pressure over the plate. It is seen that the lift is composed of parts due to the cross-flow, the axial flow and cross-product terms of these flows. In addition, the dependence on cavitation number and angle of attack is of a non-linear form and precludes any simple interpretation of the terms in the lift force as given by Ward and Sacks for the non-separated flow past a slender solid body. This is due to the fact that the present analysis represents in an approximate way the wake effects of a real fluid.

2. Formulation of the problem

The problem considered is that of the supercavitating flow past a slender pointed hydrofoil, placed at a small angle of attack in a stream of velocity V and pressure p_∞ far upstream. The hydrofoil is taken to be a plate which is pointed at the leading edge and may have a small camber in the downstream direction. A cavity, in which the pressure has a constant value p_c, is assumed to have been generated to envelop the entire upper surface of the plate, starting from the sharp side and trailing edges of the plate and extending to some position downstream of the trailing edge (see figure 1). Physically this situation can be realized at sufficiently small values of the cavitation number,

$$\sigma = (p_\infty - p_c)/\tfrac{1}{2}\rho V^2, \tag{1}$$

ρ being the density of the fluid. The total system of the plate and the cavity is assumed slender enough for the approximations adopted in the slender-body theory to be valid. The flow exterior to the plate-cavity system is assumed to be incompressible, inviscid and irrotational, in which case there will exist in this region a perturbation velocity potential which will satisfy the three-dimensional Laplace equation.

It has been pointed out in § 1 that the velocity potential of the flow past slender bodies may, in the vicinity of the body, be separated into two parts. One part is the source-like component which represents the effect of the variation of the cross-sectional area of the body; the other part is the doublet-like component which is actually the cross-flow in planes perpendicular to the body axis. Thus, in the case of non-separated (or non-cavitating) flow past a slender body, the free-stream velocity is resolved into components parallel and normal to the body axis, which is taken to pass through the geometric centroids of the cross-sectional area of the body at different stations. The situation is certainly different in the present case of the cavity flow over the slender plate, since the cavity boundary is not known *a priori* and the centroid line of the cavity-plate system must be determined as a part of the problem. Presumably, for the purpose of determining this cross-flow, the cavity boundary may be regarded as a solid boundary since the same kinematic condition is applied there as would be applied to an equivalent solid boundary. The centroid of a cavity-plate cross-section is thus taken as the geometric centre of the two-dimensional cavity behind a plate set normal to

the cross-flow, the shape of this plate being the shape of the hydrofoil at the section chosen. It is assumed that when the cavity of the slender body is sufficiently long, the curvature of the line passing through the centroids of the cavity sections is negligibly small (at least in the region over the plate), so that it may be taken as a straight line. This line will be at a small angle, say ϵ, to the free-stream direction and will lie between this direction and the inclined slender plate. It should be emphasized that the angle ϵ is to be determined in the subsequent analysis of the problem.

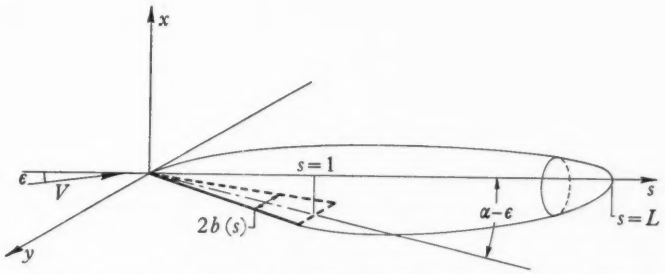

FIGURE 1. The supercavitating flow past a slender pointed hydrofoil and the co-ordinate system.

Now that the method of determining the direction of the cross-flow has been explained, it is convenient to take axes in and perpendicular to the cross-flow plane. A Cartesian co-ordinate system (x, y, s) is taken fixed at the leading edge of the hydrofoil with the s-axis pointing along the line of centroids of the cavity-plate system (which is assumed straight) and the y-axis taken parallel to the span of the hydrofoil (see figure 1). In this co-ordinate system the free-stream velocity has the vector form $(V \sin\epsilon, 0, V\cos\epsilon)$. In general, the hydrofoil may have a small camber

$$x = \xi(s). \tag{2}$$

The angle of inclination, α, of the hydrofoil is taken to be the angle between the free-stream direction and the line joining the leading edge to the mid-point of the trailing edge of the hydrofoil. The half-width of the slender plate at any station s is taken as $b(s)$, the total length of the plate being normalized to unity.

The perturbation velocity potential of the flow is taken to be $\phi(x, y, s)$, which is made non-dimensional, such that the flow velocity $\mathbf{q}$ is given by

$$\mathbf{q}/V = (\phi_x, \phi_y, \cos\epsilon + \phi_s). \tag{3}$$

Hence, at large distances from the cavity-plate system,

$$\phi - x\sin\epsilon \to 0, \quad \phi_x - \sin\epsilon \to 0, \quad \phi_y, \phi_s \to 0. \tag{4}$$

The potential ϕ satisfies, in the flow region, the Laplace equation

$$\phi_{rr} + \frac{1}{r}\phi_r + \frac{1}{r^2}\phi_{\theta\theta} + \phi_{ss} = 0, \tag{5}$$

where $r = (x^2 + y^2)^{\frac{1}{2}}$ and $\theta = \tan^{-1}(y/x)$.

In the absence of gravity, the pressure p at a point in the flow is given by the Bernoulli equation

$$p+\tfrac{1}{2}\rho q^2 = p_\infty+\tfrac{1}{2}\rho V^2. \tag{6}$$

There are boundary conditions at the plate and at the cavity boundary. The first one, which is kinematic in nature, requires that the flow be tangential to the plate and to the cavity boundary. Hence

$$\frac{\partial\phi}{\partial x} = \left[\frac{d\xi}{ds}-(\alpha-\epsilon)\right]\left[\cos\epsilon+\frac{\partial\phi}{\partial s}\right] \quad \text{at the plate} \tag{7}$$

and

$$\frac{\partial\phi}{\partial n} = \frac{d\nu}{ds}\left[\cos\epsilon+\frac{\partial\phi}{\partial s}\right] \quad \text{over the cavity boundary,} \tag{8}$$

where $\partial/\partial n$ denotes differentiation along the outward normal to the cavity boundary at station s, and $d\nu$ is the normal distance between the projections on the (x,y)-plane of the cavity boundary of two sections at a distance ds apart. The second boundary condition, which is dynamic in nature, states that

$$p = p_c \quad \text{over the cavity.} \tag{9}$$

It follows from (6) that $\mathbf{q}$ assumes the constant magnitude

$$|\mathbf{q}| = q_c \quad \text{on the cavity boundary,} \tag{9a}$$

where q_c and V are related, using (1) and (6), by

$$q_c = V(1+\sigma)^{\frac{1}{2}}. \tag{10}$$

It is to be noted that the above boundary conditions (7), (8) and (9) are of a mixed type in the sense that different conditions are imposed over different parts of the boundary. Furthermore, the fact that the location of the cavity boundary is not known *a priori* is one of the factors which makes the problem non-linear.

In the treatment of the flow past a slender body without separation or cavitation, the slender-body theory indicates that, near the body, perturbation velocities in the downstream direction are small quantities of higher order than the velocity components in the lateral directions. It is on this basis that the problem can be solved approximately by reducing it to a two-dimensional flow in the cross-flow plane. However, when a cavity is present in the flow the condition on the pressure, (9) or (9*a*), connects velocity components of different orders in one relationship, as will be shown later; the problem thus becomes more complicated. It is therefore desirable to estimate the order of magnitude of the perturbation velocities in the neighbourhood of the cavity-plate system. This is done as follows.

If the maximum lateral dimension of the cavity is t, and the length of the cavity is L, then the assumption of slenderness implies that

$$\delta = t/L \ll 1. \tag{11}$$

It is convenient for the moment to make the substitition

$$\Phi = \phi - x\sin\epsilon, \tag{12}$$

so that Φ and (grad Φ) vanish at infinity (cf. equation (4)). It is easily seen that Φ also satisfies the Laplace equation (5). Application to this equation for Φ of the Fourier transform

$$\tilde{\Phi}(x, y, \omega) = \int_{-\infty}^{\infty} e^{-i\omega s}\Phi(x, y, s)\, ds \tag{13}$$

yields

$$\frac{\partial^2\tilde{\Phi}}{\partial r^2} + \frac{1}{r}\frac{\partial\tilde{\Phi}}{\partial r} + \frac{1}{r^2}\frac{\partial^2\tilde{\Phi}}{\partial\theta^2} - \omega^2\tilde{\Phi} = 0. \tag{14}$$

This equation has the general solution, which satisfies the condition (4), of the form

$$\tilde{\Phi}(r, \theta, \omega) = A_0 K_0(|\omega| r) + \sum_{n=1}^{\infty} A_n K_n(|\omega| r)\cos(n\theta + \beta_n), \tag{15}$$

where K_n stands for the modified Bessel function of the second kind, and the coefficients A_n and the phase angles β_n may depend on ω. Near the cavity-plate system, where $r/L = O(\delta)$, use of the expansion of K_n for small argument leads to $\tilde{\Phi} = \tilde{\Phi}_0[1 + O(\delta)]$, where

$$\tilde{\Phi}_0 = -(\log \tfrac{1}{2}|\omega| r + \gamma) A_0 + \frac{1}{2}\sum_{n=1}^{\infty} (n-1)!\left(\frac{2}{|\omega|}\right)^n \frac{A_n}{r^n}\cos(n\theta + \beta_n),$$

and $\gamma = 0{\cdot}5772\ldots$ is Euler's constant.

The inverse Fourier transform of the function $\tilde{\Phi}_0$ is of the form

$$\Phi_0 = \mathrm{Re}\left[a_0 \log z + b_0 + \sum_{n=1}^{\infty} a_n z^{-n}\right], \tag{16}$$

where

$$z = x + iy = re^{i\theta}$$

and $\tilde{a} = -A_0$, $\tilde{b}_0 = -(\log \tfrac{1}{2}|\omega| + \gamma) A_0$, $\tilde{a}_n = \tfrac{1}{2}e^{-i\beta n}(n-1)!\,(2/|\omega|)^n A_n$. (16*a*)

Hence the function

$$\phi_0 = \Phi_0 + x\sin\epsilon \tag{17}$$

provides an approximation to ϕ in the neighbourhood of the cavity-plate system. Obviously ϕ_0 is a harmonic function of r and θ. Potential theory can therefore be used to determine the constants a_n, occurring in (16), from the boundary conditions. The order of magnitude of the a_n's is determined in terms of the slenderness parameter δ of the cavity-plate system as follows. Since, by assumption, when the tangent to the boundary of the cavity-plate system has no discontinuities, $dv/ds = O(\delta)$, it follows from (8) that $\partial\phi_0/\partial r = O(\delta)$ near the cavity-plate system. Also, using the condition of the continuity of the flow near the boundary, $(1/r)(\partial\phi_0/\partial\theta) = O(\delta)$ near the cavity-plate system. By making use of these order relations, one finds from the above solution (16) that

$$|a_n| = O(\delta^{n+2}) \quad (n = 0, 1, 2, \ldots). \tag{18}$$

Therefore, if the entire boundary is inside $r = R =$ constant for all s, then the series expression of ϕ_0 converges for $r > R$ and may be continued analytically

into $r < R$ if it does not converge there. From the above order of magnitude of a_n it follows immediately that near the body

$$\left.\begin{aligned} &\frac{\partial\phi_0}{\partial s}, \quad \frac{\partial^2\phi_0}{\partial s^2} = O(\delta^2 \log\delta), \\ &\frac{\partial\phi_0}{\partial x}, \quad \frac{\partial\phi_0}{\partial y}, \quad \frac{\partial^2\phi_0}{\partial x\,\partial s}, \quad \frac{\partial^2\phi_0}{\partial y\,\partial s} = O(\delta), \\ &\frac{\partial^2\phi_0}{\partial x^2}, \quad \frac{\partial^2\phi_0}{\partial y^2} = O(1). \end{aligned}\right\} \tag{19}$$

In order to determine the accuracy of this series solution, let

$$\phi = \phi_0 + \phi_1. \tag{20a}$$

Equation (5) then becomes

$$4\frac{\partial^2\phi_0}{\partial z\,\partial\bar{z}} + \left[4\frac{\partial^2\phi_1}{\partial z\,\partial\bar{z}} + \frac{\partial^2\phi_1}{\partial s^2} + \frac{\partial^2\phi_0}{\partial s^2}\right] = 0, \tag{20b}$$

where $\bar{z}$ is the complex conjugate of z. If it is now assumed that ϕ_1 and its derivatives are much smaller than those of ϕ_0 near the body, then

$$\partial^2\phi_0/\partial z\,\partial\bar{z} = 0, \tag{21a}$$

which is accurate up to $O(\delta^2 \log\delta)$. Hence, from (20*b*) and (21*a*),

$$4\frac{\partial^2\phi_1}{\partial z\,\partial\bar{z}} + \frac{\partial^2\phi_1}{\partial s^2} = -\frac{\partial^2\phi_0}{\partial s^2} = f(z,\bar{z},s) \quad \text{say}, \tag{21b}$$

the function $f(z,\bar{z},s)$ being obviously of the order $O(\delta^2 \log\delta)$. This gives

$$\phi_1 = \frac{1}{4}\int^z\int^{\bar{z}} f(z,\bar{z},s)\,d\bar{z}\,dz - \frac{1}{16}\frac{\partial^2}{\partial s^2}\int^z\int^z\int^{\bar{z}}\int^{\bar{z}} f(z,\bar{z},s)\,(d\bar{z})^2\,(dz)^2 + \ldots.$$

From this result and (19), it follows immediately that, near the body,

$$\left.\begin{aligned} &\phi_1, \quad \frac{\partial\phi_1}{\partial s}, \quad \frac{\partial^2\phi_1}{\partial s^2}, \quad \ldots = O(\delta^4 \log\delta), \\ &\frac{\partial\phi_1}{\partial x}, \quad \frac{\partial\phi_1}{\partial y}, \quad \frac{\partial^2\phi_1}{\partial x\,\partial s}, \quad \frac{\partial^2\phi_1}{\partial y\,\partial s} = O(\delta^3 \log\delta), \\ &\frac{\partial^2\phi_1}{\partial x^2}, \quad \frac{\partial^2\phi_1}{\partial y^2} = O(\delta^2 \log\delta). \end{aligned}\right\} \tag{22}$$

Therefore, combining (19) and (22), it is seen that ϕ_0 gives the velocity near the body accurately up to terms of order $\delta^2 \log\delta$, hence ϕ_1 may be neglected in the first approximation. It is to be noted that the above order-of-magnitude estimation, (19) and (22), is valid uniformly over the body surface provided that there is no discontinuity in the slope of the boundary. Over the cavity boundary in particular, however, the estimation can be made more specific, using the pressure condition (9) or (9*a*).

The pressure field, derived from (6), is

$$\frac{p - p_\infty}{\frac{1}{2}\rho V^2} = 1 - [(\cos\epsilon + \phi_s)^2 + \phi_x^2 + \phi_y^2].$$

Hence, using (19) and (22), this becomes, near the body,

$$\frac{p-p_\infty}{\frac{1}{2}\rho V^2} = \epsilon^2 - \left[2\frac{\partial\phi_0}{\partial s} + \left(\frac{\partial\phi_0}{\partial x}\right)^2 + \left(\frac{\partial\phi_0}{\partial y}\right)^2\right] \tag{23}$$

which is accurate up to terms of order $\delta^2\log\delta$. In particular, over the cavity boundary, where $p = p_c$, (23) becomes

$$2\frac{\partial\phi_0}{\partial s} + \left(\frac{\partial\phi_0}{\partial x}\right)^2 + \left(\frac{\partial\phi_0}{\partial y}\right)^2 = \sigma + \epsilon^2. \tag{24}$$

Since, as may be noted from (19), $\phi_{0s} \approx O(\delta^2\log\delta)$ and $(\phi_{0x})^2 + (\phi_{0y})^2 \approx O(\delta^2)$ for the flow past a slender body, the above result implies that the assumption of slenderness can be valid only if σ is $O(\delta^2\log\delta)$ or of smaller magnitude.

When the configuration of the body is given, the coefficients a_0 and b_0 of (16) can be obtained as follows. From the analyticity of the solution (16) it follows that conditions (7) and (8) may be applied on the contour C which is the circle $r = r_1$, large enough to include the largest cross-section of the body. Thus

$$\int_C \frac{\partial\phi_0}{\partial n}\,d\tau = \int_0^{2\pi}\left(\frac{\partial\phi_0}{\partial r}\right)_{r=r_1} r_1\,d\theta = \int_0^{2\pi}\left(\frac{\partial\Phi_0}{\partial r}\right)_{r=r_1} r_1\,d\theta = 2\pi a_0.$$

Hence, by conditions (7) and (8), and the analyticity of the solution (16)

$$a_0 = \frac{1}{2\pi}\int_{C_B}\frac{dv}{ds}\,d\tau = \frac{1}{2\pi}\frac{d}{ds}\int_{C_B} v\,d\tau = \frac{1}{2\pi}S'(s), \tag{25}$$

where C_B is the contour of the cavity-plate section and

$$S(s) = \int_{C_B} v\,d\tau \tag{25a}$$

is the cross-sectional area. Furthermore, from (16a),

$$\tilde{b}_0 = (\log\tfrac{1}{2}|\omega| + \gamma)\,\tilde{a}_0 = (\log\tfrac{1}{2}|\omega| + \gamma)\,(2\pi)^{-1} i\omega\,\tilde{S}(\omega),$$

the inverse transform of which, with the assumption that $S'(s)$ vanishes at the two ends of the cavity, is found to be

$$b_0 = \frac{S'(s)}{2\pi}\log\frac{1}{2} - \frac{1}{4\pi}\left\{\int_{-\infty}^{s} S''(\sigma)\log(s-\sigma)\,d\sigma - \int_s^{\infty} S''(\sigma)\log(\sigma-s)\,d\sigma\right\}. \tag{26}$$

The coefficient a_0 gives the strength of the source distribution to represent the longitudinal flow in the axial direction. It is noted that like $a_0(s)$, b_0 is a function of s only. The determination of the coefficients of the higher-order terms requires the solution of the cross-flow.

It should be pointed out that, in the absence of cavitation, the problem of solving ϕ_0 is clearly a two-dimensional one, since the differential equation governing ϕ_0, (21a), is two-dimensional, and no s-derivatives of ϕ_0 appear in the boundary condition of the problem. In this case the variable s enters the problem merely as a parameter through the boundary condition. Only when the pressure is calculated does the s-derivative of ϕ_0 arise. However, when a cavity is present, the pressure condition (24) contains the term $(\partial\phi_0/\partial s)$. Consequently the problem

of solving the cross-flow is no longer two-dimensional even though the differential equation (21 *a*) remains unchanged.

In the subsequent sections the potential ϕ_0 will be solved with appropriate simplifying assumptions. Since only the first-order theory is considered, ϕ_1 will be henceforth neglected and the subscript of ϕ_0 can therefore be omitted.

3. The solution in the cross-flow plane

It will be shown in this section how a solution for the velocity potential ϕ may be obtained from the cross-flow. As discussed in the previous section this solution will be accurate to terms of order $O(\delta^2 \log \delta)$ near the body. The flow near the body may be resolved into two components, representing the axial and cross-flows. This is shown by writing equations (16) and (17) in the form

$$\phi = a_0(s) \log r + b_0(s) + \phi_c = \phi_a + \phi_c, \tag{27}$$

where a_0 and b_0 are given by (25) and (26), respectively. The axial flow, with potential ϕ_a, is the source-like component of the total flow and represents the effect of variation of the cross-sectional area of the cavity. The cross-flow, with potential ϕ_c, is the doublet-like component of the total flow and represents the flow in planes perpendicular to the axis along the centroids of the cavity cross-sections. It may be seen that

$$\phi_c \sim \epsilon x \tag{28}$$

at large distances from the cavity-plate system.

It is assumed that, with the choice of the free-stream velocity of the cross-flow as indicated in § 2, the kinematic boundary condition (7), (8) is satisfied approximately by the axial component of the flow. This approximation will be good at distances near the cavity-plate system by choice of the constants a_0 and b_0; this amounts to satisfying (7) and (8) averaged over the bounding surface. Thus this method will be expected to give a well-balanced approximation of the flow quantities over the entire boundary of the cavity-plate system. With this assumption then, the kinematic boundary condition for the cross-flow potential ϕ_c on the cavity-plate surface is

$$\frac{\partial \phi_c}{\partial n} = 0. \tag{29}$$

The primary effect of the axial flow is its contribution to the local pressure field, the value of which is essential in the determination of the location of the cavity boundary. Upon substitution of (27) into (23), the pressure near the cavity-plate system may be written

$$\frac{p - p_c}{\frac{1}{2}\rho V^2} = \sigma + \epsilon^2 - \left[2\frac{\partial \phi_a}{\partial s} + \left(\frac{\partial \phi_a}{\partial x}\right)^2 + \left(\frac{\partial \phi_a}{\partial y}\right)^2\right] - \left[2\frac{\partial \phi_c}{\partial s} + \left(\frac{\partial \phi_c}{\partial x}\right)^2 + \left(\frac{\partial \phi_c}{\partial y}\right)^2\right] - 2\left(\frac{\partial \phi_a}{\partial x}\frac{\partial \phi_c}{\partial x} + \frac{\partial \phi_a}{\partial y}\frac{\partial \phi_c}{\partial y}\right). \tag{30}$$

It may be pointed out that for the case of non-cavitating flow past a body of revolution, the pressure differences $[p(r, \theta) - p(r, -\theta)]$ and $[p(r, \theta) - p(r, \pi - \theta)]$ are seen to be independent of ϕ_a. This is due to the fact that ϕ_a, given by (27), is

dependent only on r in the cross-plane, and in such a way that in (30) the cross-product terms,

$$\frac{\partial\phi_a}{\partial x}\frac{\partial\phi_c}{\partial x}+\frac{\partial\phi_a}{\partial y}\frac{\partial\phi_c}{\partial y}=\frac{a_0(s)}{r}\left[\cos\theta\frac{\partial\phi_c}{\partial x}+\sin\theta\frac{\partial\phi_c}{\partial y}\right]=\frac{a_0(s)}{r}\frac{\partial\phi_c}{\partial r}, \tag{31}$$

vanish on the body-surface of revolution because of the normal flow condition (29) on the body. Consequently the source type flow ϕ_a makes no contribution to the lateral forces and may therefore be neglected in such calculations. The same argument no longer holds true for the case of cavity flow since the location of the cavity boundary will depend on the pressure field due to ϕ_a; an approximate method is introduced here to determine this effect as follows. For the purpose of determining ϕ_a alone, the undetermined cavity shape may be assumed to approximate to a body of revolution, and the effect of ϕ_a on the pressure field may then be evaluated at an equivalent radial distance

$$r=R=[S(s)/\pi]^{\frac{1}{2}}. \tag{32}$$

Under these assumptions, the cross-product terms of ϕ_a and ϕ_c in (30) reduce to zero in virtue of (31) and condition (29), and the remaining terms in (30) involving ϕ_a are determined as

$$\left[2\frac{\partial\phi_a}{\partial s}+\left(\frac{\partial\phi_a}{\partial x}\right)^2+\left(\frac{\partial\phi_a}{\partial y}\right)^2\right]_{r=R}=\frac{1}{2\pi}S''(s)\log\frac{S}{4\pi}+\frac{1}{4\pi}\frac{1}{S}S'(s)^2$$
$$-\frac{1}{2\pi}\left[\int_{-\infty}^{s}S'''(\sigma)\log(s-\sigma)\,d\sigma-\int_{s}^{\infty}S'''(\sigma)\log(\sigma-s)\,d\sigma\right].$$

Thus (30) becomes

$$\frac{p-p_c}{\frac{1}{2}\rho V^2}=\eta^2-\left[2\frac{\partial\phi_c}{\partial s}+\left(\frac{\partial\phi_c}{\partial x}\right)^2+\left(\frac{\partial\phi_c}{\partial y}\right)^2\right], \tag{33a}$$

where

$$\eta^2=\sigma+\epsilon^2-\frac{1}{2\pi}S''(s)\log\frac{S}{4\pi}-\frac{1}{4\pi}\frac{S'^2}{S}-\frac{1}{2\pi}\int_{-\infty}^{\infty}\operatorname{sgn}(\sigma-s)\log|\sigma-s|S'''(\sigma)\,d\sigma. \tag{33b}$$

Over the cavity boundary, $p=p_c$, and hence

$$\left(\frac{\partial\phi_c}{\partial x}\right)^2+\left(\frac{\partial\phi_c}{\partial y}\right)^2=\eta^2-2\frac{\partial\phi_c}{\partial s}. \tag{34}$$

This condition now replaces (24).

For simplicity, in the remaining part of the analysis, only the flat-plate hydrofoil will be considered; the generalization to the pointed hydrofoil having a small camber can be obtained without too much difficulty. The cross-flow is then the flow past a flat plate of semi-width $b(s)$ placed normal to a stream of velocity $V\epsilon$ (see (28)). The flow separates behind the flat plate to form a cavity, on the surface of which the condition (34) is to be satisfied. In order to evaluate the flow past a cavity of finite size, the Riabouchinsky model for the flow is adopted. In this model, an image plate is introduced downstream of the real plate, the pair of plates being connected by the cavity surface (see figure 2). Introduction of the image plate serves to admit the cavitation number as a free parameter. The

Riabouchinsky model for the flow provides a good approximation of the actual flow quantities near the real plate and gives a good estimate of the drag force on the plate at moderate cavitation numbers. It should not be expected, however, that the flow near the image plate can well resemble the actual flow there.

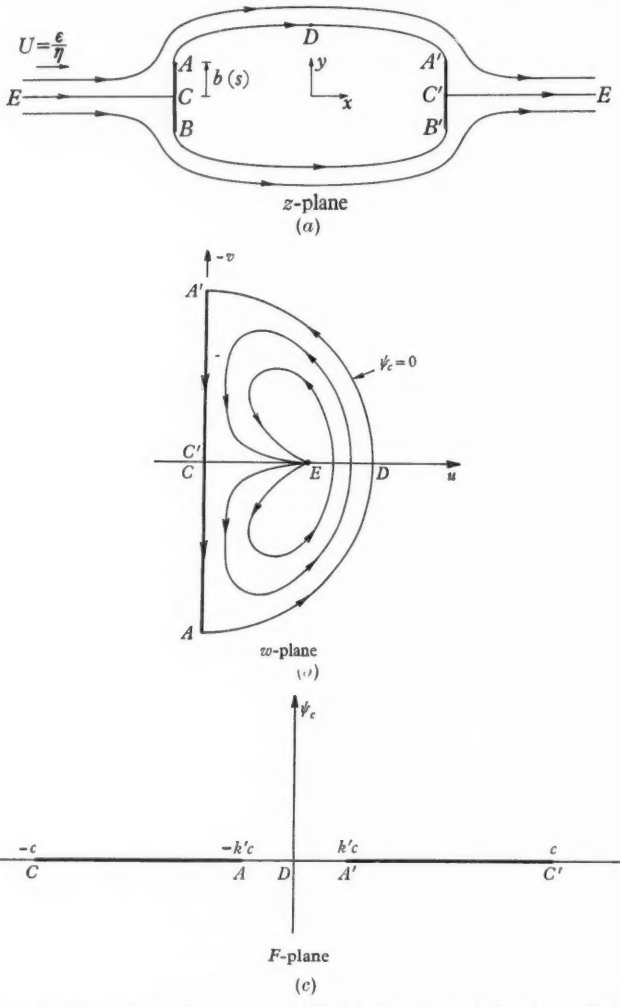

FIGURE 2. The Raibouchinsky model and its hodograph for the cross-flow.

For the cross-flow it is convenient to introduce the complex potential

$$F(z) = \phi_c(x, y) + i\psi_c(x, y), \tag{35}$$

which is an analytic function of $z = x + iy$. Here ψ_c is the stream function of the cross-flow only. In terms of ψ_c, the kinematic condition (29) reduces to

$$\psi_c = 0 \quad \text{on the plate and its image plate and on the cavity.} \tag{36}$$

In order that the cross-flow be reduced to the Riabouchinsky problem and that condition (34) be satisfied on the cavity with a good over-all accuracy, it is assumed that the term $\partial\phi_c/\partial s$ in (34) may be replaced by its average over the cavity in the cross-flow plane. It will be shown later (see equation (55)) that $\partial\phi_c/\partial s$ is an odd function of the arc length τ measured along the cavity boundary from the midsection ($x = 0$) in the cross-flow plane, and therefore the average of $\partial\phi_c/\partial s$ over the cavity vanishes, or

$$\overline{\frac{\partial\phi_c}{\partial s}} = \int_{\text{cavity}} \frac{\partial\phi_c}{\partial s}\, d\tau \Big/ \int_{\text{cavity}} d\tau = 0. \tag{37}$$

Equation (34) then becomes

$$\left(\frac{\partial\phi_c}{\partial x}\right)^2 + \left(\frac{\partial\phi_c}{\partial y}\right)^2 = \eta^2 \tag{38}$$

on the cavity, where η^2 is given by (33*b*). The free-stream velocity of the cross-flow can be derived from (28) as

$$\frac{\partial\phi_c}{\partial x} = \epsilon, \quad \frac{\partial\phi_c}{\partial y} = 0 \quad \text{at infinity.} \tag{39}$$

It is convenient to introduce the normalized cross-flow velocity components

$$u = \frac{1}{\eta}\frac{\partial\phi_c}{\partial x}, \quad v = \frac{1}{\eta}\frac{\partial\phi_c}{\partial y}, \tag{40}$$

and the complex velocity

$$w(z) = u - iv = \frac{1}{\eta}\frac{dF}{dz}, \tag{41}$$

which is also an analytic function of z. In the w-plane, or the hodograph plane of the cross-flow, the boundary conditions take the form

$$u = \operatorname{Re} w = 0 \quad \text{on the plate,} \tag{42a}$$

$$w = \epsilon/\eta = U \quad \text{at} \quad z = \infty, \tag{42b}$$

and

$$|w| = (u^2+v^2)^{\frac{1}{2}} = 1 \quad \text{on the cavity boundary.} \tag{42c}$$

Furthermore, condition (36) still holds. The sketch of a few streamlines, ψ_c = constant, are shown in figure 2. It is to be noted that with the assumption that $\partial\phi_c/\partial s$ be replaced by its average value over the cavity, which is zero, the three-dimensional effect on the cross-flow is thereby eliminated and the problem of the cross-flow then reduces exactly to the Riabouchinsky flow over a flat plate, the solution of which is already known (e.g. Birkhoff & Zarantonello 1957). In order to facilitate the subsequent analysis, the result is reproduced briefly as follows.

The flow in the hodograph plane and the potential plane are shown in figure 2. The upper half F-plane is mapped on to the hodograph plane by the transformation

$$\frac{1}{w} = \frac{kF}{k'(F^2-c^2)^{\frac{1}{2}}} + \frac{1}{k'}\left(\frac{F^2-k'^2c^2}{F^2-c^2}\right)^{\frac{1}{2}}, \tag{43}$$

where

$$c = -F(z = z_c) = F(z = z_{c'}),$$

which is to be determined, and k, k' are defined by

$$k = \frac{1-U^2}{1+U^2}, \quad k' = (1-k^2)^{\frac{1}{2}} = \frac{2U}{1+U^2}, \quad U = \frac{\epsilon}{\eta}. \tag{44}$$

At the point A, $w = -i$, so $\quad F_A = \phi_{cA} = -k'c,$ (45a)

and at the point D, $w = 1$, so $\quad F_D = \phi_{cD} = 0.$ (45b)

The physical plane, z, can be obtained by integration as

$$z - z_c = \frac{1}{\eta}\int_{-c}^{F} \frac{1}{w}\, dF = \frac{1}{\eta k'}\left[k(F^2-c^2)^{\frac{1}{2}} + \int_{-c}^{F}\left(\frac{F^2-k'^2c^2}{F^2-c^2}\right)^{\frac{1}{2}} dF\right]. \tag{46}$$

Hence on the plate AC, where $-c \leqslant \phi_c \leqslant -k'c$ and $\psi_c = 0$,

$$z - z_c = \frac{ik}{\eta k'}\left\{(c^2-\phi_c^2)^{\frac{1}{2}} + ckB\left(k, \sin^{-1}\left[\frac{(c^2-\phi_c^2)^{\frac{1}{2}}}{ck}\right]\right)\right\}, \tag{47}$$

where the function $B(k,\theta)$ represents the elliptic integral (see Jahnke & Emde 1945),

$$B(k,\theta) = \int_0^{\theta} \frac{\cos^2 x\, dx}{(1-k^2\sin^2 x)^{\frac{1}{2}}} \quad \text{and} \quad B(k) = B(k, \tfrac{1}{2}\pi). \tag{48}$$

On the streamline AD, where $-k'c \leqslant \phi_c \leqslant 0$ and $\psi_c = 0$, the streamline has the parametric representation

$$z = x(\phi_c) + iy(\phi_c), \tag{49a}$$

where

$$x - x_c = \frac{ck'}{\eta}\left\{B(k') - B\left(k', \sin^{-1}\left[-\frac{\phi_c}{ck'}\right]\right)\right\} \tag{49b}$$

and

$$y = \frac{k}{k'\eta}[(c^2-\phi_c^2)^{\frac{1}{2}} + ckB(k)]. \tag{49c}$$

Therefore at the point A, $\phi_c = -k'c$, $z - z_c = ib(s)$, and hence, from (47) or (49),

$$b(s) = \frac{ck^2}{\eta k'}[1 + B(k)], \tag{50}$$

which provides one relation between c, η, and k in terms of the half-width of the plate, $b(s)$. Furthermore, at the point D, $x_D = 0$ and $\phi_{cD} = 0$, hence

$$-x_c = (ck'/\eta)\, B(k'). \tag{51}$$

Since $z = 0$ is the centroid of the cavity volume, it follows that

$$\alpha - \epsilon = \frac{-x_c}{s} = \frac{b(s)}{s} G(k), \quad G(k) = \frac{k'^2 B(k')}{k^2[1+B(k)]}, \tag{52}$$

where use has been made of (50). This gives one relation between ϵ and k. The cross-sectional area of the cavity is given by the integral

$$S(s) = 4\int_{x_A}^{x_D} y\, dx = 4\int_{-k'c}^{0} y(\phi_c)\frac{dx(\phi_c)}{d\phi_c}\, d\phi_c,$$

where x and y are given by (49). Carrying out the integration, one obtains

$$S(s) = \frac{4c^2k}{\eta^2 k'^2}\left[\int_0^{k'} (k'^2-t^2)^{\frac{1}{2}}\, dt + kB(k)\int_0^{k'}\left(\frac{k'^2-t^2}{1-t^2}\right)^{\frac{1}{2}} dt\right] = \frac{c^2k}{\eta^2}[\pi + 4kB(k)\, B(k')],$$

which becomes, after using (50),

$$S(s) = b^2(s)\,H(k), \quad H(k) = \frac{k'^2[\pi + 4kB(k)\,B(k')]}{k^3[1+B(k)]^2}. \tag{53}$$

It will now be shown that $\partial\phi_c/\partial s$ on the cavity boundary is an odd function of ϕ_c. In fact, at a fixed point on the cavity, the variation of ϕ_c with respect to s can be obtained from

$$\left[\frac{\partial}{\partial c} + \frac{\partial\phi_c}{\partial c}\frac{\partial}{\partial\phi_c}\right]\begin{bmatrix} y(\phi_c) \\ x(\phi_c) \end{bmatrix} = 0,$$

where x and y are given by (49). Since y/x is seen to depend on ϕ_c and c only in the combined form ϕ_c/c, it follows that

$$\frac{\partial\phi_c}{\partial c} = \frac{\phi_c}{c} \quad \text{on} \quad \psi_c = 0, \quad |\phi_c| < k'c. \tag{54}$$

Hence on the cavity

$$\frac{\partial\phi_c}{\partial s} = \frac{\partial\phi_c}{\partial c}\frac{dc}{db}\frac{db}{ds} = \frac{\phi_c}{c}\frac{dc}{db}\frac{db}{ds}, \tag{55}$$

which is an odd function of ϕ_c. This implies that the average of $\partial\phi_c/\partial s$ over the cavity boundary vanishes, as stated in (37).

For given plan form $b(s)$, attack angle α, and cavitation number σ, the above solution contains four unknowns, namely, η, ϵ, k and S, which are related to each other by the four equations (33*b*), (44), (52) and (53). Strictly speaking, the determination of these quantities further requires the solution of the flow field over the cavity downstream of the plate since the definition of η, (33*b*), contains $S(s)$ over the entire range of the cavity. The problem of the trailing cavity flow is very complicated, since either it involves the direct treatment of the turbulent wake to the rear of the cavity or at least it would require an appropriate potential flow model to account for the real fluid effect in the wake. Even with the trailing cavity assumed to take a well-defined (but unknown) profile, the problem still involves the solution of a complicated integral equation since in (33*b*) the unknown $S(s)$ appears in the integral over the entire cavity region. It can be seen, however, that the contribution of these two integrals is, at most, of order δ^2 as compared with the order of magnitude $O(\delta^2\log\delta)$ of the remaining terms in (33*b*). In particular, the contribution of these integrals would be negligible in the region over the plate if $S'''(s)$ is small in that region, as would be expected in the case of a triangular plate, since the flow near the plate would be approximately conical and hence $S(s)$ would be proportional to s^2 (this feature will be pointed out in the following example). Furthermore, it will be assumed that the cavity is sufficiently long (which can be realized with sufficiently small σ) so that the region in which $S'''(s)$ may not be small will be far enough downstream to cause its effect on the flow field near the plate to be negligible. Therefore, in a first-order approximation for calculating the aforementioned quantities, or at least in the first-order computation of a more accurate iteration procedure, these integrals may be neglected. For this reason the flow field downstream of the plate will not be further considered here. With this simplification, it was found that k, η, ϵ and S can be obtained as functions of s in a straightforward manner.

4. Calculation of the normal force

The force acting perpendicular to the cavitated hydrofoil considered in the previous sections can be calculated by integration of the normal pressure over the plate. On the plate, $\partial\phi_c/\partial x = 0$ and $\partial\phi_c/\partial y = \eta v$ (see (40) and (42)). Hence the difference between the pressure at a point on the wetted side of the plate and the cavity pressure can be deduced from (33) and may be written as

$$\frac{p-p_c}{\frac{1}{2}\rho V^2} = \eta^2(1-v^2) - 2\left[\frac{\partial\phi_c}{\partial s} - \left(\frac{\partial\phi_c}{\partial s}\right)_A\right], \tag{56}$$

where $(\partial\phi_c/\partial s)_A$ is the value of $(\partial\phi_c/\partial s)$ at the point A, the side edge of the plate. The reason for introducing this constant term may be explained as follows. In the determination of the cross-flow, the variation of $(\partial\phi_c/\partial s)$ over the cavity is approximated by the average of $(\partial\phi_c/\partial s)$ on the cavity, as given by (37), so that a good estimate of the cavity shape may be obtained by a relatively simple analysis. When the pressure p on the plate is now calculated, the variation of $(\partial\phi_c/\partial s)$ on the plate is taken into account and the constant $(\partial\phi_c/\partial s)_A$ is introduced to make p continuous at the edge of the plate, that is $p = p_c$ at the point A, where $v = 1$. In other words, $(\partial\phi_c/\partial s)$ is approximated by a piecewise continuous function, its value on the cavity being replaced by its average in that region, for the purpose of evaluating the cross-flow. After ϕ_c is so determined, the variation of $\partial\phi_c/\partial s$ from its value at the point A, namely $[\partial\phi_c/\partial s - (\partial\phi_c/\partial s)_A]$, is restored in the expression (56) for the pressure on the plate. Furthermore, as was already explained in the derivation of (33), the cross-product terms of ϕ_a and ϕ_c in (30) vanish when evaluated at the equivalent radial distance $r = R(s)$, given by (32). The deviation of the plate-form from the equivalent circular cross-section is generally very small; consequently this effect will remain neglected in the present analysis.

The normal force element dN experienced by an element of the plate ds at station s will be given by the spanwise integration of the pressure (56). That is

$$dN = dN_1 + dN_2, \tag{57}$$

where

$$dN_1 = \rho V^2\eta^2 ds \int_0^{b(s)} (1-v^2)\,dy, \tag{57a}$$

$$dN_2 = -2\rho V^2 ds \frac{\partial}{\partial s}\int_0^{b(s)} [\phi_c - \phi_{cA}]\,dy, \tag{57b}$$

The integral in (57a) is readily evaluated by using the solution (43),

$$\int_0^{b(s)} (1-v^2)\,dy = \frac{1}{\eta}\int_{-c}^{-k'c}\left(\frac{1}{v}-v\right)d\phi_c = \frac{2c}{\eta k'}\int_{k'}^{1}\left(\frac{t^2-k'^2}{1-t^2}\right)^{\frac{1}{2}}dt = \frac{2ck^2}{\eta k'}B(k),$$

where $B(k)$ is defined by (48). Hence, using (50), it follows that

$$dN_1 = 2\rho V^2\eta^2 \frac{B(k)}{1+B(k)}\,b(s)\,ds. \tag{58}$$

By making use of (43), the integral in (57*b*) can be evaluated as

$$\int_0^b [\phi_c - \phi_{cA}]\,dy = \frac{1}{\eta}\int_{-c}^{-k'c} (\phi_c + k'c)\frac{1}{v}\,d\phi_c = \frac{c^2}{\eta k'}\int_{k'}^{1} (-t+k')\left[\frac{kt}{(1-t^2)^{\frac{1}{2}}} + \left(\frac{t^2-k'^2}{1-t^2}\right)^{\frac{1}{2}}\right] dt$$

$$= -\frac{c^2 k}{2\eta k'}[\cos^{-1} k' - kk' + \tfrac{1}{2}\pi k - 2k'kB(k)].$$

Therefore, using (50), we obtain

$$dN_2 = \rho V^2 \frac{\partial}{\partial s}\left\{\frac{\eta k'}{k^3}\frac{\cos^{-1} k' - kk' + \frac{1}{2}\pi k - 2k'kB(k)}{[1+B(k)]^2} b^2(s)\right\} ds. \tag{59}$$

Finally, the total normal force N experienced by the plate is obtained by integrating $dN(s)$ along the chord from $s = 0$ to the trailing edge $s = 1$. This will be carried out for the following example.

5. Example—triangular plate

Consider the special case of a triangular plate of small vertex angle and length unity so that

$$b = s\tan\tfrac{1}{2}\gamma \quad \text{for} \quad 0 \leqslant s \leqslant 1. \tag{60}$$

The plate area is given by $A = \tan\frac{1}{2}\gamma$, and the aspect-ratio of this hydrofoil is then $4b^2(1)/A = 4\tan\frac{1}{2}\gamma$. Substituting (60) in (52), we obtain

$$\alpha - \epsilon = (\tan\tfrac{1}{2}\gamma)\,G(k). \tag{61}$$

Since ϵ is assumed to be constant, it follows that k is independent of s. From (53) and (60),

$$S(s) = s^2(\tan^2\tfrac{1}{2}\gamma)\,H(k), \tag{62}$$

which now indicates that the cavity cross-sectional area in the region over the plate is proportional to s^2, implying that the local flow is essentially conical. Furthermore, under the present assumption that the integrals containing S''' in the expression for η may be neglected, (33*b*) reduces to

$$\eta^2 = \sigma + \epsilon^2 - \frac{1}{2\pi}S''(s)\log\frac{S}{4\pi} - \frac{1}{4\pi}\frac{S'^2}{S}.$$

Upon substitution of (62) into the above equation, it is noted that the only term depending on s is $(S''/2\pi)\log s^2$, which is of order $O(\delta^2)$, while the most important terms in that equation are of order $O(\delta^2\log\delta)$. For the present first-order theory we may approximate $\log s$ by its average over the plate, that is, by replacing $\log s$ by

$$\int_0^1 s\log s\,ds \Big/ \int_0^1 s\,ds = -\tfrac{1}{2}.$$

With this approximation, we obtain

$$\eta^2 = \sigma + \epsilon^2 + \frac{1}{\pi}\tan^2\tfrac{1}{2}\gamma\,H(k)\log[4\pi\cot^2\tfrac{1}{2}\gamma/H(k)]. \tag{63}$$

From (61), (63), and (44), one readily derives the result

$$\alpha\cot\tfrac{1}{2}\gamma = G(k) + \left(\frac{1-k}{2k}\right)^{\frac{1}{2}}\left\{\sigma\cot^2\tfrac{1}{2}\gamma + \frac{1}{\pi}H(k)\log[4\pi\cot^2\tfrac{1}{2}\gamma/H(k)]\right\}^{\frac{1}{2}}, \tag{64}$$

where $G(k)$ and $H(k)$ are defined in (52) and (53). This equation, which is easily solved by a graphical method, determines k for given γ, σ and $\varkappa$

In consequence of the above result, (58) is readily integrated to yield

$$N_1 = \rho V^2 \eta^2 (\tan \tfrac{1}{2}\gamma) \frac{B(k)}{1+B(k)}. \tag{65}$$

Integration of (59) gives

$$N_2 = \rho V^2 (\tan^2 \tfrac{1}{2}\gamma) \frac{\eta k'}{k^3} \frac{\cos^{-1} k' + \frac{1}{2}\pi k - k k'[1+2B(k)]}{[1+B(k)]^2}. \tag{66}$$

The total normal force coefficient may be defined as

$$C_N = N/(\tfrac{1}{2}\rho V^2 A) = (N_1 + N_2)/(\tfrac{1}{2}\rho V^2 A). \tag{67}$$

Since there is no singular leading edge force in this supercavitating flow, the resultant force must act normal to the delta flat-plate. It then follows that the lift coefficient and the drag coefficient of the plate in the cavity flow are

$$C_L = C_N \cos\alpha, \quad C_D = C_N \sin\alpha. \tag{68}$$

The drag due to the skin friction over the wetted surface of the plate is generally negligible compared with the cavity-flow drag.

A limiting case of interest is for vanishingly small α, provided the fully-developed cavity can be sustained. As $\alpha \to 0$, one finds from (64) that $k \to 1$, $k' \to 0$. Hence, from (61) and (63), $\epsilon \to 0$, and $\eta^2 \to \sigma$. The corresponding C_L is given by

$$C_L \to C_N \to \sigma \quad \text{as} \quad \alpha \to 0, \tag{69}$$

this limit of C_L being independent of γ. This result may be interpreted as implying that the hydrodynamic pressure on the wetted side of the plate is negligible compared with the cavity pressure at vanishingly small α.

Another special limiting case is when $\gamma \to 0$ and $\alpha^2 \ll \sigma$. In this case we also have $k \to 1$. The corresponding C_L is given by

$$C_L \to \sigma + \alpha^2, \tag{70}$$

which indicates the behaviour of C_L at small α and moderate σ.

For the general case, the value of C_N is calculated from the above equations and is plotted versus σ with $\alpha = 5°$, $10°$, $15°$, $20°$, $25°$ for each of the cases $\gamma = 5°$, $10°$, $15°$ in figures 3–5 and versus α for several small values of σ in figures 6–8. In the numerical calculation it is found that the major contribution to the total force comes from N_1.

When this theoretical study was completed, the authors were given some preliminary experimental data by Mr Taras Kiceniuk of the Hydrodynamics Laboratory, California Institute of Technology. These data are compared with the theory in figure 5. Although the data available at present are not extensive enough to make an overall comparison, figure 5 indicates that the present theory is in good agreement with experiment. The details of the experimental arrangement and the final results will be reported later elsewhere.

FIGURE 3. Dependence of the normal-force coefficient on the cavitation number σ, for a cavitating triangular plate of vertex angle, $\gamma = 5°$.

FIGURE 4. Dependence of the normal-force coefficient on the cavitation number σ, $\gamma = 10°$.

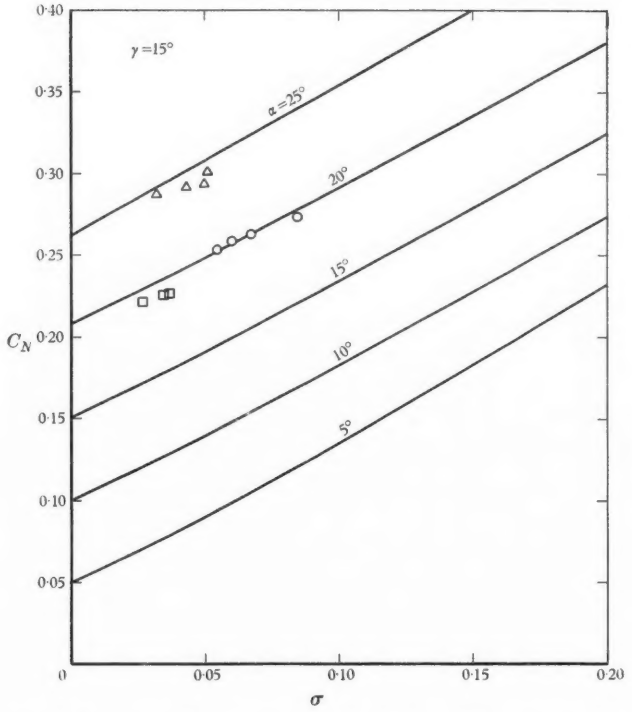

FIGURE 5. Theoretical and experimental normal-force coefficient curves for a cavitating triangular plate of vertex angle, $\gamma = 15°$. Experimental data: □, $\alpha = 20°$; ○, $\alpha = 21°$; △, $\alpha = 25°$.

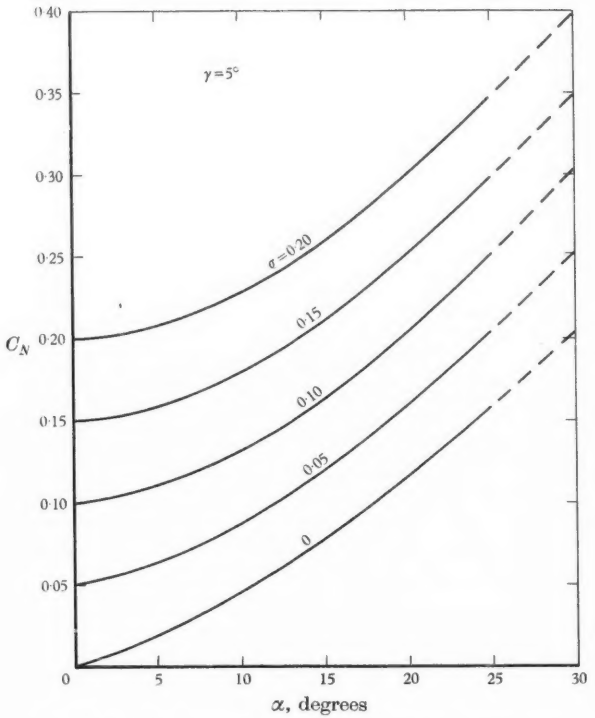

FIGURE 6. Variation of the normal-force coefficient with the angle of attack, $\gamma = 5°$.

Experimental data: □, $\alpha = 20°$; ○, $\alpha = 21°$; △, $\alpha = 25°$.

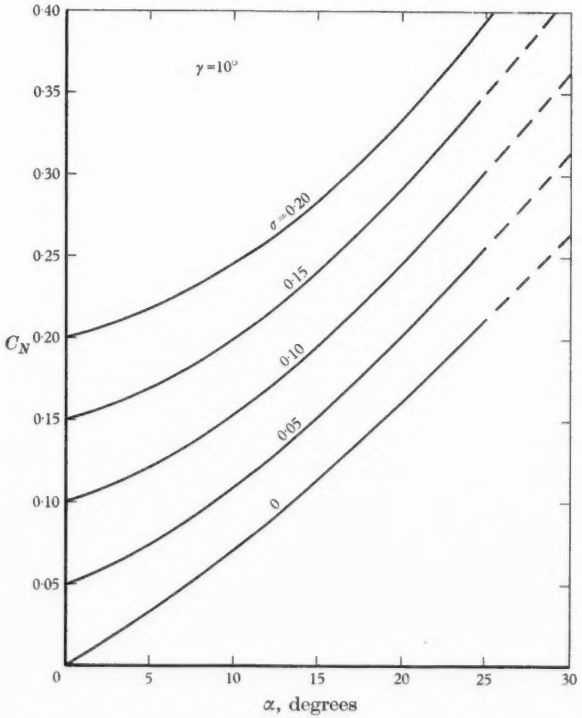

FIGURE 7. Variation of the normal-force coefficient with the angle of attack, $\gamma = 10°$.

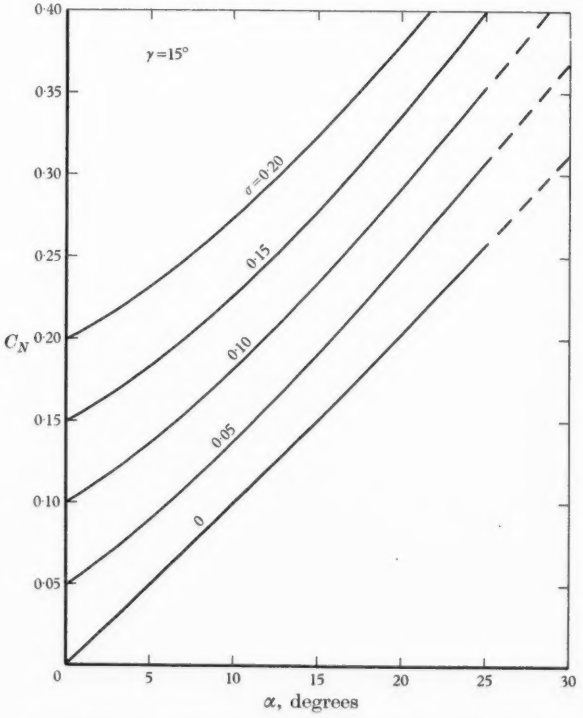

FIGURE 8. Variation of the normal-force coefficient with the angle of attack, $\gamma = 15°$.

In conclusion, the following features of and comments on the solution may be pointed out.

(1) For fixed α, C_N increases approximately linearly with σ, the slope $(\partial C_N/\partial\sigma)$ being approximately the same (slightly less than unity) throughout the range of α considered.

(2) For fixed σ, the non-linear dependence of C_N on α is exhibited in figures 6–8.

(3) The present analysis does not provide the criterion for conditions under which the cavity will be shorter than the plate and the cavity-plate system will no longer be slender. It is to be expected that as $\alpha \to 0$, the cavity length will decrease and become terminated on the plate such that the assumption of slenderness as well as of the cavity-flow model will be violated. The result for very small values of α (say less than 2°), obtained from this theory, will therefore not be expected to apply.

(4) It may be noted that the other potential flow models (such as the re-entrant jet model) may also be adopted to calculate the cross-flow provided that the cavity volume in such a model is interpreted appropriately. Since the equivalent cavitation number for the cross-flow is in general not small, the use of the non-linear two-dimensional cavity-flow model (the Riabouchinsky model in the present case) really implies putting on test the validity of the model for the case of small cavity cross-section (or large cavitation number for the cross-flow) together with the simplifying assumptions introduced here.

This work was carried out under the Bureau of Ships fundamental hydrodynamics research programme, Project NS 715-102, David Taylor Model Basin. Reproduction in whole or in part is permitted for any purpose of the United States Government. The authors wish to thank Mr T. Kiceniuk for his courtesy in furnishing the preliminary data used here. The assistance rendered by Mrs Rose Grant, Mrs Barbara Cumberbatch, and Mrs Zora Harrison in preparation of the manuscript is greatly appreciated.

REFERENCES

Birkhoff, G. & Zarantonello, E. H. 1957 *Jets, Wakes and Cavities.* New York: Academic Press.

Jahnke, E. & Emde, F. 1945 *Tables of Functions.* New York: Dover Publications.

Sacks, A. H. 1954 On slender body theory and apparent mass. *J. Aero. Sci.* **21**, 713.

Tulin, M. P. 1959 Supercavitating flow past slender wings. *J. Ship Res.* **3**, 17.

Ward, G. N. 1949 Supersonic flow past slender pointed bodies. *Quart. J. Mech. Appl. Math.* **2**, 75.

Wu, T. Y. 1956 A free streamline theory for two-dimensional fully cavitated hydrofoils. *J. Math. Phys.* **35**, 236.

A theory for the core of a leading-edge vortex

By M. G. HALL

Royal Aircraft Establishment, Farnborough, Hampshire

(Received 28 February 1961)

In the flow past a slender delta wing at incidence one can observe a roughly axially symmetric core of spiralling fluid, formed by the rolling-up of the shear layer that separates from a leading edge. The aim in this paper is to predict the flow field within this vortex core, given appropriate conditions at its outside edge.

The basic assumptions are (i) that the flow is continuous and rotational, and (ii) that viscous diffusion is confined to a relatively slender subcore. In addition it is assumed that the flow is axially symmetric and incompressible. Together, these admit outer and inner solutions for the core from the equations of motion. For the outer solution the subcore is ignored, and the flow is taken to be inviscid (but rotational) and conical. The resulting solution consists of simple expressions for the velocity components and pressure. For the inner solution, which applies to the diffusive subcore, the flow is taken to be laminar, and certain approximations are made, some based on the boundary conditions and some analogous to those of boundary-layer theory. The solution obtained in this case is a first approximation, and has been computed.

A sample calculation yields results which are in good qualitative and fair quantitative agreement with experimental measurements.

1. Introduction

A core of spiralling fluid can be observed in the flow past a slender delta wing at incidence. Its position is shown in figure 1, which is a sketch of the over-all flow pattern. Separation of a shear layer takes place from the neighbourhood of each leading edge. The layer curves upward and inboard and eventually rolls up, forming a core in which the velocity and pressure fields are roughly axially symmetric. This over-all pattern is well established experimentally. It appears essentially unchanged through the speed range and for most operating incidences as long as the leading edges are subsonic, and it is found also with slender wings other than deltas. Such a vortex core may have a diameter as large as one-third of the semi-span, and within it have been found velocities so high and pressures so low as to create some speculation and controversy. The aim in this paper is to predict theoretically the velocity and pressure fields within a core, given appropriate conditions at its outside edge, and to explain the core structures that have been observed.

The recent experimental studies by Earnshaw (1961) and Lambourne &

Bryer (1959) have established the structural form taken by the vortex core. Figures 2–5 show results at 70 % chord of measurements by Earnshaw over a delta wing of aspect ratio one and 56 in. centre line, at 14·9° incidence and with a free-stream velocity of 100 ft./sec. Figure 2 is a cross-sectional view showing the formation of the core. The closed contour drawn as a broken line marks the

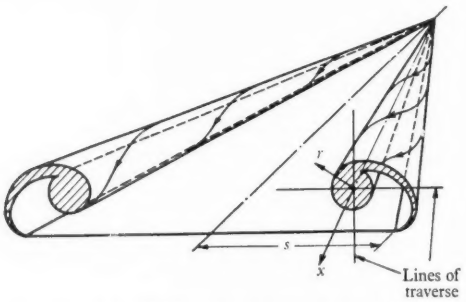

FIGURE 1. Basic pattern for flow over a slender delta wing at incidence.

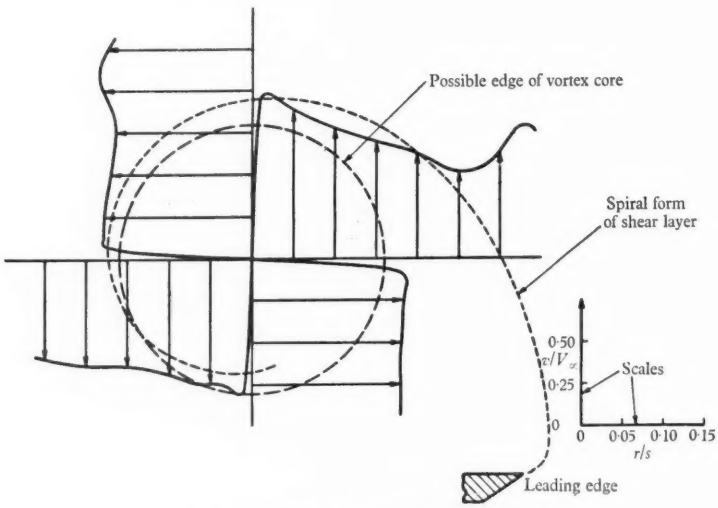

FIGURE 2. Profiles of the circumferential velocity v, derived from Earnshaw's measurements.

outside edge of the core (its size is somewhat arbitrary), the choice being guided only by the criterion of axial symmetry. The ordinate r/s is the ratio of the radial distance r from the axis of the core to the semi-span s (see figure 1). V_∞ is the free-stream velocity. Figures 3–5 show pairs of profiles obtained by traversing through the core in a pair of mutually perpendicular directions (figure 1). Corresponding theoretical profiles are included also: these will be referred to after the theory has been presented. The striking feature here is that there are axial velocities (figure 3) within the core over twice the magnitude of the free

stream velocity and, associated with them, pressure coefficients (figure 5) of less than -6. This stands in sharp contrast to the much smaller perturbations of the free-stream values elsewhere over the wing.

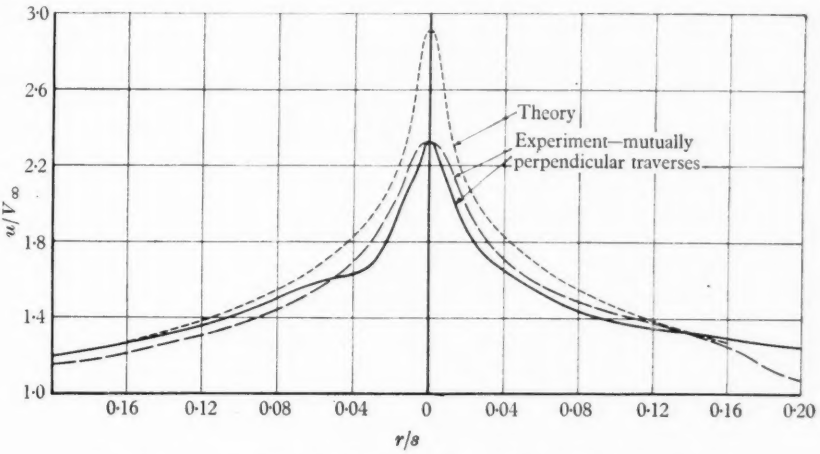

FIGURE 3. Experimental and theoretical profiles of axial velocity u.

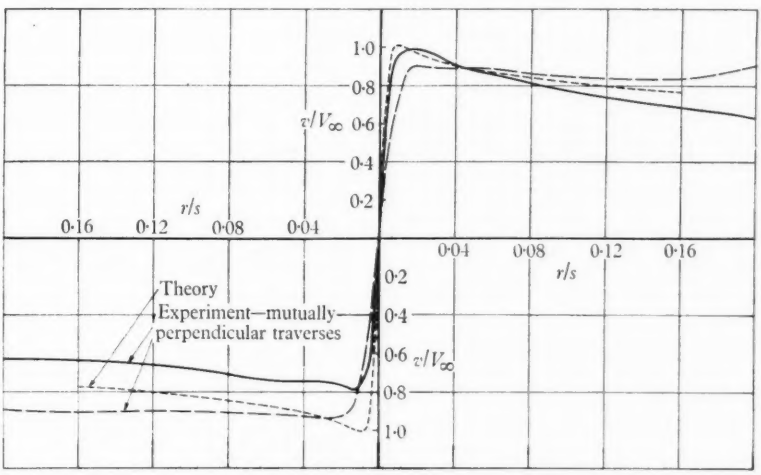

FIGURE 4. Experimental and theoretical profiles of circumferential velocity v.

Certain other features of the observed core structure should be noted, since they suggest the form of a possible simplified model of the core. First, the shear layer from the leading edge diffuses rapidly (figure 2) and is barely distinguishable after less than one convolution of a spiral, before the core is even reached. Secondly, the gradients of total pressure within the core (figure 5) are small except for a very slender region along the axis. It has been found that where the gradients

of total pressure are small the velocity and pressure fields are approximately conical, which is consistent with Jones's wing theory.

A simplified model of the vortex core is adopted here, with two distinctive properties that are suggested by the above. The first property is that the flow is continuous, i.e. it includes no vortex sheet. Thus, the flow must be rotational to allow a convection of vorticity. The second is that diffusion of vorticity (associated with a loss of total pressure) is confined to a relatively slender subcore. In this way the core is divided into a convective outer part and a diffusive subcore. This is justifiable for large Reynolds numbers, and it reduces the problem of solving

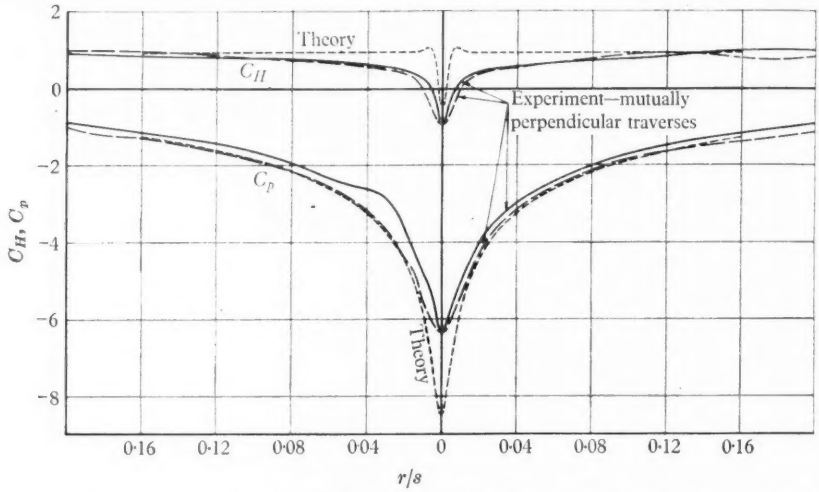

FIGURE 5. Experimental and theoretical profiles of total and static pressure coefficients, $C_H = (p_0 - p_\infty)/\frac{1}{2}\rho V_\infty^2$ and $C_p = (p - p_\infty)/\frac{1}{2}\rho V_\infty^2$ respectively.

the equations of motion for the core to that of obtaining an inviscid outer solution for the convective part—for which the subcore is ignored—and then, using this outer solution to specify boundary conditions, obtaining a viscous inner solution for the subcore. In addition to the distinctive properties, the fluid is taken to be incompressible, and the velocity and pressure fields are taken to be axially symmetric. For the outer solution, these fields are taken to be conical as well, which implies a constant total pressure. Advantage will be taken of the fact that the core is slender to neglect terms of order $(r/x)^2$, where, as shown in figure 1, x is the distance along the axis of the core from the apex of the wing. For the inner solution the flow is taken to be laminar, and the Reynolds number will be supposed to be large enough for approximations analogous to those of boundary-layer theory to be made.

Mangler & Smith (1959) have previously obtained a solution for the vortex core in the course of investigating the flow past the wing as a whole. No specific steps were taken to elucidate the core structure in detail. The flow was treated by slender-wing theory, and only constant values through the core of circumferential and axial velocity were obtained.

In the model of Mangler & Smith, the core consists of a tightly rolled vortex sheet (representing the shear layer) imbedded in a potential flow. This provides an exact representation of the core for the flow past a wing in the limit of infinite Reynolds number, and it is of interest to compare such a model with the present one. Corresponding profiles of the circumferential velocity component are sketched in figure 6. Observe that in the present model the steps due to the vortex sheet have been smoothed out, so that no part of the profile can be that of a potential flow. Because finite Reynolds numbers are admitted here, the profile passes smoothly through the axis no matter what its shape in the outer part of the core. This stricter condition is also satisfied by the profile of the hypothetical

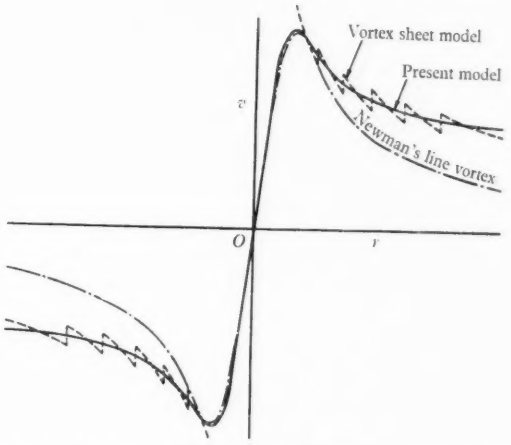

FIGURE 6. Qualitative comparison of different types of profile of the circumferential velocity v.

Rankine vortex, or by a more realistic counterpart, Newman's (1959) theoretical profile for a viscous line vortex of constant strength. A sketch of Newman's profile is included in the figure. If the present profile for a leading-edge vortex were extended far enough from the axis, it would tend to that of a potential flow, as Newman's profile does in the figure. Closer to the axis, the present profile shows (as sketched) a departure from potential flow, as also does Newman's profile. However, the departure in Newman's case is associated solely with a significant increase of viscous diffusion, and leads directly to a 'solid body' rotation, whereas in the present case diffusion is still insignificant and the departure is associated with a convection of vorticity; of course, viscous diffusion eventually does become appreciable here also sufficiently close to the axis. Newman's flow configuration was simple enough for him to obtain a neat approximate solution of the Navier–Stokes equations without having to divide his vortex into outer and inner parts.

2. Outer solution

2.1. *Equations of motion and their solution*

When the velocity and pressure fields are axially symmetric, the Navier–Stokes equations for the steady flow of an incompressible fluid are, in cylindrical coordinates (r, x),

$$\frac{\partial u}{\partial x}+\frac{\partial w}{\partial r}+\frac{w}{r}=0, \tag{1a}$$

$$u\frac{\partial u}{\partial x}+w\frac{\partial u}{\partial r}=-\frac{1}{\rho}\frac{\partial p}{\partial x}+\nu\nabla^2 u, \tag{1b}$$

$$u\frac{\partial v}{\partial x}+w\frac{\partial v}{\partial r}+\frac{vw}{r}=\nu\left(\nabla^2 v-\frac{v}{r^2}\right), \tag{1c}$$

$$u\frac{\partial w}{\partial x}+w\frac{\partial w}{\partial r}-\frac{v^2}{r}=-\frac{1}{\rho}\frac{\partial p}{\partial r}+\nu\left(\nabla^2 w-\frac{w}{r^2}\right), \tag{1d}$$

where

$$\nabla^2\equiv\frac{\partial^2}{\partial r^2}+\frac{1}{r}\frac{\partial}{\partial r}+\frac{\partial^2}{\partial x^2},$$

u and w are the axial and radial velocity components, v is the circumferential velocity component, and p, ρ and ν are the pressure, density and kinematic viscosity, respectively.

The values taken by u, v and w in the outer solution will be denoted by U, V and W respectively. Since the velocity and pressure fields are conical here, U, V, W and p will be functions of the conical parameter $\theta = r/x$ alone. Thus, for the outer solution, where the flow is inviscid (but rotational) and conical, equations (1) reduce to

$$-\theta\frac{d}{d\theta}\left(U-\frac{W}{\theta}\right)+\frac{2W}{\theta}=0, \tag{2a}$$

$$-\left(U-\frac{W}{\theta}\right)\frac{dU}{d\theta}=\frac{1}{\rho}\frac{dp}{d\theta}, \tag{2b}$$

$$-\theta\left(U-\frac{W}{\theta}\right)\frac{dV}{d\theta}+\frac{VW}{\theta}=0, \tag{2c}$$

$$-\theta\left(U-\frac{W}{\theta}\right)\frac{dW}{d\theta}-\frac{V^2}{\theta}=-\frac{1}{\rho}\frac{dp}{d\theta}. \tag{2d}$$

The boundary conditions are taken to be

$$\left.\begin{aligned}&\theta=0, \quad W=0,\\ &\theta=\theta_2, \quad U=U_2, \quad V=V_2, \quad p=p_2,\end{aligned}\right\} \tag{3}$$

where the subscript 2 identifies quantities at the outside edge of the core $\theta = \text{const.} = \theta_2$. The subscript 1 will identify quantities at the outside edge of the subcore. Observe that the solution is here formally extended to the axis, $\theta = 0$, following the stipulation that the viscous subcore is relatively slender. The tacit assumption is that the effects of the subcore on the outer part of the core are negligible. The first condition, that of zero radial flow on the axis, is an

important one. It expresses a continuity condition and implies an absence of sources or sinks. It appears to be the sole condition applicable to the axis of an inviscid rotating flow, for infinite velocities and gradients cannot be ruled out. The ratio V/U, which is a measure of the helix angle of the spiralling streamlines, will appear frequently, and is therefore denoted by the symbol ϕ. The value ϕ_2 may be related to the rate of increase of the strength of the core along its length or, what is equivalent, to the rate at which vorticity is fed in, by taking the circulation $2\pi r_2 V_2$ around the core as a measure of its strength and differentiating: thus

$$\frac{d}{dx}(2\pi r_2 V_2) = 2\pi U_2 \theta_2 \phi_2.$$

The equations (2) are easily integrated. Equations (2*a*) and (2*c*) yield

$$\left(\frac{V}{V_2}\right)^2 = \frac{U - W/\theta}{U_2 - W_2/\theta_2}. \tag{4}$$

Equation (4), together with (2*a*) and (2*b*), enables V and p to be eliminated from equation (2*d*), which becomes

$$(1+\theta^2)\frac{dW}{d\theta} + \frac{W}{\theta} = -\frac{V_2^2}{U_2 - W_2/\theta_2}. \tag{5}$$

Therefore, since the term $\theta^2 = (r/x)^2$ in the bracket may be neglected for a slender core,† the solution for W is

$$\left.\begin{aligned} W/W_2 &= \theta/\theta_2, \\ W_2 &= -\tfrac{1}{2}(\theta_2 U_2)\{\sqrt{(1+2\phi_2^2)} - 1\} < 0. \end{aligned}\right\} \tag{6}$$

Note that $\sqrt{(1+2\phi_2^2)}$ is positive; the possible ambiguity of sign in the expression for W_2 has been removed by applying the condition $W/U < \theta$, which follows from Kelvin's circulation theorem. The substitution of (6) in equation (2*a*) leads to the result

$$\frac{U}{U_2} = 1 - \{\sqrt{(1+2\phi_2^2)} - 1\}\log\left(\frac{\theta}{\theta_2}\right), \tag{7}$$

and the substitution of (6) and (7) in (4) yields

$$\left(\frac{V}{V_2}\right)^2 = 1 - \left[\frac{\sqrt{(1+2\phi_2^2)} - 1}{\phi_2}\right]^2 \log\left(\frac{\theta}{\theta_2}\right). \tag{8}$$

Finally, the neglect of the term θ^2 in equation (5) implies that (2*d*) can be reduced to

$$\frac{1}{\rho}\frac{dp}{d\theta} = \frac{V^2}{\theta}; \tag{9}$$

and the expression for V^2 given by equation (8) enables this to be integrated, with the result

$$\frac{p - p_2}{\rho V_2^2} = \log\left(\frac{\theta}{\theta_2}\right) - \frac{1}{2}\left[\frac{\sqrt{(1+2\phi_2^2)} - 1}{\phi_2}\right]^2 \log^2\left(\frac{\theta}{\theta_2}\right). \tag{10}$$

† Equation (5) can be solved without neglecting θ^2, but the expressions for the other velocity components then become unduly complicated for this particular problem.

2.2. *Discussion of the outer solution*

Equations (6), (7), (8) and (10) constitute a solution for the flow in the convective outer part of the core. Equations (6) show that the radial flow is always small and always directed inwards toward the axis, and that it decreases linearly in magnitude with decreasing distance from the axis. Also, the larger the ratio ϕ_2,

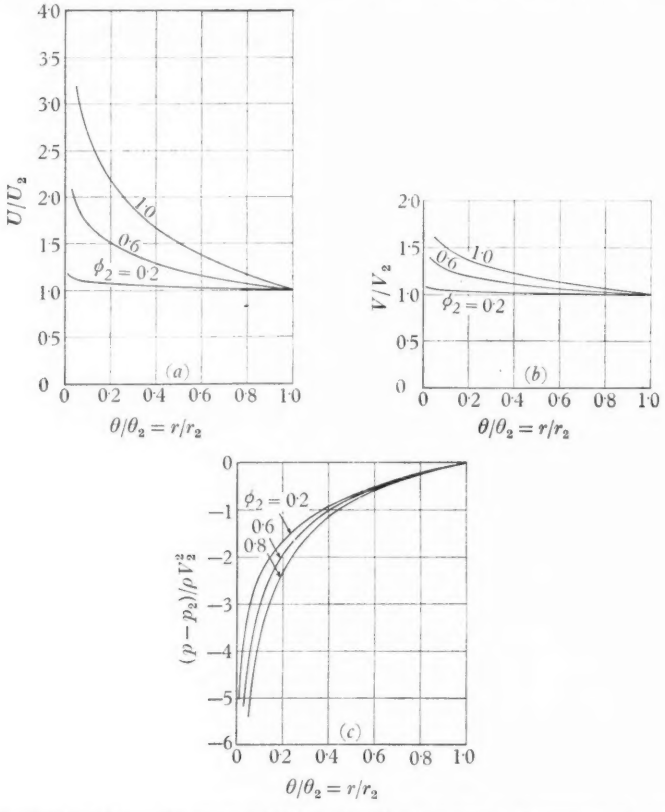

FIGURE 7. Profiles from the outer solution, showing the effect of varying ϕ_2, for (*a*) the axial velocity U, (*b*) the circumferential velocity V, and (*c*) the static pressure p.

the larger is the radial in-flow. Some representative profiles of the axial and circumferential velocity components U and V and of the pressure p have been calculated from equations (7), (8) and (10), respectively, and are shown in figure 7. The abscissae on the figures denote the non-dimensional distance from the axis of symmetry. Each figure is concerned with one of the velocity components or with the pressure, and the different curves in the figure correspond to different values of ϕ_2.

The figures show that U/U_2, V/V_2 and the pressure drop $(p_2-p)/\rho V_2^2$ all decrease with increasing distance from the axis, and all increase with increasing ϕ_2. It may be observed that the increase in axial velocity U and the drop in pressure

within the core may be very considerable. Such a pressure drop is to be expected in a spiralling flow, but the considerable increase in axial velocity is perhaps surprising. This increase is, however, a natural consequence of the original assumptions of conical field, etc., for the structure of the core. The phenomenon may be easier to understand if it is noted that according to the theory the pressure gradient in the direction of the spiralling path of a fluid element is negative and sustained, though not in general large: the core is such that it entrains fluid and retains it in a pressure field, which subjects each element to a continuous accelerating force. Alternatively, it can be shown that the vortex lines in the outer solution nearly coincide with the spiralling streamlines, so that there exists a circumferential component of vorticity for which the induced flow is axial. Since the distribution of this vorticity is symmetrical about the axis of the core, there will be, in effect, a focusing or concentrating action which yields a high resultant velocity along the axis.

The outer solution is clearly singular on the axis of symmetry, but even as the axis is approached the solution becomes invalid. Towards the axis, the gradients of vorticity become increasingly large, so that it is to be expected that viscous diffusion will become appreciable. In addition, according to equation (10) the pressure p becomes negative for sufficiently small θ/θ_2. It is supposed here, however, that before this occurs the diffusion effects have invalidated the solution. An *a posteriori* check of the viscous diffusion effects implied by the outer solution is therefore worth while.

The procedure is to feed back the above (inviscid) solutions for U, V and W into the full Navier–Stokes equations (1), and to compare the magnitudes of the terms representing inertia and viscous forces. It can be shown, if this is done, that the outer solution implies negligible viscous forces in the axial direction. But circumferential viscous forces are implied: the ratio of inertia to viscous terms, if we assume that ϕ_2 is not large compared with unity, is found to be

$$O\left(\frac{\phi^2 U x\theta^2}{\nu}\right) = O\left(\frac{\phi_2^2 U_2 x\theta^2}{\nu}\right).$$

The product

$$\phi_2^2 R_2 \equiv \frac{\phi_2^2 U_2 x}{\nu}$$

is of special significance. It is clear that in a region of dimensions $\theta = O(\phi_2^{-1} R_2^{-\frac{1}{2}})$ diffusion effects must become appreciable, and the outer solution must become unrealistic. Thus it can be deduced from the outer solution that a diffusive subcore exists and, moreover, that circumferential viscous forces play the dominant role in its generation. Note that this subcore can be made as slender as desired by taking R_2 sufficiently large. The limit (with ϕ_2 bounded) $R_2 \to \infty$ therefore constitutes the formal condition for the present model of the vortex core to be self-consistent, because only in this limit will an inviscid outer flow which is conical be compatible with an inner diffusive subcore which cannot be conical. Note finally that as $R_2 \to \infty$ then, for the edge of the subcore, $\theta_1/\theta_2 \to 0$, and, from equations (7) and (8),

$$\frac{V_1^2}{U_1^2} \equiv \phi_1^2 \to 0.$$

3. Inner solution†

3.1. *Approximation of the equations of motion*

Equations (1) apply to the diffusive subcore, but they are intractable as they stand. In this subsection, approximations will be made to simplify the equations. What is wanted is an approximate solution valid for large but finite Reynolds numbers. The first step would be to make the usual boundary-layer assumptions (that the Reynolds number tends to infinity, and so on), and to seek an inner solution which satisfies the proper conditions on the axis of symmetry and tends asymptotically to the outer solution with increasing distance from the axis. If no more than this is done, however, it is found that the equations of motion are still intractable, mainly because large variations of the axial velocity are not excluded. Fortunately, the boundary-layer assumptions can be coupled with other assumptions based on the boundary conditions. The symbols u, v, w will be retained for the velocity components within the subcore. On the axis of symmetry, $r = 0$, a diffusive fluid satisfies the conditions

$$\frac{\partial u}{\partial r} = v = w = 0.$$

At the edge, $r = r_1$, of the subcore, we have, in the limit as viscous diffusion becomes negligible,

$$u = U_1, \quad v = V_1 \quad \text{and} \quad p = p_1.$$

The assumptions suggested by the above boundary conditions are, first, that

$$u = \text{const.} + O(\epsilon u), \tag{11a}$$

where ϵ is small; secondly, since the outer solution suggests (§ 2.2) that axial viscous forces will not be significant in the outer part $r > \delta$, say, of the subcore,

$$\left.\begin{aligned} \left(\frac{\partial u}{\partial r}\right)_{r \geqslant \delta} &= O\left(\frac{\partial U}{\partial r}\right), \\ \left(\frac{\partial u}{\partial r}\right)_{r < \delta} &= O\left[\left(\frac{\partial U}{\partial r}\right)_{r=\delta}\right]; \end{aligned}\right\} \tag{11b}$$

and, thirdly,

$$w = O(W) = O(W_1 r/r_1). \tag{11c}$$

The first of these, (11a), will be justified eventually: it is not introduced merely to simplify the equations of motion. An expression for ϵ,

$$\epsilon = \phi_1^2 \log(\theta_1 R_1^{\frac{1}{2}}), \tag{12}$$

can be deduced, by establishing from equation (1b) that $\delta = O(xR_1^{-\frac{1}{2}})$ and integrating $\partial u/\partial r$. But it can be shown from the outer solution that $\theta_1 R_1^{\frac{1}{2}}$ is large for large Reynolds numbers. If ϵ is to be small, therefore, a limit will have to be placed on the magnitude of $\theta_1 R_1^{\frac{1}{2}}$.

The assumptions similar to those made in boundary-layer theory are that (i) the Reynolds number is large or, formally, $R_2 \to \infty$, and (ii) the circum-

† A more detailed account has been given (1960) by the author.

ferential viscous forces, which have the dominant role in generating the subcore, must be as important as the circumferential inertia forces (within the subcore) and must be negligible at the edge.

These two sets of assumptions—from the boundary conditions and from boundary-layer theory—enable the orders of magnitude of the terms in equations (1) to be specified in such a way that solution becomes practicable. Now, as pointed out in the previous section, the condition $R_2 \to \infty$ implies that $\theta_1/\theta_2 \to 0$ and that $\phi_1^2 \to 0$. The basis of the present approximation to the equations of motion will be to make use of the smallness of ϕ_1^2 and ϵ to simplify the equations. ϕ_1^2 will be treated as a small parameter; unlike θ_1/θ_2, it remains a meaningful parameter for finite Reynolds numbers. It can be deduced from the outer solution that, for $\phi_1^2 \to 0$,

$$\phi_1^2 = -\frac{1}{\log \theta_1} = -\frac{2W_2}{\theta_2 U_1} = -\frac{2W_1}{\theta_1 U_1}, \tag{13}$$

so that ϕ_1^2 is a measure not only of the helix angle of the spiralling streamlines at the edge of the subcore but also of the rate of convergence of the streamlines.

On neglect of the terms in equations (1) that are smaller by a factor of either ϕ_1^2 or ϵ, the equations reduce to

$$\frac{\partial u}{\partial x} + \frac{\partial w}{\partial r} + \frac{w}{r} = 0, \tag{14a}$$

$$U_1 \frac{\partial u}{\partial x} = -\frac{1}{\rho}\frac{\partial p}{\partial x} + \nu\left(\frac{\partial^2 u}{\partial r^2} + \frac{1}{r}\frac{\partial u}{\partial r}\right), \tag{14b}$$

$$U_1 \frac{\partial v}{\partial x} + w\frac{\partial v}{\partial r} + \frac{vw}{r} = \nu\left(\frac{\partial^2 v}{\partial r^2} + \frac{1}{r}\frac{\partial v}{\partial r} - \frac{v}{r^2}\right), \tag{14c}$$

$$\frac{v^2}{r} = \frac{1}{\rho}\frac{\partial p}{\partial r}. \tag{14d}$$

As the equations stand, they are still intractable, but clearly if some approximation to w could be substituted in (14c), so that the equation yielded a satisfactory first approximation to v, completion of the solution would be straightforward. Now, for $r \ll r_1$, the terms in (14c) containing w become negligible anyway, so that any chosen w need be an adequate approximation to the correct w for larger r only. The obvious choice, therefore, is the formula given by equations (6) respective to the outer solution, namely

$$w = \frac{W_2}{\theta_2}\frac{r}{x}.$$

Thus w is assigned its correct magnitude and gradient at $r = r_1$, and its correct magnitude at $r = 0$. Substitution in equation (14c) yields

$$U_1 \frac{\partial v}{\partial x} + \frac{W_2}{\theta_2}\frac{r}{x}\frac{\partial v}{\partial r} + \frac{W_2}{\theta_2}\frac{v}{x} = \nu\left(\frac{\partial^2 v}{\partial r^2} + \frac{1}{r}\frac{\partial v}{\partial r} - \frac{v}{r^2}\right). \tag{15}$$

The equations (15), (14d), (14b) and (14a) can be solved successively, to yield first approximations to v, p, u and w, respectively. This would in fact be the first step in a process of solution by iteration. In this process the adoption of the

formula given by the outer solution for w would constitute the 'zeroth' approximation. However, only the first approximations will be sought here, and whether the process of iteration is justified will be put aside.

3.2. *Transformation of the equations and the form of the solution*

The equations for the subcore are still not easy to solve, because they contain partial derivatives. This would be remedied if, by transformation of the variables, similar solutions could be found. A new independent variable

$$\zeta = \left[\frac{U_1(x)\,x}{\nu}\right]^{\frac{1}{2}} \frac{r}{x} \tag{16}$$

is therefore introduced to replace r as the measure of the radial distance from the axis. For the region within which viscous diffusion must, according to the *a posteriori* check, become appreciable, it can be shown that $\zeta^2 = O(1/\phi_1^2)$; and, for the edge of the subcore, $\zeta_1^2 \gg 1/\phi_1^2$. Similar solutions of the form

$$u = U_1(x) f(\zeta), \quad v = V_1(x)\, g(\zeta), \quad \zeta_1 = \text{const.} \tag{17}$$

will be sought, where $df/d\zeta = g = 0$ at $\zeta = 0$ and $f = g = 1$ at $\zeta = \zeta_1$. The value of ζ_1 may be arbitrarily chosen, provided it is large enough to satisfy the condition $\zeta_1^2 \gg 1/\phi_1^2$ and not so large that the assumption (11*a*) is invalidated.

Equations (15), (14*d*), (14*b*) and (14*a*) are now transformed by substitution of the new variables f, g and ζ. After some labour, in which the outer solution is used, terms that are smaller by the factors ϕ_1^2 and ϵ are again neglected, and the result is

$$\frac{d^2g}{d\zeta^2} + \left(\frac{\zeta}{2} + \frac{1}{\zeta}\right)\frac{dg}{d\zeta} + \left(\frac{\phi_1^2}{4} - \frac{1}{\zeta^2}\right) g = 0, \tag{18}$$

$$\frac{1}{\rho}\frac{\partial p}{\partial \zeta} = V_1^2 \frac{g^2}{\zeta}, \tag{19}$$

$$\frac{d^2f}{d\zeta^2} + \left(\frac{\zeta}{2} + \frac{1}{\zeta}\right)\frac{df}{d\zeta} = -\frac{\phi_1^2}{2} g^2 + \frac{\phi_1^4}{2}\int_{\zeta_1}^{\zeta} \frac{g^2}{\zeta}\, d\zeta, \tag{20}$$

$$\left(\frac{x}{\nu U_1}\right)^{\frac{1}{2}} \frac{\partial}{\partial \zeta}(\zeta w) = -\frac{\phi_1^2}{2}\zeta + \frac{\zeta^2}{2}\frac{df}{d\zeta}. \tag{21}$$

It is clear from equations (18) to (21) that the form of solution specified by equations (17) is compatible with the equations of motion. Therefore, since the boundary conditions are already satisfied, the similar solutions (17) exist, and the calculations of the solutions can proceed.

3.3. *Solutions of the transformed equations*

Once a solution for g is obtained from equation (18), solutions for p, f and w are readily derived. The solution of equation (18) is

$$\begin{aligned} g = kG(\phi_1^2, \zeta) &= k\zeta \exp(-\tfrac{1}{4}\zeta^2)\, {}_1F_1(\tfrac{3}{2} - \tfrac{1}{4}\phi_1^2, 2, \tfrac{1}{4}\zeta^2) \\ &= k\zeta \exp(-\tfrac{1}{4}\zeta^2)\left[1 + \frac{\frac{3}{2} - \frac{1}{4}\phi_1^2}{2}\,\tfrac{1}{4}\zeta^2 + \frac{(\frac{3}{2} - \frac{1}{4}\phi_1^2)(\frac{5}{2} - \frac{1}{4}\phi_1^2)}{2! \times 2 \times 3}(\tfrac{1}{4}\zeta^2)^2 + \ldots\right], \end{aligned} \tag{22}$$

where k is a constant fixed by the boundary condition $g = 1$ at $\zeta = \zeta_1$, and ${}_1F_1$ is a confluent hypergeometric function (see, for example, Jeffreys & Jeffreys 1956, ch. 23).

By substituting $kG(\phi_1^2, \zeta)$ for g, equations (19) and (20) can be integrated to yield p and f respectively, and substitution for $df/d\zeta$ in (21) then enables w to be calculated. The results may be expressed in the forms

$$f = 1 + k^2\phi_1^2[(F_1 - F) + \phi_1^2(\alpha_1 - \alpha)P_1], \tag{23}$$

$$\frac{w}{W_2} = \frac{\theta}{\theta_2}[\tfrac{1}{2} + k^2(H + \phi_1^2\beta P_1)], \tag{24}$$

$$\frac{p}{\rho U_1^2} = \frac{p_1}{\rho U_1^2} - k^2\phi_1^2(P_1 - P), \tag{25}$$

where F, H and P are functions of ϕ_1^2 and ζ, given by

$$F = \frac{1}{2}\int_0^\zeta \left\{\frac{1}{\zeta \exp(\frac{1}{4}\zeta^2)}\int_0^\zeta \zeta \exp(\tfrac{1}{4}\zeta^2)\left(G^2 - \phi_1^2\int_0^\zeta \frac{G^2}{\zeta}d\zeta\right)d\zeta\right\}d\zeta,$$

$$H = \frac{1}{2\zeta^2}\int_0^\zeta \left\{\frac{\zeta}{\exp(\frac{1}{4}\zeta^2)}\int_0^\zeta \zeta \exp(\tfrac{1}{4}\zeta^2)\left(G^2 - \phi_1^2\int_0^\zeta \frac{G^2}{\zeta}d\zeta\right)d\zeta\right\}d\zeta,$$

$$P = \int_0^\zeta \frac{G^2}{\zeta}d\zeta,$$

and α and β are functions of ζ only, given by

$$\alpha = \int_0^\zeta \frac{\exp(\frac{1}{4}\zeta^2) - 1}{\zeta \exp(\frac{1}{4}\zeta^2)}d\zeta$$

$$\beta = \frac{1}{\zeta^2}\int_0^\zeta \frac{\zeta[\exp(\frac{1}{4}\zeta^2) - 1]}{\exp(\frac{1}{4}\zeta^2)}d\zeta.$$

To the above may be added an expression for the total pressure p_0, derived from equations (22) to (25) and (17):

$$p_0 = p_{01}(= p_{02}) - \tfrac{1}{2}\rho V_1^2(1 - k^2G^2)$$
$$- k^2\phi_1^2\rho U_1^2[(P_1 - P) - (F_1 - F) - \phi_1^2(\alpha_1 - \alpha)P_1]. \tag{26}$$

The functions F, G, H and P have been computed for ϕ_1^2 ranging from 0 to 0·6 in increments of 0·1, and the numerical results have been tabulated by the author (1960), together with numerical values of α and β. Curves of the function $G\,(= v/(kV_1))$ are plotted in figure 8. For large ζ, the asymptotic form of the confluent hypergeometric function gives

$$G \doteq \frac{2}{(\frac{1}{2} - \frac{1}{4}\phi_1^2)!}\left(\frac{\zeta^2}{4}\right)^{-\frac{1}{4}\phi_1^2}.$$

As might be expected, this is the same as would be obtained from equation (18) if the viscous terms therein were neglected.

Comparison of the solution for G with its asymptotic form indicates how viscous diffusion effects vary within the subcore. Included in figure 8 are the asymptotic curves for the cases $\phi_1^2 = 0$ and $\phi_1^2 = 0{\cdot}6$. It can be seen from these that the effects decrease rapidly as ζ increases, up to about $\zeta = 6$, and that by $\zeta = 10$ they are small. A close examination shows also that the decrease is more marked for

$\phi_1^2 = 0{\cdot}6$ than for $\phi_1^2 = 0$. Thus, the comparison shows the results to be consistent with the condition $\zeta_1^2 \gg 1/\phi_1^2$: the magnitude of ζ at the edge of the subcore must indeed be large for diffusion effects to be vanishingly small, and the smaller the magnitude of ϕ_1^2 the larger must ζ_1 be. But the comparison shows, in addition, that it will be sufficient for a first approximation to take ζ_1 equal to, say, 8 or 10, independently of ϕ_1^2. For although a smaller ϕ_1^2 will imply that diffusion effects will persist to a larger ζ, those effects will be small enough to be neglected anyway for ζ beyond 8 or 10.

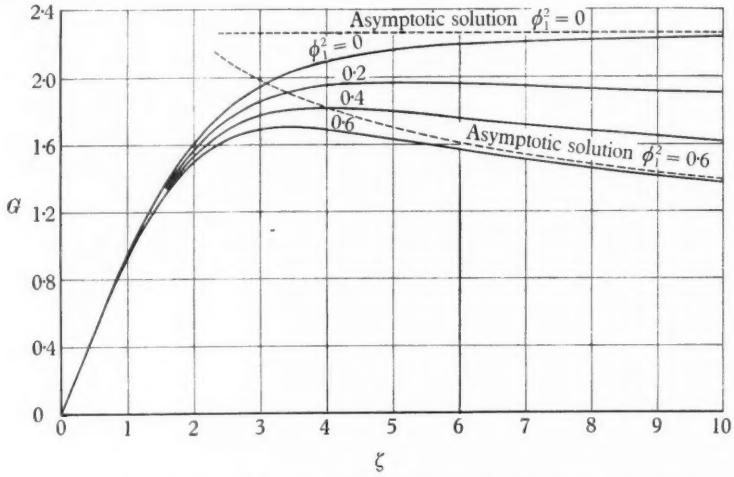

FIGURE 8. Curves of the function G from the inner solution, together with asymptotic solutions, for different values of ϕ_1^2.

Equations (22) to (26), together with (17), constitute an approximate inner solution, and describe the structure of the diffusive subcore. On the axis the circumferential and radial velocity components, v and w, are zero, and so also are the radial gradients of the axial velocity u, the static pressure p, and the total pressure p_0, with u taking a maximum value and p and p_0 minimum values there. The circumferential velocity is a maximum at a distance from the axis which decreases with both increasing ϕ_1^2 and increasing R_2. The radial velocity, which describes an inward flow, grows with increasing distance from the axis, from half the magnitude given by the outer solution. The circumferential and axial components, and the pressures, have magnitudes at the edge of the subcore equal to those given by the outer solution.

From the inner solution the effects of variations of Reynolds number can be worked out, and a brief illustration of this is given in the following section.

3.4. *Reynolds number effects*

Given a vortex core for which θ_2, U_2/V_∞, V_2/V_∞ and $C_{p2} = (p_2 - p_\infty)/\frac{1}{2}\rho V_\infty^2$ are specified, what are the effects of variations of the Reynolds number $R = V_\infty x/\nu$ on the core structure? Evidently the effects must be confined to the subcore.

As suggested in the previous subsection, ζ_1 is taken to be constant, independent of ϕ_1^2 and, consequently, independent of R. Such a constant ζ_1 is in fact a measure of the size of a subcore, for, as can be seen in figure 8, the range of ζ over which viscous diffusion effects become small is roughly the same for different solutions of the subcore.

From equations (16) and (7), we get

$$\zeta_1 = R^{\frac{1}{2}}\left(\frac{U_2}{V_\infty}\right)^{\frac{1}{2}}\theta_1\left(\frac{U_1}{U_2}\right)^{\frac{1}{2}} = R^{\frac{1}{2}}\left(\frac{U_2}{V_\infty}\right)\theta_1\left[1-\{\sqrt{(1+2\phi_2^2)}-1\}\log\left(\frac{\theta_1}{\theta_2}\right)\right]^{\frac{1}{2}} = \text{const.} \tag{27}$$

It follows that $d\theta_1/dR < 0$, or that θ_1 decreases as R increases. θ_1 is a direct measure of the slenderness of the subcore: the larger the Reynolds number, the slenderer is the subcore.

A number of trends can be deduced. Suppose the Reynolds number is increased from R to R', so that $\theta_1' < \theta_1$. From equations (7), (8) and (10), respectively, $U_1' > U_1$, $V_1' > V_1$, and $p_1' < p_1$. Since $U_1' > U_1$, equation (13) yields $\phi_1'^2 < \phi_1^2$. From equations (17), (13) and (23), it appears that

$$u'_{\max} - u_{\max} = \frac{2W_2}{\theta_2}[k^2(F_1+\alpha_1\phi_1^2P_1)+\phi_1^2-k'^2(F_1'+\alpha_1\phi_1'^2P_1')-\phi_1'^2],$$

and from equations (25) and (26), respectively, again with use of (13),

$$p'_{\min} - p_{\min} = p_1' - p_1 + \frac{4\rho W_2^2}{\theta_2^2}\left[\frac{k^2P_1}{\phi_1^2}-\frac{k'^2P_1'}{\phi_1'^2}\right],$$

and
$$p'_{0\min} - p_{0\min} = \tfrac{1}{2}\rho V_1^2 - \tfrac{1}{2}\rho V_1'^2 + \frac{4\rho W_2^2}{\phi_2^2}\left[\frac{k^2}{\phi_1^2}(P_1-F_1-\alpha_1\phi_1^2P_1)-\frac{k'^2}{\phi_1'^2}(P_1'-F_1'-\alpha_1\phi_1'^2P_1')\right].$$

Now it can be checked from the tables that, for $\zeta_1 = 8$ or 10, each of the expressions in square brackets in the above three equations is negative. Furthermore, $p_1' < p_1$ and $V_1' > V_1$. Therefore the three equations yield $u'_{\max} > u_{\max}$, $p'_{\min} < p_{\min}$, and $p'_{0\min} < p_{0\min}$. Thus an increase of the Reynolds number yields, on the axis, an increase of the velocity and a lowering of both the static and total pressures. Alternatively, for any particular vortex core, the Reynolds number $R = V_\infty x/\nu$ grows with the distance x from the apex. Along the axis, therefore, the velocity increases, and the static and total pressures drop, with increasing distance from the apex.

4. Comparison with experimental results

The above theory has been employed to calculate the velocity and pressure fields within a particular vortex core. For the boundary conditions at the outside edge of the core, numerical values based on Earnshaw's measurements (1961) were used, so that the theoretical results are directly comparable with the experimental profiles of figures 3–5. The numerical results for u/V_∞, v/V_∞ (u and v now are taken to refer also to the outer solution), C_p, and $C_H = (p_0 - p_\infty)/\frac{1}{2}\rho V_\infty^2$ have been superimposed on the corresponding experimental results in figures 3–5.

The joining of the inner and outer solutions for u/V_∞, v/V_∞ and w/W_2 is shown in figure 10, but this will be discussed in the final section rather than here.

In addition, the variation with the Reynolds number $R = V_\infty x/\nu$ of $U_{\max}/V_\infty$ in subcores corresponding to the particular outer solution considered here has been calculated for R ranging from $10^{5\cdot5}$ to 10^8. Values of R below $10^{5\cdot5}$ were excluded because, with the present outer solution, errors in the inner solution are then likely to be appreciable. For example, in the experiment $R = 2{\cdot}22 \times 10^6$,

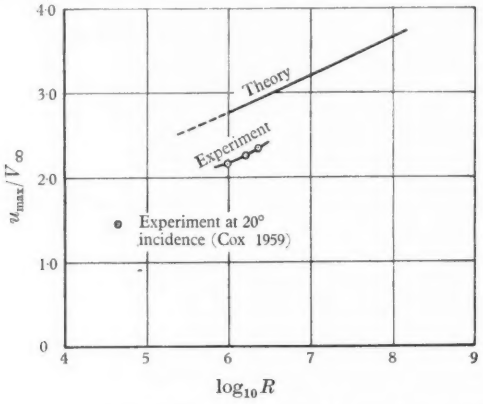

FIGURE 9. Variation with the Reynolds number R of the velocity along the axis of the vortex core of §4.

and this gives $\phi_1^2 \sim 0{\cdot}2$ and $\epsilon \sim 0{\cdot}4$, whereas the theory requires $\phi_1^2 \ll 1$ and $\epsilon \ll 1$. For smaller R, ϕ_1^2 and ϵ are still larger. It is thus perhaps questionable whether this comparison is a fair test of the theoretical inner solution. The resulting curve of $u_{\max}/V_\infty$ is plotted in figure 9, together with the few available experimental results, and it can be seen that theory and experiment give similar upward trends of $u_{\max}/V_\infty$ with increasing Reynolds number.

Compare now the theoretical and experimental profiles of figures 3–5. The outer solution is seen to give results which agree fairly well with the experimental results. The static pressure profiles, outside the subcore, are in markedly good agreement. That there are some discrepancies may be attributed to the theoretical assumption that the flow field is inviscid, exactly axially symmetric, and exactly conical. On the other hand, the inner solution gives results which differ appreciably from the experimental results: the predictions are only qualitatively correct. The theoretical velocity and pressure gradients in the subcore are too large, and the peaks are too pronounced. The theoretical subcore is too slender. Now, it does not seem likely that instrument errors, or too large a value of ϕ_1^2 or ϵ, can account for the discrepancies. So, while the viscous diffusion outside the subcore and effects of the flow near the apex should not be overlooked, it is natural to question the assumption of laminar flow in the subcore. Measurements by Lambourne & Bryer (1959) in a similar leading-edge vortex have suggested that the flow in the core is turbulent. The poor agreement here also suggests this. If this is so, the laminar theory might still be applied, but only

in a limited way: theoretical and experimental results might be matched by the introduction of an eddy viscosity, for example as Newman (1959) has done. From experience with wakes, the introduction of an eddy viscosity into the theoretical results for laminar flow would give increased diffusion, or a smaller effective Reynolds number, and this would improve the agreement.

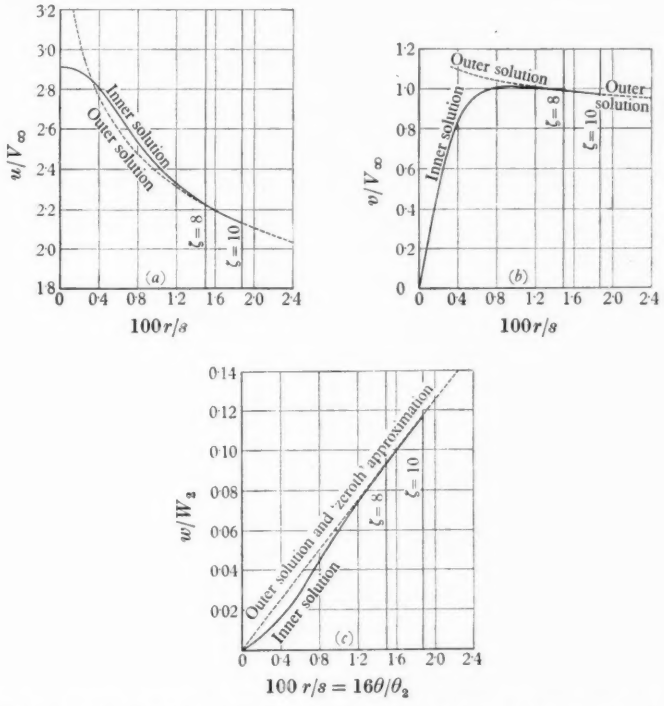

FIGURE 10. Joining of the inner and outer solutions (§ 4) for (*a*) the axial velocity u, (*b*) the circumferential velocity v, and (*c*) the radial velocity w.

5. Discussion

First, the present work will be briefly summarized. Then, the joining of the inner and outer solutions, and the validity of the theory will be discussed. Finally, some extensions of the work will be considered.

The theoretical results obtained stem from the type of vortex core model originally chosen. The essential features of the model were (i) that the flow is continuous and rotational, and (ii) that viscous diffusion is confined to a relatively slender subcore. Allied with the assumption that the flow is axially symmetric and incompressible, these admitted outer and inner solutions for the core. For the outer solution the subcore was ignored and the flow was taken to be inviscid and conical. The results (§ 2.1) were in simple logarithmic form. For the inner solution, which applied to the subcore, the flow was taken to be laminar, and approximations, some based on the boundary conditions and some analogous to

those of boundary-layer theory, were made. The results of § 3.3, in this case first approximations, appeared as similar solutions. Given the axial and circumferential velocities, the pressure, and the Reynolds number at the outside edge of the core, the velocity and pressure fields within the core can be calculated. The comparison with experimental results (§ 4) showed fair agreement, except in the details of the subcore, and this does not necessarily imply a fault in the model chosen, because it seems likely that the flow in the subcore of the experiment was significantly turbulent. Over-all qualitative agreement was good.

Figure 10 shows the joining of the profiles of the axial (u), circumferential (v), and radial (w) components of velocity, respectively, for the particular vortex core of § 4. For u and v, the magnitudes given by the inner and outer solutions at $\zeta_1 = 8$ were equated. Each join is seen to be smooth: the gradient is so nearly continuous that the extension of the inner solution to $\zeta_1 = 10$ virtually coincides with the outer solution. ζ_1 could equally well have been taken to be 10, say, but could not have been taken much larger without violating the condition ϵ $(= \phi_1^2 \log \zeta_1) \ll 1$. For w, the only boundary condition satisfied was $w = 0$ at $\zeta = 0$, and yet the inner and outer solutions very nearly coincide at ζ equal to 8 or 10. Had the Reynolds number been larger, even smoother joins could have been obtained.

The smoothness of the joins justifies two assumptions that were introduced tentatively. The first is the approximation made for w in equation (14*c*). The second is the vital simplifying assumption (§ 3.1) that the variations of axial velocity in the subcore are small, or $\epsilon \ll 1$: since the join *is* smooth, it can be said that at the edge of *some* region for which $\epsilon \ll 1$ does hold, viscous diffusion is indeed negligible, and thus there is a sound physical basis for the assumption.

The above points are related to the internal consistency of the theory. For example, it can be shown from equation (23) that $f\ (= u/U_1) = 1 + O(\phi_1^2 \log \zeta_1)$, as is required by (11*a*) and (12). Again, it can be shown from the outer solution that as $\theta \to 0$ equations (2) can be reduced to the equations obtained by omitting the viscous terms in (14). Therefore, with increasing distance from the axis, a solution of (14) must tend to one given by (2)—until ϵ and the errors in equations (14) become appreciable and the solutions diverge. For sufficiently large Reynolds numbers there is an intermediate region, where diffusion is negligible and before the solutions diverge, in which a join can be made. This join specifies an approximate solution. The exploitation of the smallness of the variations of the axial velocity in the subcore thus enables an approximate solution of the Navier–Stokes equations to be obtained; but it makes an intermediate join necessary, and the solution remains approximate in the limit of infinite Reynolds number, unlike boundary-layer solutions which become exact.

A number of extensions of the present work may be considered. The author has obtained (1959) outer solutions for which the pressure field was not necessarily conical, nor the radial velocity on the axis necessarily zero. For this more complicated problem it was convenient to introduce a stream function ψ, defined (in the present notation) by

$$U = 2\psi + \theta d\psi/d\theta, \quad W = \theta^2 d\psi/d\theta.$$

It turned out that $V^2 = K\psi$, with K = const., and the problem reduced to that of solving the ordinary non-linear equation

$$\theta^2 \frac{d^2\psi}{d\theta^2} + 3\theta \frac{d\psi}{d\theta} = -\frac{K}{2} + \frac{l}{\psi}, \tag{28}$$

where, in order that the velocity field be conical,

$$l = \frac{x}{2\rho}\left(\frac{\partial p}{\partial x}\right)_{\theta=\text{const.}} = \text{const.}$$

It was found, other conditions being equal, that a positive pressure gradient $\partial p/\partial x$ along θ_2 reduced the axial velocity within the core, increased the circumferential velocity, reduced the radial velocity, and increased the magnitude of the pressure difference $(p_2 - p)$. A negative pressure gradient had the reverse effect. The relaxation of the condition of zero radial velocity at the axis left the boundary condition W_2, which is a measure of the rate of flow into the core, free to be varied. It was found that small variations in W_2 produced comparatively large changes in the flow field within the core.

It should be mentioned that if the field for U and V is paraboloidal, depending on $\Theta = r/x^n$, n = const., instead of conical and dependent on θ, then (if one supposes that $x^{2n-2} = O(1)$ and $\Theta d\psi/d\Theta = O(\psi)$) an equation identical in form to (28) is obtained, with Θ replacing θ, and

$$L = \frac{x}{2n\rho}\left(\frac{\partial p}{\partial x}\right)_{\Theta=\text{const.}} = \text{const.}$$

replacing l. It is still true that $U = 2\psi + \Theta d\psi/d\Theta$ and $V^2 = K\psi$, but

$$W = nx^{n-1}\Theta^2 d\psi/d\Theta.$$

Therefore the solutions for U and V in a paraboloidal field, as functions of Θ, are identical to the solutions for U and V in a conical field, as functions of θ, for $L = l$.

Should practical reasons require the calculation of solutions for small perturbations of conical or paraboloidal field, or axial symmetry, this should be straightforward.

The present results also provide a basis for the investigation of 'vortex breakdown', an abrupt change in the flow from the pattern considered here, at some position downstream of the apex. This has been studied experimentally by Elle (1958), Peckham (1958), and Gray (unpublished), and theoretically by Squire (1960) and Jones (1960) who suggest plausible, but different, explanations for the phenomenon.

Finally, a first approximation to the temperature distribution in a real vortex core may be obtained by substituting the (incompressible) results for the velocity components into the energy equation, for example as Rott (1959) has done. This would constitute the first step in an iterative solution for a compressible vortex core.

REFERENCES

Cox, A. P. 1959 Measurements of the velocity at the vortex centre on an A.R.1 delta wing by means of smoke observations. *Aero. Res. Coun., Lond., Rep.* no. 21,116.

Earnshaw, P. B. 1961 An experimental investigation of the structure of a leading edge vortex. *Aero. Res. Coun., Lond., Rep.* no. 22,876.

Elle, B. J. 1958 An investigation at low speed of the flow near the apex of thin delta wings with sharp leading edges. *Aero. Res. Coun., Lond., Rep.* no. 19,780.

Hall, M. G. 1959 On the vortex associated with flow separation from a leading edge of a slender wing. *Aero. Res. Coun., Lond., Rep.* no. 21,117.

Hall, M. G. 1960 A theory for the core of a leading edge vortex. *Aero. Res. Coun., Lond., Rep.* no. 22,660.

Jeffreys, H. & Jeffreys, B. S. 1956 *Methods of Mathematical Physics*, 3rd ed. Cambridge University Press.

Jones, J. P. 1960 The breakdown of vortices in separated flow. *University of Southampton, U.S.A.A. Report*, no. 140.

Lambourne, N. C. & Bryer, D. W. 1959 Some measurements in the vortex flow generated by a sharp leading-edge having 65° sweep. *Aero. Res. Coun., Lond., Rep.* no. 21,073, *Curr. Pap.* no. 477.

Mangler, K. W. & Smith, J. H. B. 1959 A theory of the flow past a slender delta wing with leading edge separation. *Proc. Roy. Soc.* A, **251**, 200.

Newman, B. G. 1959 Flow in a viscous trailing vortex. *Aero. Quart.* **10**, 149.

Peckham, D. H. 1958 Low speed wind tunnel tests on a series of uncambered slender pointed wings with sharp edges. *Aero. Res. Coun., Lond., Rep.* no. 20,727.

Rott, N. 1959 On the viscous core of a line vortex. II. *Z. angew. Math. Phys.* **10**, 82.

Squire, H. B. 1960 Analysis of the 'vortex breakdown' phenomenon. Part 1. *Imperial College Aero. Dep., Rep.* no. 102.

Ship waves in a stratified ocean

By ALBERT A. HUDIMAC

U.S. Navy Electronics Laboratory, San Diego 52, California

(Received 5 July 1960 and in revised form 20 March 1961)

The velocity potential for a simple source moving in a straight line at constant depth in a two-layer ocean is obtained by the Fourier transform method. It is used to develop a formula for the wave-making resistance of a 'thin' ship for both surface and internal waves. An asymptotic expansion is used to delineate quantitatively the internal wave system. It is shown that at speeds less than the critical speed transverse and divergent wave systems are excited, while at speeds greater than the critical internal wave speed only the divergent wave system is excited. Examples of the shape of wave crests and of wave heights are given.

1. Introduction

Free waves in a homogeneous fluid with a free surface are characterized by a maximum vertical displacement at the surface. In deep water, the vertical displacement of a water particle decreases exponentially downward. In stratified water, other types of free waves may occur which are called 'boundary waves' or 'internal waves'. They are characterized by having their greatest vertical displacement in the interior.

The ocean has a vertical density structure. There often is a surface layer (usually quite homogeneous) which is separated from the denser fluid below by a more or less narrow thermocline region. Such layers may be caused by heating, cooling, mixing, and the advection of water masses.

The excitation of waves on the surface of the ocean by a displacement ship has been treated by various approximations. A comprehensive survey is given by Lunde (1951). In practically all cases the ocean is treated as if it were homogeneous; there is very little early literature (see Lamb 1916) on the excitation of internal waves. There has been work on the comparable situation in the stratified atmosphere, e.g. the work of Kochin (1949) and Warren (1960). Ekman (1904) has shown experimentally that a ship moving near the critical internal wave velocity (velocity of waves for which the wavelength is large compared to the thickness of the layer) strongly excites internal waves if the keel depth is about equal to the thickness of the layer. The transfer of energy from the ship to the internal waves is manifested by an increase in resistance to the motion of the ship. Under suitable circumstances, this increase of resistance can be manifold. The phenomenon is referred to as 'dead water'.

The author (1958) developed a formula for the resistance of a 'thin ship' in a two-layer ocean. An algebraic error invalidated the results. One purpose

of this paper is to present the correct results. Sretenskii† (1959) used a somewhat different method of analysis to derive such a formula. It can be shown that the results are exactly equivalent.

Another aspect of ship-excited waves is their peculiar pattern. For a homogeneous ocean, an explanation and treatment of this effect was first given by Kelvin (1887); it has also been treated by many others, e.g. Hogner (1923) and Peters (1949). The pattern of the corresponding internal waves formed in a two-layer ocean is delineated in this paper.

2. Motion of a simple source at constant speed, direction, and depth in a two-layer ocean

For simplicity, a two-layer model of the ocean will be considered. Perturbation theory (see Lunde 1951) can be used to replace a 'thin ship', to the first approximation, by a distribution of simple sources over the centre-plane section. The velocity potential for a simple source in a homogeneous fluid with a free surface has been determined in several ways; it is occasionally called a Havelock source. The objective of this section is to find the corresponding Green's function for a two-layer ocean. The mathematical statement of the problem is given in the next few paragraphs.

Fix a co-ordinate system in space such that the (x, z)-plane lies in the undisturbed interface between a layer of fluid of density ρ, and thickness h, lying on another fluid of density $\rho' = \Delta\rho + \rho$, of semi-infinite extent. Consider a simple point-source moving with constant velocity, c, in the direction of increasing x at a constant distance, f, above the undisturbed interface. If the layer were of infinite extent, the potential would be

$$\phi = m/r_1, \quad r_1^2 = (x-ct)^2 + (y-f)^2 + z^2, \tag{1}$$

assuming the source of strength m to pass over the origin at $t = 0$.

If the source is assumed to have started at $x = -\infty$, then at any finite distance from the origin, the potential ϕ, in the layer, the potential ϕ', below the layer, the pressure, p, the displacement of the free surface, η_s, and the displacement of the interface, η_i, are of the form

$$\left.\begin{aligned} \phi &= \phi(x-ct, y, z), \quad p = p(x-ct, y, z), \quad \eta_s = \eta_s(x-ct, y, z), \\ \phi' &= \phi(x-ct, y, z), \quad \eta_i = \eta_i(x-ct, y, z). \end{aligned}\right\} \tag{2}$$

Now consider a co-ordinate system moving with the source such that the axes $(\bar{x}, \bar{y}, \bar{z})$ are parallel to the stationary axes. Let

$$\bar{x} = x - ct, \quad \bar{y} = y, \quad \bar{z} = z, \quad \bar{t} = t. \tag{3}$$

In the fixed co-ordinate system, the potentials ϕ and ϕ' satisfy Laplace's equation, the former everywhere in the layer except at the source, and the latter everywhere in the lower fluid. The potentials $\overline{\phi}$ and $\overline{\phi}'$ in the moving co-ordinate system still satisfy Laplace's equation, i.e.

$$\Delta\overline{\phi}_b = 0, \quad \overline{\phi} = \overline{\phi}_b + \frac{m}{\bar{r}_1}, \tag{4}$$

† The author is indebted to the referee for having Sretenskii's work brought to his attention.

where the second equation defines $\overline{\phi}_b$, which is assumed to be regular, and

$$\Delta\overline{\phi}' = 0. \tag{5}$$

The boundary conditions can be linearized by a perturbation method. They become, in the moving co-ordinate system,

$$\overline{\phi}_{\bar{y}}(\bar{x}, h, \bar{z}) + c^2 g^{-1}\overline{\phi}_{\bar{x}\bar{x}}(\bar{x}, h, \bar{z}) = 0, \tag{6}$$

$$\rho c^2\overline{\phi}_{\bar{x}\bar{x}}(\bar{x}, 0, \bar{z}) + \rho g\overline{\phi}_{\bar{y}}(\bar{x}, 0, \bar{z}) = \rho' c^2\overline{\phi}'_{\bar{x}\bar{x}}(\bar{x}, 0, \bar{z}) + \rho' g\overline{\phi}'_{\bar{y}}(\bar{x}, 0, \bar{z}), \tag{7}$$

$$\overline{\phi}_{\bar{y}}(\bar{x}, 0, \bar{z}) = \overline{\phi}'_{\bar{y}}(\bar{x}, 0, \bar{z}) = -c\eta_x, \tag{8}$$

where (6) is the combination of the kinematic and dynamic conditions at the free surface (and g is the acceleration of gravity), (7) is the dynamic condition at the interface, and (8) is the kinematic condition at the interface. Also, $\overline{\phi}'$ satisfies the condition

$$\lim_{\bar{y}\to-\infty} \overline{\phi}' = 0, \tag{9}$$

and the condition at infinity has the form

$$\lim_{\bar{x}\to\infty} \overline{\eta}_s = \lim_{\bar{x}\to\infty} \overline{\eta}_i = 0. \tag{10}$$

There is no restriction placed on the η's for $\bar{x} \to -\infty$ except that they be bounded. In sequel, only the moving reference-frame is used and so the bars will be dropped.

The solution of the problem is obtained by application of the Fourier transform method.† The Fourier transform of ϕ_b is

$$\tilde{\phi}_b(\xi, \zeta) = \frac{1}{2\pi}\iint_{-\infty}^{\infty} \phi_b(x, y, z)\exp\{-i(\xi x + \zeta z)\}\,dx\,dz, \tag{11}$$

and the inverse transform is

$$\phi_b(x, z) = \frac{1}{2\pi}\iint_{-\infty}^{\infty} \tilde{\phi}_b(\xi, \zeta)\exp\{i(\xi x + \zeta z)\}\,d\xi\,d\zeta.$$

The transform of (4) is

$$\tilde{\phi}_{byy} - (\xi^2 + \zeta^2)\tilde{\phi}_b = 0.$$

Let $\xi^2 + \zeta^2 = \varpi^2$. This has the fundamental solution

$$\tilde{\phi}_b = A(\xi, \zeta)\,e^{y\varpi} + B(\xi, \zeta)\,e^{-y\varpi}. \tag{12}$$

Similarly

$$\tilde{\phi}' = A'(\xi, \zeta)\,e^{y\varpi} + B'(\xi, \zeta)\,e^{-y\varpi}. \tag{13}$$

Because of condition (9), $B' = 0$.

The Fourier transform of the surface boundary condition (6) is

$$g\tilde{\phi}_{by}(\xi, h, \zeta) - c^2\xi^2\tilde{\phi}_b(\xi, h, \zeta) - mg\exp\{-\varpi(h-f)\} - \frac{mc^2}{\varpi}\xi^2\exp\{-\varpi(h-f)\} = 0. \tag{14}$$

Here use is made of the well-known relation

$$\frac{1}{(x^2 + (y-f)^2 + z^2)^{\frac{1}{2}}} = \frac{1}{2\pi}\iint_{-\infty}^{+\infty} \frac{\exp\{\pm\varpi(y-f)\}}{\varpi}\exp\{i(\xi x + \zeta z)\}\,d\xi\,d\zeta, \tag{15}$$

† The method is similar to that used by Timman & Vossers (1953).

where '$-$' is used for $y > f$ and '$+$' is used for $y < f$. Thus the transform of

$$(x^2+(y-f)^2+z^2)^{-\frac{1}{2}}$$

is
$$\mathscr{F}(\exp-[x^2+(y-f)^2+z^2]) = \varpi^{-1}\exp\{\pm\varpi(y-f)\}. \tag{16}$$

The Fourier transforms of the boundary conditions (7) and (8) are

$$\bar{\phi}_{by}(\xi,0,\zeta)+me^{-\varpi f} = \bar{\phi}'_y(\xi,0,\zeta), \tag{17}$$

$$-\rho c^2\xi^2\bar{\phi}_b(\xi,0,\zeta)+\rho g\bar{\phi}_{by}(\xi,0,\zeta)-\rho c^2\varpi^{-1}\xi^2me^{-\varpi f}+\rho gme^{-\varpi f}$$
$$= -\rho' c^2\xi^2\bar{\phi}'(\xi,0,\zeta)+\rho' g\bar{\phi}'_y(\xi,0,\zeta). \tag{18}$$

Substitution of (12) and (13) into (14), (17), and (18) gives a set of three simultaneous equations in A, B, and A'. Solutions are obtained and substituted in (12) and (13) to give $\bar{\phi}_b$ and $\bar{\phi}'$. The inverse transform of $\bar{\phi}_b$ and $\bar{\phi}'$ then gives the formal solutions, ϕ_0 and ϕ'_0, which are not the complete expressions for ϕ and ϕ',

$$\phi_0 = \frac{m}{r_1}+\frac{m}{2\pi}\iint_{-\infty}^{\infty}\frac{P\exp\{i(\xi x+\zeta z)\}}{Q}\,d\xi\,d\zeta, \tag{19}$$

$$\phi'_0 = \frac{\rho m}{2\pi}\iint_{-\infty}^{\infty}\frac{2c^2\xi^2R\,e^{y\varpi}\exp\{i(\xi x+\zeta z)\}}{Q}\,d\xi\,d\zeta, \tag{20}$$

where

$$P = (c^2\xi^2+g\varpi)[-(\rho'+\rho)c^2\xi^2+(\rho'-\rho)g\varpi]\exp\{-(h-f-y)\varpi\}$$
$$-(c^2\xi^2+g\varpi)(c^2\xi^2-g\varpi)(\rho'-\rho)[\exp\{-(h+f-y)\varpi\}+\exp\{-(h-f+y)\varpi\}]$$
$$+(c^2\xi^2-g\varpi)^2(\rho'-\rho)\exp\{(h-f-y)\varpi\},$$

$$Q = \varpi(c^2\xi^2-g\varpi)\{[(\rho'+\rho)c^2\xi^2-(\rho'-\rho)g\varpi]e^{h\varpi}+(c^2\xi^2+g\varpi)(\rho'-\rho)e^{-h\varpi}\},$$

and
$$R = (c^2\xi^2-g\varpi)\exp\{(h-f)\varpi\}-(c^2\xi^2+g\varpi)\exp\{-(h-f)\varpi\}.$$

When expressed in polar co-ordinates, which are defined by

$$\xi = \varpi\cos\theta, \quad \zeta = \varpi\sin\theta, \tag{21}$$

equation (19) becomes

$$\phi_0 = \frac{m}{r_1}+\frac{m}{\pi c^2}\int_0^{\frac{1}{2}\pi}d\theta\int_0^{\infty}\frac{M(\theta,\varpi)\cos(\varpi x\cos\theta)\cos(\varpi z\sin\theta)}{(\varpi-\varpi_0)g(\theta,\varpi)}\,d\varpi, \tag{22}$$

where

$$M(\theta,\varpi) = \sec^2\theta\{(c^2\varpi\cos^2\theta+g)$$
$$\times[-(\rho'+\rho)c^2\varpi\cos^2\theta+(\rho'-\rho)g]\exp\{-(h-f-y)\varpi\}$$
$$-(\rho'-\rho)(c^2\varpi\cos^2\theta-g)(c^2\varpi\cos^2\theta+g)\exp\{-(h+f-y)\varpi\}$$
$$+(\rho'-\rho)(c^2\varpi\cos^2\theta-g)^2\exp\{(h-f-y)\varpi\}$$
$$-(\rho'-\rho)(c^2\varpi\cos^2\theta+g)(c^2\varpi\cos^2\theta-g)\exp\{-(h-f+y)\varpi\}, \tag{23}$$

$$\varpi_0 = gc^{-2}\sec^2\theta, \tag{24}$$

$$g(\theta,\varpi) = \cos^2\theta(\varpi\rho'c^2\cosh h\varpi+\varpi\rho c^2\sinh h\varpi)-(\rho'-\rho)g\sinh h\varpi. \tag{25}$$

To check the condition (10), it will be necessary to find the limit of this integral as $x\to\infty$. To do this, first note that the singularities of the integrand lie on two

curves, $\varpi = \varpi_0$, where ϖ_0 is given by (24) and $\varpi = \varpi_1$, where ϖ_1 is given by the implicit relation

$$g(\theta, \varpi_1) = 0. \tag{26}$$

The curves do not intersect. They are shown roughly in figure 1. The second of these curves behaves in a manner dependent on F, the ratio of the speed to the critical internal wave speed, i.e.

$$F^2 = c^2\rho'/\Delta\rho g h, \quad \Delta\rho = \rho' - \rho. \tag{27}$$

Now consider the integration with respect to ϖ for a fixed value of θ and for large x. It is clear that the interval of integration can be broken into two parts: I_1 from 0 to ϖ_2 and I_0 from ϖ_2 to ∞, where $\varpi_0 > \varpi_2 > \varpi_1$.

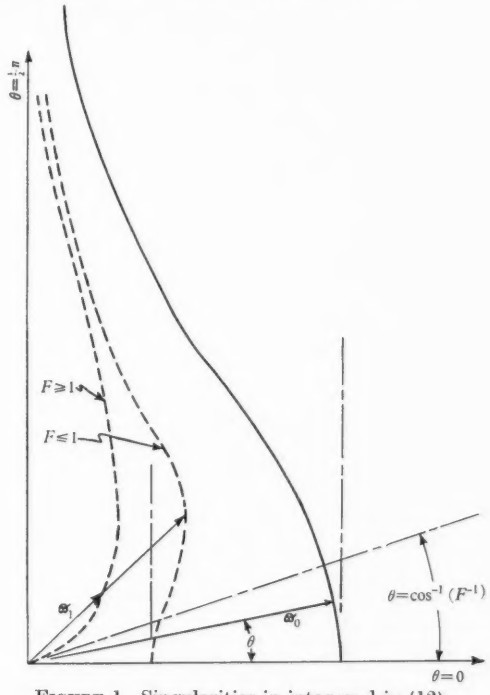

FIGURE 1. Singularities in integrand in (12).

The limit of the integral over each interval as x goes to ∞ may now be evaluated† by means of the Fourier single-integral limit theorem

$$\lim_{t\to\infty}\int_a^b f(s)\frac{\sin[t(s-s_0)]}{s-s_0}\,ds = \begin{cases} \frac{1}{2}\pi[f(s_0+0)+f(s_0-0)] & (a < s_0 < b), \\ \frac{1}{2}\pi f(a+0) & (a = s_0), \\ \frac{1}{2}\pi f(b-0) & (b = s_0), \\ 0, \quad a > s_0 \quad \text{or} \quad b < s_0. \end{cases} \tag{28}$$

The limit is zero in each case if the cosine function occurs instead of the sine function in (28).

† The application of this theorem to the question of the condition at infinity in ship wave problems is due to John V. Wehausen.

For the interval that includes the singularity at ϖ_0, only the first term in $M(\theta, \varpi)$ gives a non-zero contribution. That term can readily be written in a form such that the foregoing theorem applies. This part of the integral then gives

$$\lim_{x\to\infty} I_0 = \frac{4m\rho g}{c^2}\int_0^{\frac{1}{2}\pi} \frac{\exp\{-(h-f-y)\varpi_0\}\sec^2\theta\sin(xg\sec\theta/c^2)\cos(zg\sin\theta\cos^2\theta/c^2)\,d\theta}{\rho\exp(h\varpi_0)+(\rho'-\rho)\exp(-h\varpi_0)}. \tag{29}$$

Since this term is not zero, ϕ_0 as given by (22) violates the condition at $x = +\infty$. This can be rectified by subtracting this expression from (22). It is clear that this expression satisfies Laplace's equation; together with the other parts of the solution, it satisfies the boundary conditions.

The integral over the interval that includes the singularity at ϖ_1 can also be put into a form such that the theorem applies, although the fact that ϖ_1 is given only implicitly by $g(\theta, \varpi_1)$ requires special treatment. This part of the integral then gives

$$\lim_{x\to\infty} I_1 = -\frac{m}{c^2}\int_a^{\frac{1}{2}\pi} \frac{M(\theta,\varpi)\sin(x\varpi_1\cos\theta)\cos(z\varpi_1\sin\theta)\,d\theta}{(\varpi_1-\varpi_0)\,G(\theta,\varpi_1)}, \tag{30}$$

where $a = \cos^{-1}(F^{-1}), \quad F \geqslant 1; \quad a = 0, \quad F < 1,$

$$\begin{aligned} G(\theta,\varpi_1) = {} & \rho' c^2\cos^2\theta\cosh h\varpi_1 + h\rho'\varpi_1 c^2\cos^2\theta\sinh h\varpi_1 \\ & + h\varpi_1\rho c^2\cos^2\theta\cosh h\varpi_1 + \rho c^2\cos^2\theta\sinh h\varpi_1 \\ & - h(\rho'-\rho)\,g\cosh\varpi_1. \end{aligned}$$

Since this term is not zero, it too is subtracted from (22). Thus the total expression for the velocity potential in the layer,

$$\phi = \phi_0 - \lim_{x\to\infty} I_0 - \lim_{x\to\infty} I_1,$$

is obtained from (22), (29), and (30).

3. Forces on a thin ship

Consider a 'thin' ship in steady motion having a speed c in the direction of the x-axis, the co-ordinate system being the same as that used previously. For a deep ocean, the linearized equations have been used† to demonstrate that the ship may be replaced effectively by a distribution of sources over the centreplane section whose strength is given by $-\frac{1}{2}c\pi^{-1}\zeta_x(\alpha,\beta)$, where the shape of the hull is given by $\zeta(x, y)$. This leads to a velocity potential

$$\Phi(x,y,z) = \iint_{S_0} -\tfrac{1}{2}c\pi^{-1}\zeta_\alpha(\alpha,\beta)\,H(x,y,z;\alpha,\beta,0)\,d\alpha\,d\beta, \tag{31}$$

where S_0 is the area of the centreplane section, and H is the potential for a 'Havelock source'. The resistance, R, to the motion of the ship is then given by

$$R = 2\rho c\iint_{S_0} \Phi_x(x,y,0)\,\zeta_x(x,y)\,dx\,dy, \tag{32}$$

where, it turns out, some of the terms in Φ_x make no contribution.

† See Lunde (1951).

The same procedure may be applied to the case of a thin ship in a two-layer ocean. Again, the ship may be replaced effectively by a distribution of sources over the centreplane section whose strength is given by $-\frac{1}{2}c\pi^{-1}\zeta_x(\alpha,\beta)$, where the shape of the hull is given by $\zeta(x,y)$. The velocity potential is

$$\Phi(x,y,z) = \iint_{S_0} -\tfrac{1}{2}c\pi^{-1}\zeta_x(\alpha,\beta)\,\phi(x,y,z;\alpha,\beta,0)\,d\alpha\,d\beta, \tag{33}$$

where $\phi(x,y,z;\alpha,\beta,0)$ is given by (22) minus (29) and (30), with the following modification. The source had been taken at $(0,f,0)$. We now replace f by β and x by $(x-\alpha)$. The resistance to the motion of the ship is given by substituting this into (32).

The contribution to R from the x-derivative of the part of ϕ given by (22) is zero. Thus

$$\begin{aligned} R = \frac{4\rho^2 g^2}{\pi c^2}\iint_{S_0} dx\,dy\,\zeta_x(x,y)\iint_{S_0} d\alpha\,d\beta\,\zeta_x(\alpha,\beta) \\ \times\int_0^{\frac{1}{2}\pi}\frac{\exp\{-(h-\beta-y)\,\varpi_0\}\sec^3\theta\cos\{g(x-\alpha)\sec\theta/c^2\}}{\rho\exp(h\varpi_0)+(\rho'-\rho)\exp(-h\varpi_0)}\,d\theta \\ -\frac{\rho}{\pi}\iint_{S_0} dx\,dy\,\zeta_x(x,y)\iint_{S_0} d\alpha\,d\beta\,\zeta_x(\alpha,\beta) \\ \times\int_a^{\frac{1}{2}\pi}\frac{\varpi_1\cos\theta\,M(\theta,\varpi_1)\cos[(x-\alpha)\,\varpi_1\cos\theta]}{(\varpi_1-\varpi_0)\,G(\theta,\varpi_1)}\,d\theta. \end{aligned} \tag{34}$$

If h is made infinitely great, the second term goes to zero, and the first term goes over into the well-known Michell's integral for the wave-making resistance of thin ships

$$\begin{aligned} R = \frac{4g^2\rho}{\pi c^2}\iint_{S_0} dx\,dy\,\zeta_x(x,y)\iint_{S_0} d\alpha\,d\beta\,\zeta_x(\alpha,\beta)\int_0^{\frac{1}{2}\pi} d\theta\sec^3\theta \\ \times\exp\{g(y+\beta)\sec^2\theta/c^2\}\cos\{g(x-\alpha)\sec\theta/c^2\}, \end{aligned} \tag{35}$$

where here the origin lies in the undisturbed free surface. Thus (34) is a generalization of Michell's integral to the case of the two-layer ocean.

4. The asymptotic evaluation of the velocity potential of the ship's internal wave system

The results given above for the velocity potential due to a moving simple source are so complex that a general evaluation of the integrals does not appear to be possible. However, an asymptotic solution for large negative values of x would be useful in delineating the wave pattern far aft of the moving source.

The double integral in (22) is first reduced (asymptotically) to a single integral. The method used is exactly the same as that used to obtain (29) and (30). Note, however, that large negative values of the parameter, x, are considered. This changes the sign of the limits given by (29) and (30) and further leaves error terms of Ox^{-1}. Thus, to this degree of approximation, for $x<0$,

$$\begin{aligned} \phi(x) \sim \frac{-8\rho g m}{c^2}\int_0^{\frac{1}{2}\pi}\frac{\exp\{-(h-f-y)\,\varpi_0\}}{\rho\exp(h\varpi_0)+(\rho'-\rho)\exp(-h\varpi_0)}\sec^2\theta\sin(gx\sec\theta/c^2) \\ \times\cos(gz\sec^2\theta\sin\theta/c^2)\,d\theta \\ +\frac{2m}{c}\int_a^{\frac{1}{2}\pi}\frac{M(\theta,\varpi_1)\sin(x\varpi_1\cos\theta)\cos(z\varpi_1\sin\theta)}{(\varpi_1-\varpi_0)\,G(\theta,\varpi_1)}\,d\theta. \end{aligned} \tag{36}$$

The first integral has been evaluated for $z = 0$ (i.e. on the track) by the method of steepest descent, but the details will not be presented here. The result of the evaluation showed that the wavelength on the axis was exactly the same as that for a homogeneous ocean, and that the amplitude was only slightly different. The first integral will not be considered further here.

The second integral term in (36) describes the internal wave mode for large negative values of x. The asymptotic evaluation is difficult because ϖ_1 is not given as an explicit function of θ; there is only the implicit relation (26). Simplification is achieved if (26) is used to transform the integral so that the variable of integration is ϖ. It helps further if polar co-ordinates are used for the point of observation, i.e.

$$x = R\cos\gamma, \quad z = R\sin\gamma. \tag{37}$$

The second integral in (36), (call it I_2), has the form

$$I_2(R,\gamma) = \operatorname{Im}\int_b^\infty g(\varpi)\left[\exp\{iRh_+(\varpi)\} + \exp\{iRh_-(\varpi)\}\right]d\varpi, \tag{38}$$

where $b = 0$, $F \geqslant 1$; $b = \varpi_1(0)$, $F < 1$, and where $g(\varpi)$ is continuous and the $h(\varpi)$'s have non-zero second derivatives almost everywhere in the interval of integration, and $\varpi_1(0)$ is obtained from (26) with $\cos\theta$ set equal to unity.

It is well known that the major part of the value of the integrals in (38) arises from the vicinity of the end-points and from the vicinity of those ϖ at which $h(\varpi)$ is stationary, i.e. $h'(\varpi) = 0$; the first-order approximation of the contribution of the stationary points, being of $O(R^{-\frac{1}{2}})$, is more important than the contribution from the end-points which are of $O(R^{-1})$. If there is a stationary point, the first approximation is

$$\begin{aligned} I_2(R,\gamma) \sim{}& \operatorname{Im}\left[2\pi/Rh''_+(\varpi_2)\right]^{\frac{1}{2}} g(\varpi_2)\exp\{i[Rh_+(\varpi_2)+\tfrac{1}{4}\pi]\} \\ &+ \operatorname{Im}\left[2\pi/Rh''_-(\varpi_3)\right]^{\frac{1}{2}} g(\varpi_3)\exp\{i[Rh_-(\varpi_3)+\tfrac{1}{4}\pi]\}; \end{aligned} \tag{39}$$

here ϖ_2, ϖ_3, are the stationary points. The stationary points are given by the solutions of

$$\left.\begin{aligned} \mp\tan\gamma &= \frac{A\sinh Z + Z}{2F^2ZA^2 - A\sinh Z - Z}\left(\frac{F^2ZA - \sinh Z}{\sinh Z}\right)^{\frac{1}{2}}, \\ A &= \cosh Z + (\rho/\rho')\sinh Z \quad (Z = h\varpi). \end{aligned}\right\} \tag{40}$$

The right side of (40) is real and non-negative for all values of Z in the interval of integration. Hence, for all Z there is a γ for which (40) is satisfied. For h_+, the upper sign is used and γ is the second quadrant; for h_-, the lower sign is used and γ is in the third quadrant. The two γ's are symmetrical about π, and the two terms in (39) are equal for these values of γ. Thus only one of the terms in (39) need be computed; let it be the first.

The solution of (40) is plotted in figure 2 for $F = \frac{1}{2}$. The value of γ is π at the lower limit of the range of Z. As Z increases, γ decreases to a minimum, then increases and becomes asymptotic to π as $Z \to \infty$. The minimum point on the curve defines a critical angle, $\gamma_c = 2{\cdot}7933$. For γ smaller than γ_c, there is no solution, and hence no stationary point. Thus for $\gamma_c > \gamma$, ϕ is $O(R^{-1})$. For $\gamma_c < \gamma \leqslant \pi$, there are two solutions to (40), and hence two contributions to ϕ

of the form (39). These represent waves (as will be emphasized later), and hence there are two sets of waves for this case. This picture is true for quite a range of F for which calculations have been made, (see figure 4 for γ_c as a function of F), and is probably true for all $F < 1$.

The solution of (40) is plotted in figure 3 for $F = 2$. The value of γ_c is 2·618 for $Z = 0$, increases monotonically with increase in Z, and it becomes asymptotic to π for large values of Z. Thus for $\gamma < \gamma_c$, ϕ is $O(R^{-1})$ while within the sector ϕ is $O(R^{-\frac{1}{2}})$. Note that for $\gamma_c \leqslant \gamma \leqslant \pi$ there is only one stationary point and, hence,

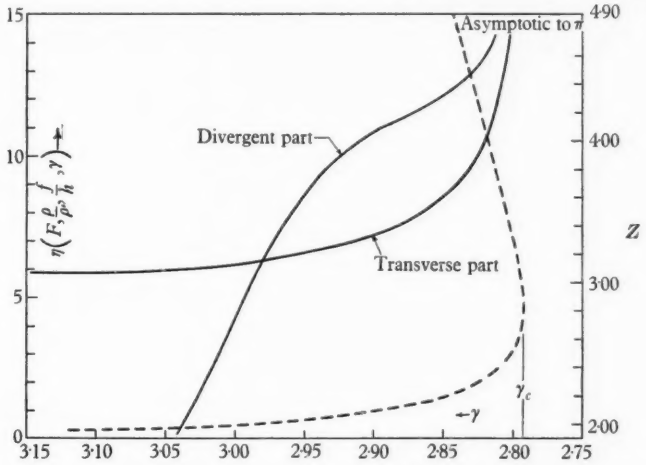

FIGURE 2. Stationary points, Z, and non-dimensional displacement factor η *vs* γ for $F = \frac{1}{2}$, $\rho/\rho' = 0{\cdot}999$, $f/h = 0{\cdot}1$. — Non-dimensional displacement factor, $\eta(F, \rho/\rho', f/h, \gamma)$. – – – Stationary points Z.

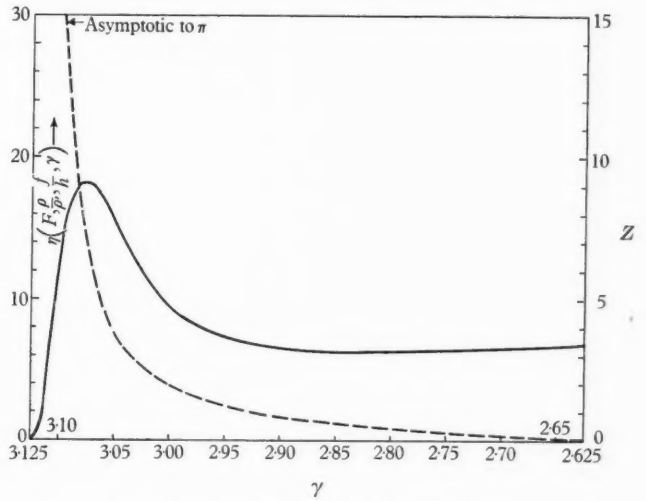

FIGURE 3. As for figure 2, but with $F = 2$.

only one set of waves propagates. This also has been verified for a wide range of values of $F > 1$. A remarkably simple expression can be obtained from (40) for γ_c when $F > 1$,

$$\pi - \gamma_c = \sin^{-1}(F^{-1}). \tag{41}$$

This is just the Mach shock angle formula! This is also plotted in figure 4.

Let the symbol Z now stand for a stationary value of Z. The first approximation of the contribution of a stationary point to the velocity potential of the internal wave is

$$\begin{aligned} I_2(R,\gamma) \sim \operatorname{Im} m &\left[\frac{\pi F A^{\frac{3}{2}}}{Rh}\right]^{\frac{1}{2}} \\ &\times \left\{ \frac{\cos\gamma}{Z\sin Z}\left[2A\cosh Z\,(Z\sinh Z)^{\frac{1}{2}} - (A\sinh Z + Z)\,\frac{(\sinh Z + Z\cosh Z)}{2(Z\sinh Z)^{\frac{1}{2}}}\right]\right. \\ &+ \frac{\sin\gamma}{F^2Z^2A - Z\sinh Z}\left[(F^2Z^2A - Z\sinh Z)^{\frac{1}{2}}\,(2F^2A^2 + 4F^2ZAB - 2A\cosh Z)\right. \\ &\left.\left. - (2F^2Z^2A^2 - A\sinh Z - \dot{Z})\,\frac{(2F^2ZA + F^2Z^2B - \sinh Z - Z\cosh Z)}{2(F^2Z^2A - Z\sinh Z)^{\frac{1}{2}}}\right]\right\}^{-\frac{1}{2}} \\ &\times \left\{ -(\rho C + \rho' D)\,C\exp\left[-\left(1 - \frac{f}{h} - \frac{y}{h}\right)Z\right] - (\rho' - \rho)\,CD\exp\left[-\left(1 - \frac{f}{h} + \frac{y}{h}\right)Z\right]\right. \\ &\left. + (\rho' - \rho)\,D^2\exp\left[\left(1 - \frac{f}{h} - \frac{y}{h}\right)Z\right] - (\rho' - \rho)\,CD\exp\left[-\left(1 - \frac{f}{h} + \frac{y}{h}\right)Z\right]\right\} \\ &\times [D\cos\theta\sin\theta\,\rho' c^2 ZA]^{-1}\exp\{i[RZ\cos(\theta - \gamma)/h + \tfrac{1}{4}\pi]\}, \end{aligned} \tag{42}$$

where

$$B = \sinh Z + \frac{\rho}{\rho'}\cosh Z, \quad C = \frac{c^2\sinh Z}{F^2A} + gh, \quad D = \frac{c^2\sinh Z}{F^2A} - gh.$$

Here the angle θ is computed from (26), with Z taken at the stationary point. For $F < 1$, there would be two such terms, one for each stationary point at a given γ; for $F > 1$, there would be only one term.

5. The evaluation of the displacement of the interface

We recall a relation at the interface

$$\phi_y(x, 0, z) = -c\eta_x. \tag{43}$$

The expression for η, the displacement of the interface† can readily be obtained for values of γ restricted to $\gamma_c \leqslant \gamma \leqslant \pi$. The solutions can be written in the form

$$\eta = \frac{1}{c}\frac{m}{R^{\frac{1}{2}}h^{\frac{1}{2}}}\eta\left(F, \frac{\rho}{\rho'}, \frac{f}{h}, Z\right)\begin{matrix}\cos\\ \sin\end{matrix}[RZ\cos(\theta - Z)/h + \tfrac{1}{4}\pi], \tag{44}$$

† The displacement of the interface due to the surface mode will not be considered. Thus, only the first-order contribution to the velocity potential from the stationary points in I_2 as given by (42) is used.

where

$$\eta\left(F, \frac{\rho}{\rho'}, \frac{f}{h}, Z\right) = (\pi FA)^{\frac{1}{2}} (ZA \sin\theta \cos^2\theta)^{-1}$$

$$\times \left\{ \frac{\cos\alpha}{Z \sinh Z} \left[2A \cosh Z (Z \sinh Z)^{\frac{1}{2}} - (A \sinh Z + Z) \frac{\sinh Z + Z \cosh Z}{2(Z \sinh Z)^{\frac{1}{2}}} \right] \right.$$

$$+ \frac{\sin\alpha}{F^2Z^2A - Z \sinh A} \left[(F^2Z^2A - Z \sinh Z)^{\frac{1}{2}} (2F^2A^2 + 4F^2ZBA - 2A \cosh Z) \right.$$

$$\left. \left. - (2F^2ZA^2 - A \sinh Z - Z) \frac{(2F^2ZA - F^2Z^2B - \sinh Z - Z \cosh Z)}{2(F^2Z^2A - Z \sinh Z)^{\frac{1}{2}}} \right] \right\}^{-\frac{1}{2}}$$

$$\times \left\{ -\frac{C}{D} \frac{(\rho C + \rho' D)}{\rho' c^2} \exp\left\{ -\left(1 - \frac{f}{h}\right) Z \right\} - \frac{\Delta\rho}{\rho' c^2} D \right.$$

$$\left. \times \exp\left\{ \left(1 - \frac{f}{h}\right) Z \right\} + \frac{2\Delta\rho}{\rho' c^2} C \exp(-Z) \sinh Z \right\}$$

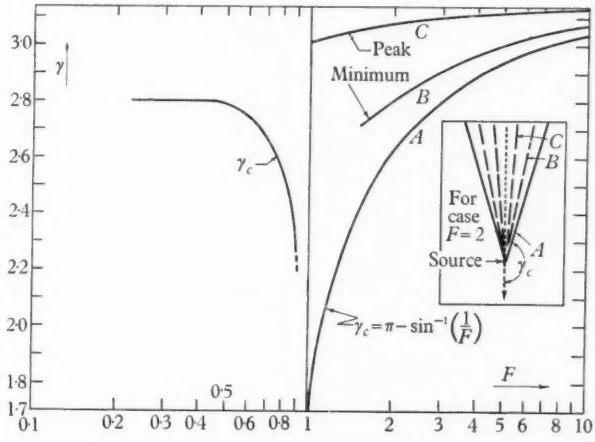

FIGURE 4. Features of $\eta(F, \rho/\rho', f/h, \gamma)$ *vs* F. Curve A gives the value of γ_c, curve B the value of γ for which η is a minimum, and curve C that for which η is a maximum.

is a non-dimensional displacement factor which is a function of the non-dimensional parameters F, ρ/ρ', f/h and the variable Z. This non-dimensional displacement factor has been computed and is plotted *vs* Z in figures 2 and 3 for $F = \frac{1}{2}$ and $F = 2$, with $\rho/\rho' = 0{\cdot}999$ and $f/h = 0{\cdot}1$. On the same graphs is plotted γ *vs* Z for the stationary values of Z.

Note that $\eta(\frac{1}{2}, \rho/\rho', f/h, Z)$ has a singularity at γ_c because $h''(\gamma_c)$ is zero. For $F = 2$, $\eta(F, \rho/\rho', f/h, Z)$ is well behaved for all Z. Here, there is a maximum at $\gamma = 3{\cdot}075$ and a minimum at $\gamma = 2{\cdot}807$.

Computations for a wide range of ratios of speed to the critical internal wave speed, i.e. F, are summarized in figures 4 and 5. In figure 4 the critical angle is plotted as a function of F for a range of $F < 1$, and for $1 \leqslant F \leqslant 10$. Note that as

F increases from a small value to unity, the half-angle of the wedge, $\pi - \gamma_c$, within which the sensible waves are contained, increases; at $F = 1$, it is $\frac{1}{2}\pi$, and for $F > 1$ it obeys the law: $\pi - \gamma_c = \sin^{-1}(F^{-1})$. Also plotted in this figure are the positions of the maxima and the minima of the non-dimensional amplitude as functions of F. In figure 5, the amplitudes of the non-dimensional amplitude at the maxima, minima, and boundary points are plotted as functions

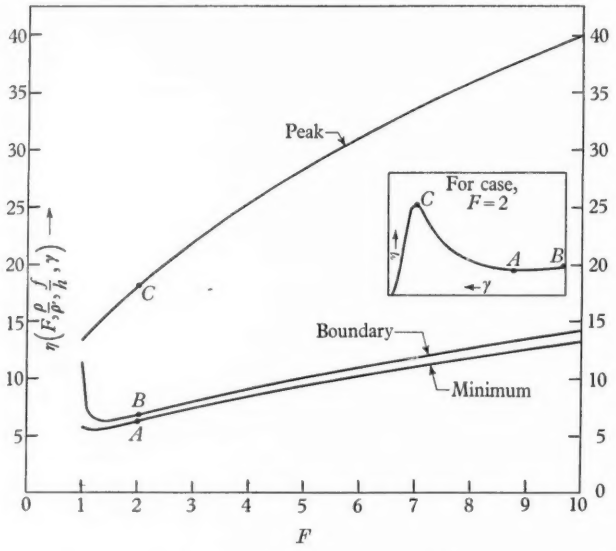

FIGURE 5. Amplitudes of maxima, minima and boundary points of $\eta(F, \rho/\rho', f/h, \gamma)$ *vs* F.

of F. Note the increase with F, which is surprising in view of the commonly held notion that the 'dead water' effect is greatly decreased for F even a small amount larger than unity.

Consider the argument of the oscillatory factor in (44). It can be written

$$RZ\cos(\theta - \gamma)/h + \tfrac{1}{4}\pi = 2\pi R/\lambda(Z) + \tfrac{1}{4}\pi, \tag{45}$$

from which it is clear that the displacement, η, along a ray, γ = constant, is wavelike. If there are two stationary values of Z for a given γ, there are two terms in (44), and hence two λ's. Thus for $F < 1$, there are two wave systems. This can be brought out further by delineating the position of the crests. This is done by setting

$$RZ\cos(\theta - \gamma)/h + \tfrac{1}{4}\pi = 2\pi N \quad \text{or} \quad 2\pi N + \tfrac{1}{2}\pi, \tag{46a, b}$$

for the cosine case and the sine case respectively, in (44), and where N is an integer. Here, Z is the stationary value for the given γ, and θ is a function of Z as previously given. Computations have been made using (26) and (40) in (46) for the same set of parameters as in figures 2 and 3. The results for $F = \frac{1}{2}$ are shown in figure 6 for four values of N. That there are two sets of waves is clear; they are

quite similar to the sets of transverse waves and divergent waves caused by a ship in an infinitely deep, homogeneous ocean. The wavelength of the transverse wave on the track is such that a plane wave having that wavelength travels at one half the critical internal wave speed. But this is just the assumed speed of the simple source. Note that the crests of the two different waves do not meet at the edge of the wedge. There is a singularity in the displacement due to the breakdown in the usual first term in the expansion by the method of stationary

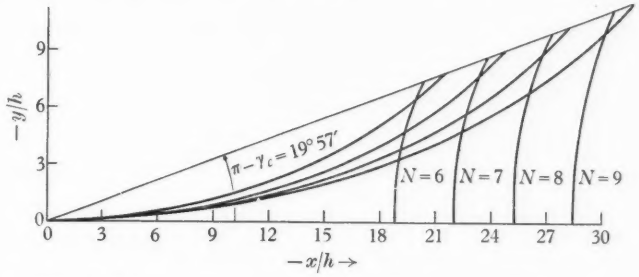

FIGURE 6. Internal wave crests for $F = \frac{1}{2}$, $\rho/\rho' = 0{\cdot}999$, $f/h = 0{\cdot}1$.

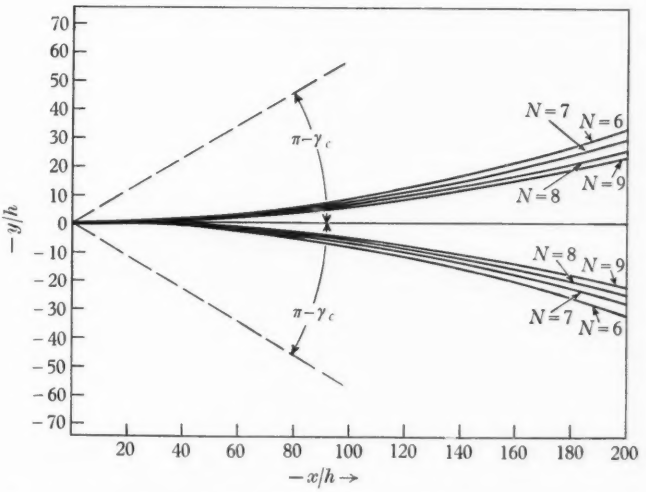

FIGURE 7. Internal wave crests for $F = 2$, $\rho/\rho' = 0{\cdot}999$, $f/h = 0{\cdot}1$.

phase. A modification of the computation in the vicinity of this point (it would be almost intractable) would probably show a gradual transition in the wave front here. The results for $F = 2$ are shown in figure 7. Here there is only one set of waves, the divergent waves.

From (44) it is clear that the displacement for any point of the crest is proportional to the product of the factors $R^{-\frac{1}{2}}$ and $\eta(F, \rho/\rho', f/h, Z)$. To visualize the amplitude of the crest, an interval, proportional to this product, perpendicular to the curve of the crest at each point on the crest is drawn, and the end-points

are connected. In figure 8 this is done for a single crest ($N = 6$) for $F = \frac{1}{2}$, and in figure 9 this is done for a single crest ($N = 6$) for $F = 2$. In each case, a three-dimensional sketch is also given to give a clearer picture of the amplitude of the crest.

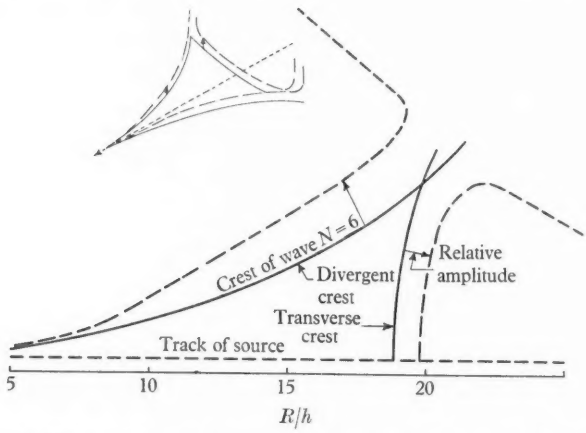

FIGURE 8. Height of internal wave crest for $F = \frac{1}{2}$, $\rho/\rho' = 0{\cdot}999$, $f/h = 0{\cdot}1$.

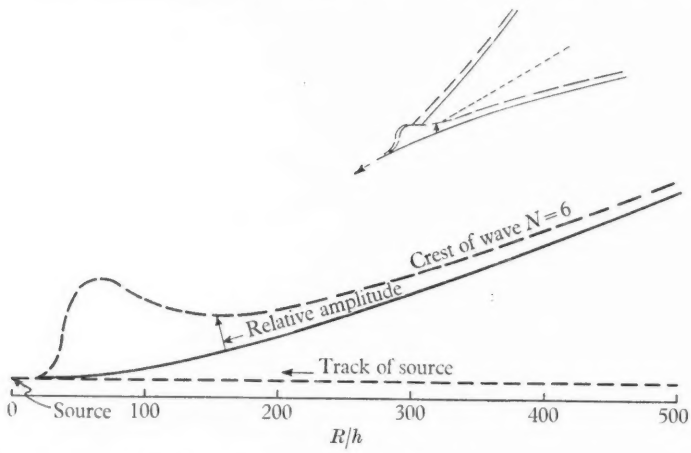

FIGURE 9. Height of internal wave crest for $F = 2$, $\rho/\rho' = 0{\cdot}999$, $f/h = 0{\cdot}1$.

6. Discussion

An integral formula for the wave-making resistance has been developed. It would be worthwhile to use this result to show how the resistance varies with speed. In particular, it would be of interest to see if there is a sudden decrease in resistance with speed at the critical internal wave velocity.

The displacement of the interface due to the internal wave mode has been described in some detail. It would also be worthwhile to treat in detail the surface wave mode to see what effect the stratification of the water has on it.

The author wishes to acknowledge the many helpful suggestions given by Professor John V. Wehausen of the University of California, Berkeley. He is also indebted to Robert Arenz for programming and executing many of the computations, and to David Brumley and the NEL drafting staff for assistance with the figures.

REFERENCES

Ekman, V. W. 1904 On dead water. Norwegian North Polar Expedition, 1893–1896. *Sci. Res.* **5**, Christiana.

Hogner, E. 1923 Contributions to the theory of ship waves. *Arch. Mat. Astr. Fys.* **17**, 1–50.

Hudimac, A. A. 1958 The motion of a body in a fluid with a free surface and irregular solid boundaries. Dissertation Univ. Calif. May 1958; also *Univ. Calif. Inst. Engng Res.* Berkeley, Calif. Ser. **85**, no. 5.

Kelvin, Lord, 1887 On the waves produced by a single impulse in water of any depth, or in a dispersive medium. *Proc. Roy. Soc.* A, **42**, 80–5.

Kochin, N. E. 1949 *Collected Works* (Academy of Sciences USSR), Vol. I, pp. 448, 508.

Lamb, H. 1916 On waves due to a travelling disturbance, with an application to waves in superposed fluids. *Phil. Mag.* **31**, 386–99.

Lunde, J. K. 1951. On the linearized theory of wave resistance of displacement ships in steady and accelerated motion. *SNAME*, **59**, 26–76.

Peters, A. S. 1949 A new treatment of the ship wave problem. *Commun. Pure Appl. Math.* **2**, 123–48.

Sretenskii, L. N. 1959 On the wave resistance of ships in the presence of internal waves. *Izv. Akad. Nauk C.C.C.R., Otdelenie Tekhnicheskikh*, **1**, 56–63.

Timman, R. & Vossers, G. 1953 The linearized velocity potential round a Michell-ship. *Technische Hogeschool, Laboratoriam voor Scheepsbouwkaunde, Delft, Rappart* **1**,

Warren, F. W. G. 1960 Wave resistance to vertical motion in a stratified fluid. *J. Fluid Mech.* **7**, 209–29.

An experimental investigation of the oscillating lift and drag of a circular cylinder shedding turbulent vortices

By J. H. GERRARD

Department of the Mechanics of Fluids, Manchester University

(Received 13 March 1961)

The oscillating lift and drag on circular cylinders are determined from measurements of the fluctuating pressure on the cylinder surface in the range of Reynolds number from 4×10^3 to just above 10^5.

The magnitude of the r.m.s. lift coefficient has a maximum of about 0·8 at a Reynolds number of 7×10^4 and falls to about 0·01 at a Reynolds number of 4×10^3. The fluctuating component of the drag was determined for Reynolds numbers greater than 2×10^4 and was found to be an order of magnitude smaller than the lift.

1. Introduction

In the last 30 years more than sixty papers have been published on subjects closely related to vortex shedding from circular cylinders in subsonic flow. Apart from the fact that the phenomenon is far from completely understood, this continued interest in a classical subject is partly due to improved instrumentation, making possible the measurement of the intensity of fluctuating quantities. Recently renewed interest has followed on Lighthill's publications (1952, 1954) on aerodynamic sound. Fifteen of the papers mentioned above are concerned with the acoustical concomitant of vortex shedding known as Aeolian tones. Lighthill's theory was applied to the problem of Aeolian tones by Curle (1955) and Phillips (1956). They show that in the presence of a rigid body the sound field is dominated at low Mach numbers by dipole radiation attributable to the fluctuating pressure at the surface of the body.

In the case of a circular cylinder shedding vortices, the main component of the acoustic radiation is a single dipole field which results from a surface pressure distribution, equivalent to that which would be produced by a fluctuating circulation round the cylinder in inviscid flow: the integral of this surface pressure distribution is the fluctuating lift. A second but smaller component is also produced as vortices of alternate sign grow and pass downstream; it has twice the frequency of the fluctuating lift and arises from the pressure distribution responsible for the fluctuating drag.

It can be shown, by applying dimensional analysis to the fundamental equation of Curle and Phillips, that the acoustic intensity at large distances

from a cylinder of finite length in the plane of symmetry bisecting the cylinder at right angles, is given by

$$I \propto \frac{\rho}{a^3} \frac{\sin^2\theta}{r^2} U^6 S^2 \overline{l^2}\, \overline{C_L^2}. \tag{1}$$

Bars denote means with respect to time, and

ρ = free stream density,
a = free stream speed of sound,
r, θ = polar co-ordinates, $\theta = 0$ being the upstream direction,
U = free stream velocity,
$S = Nd/U$ = Strouhal number,
d = cylinder diameter,
N = vortex shedding frequency,
l = a representative length of the cylinder which will depend on the phase variation along the cylinder length
C_L = lift coefficient = (lift per unit length)/$\frac{1}{2}\rho U^2 d$.

Equation (1) relates the intensity of Aeolian tones to the parameters of the flow. In order to compare experimental investigations of the radiated sound with this equation, resort must be had to experimental evidence or to assumptions concerning the parameters S, l and C_L. The Strouhal number, S, is a well-established function of Reynolds number for the whole of the range (35 to 10^5) within which vortices are shed; see, for example, Cometta (1957), Gerrard (1955). The value of S, in fact, differs by less than 10 % from the value 0·20 for Reynolds numbers greater than about 300. This parameter will produce no spectacular variation in equation (1).

The purpose of the present investigations is to determine the fluctuating lift coefficient as a function of Reynolds number. The spanwise correlation of the oscillations which determine the effective length l will not be discussed here.

2. Experimental apparatus

2.1. *The wind tunnel*

A return-circuit wind tunnel of 20 in. × 20 in. working section was used for these experiments. The tunnel was designed to have a low turbulence level. The intensity of the axial component of turbulence was less than 0·30 % at distances greater than 3 in. from the walls. The thickness of the boundary layer on the tunnel walls at the model position was $1\frac{1}{2}$ in.

The models were mounted in the centre of the 10 ft. long working section; they spanned the tunnel vertically mid-way between the side walls. The static pressure varied from floor to roof at the model position by about $\frac{3}{4}$ % of the kinetic pressure. The working section static pressure was atmospheric and made constant along the working section in the absence of the model by adjustment of the position of the roof.

Corrections to the velocity of the air flow to account for the effect of the tunnel walls were investigated in the manner described by Pankhurst & Holder (1952).

These included a consideration of the lift correction. The only significant corrections were found to be those due to the blockage of the flow by the cylinder and its wake.

2.2. *Models*

The circular-cylinder models were metal tubes and had outside diameters of 3, $1\frac{1}{2}$, 1, $\frac{9}{16}$ and $\frac{1}{4}$ in., there being two models of 1 in. diameter. The pressure pick-ups were mounted midway along the length of the cylinders. In the case of the cylinders of smaller diameter, electrical connexions were taken along the axis of the cylinder from the pick-up to a pre-amplifier outside the tunnel. The

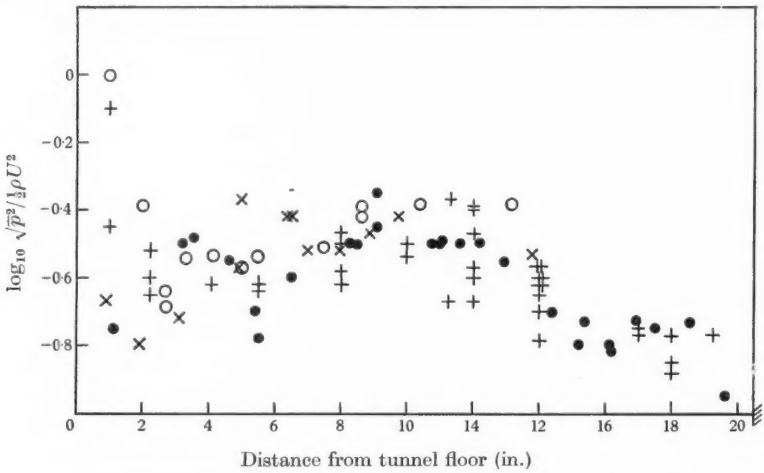

FIGURE 1. Spanwise variation of the fundamental component of oscillating pressure 120° from the front of the cylinder ($\theta = 0°$) on 1in. diameter cylinders.

	Tunnel	Model	$\log_{10} R$
●	Low turbulence	No. 1	4·46
+	Low turbulence	No. 2	4·46
×	Open circuit	No. 2	4·36
○	Open circuit	No. 2	4·59

3 in., $1\frac{1}{2}$ in., and one of the 1 in. diameter models had the preamplifier mounted inside the model close to the pressure pick-up. This was found not to increase the true to spurious signal ratio because vibration of the leads and of the pre-amplifier produced roughly equal effects.

Various types of cylinder mounting were tried in an attempt to reduce cylinder vibration to a minimum. Rigid contact with the tunnel floor and roof increased the vibrations since these vibrated at the vortex shedding frequency under the driving force of the wake. No appreciable effect on the cylinder surface pressure at the centre of the tunnel was observed when the mounting was changed. Resonance vibration was, of course, avoided but the conclusion reached after many unsuccessful attempts to eliminate vibration was that it is virtually impossible to produce a rigid cylinder.

2.3. *Pressure pick-up position*

The sensitive area of the pressure pick-up was flush with the cylinder surface. Measurements at various positions round the circumference of the model were made by rotating the cylinder. The 3 in. diameter cylinder carried two pressure pick-ups separated by 1 in. in the spanwise direction: these could be rotated independently to determine the phase distribution of the fluctuating pressure round the circumference.

The pressure pick-up was generally at the centre of the tunnel. Only with the 1 in. models was a spanwise traverse made. The results are shown in figure 1. This graph also illustrates the repeatability of the results. The measurements in the low turbulence tunnel were made with two models (both 1 in. diameter) and with different mountings. Some measurements were made in an open-circuit wind tunnel of the same working-section cross-section. This had a free stream turbulence intensity of 7–10 %, some 200 times greater. At the Reynolds numbers investigated this increased turbulence had no apparent effect.

Despite the large scatter (the greatest spread excluding points close to the floor is about 6db), there appears to be some systematic variation across the span. There is little variation over the centre third of the model length and end-effects, if such they be, have not been investigated. In what follows all the measurements were obtained at the centre of the low-turbulence tunnel.

2.4. *The pressure pick-ups*

The pressure pick-ups used are essentially condenser microphones. Piezoelectric gauges were tried but proved in this application to be more sensitive to vibration than to the pressure on their surface. The pressure pick-ups are the only part of the instrumentation which is in any way novel and they will therefore be described fully. They are easily made and fit flush with the cylinder surface. A cross-section of what may be called the standard pressure gauge fitted in most models is shown in figure 2. Those in the 3 and $\frac{1}{4}$ in. diameter models are differently mounted but the same in principle.

The design is based on the 'condenser microphone with solid dielectric' described by Kuhl *et al.* (1954). In essence the microphone consists of an insulated back-plate and a metal-foil front plate separated by a dielectric foil. The microphone functions by the applied pressure compressing the occluded air between the solid dielectric and the back-plate; the signal is produced by the fluctuations in capacity.

Here the back-plate is simply a 4 BA cheesehead screw with the head turned down beyond the slot and then grooved. This is held in a $\frac{1}{2}$ in. Perspex cylinder which fits across the inside of the model as shown in the figure, and the part protruding is machined off. The signal lead (a metal rod) is held against the back-plate screw. The front plate of the condenser microphone is a 0·001 in. silver foil which is soldered at one point to the cylinder surface which is the earth connexion. The solid dielectric consists of a thin piece of paper (typing copy paper) soaked in a silicone preparation and dried. Without the silicone treatment the microphone self-noise is high. The paper and silver foil are

smoothed in place and pressed hard onto the back-plate and secured with a little silicone varnish.

The sensitivity of such an instrument with a circular sensitive area of $\frac{1}{4}$ in. diameter is about -110 db on 1 V/dyne cm^{-2} or 3·16 μV/dyne cm^{-2}, and this remains constant to within a few decibels in 12 months; the short-term stability is also good. When the mean ambient pressure changes, the calibration changes if there is no leak between the atmosphere and the occluded air within the microphone. No leakage was included in these pressure gauges and so a small error is introduced. The mean pressure on the cylindrical-model surface differed from atmospheric between the limits of $+7$ cm of water and -20 cm of water according to position at the highest tunnel speed. Calibration of the microphones with varying ambient pressure showed that for this range of ambient

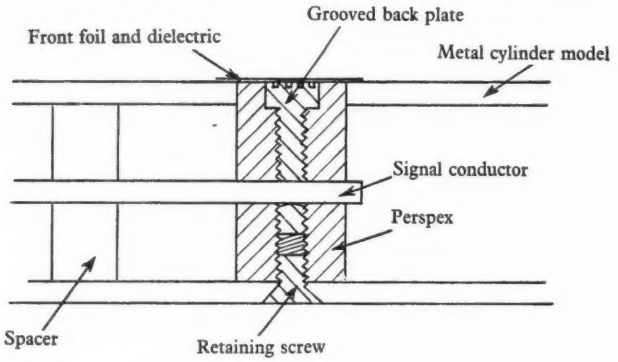

FIGURE 2. Pressure pick-up.

pressure the sensitivity varied by less than 1 db from -110 db on 1 V/dyne cm^{-2} and so no effort has been made to correct for the variation or to construct a leak in the pressure gauge.

The pressure pick-ups covered a large angular range on the cylinder surface. It was fortunate that in this application the large size of the sensitive area was relatively unimportant. The fluctuating pressure intensity only varies rapidly with position at the front and rear of the cylinder where it contributes little to the lift. Pressure distributions were measured with the larger models. With models of diameter less than 1 in. measurements were made in the region $90° < \theta < 150°$, in which the intensity is almost independent of the angle θ, where θ is the angle subtended at the axis, and is measured from the front of the cylinder. To determine the lift it was assumed that the angular distribution of pressure was the same on the smaller diameter cylinders as it was on the larger.

2.5. *Measuring apparatus*

A block diagram of the measuring and calibration apparatus is shown in figure 3 which needs little explanation. The pressure pick-up was calibrated by comparison with a B and K type 4111 condenser microphone by enclosing both in a closed coupler driven by a loudspeaker. This was done during each series of

measurements whilst the model was in the wind tunnel. The electronic apparatus following the pre-amplifier was also calibrated by inserting a standard signal at the relevant frequencies during each set of measurements.

Initially the wave analyser was a set of $\frac{1}{3}$-octave filters centred at fixed frequencies; later, a Muirhead D-788-A low-frequency analyser was used.

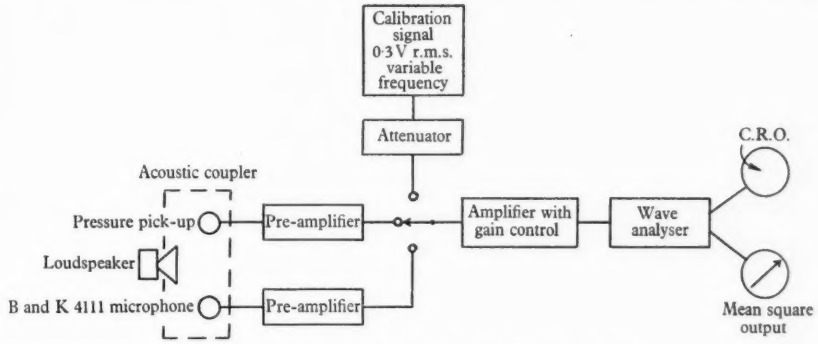

FIGURE 3. Measuring and calibration apparatus.

3. Experimental results

Extensive measurements have only been made with models of diameters 1 and 3 in. The other models were used to extend the Reynolds number range of the measurements. The appearance of the signal from the pressure pick-up was similar in all cases: frequency and intensity varied with position on the cylinder and with the flow parameters, but in all cases the signal had the appearance of a narrow band of noise, that is, a pure-tone amplitude modulated with lower frequencies. Some examples of the appearance of the traces on the cathode-ray tube are shown in figure 4. The modulation of the signal appears random, as would be expected if the governing mechanism depended on the details of a flow structure which was turbulent.

3.1. *Frequency*

The signal is close enough to a pure tone for frequencies to be determined by means of a Lissajous figure. It is simple, however, to use a narrow band filter of variable frequency. In all cases the latter method was used. This measurement served as a check that the cylinder was not executing some strong vibration. When this occurred the results were discarded. Some of the frequency measurements are plotted in figure 5, which shows agreement with previous measurements. The symbols on figure 5 refer to the same cylinder diameters as those on figure 10.

3.2. *Spectra*

The spectrum of the pressure fluctuations varied with position round the cylinder. It was rich in the second harmonic (the frequency of the fluctuating drag) at the rear of the cylinder ($\theta = 180°$), but almost lacking in harmonics at

angles θ less than 120°. In general, the width of the spectrum increased with increased velocity. Three observed spectra are shown in figure 6. As velocity increases there appears to be a relative increase in the signal at frequencies above the fundamental. Only at high fundamental frequencies does the signal below the fundamental frequency increase with velocity. The trend, however, is a broadening of the spectra as velocity is increased. If the broadening is due

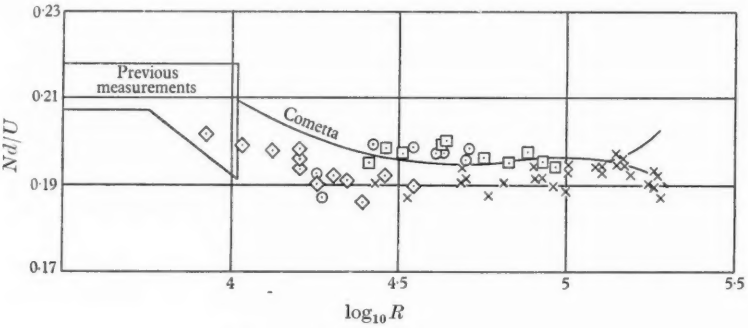

FIGURE 5. Strouhal number.

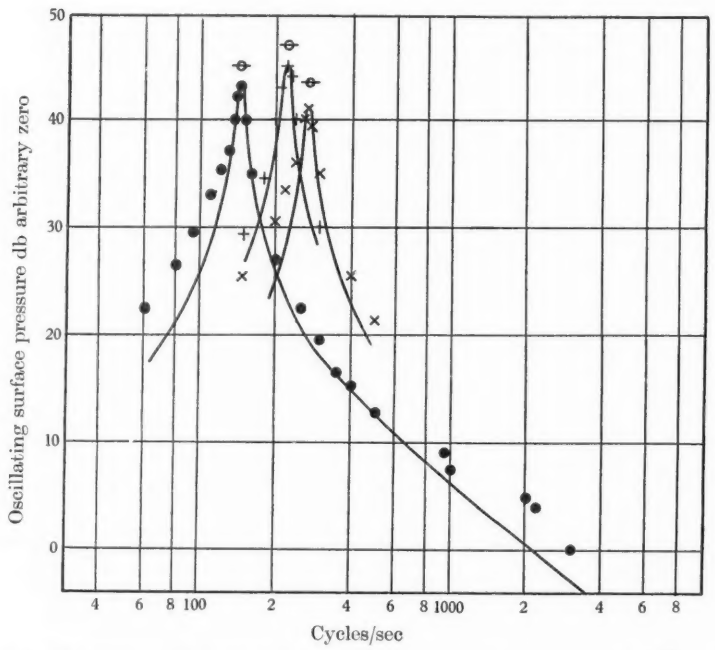

FIGURE 6. The increase of spectral width with increase of free-stream velocity; cylinder diameter 1 in., measurements at the surface 90° from the front of the cylinder. ●, 1660 cm sec^{-1}; +, 2670 cm sec^{-1}; ×, 3230 cm sec^{-1}; ⊖, level measured with no filter; ——, curve for pure tone signal.

to turbulent fluctuations we can expect the spectra to be broader at higher Reynolds numbers.

The reduced intensity at the higher velocity was often observed: two different readings appear to be possible at the high velocities as can be seen in figure 10. This behaviour is unexplained. It is perhaps worth noting in connexion with these spectra that some measurements were made up to 16·5 kc/sec on signals such as those in figure 6. The level fell off monotonically as it is shown doing in figure 6 and no peaks were observed in the spectrum at higher frequencies. This is contrary to the findings of Shaw (1951).

3.3. *Angular distribution of phase*

The 3 in. model was equipped with two pressure gauges separated by 1 in. in the spanwise direction; these could be rotated independently. Measurements were thus taken of the phase difference between the fundamental-frequency

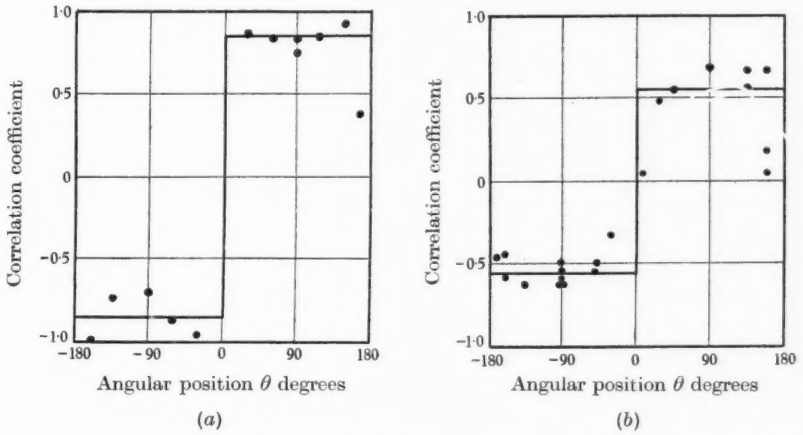

FIGURE 7. Angular distribution of surface-pressure correlation-coefficient on the 3 in. diameter model. (*a*) Reynolds number = 114,000. (*b*) Reynolds number = 85,400.

signals of the two gauges, one at a fixed position at $\theta = 90°$, the other in positions from $\theta = -180°$ to 180°. The results are shown in figure 7. They indicate essentially that the pressure is in phase over one side of the model and 180° out of phase with that on the other side. It is seen, however, that the correlation has dropped significantly from unity even in the $\frac{1}{3}$ diameter separation of the gauges. Lack of correlation may be due either to phase change of the fundamental frequency or to the change in phase of the fluctuations in the amplitude along the span. Spanwise-variation investigations have been deferred to later and will involve further experimental work. Little error will be introduced by assuming that the signal is in phase from 0 to 180 ° and of opposite phase on the other side. Though the transition may not occur rapidly at $\theta = 0$ and 180° the signal level is small in these regions.

3.4. *Angular distribution of intensity*

The distribution of oscillating pressure round the cylinder is shown in figure 8 for the fundamental-frequency component. It is seen not to vary significantly with Reynolds number. Comparison is made with the experimental results of McGregor (1957) obtained with a $1\frac{1}{8}$ in. cylinder. The values plotted are uncorrected for the size of the sensitive area of the pressure gauge.

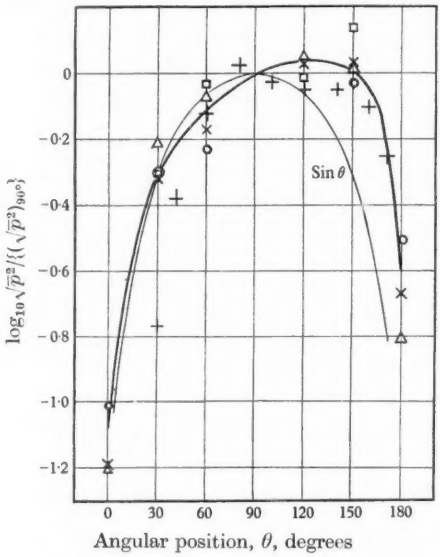

FIGURE 8. Angular distribution of intensity of surface pressure at the fundamental frequency. $\log_{10}R$: □, 4·1; △, 4·3; ×, 4·8; ○, 5·2; +, McGregor 4·64.

The second harmonic distribution is shown in figure 9 for several velocities and three cylinder diameters. McGregor's values are again included. The measurement of second harmonic intensity is difficult because it is so much smaller than the fundamental, except at $\theta = 180°$. The measurements fall reasonably on one curve nevertheless.

Measurements with the cylinders of diameters other than 1–3 in. inclusive were confined almost entirely to the fundamental frequency in the angular range 90–150°. It was assumed that the angular distribution of intensity was the same in all cases. The fundamental-fluctuating pressure coefficient is plotted as a function of Reynolds number in figure 10 for several positions on the cylinders. At high velocities there appear to be two intensities possible in some cases. These are joined by vertical lines on figure 10. No explanation is offered for this behaviour.

3.5. *The lift and drag*

The fact that the pressure is in phase on one side of the cylinder and out of phase with that on the other side allows us to calculate the lift on the cylinder by integrating the pressure. The assumption of no change in the angular dis-

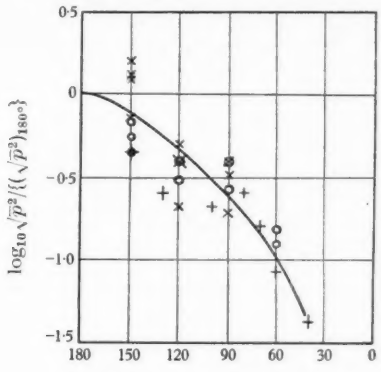

FIGURE 9. Angular distribution of intensity of surface pressure at the second harmonic frequency. ⊙, 1 in. diam. cylinder; ×, 3 in. diam. cylinder; +, McGregor, $1\frac{1}{8}$ in. diam.

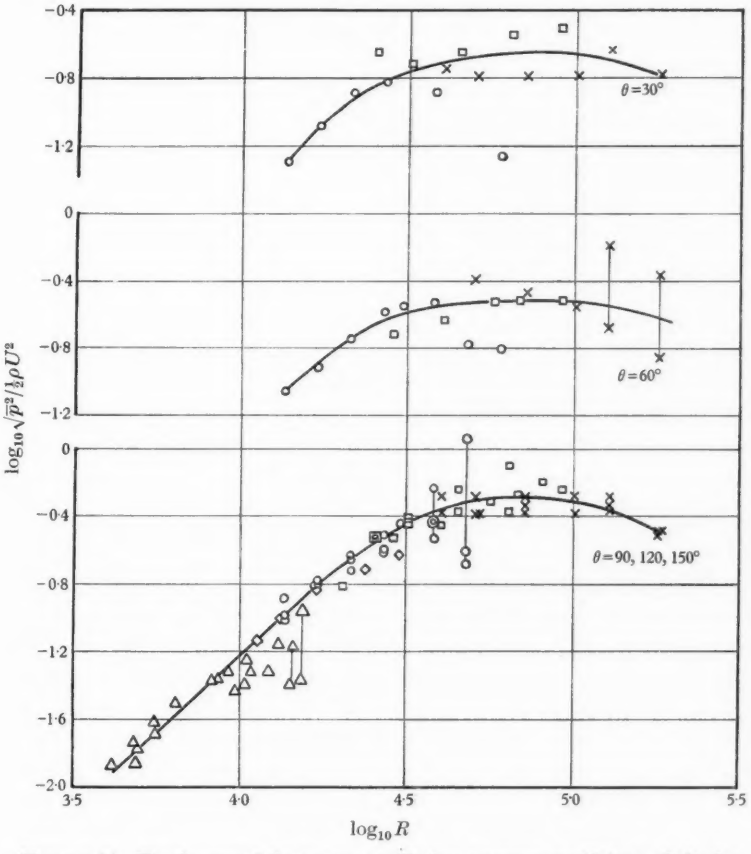

FIGURE 10. Fundamental frequency oscillating pressure coefficient. Cylinder diameter in in.: ◇, 0·56; ○, 1; □, 1·5; ×, 3; △, 0·25.

tribution of phase or intensity down to the lowest Reynolds numbers investigated seems unlikely to produce a large error in the lift. There appears to be no reason why the phase distribution should change with Reynolds number: this belief is substantiated by the predicted dipole nature of the radiated sound field (Curle 1955) which has also been observed at lower Reynolds numbers (Gerrard 1955). The intensity distribution may depend upon the Reynolds number for it was only measured in that range in which the r.m.s. lift does not vary. Even if the angular distribution of intensity changes to a $\sin\theta$ curve, the resulting change in the lift is only about 10 %.

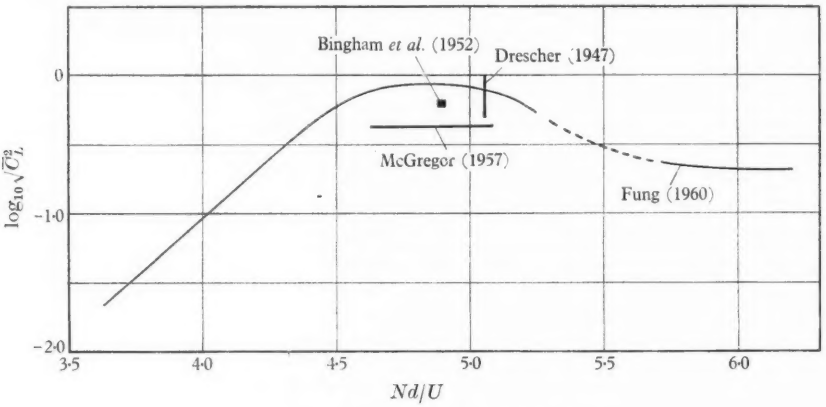

FIGURE 11. Root-mean-square lift coefficient.

The calculated lift coefficient is plotted in figure 11 and compared with the measurements of other workers. The agreement is seen to be fairly good. The measurements of Bingham, Weimer & Griffith (1952) were obtained in a shock tube during the first few cycles of oscillation of the lift. Drescher's (1947) measurements were in water at a frequency low enough to follow with a manometer. Fung's (1960) measurements refer to the more random fluctuations beyond the critical Reynolds number and were obtained directly as the lift force on a section of the cylinder about two diameters in length. The cylinder was 12 in. diameter and 72 in. long. McGregor's (1957) experimental arrangement was similar to that of the author. His measurements lie below those reported here by about 6 db, which is larger than the errors believed to be present by either author. More recent measurements by Humphreys (1960) at Reynolds numbers above 4×10^4 agree with both those of McGregor and those of the author. Humphreys's two sets of measurements were obtained by altering the geometry at the cylinder-wall junction. We have observed an effect of small disturbances at the cylinder ends (Gerrard 1958): the pressure at the cylinder centre was found to be altered by 1 db (10 % of p^2) by small alterations of end geometry. The 6 db change reported by Humphreys may be attributable to the fact that his measurements are an average over the whole cylinder and therefore include any changes of spanwise distribution caused by the change in end conditions.

The fluctuating component of the drag may be determined from the second harmonic pressure intensities if we make an assumption about the phase. The most logical assumption is that the second harmonic pressure is of the same phase over all the cylinder. The resulting drag coefficients are between 10 and 13 times less than the lift coefficients and are plotted in figure 12. They are seen to agree with McGregor's values which are included for comparison. There is a large scatter in the measurements which is attributed to the difficulty of accurate measurements of the second harmonic in the presence of the much larger fundamental component.

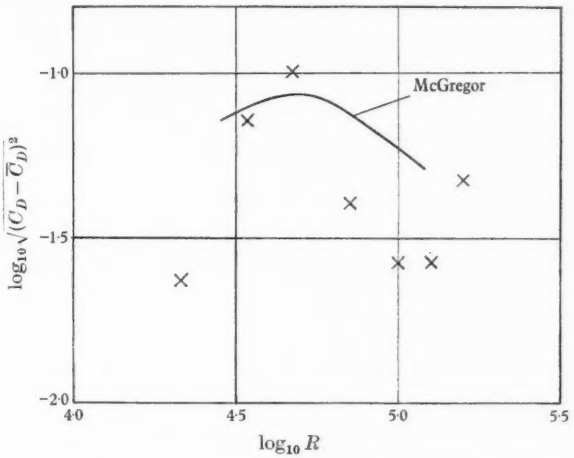

FIGURE 12. Root-mean-square oscillating component of the drag.

4. Discussion

The work reported in this paper extends the range of measured lift coefficient to lower Reynolds numbers than other workers achieved. The result of this extension of the Reynolds number range is the observed large change in lift coefficient, by nearly two orders of magnitude, as the Reynolds number changes from 4000 to 20,000. In this range the experiments indicate a power law relation between lift coefficient and Reynolds number, viz. $\sqrt{\bar{C}_L^2} \propto R^{1\cdot7}$. From equation (1) we expect the intensity of the sound radiated by the flow past the cylinder to vary with Reynolds number like $\bar{C}_L^2 \bar{l}^2$. In the Reynolds number range from 1500 to 10,000 the measured sound intensity was found to vary like R^3 by Gerrard (1955). The implication is that the effective length, l, of the cylinder varies little with Reynolds number in this range since almost all the Reynolds number variation of the sound intensity can be accounted for by that of the lift coefficient. Our intention is to investigate the spanwise structure of the flow over this Reynolds number range. The measurement of the oscillating component of the drag is difficult at Reynolds numbers less than 10^4 since large pressures are expected only on small diameter cylinders. Whether or not the oscillating drag coefficient falls off below this Reynolds number is unknown.

REFERENCES

Bingham, H. H., Weimer, D. K. & Griffith, W. 1952 The cylinder and semicylinder in subsonic flow. *Princeton Univ. Tech. Rep.* II-13.

Cometta, C. 1957 An investigation of the unsteady flow pattern in the wake of cylinders and spheres using a hot-wire probe. *Brown Univ. Tech. Rep.* WT-21.

Curle, N. 1955. The influence of solid boundaries on aerodynamic sound. *Proc. Roy. Soc.* A, **231**, 505.

Drescher, H. 1947 *Model Testing Techniques. II.* 6. *Measurement of unsteady pressure.* AVA monographs D2. (Translation: *Aero. Res. Counc. Rep.* no. 11,391.)

Fung, Y. C. 1960 Fluctuating lift and drag acting on a cylinder in a flow at supercritical Reynolds numbers. *J. Aerospace Sci.* **27**, 801.

Gerrard, J. H. 1955 Measurements of the sound from circular cylinders in an air stream. *Proc. Phys. Soc.* B, **68**, 453.

Gerrard, J. H. 1958 Measurements of the fluctuating pressure on the surface of a circular cylinder. Part I. Cylinder of 1 in. diameter. *Aero. Res. Counc. Rep.* no. 19,844.

Humphreys, J. S. 1960 On a circular cylinder in a steady wind at transition Reynolds numbers. *J. Fluid Mech.* **9**, 603.

Kuhl *et al.* 1954 Condenser transmitters and microphones with solid dielectric for airborne ultrasonics. *Acustica*, **4**, 519.

Lighthill, M. J. 1952 On sound generated aerodynamically. *Proc. Roy. Soc.* A, **211**, 564.

Lighthill, M. J. 1954 On sound generated aerodynamically. *Proc. Roy. Soc.* A, **222**, 1.

McGregor, D. M. 1957 An experimental investigation of the oscillating pressures on a circular cylinder in a fluid stream. *Univ. Toronto Inst. Aerophys. Tech. Note* 14.

Pankhurst, R. C. & Holder, D. W. 1952 *Wind Tunnel Technique*, Ch. 18. London: Pitman.

Phillips, O. M. 1956 The intensity of Aeolian tones. *J. Fluid Mech.* **1**, 607.

Shaw, R. A. 1951 A preliminary investigation of the acoustic theory of airflow. Low speed wind tunnel tests on an aerofoil and a cylinder. *Aero. Res. Counc. Rep.* no. 13,795.

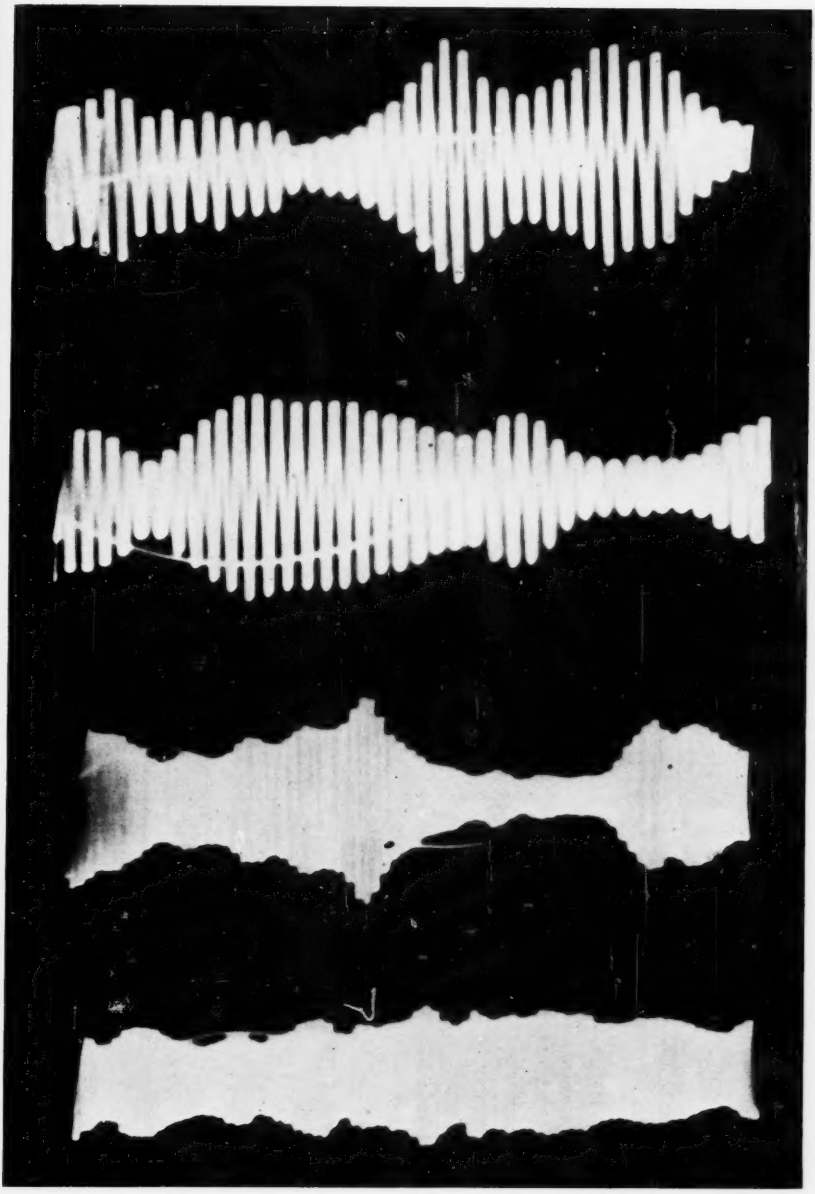

FIGURE 4. Cathode ray oscillograms of surface pressure.

Analytical theory of turbulent diffusion

By P. H. ROBERTS†

Institute of Mathematical Sciences, New York University, New York 3

(Received 27 June 1960 and in revised form 7 March 1961)

Recently Kraichnan (1959) has propounded a theory of homogeneous turbulence, based on a novel perturbation method, that leads to closed equations for the velocity covariance. In the present paper, this method is applied to the theory of turbulent diffusion and closed equations are derived for the probability distributions of the positions of marked fluid elements released in a turbulent flow.

Two topics are discussed in detail. The first is the probability distribution, at time t, of the displacement of an element from its initial position. In homogeneous flows, this distribution is found to resemble that for classical diffusion but with a variable coefficient of diffusion which is proportional to $v_0^2 t$ for $t \ll l/v_0$ and which approaches a constant value $\doteq lv_0$ for $t \gg l/v_0$ (l = macroscale, v_0 = r.m.s. turbulent velocity).

The second topic treated is the joint probability distribution of the displacements of two fluid elements. Particular attention is focused upon the probability distribution of relative displacement, i.e. Richardson's distance-neighbour function. This is found to be Gaussian for separations r which are large ($\gg l$). For smaller separations ($r \ll l$), its behaviour at high Reynolds numbers is found to be quite well expressed in terms of a variable diffusion coefficient $K(r,t)$, as suggested by Richardson (1926). For all but extremely short times, $K(r,t)$ is found to depend only on r and on the form of the inertial range spectrum $E(k)$. On assuming $E(k) \propto v_0^2 l(kl)^{-\frac{5}{3}}$ as results from Kraichnan's approximation (1959), one finds $K(r) \propto v_0 l(r/l)^{\frac{4}{3}}$. On the basis of similarity arguments of the Kolmogorov type, which give $E(k) \propto v_0^2 l(kl)^{-\frac{5}{3}}$, one finds $K(r) \propto v_0 l(r/l)^{\frac{4}{3}}$ as, in fact, Richardson originally proposed. The dispersion $\langle r^2 \rangle$ is proportional to $l^2(v_0 t/l)^4$ on Kraichnan's theory; while $\langle r^2 \rangle \propto l^2(v_0 t/l)^3$ on the similarity theory. This illustrates that the behaviour of $\langle r^2 \rangle$ is very sensitive to the spectrum.

1. Introduction

The aim of the theory of turbulent diffusion is to determine in a statistical sense the migration of marked particles as they are carried along with a turbulent flow. Like molecular motion in a dilute gas of discrete particles, turbulent diffusion is a linear process if the convected particles have no reaction on the flow; i.e. the probability distribution for the position of a marked particle in space obeys the superposition rule and changes in time according to a linear equation. Unlike classical molecular motion, the motion of neighbouring fluid elements in a

† Present address: Physics Department, King's College, Newcastle upon Tyne 1.

continuum is correlated, although one expects that over distances large compared to the macroscale l of the turbulence this correlation is weak and that elements separated by such distances move almost independently. Furthermore, unlike classical molecular diffusion, turbulent diffusion is not a Markoff process. However, one expects that over times large compared to l/v_0, where v_0 is the root mean square fluid velocity, the fluid elements will suffer many essentially uncorrelated deflexions by the energy-containing eddies and that accordingly their displacement distribution will be almost Gaussian. Under such circumstances, one expects that the spread of marked particles carried by the fluid will indeed resemble classical diffusion, and that it will be possible to define a coefficient of eddy diffusivity. An analytical basis for these qualitative observations is given in § 2.

Particles which start out simultaneously at nearby points have closely similar histories in any one realization of the turbulent flow (and over times which are not too long). For such times, their relative motion is unaffected by eddies whose spacial scale is large compared to the initial separation; such eddies give nearly equal displacements to the two points. The change in the separation r is governed by the smaller eddies, particularly those whose length scale is of the same order as r. Thus, in a flow of the high Reynolds number, we expect that while the particles are separated by a distance appropriately small compared to l their relative diffusion will be governed by the inertial range spectrum of the turbulent flow, and will be unaffected by the structure of the energy-containing eddies. An analytical basis for these surmises is given in § 3, and a form is proposed for the variable diffusion coefficient $K(r)$ introduced by Richardson (1926). This form for $K(r)$ is very sensitive to the inertial range spectrum $E(k)$. On assuming that $E(k) \propto v_0^2 l(kl)^{-n}$, it is shown that $K(r) \propto v_0 l(r/l)^n$ and that, in consequence, $\langle r^2 \rangle \propto l^2(v_0 t/l)^{2/(2-n)}$. However, on the basic approximation from which these results are derived, the energy-containing eddies do play a part in the relative diffusion process. It is shown, however, that when modifications of the theory are made to exclude this effect, Kolmogoroff's spectrum $E(k) \propto v_0^2 l(kl)^{-\frac{5}{3}}$ implies $K(r) \propto v_0 l(r/l)^{\frac{4}{3}}$, as in fact Richardson (1926) originally proposed.

Turbulent diffusion is a simple example of turbulence dynamics and is therefore a suitable testing ground for examining the consequences of various approximations. Included in § 2.2 is a brief comparison between our basic analytical method and some alternative approximations.

2. Diffusion from a fixed source

2.1. *Methods of approach*

There are two main ways of attempting to give an analytical framework to the qualitative arguments of § 1. In the Lagrangian framework (as distinct from the Eulerian approach to be described presently), probability distributions are defined for the displacements, velocities, etc., of given marked particles, and the relationships between them are studied. For example, let $G(\mathbf{x}, t \,|\, \mathbf{x}_0, t_0)\, d\mathbf{x}$ be the probability that a fluid particle lying at the point $\mathbf{x}_0$ at time t_0 should, at the later time t, lie within a volume $d\mathbf{x}$ at the point $\mathbf{x}$. Let $V(\mathbf{x}, \mathbf{u}, t \,|\, \mathbf{x}_0, t_0)\, d\mathbf{x}\, d\mathbf{u}$ be

the probability that this same particle should at that time lie within $d\mathbf{x}$ and have a velocity between $\mathbf{u}$ and $\mathbf{u}+d\mathbf{u}$. Then it is not difficult to show that

$$\frac{\partial}{\partial t}G(\mathbf{x},t\,|\,\mathbf{x}_0,t_0)+\frac{\partial}{\partial x_i}\int V(\mathbf{x},\mathbf{u},t\,|\,\mathbf{x}_0,t_0)\,u_i d\mathbf{u}=0. \tag{2.1}$$

(In 2.1 and elsewhere, we use the summation convention.) Through the hydrodynamical equations, it is possible to derive a similar, though far more involved equation, relating V to another probability function, and this, in its turn, to yet another. It would be necessary to close this hierarchy of equations in some way in order to obtain from it an evaluation of $G(\mathbf{x},t\,|\,\mathbf{x}_0,t_0)$.

The second approach was first formulated by Batchelor (1952*b*); for a discussion of the general physical interpretation of the method the reader is referred to this paper, and for other applications to papers by Reid (1955) and Roberts (1957). The basic idea is one of reformulating the problem of finding Lagrangian probability functions as one of determining certain Eulerian moments. A passive scalar quantity $\psi(\mathbf{x},t)$ is introduced which satisfies the equation

$$\frac{\partial}{\partial t}\psi(\mathbf{x},t)+\frac{\partial}{\partial x_i}[\psi(\mathbf{x},t)\,u_i(\mathbf{x},t)]=0, \tag{2.2}$$

where $u_i(\mathbf{x},t)$ is the velocity field. This quantity is therefore carried by the turbulent fluid, but does not affect its motion. It is clear that if we take

$$\psi(\mathbf{x},t_0)=\delta(\mathbf{x}-\mathbf{x}_0), \tag{2.3}$$

where $\delta(\mathbf{x})$ is the three-dimensional Dirac δ-function, then

$$\psi(\mathbf{x},t)=\delta(\mathbf{x}-\mathbf{x}_t), \tag{2.4}$$

where $\mathbf{x}_t$ is the position at time t (in this particular realization of $\mathbf{u}$) of the fluid element which was initially at $\mathbf{x}_0$. By averaging over all realizations, we see that the solution of

$$\frac{\partial}{\partial t}\langle\psi(\mathbf{x},t)\rangle+\frac{\partial}{\partial x_i}\langle\psi(\mathbf{x},t)\,u_i(\mathbf{x},t)\rangle=0, \tag{2.5}$$

which satisfies the initial condition

$$\langle\psi(\mathbf{x},t_0)\rangle=\delta(\mathbf{x}-\mathbf{x}_0), \tag{2.6}$$

is

$$\langle\psi(\mathbf{x},t)\rangle=G(\mathbf{x},t\,|\,\mathbf{x}_0,t_0). \tag{2.7}$$

Through a similar though more complicated equation, $\langle\psi u_i\rangle$ is related to higher moments, and so on. Again, we have an hierarchy of equations which must be closed in some way in order to evaluate $G(\mathbf{x},t\,|\,\mathbf{x}_0,t_0)$.

In the present paper, we adopt the second of these two approaches and employ an approximation method for closing the equations devised by Kraichnan (1959). However, before presenting this approximate analysis, we shall derive some results which are asymptotically exact for small $t-t_0$.

2.2. *Exact results for short times*

For $t-t_0 \ll l/v_0$, the fluid particles are simply swept from their points of origin with whatever velocity the turbulent fluid happens to have at the moment of their release, i.e.

$$V(\mathbf{x},\mathbf{u},t\,|\,\mathbf{x}_0,t_0)=P[\mathbf{u}(\mathbf{x}_0,t_0)]\,\delta[(\mathbf{x}-\mathbf{x}_0)-\mathbf{u}(t-t_0)], \tag{2.8}$$

where $P[\mathbf{u}(\mathbf{x}_0, t_0)]$ is the probability density function (p.d.f.) of $\mathbf{u}$ at position $\mathbf{x}_0$ and time t_0. Thus, by (2.1), or by inspection,

$$G(\mathbf{x}, t \mid \mathbf{x}_0, t_0) = \frac{1}{(t-t_0)^3} P\left(\frac{\mathbf{x}-\mathbf{x}_0}{t-t_0}\right), \tag{2.9}$$

a result due to Batchelor (1952*a*).

This result can also be deduced from the formal solution

$$\psi(\mathbf{x}, t) = \psi(\mathbf{x}, t_0) - \int_{t_0}^{t} dt' \frac{\partial}{\partial x_i} [u_i(\mathbf{x}, t') \psi(\mathbf{x}, t_0)] + \int_{t_0}^{t} dt' \frac{\partial}{\partial x_i} \left\{ u_i(\mathbf{x}, t') \int_{t_0}^{t'} dt'' \frac{\partial}{\partial x_j} [u_j(\mathbf{x}, t'') \psi(\mathbf{x}, t_0)] \right\} - \ldots, \tag{2.10}$$

which one obtains from (2.2) by integration and iteration. When $t - t_0 \ll l/v_0$, then $\mathbf{u}(\mathbf{x}, t) \doteq \mathbf{u}(\mathbf{x}_0, t_0)$, and it follows that

$$\psi(\mathbf{x}, t) \doteq \left[1 - (t-t_0) u_i(\mathbf{x}_0, t_0) \frac{\partial}{\partial x_i} + \frac{1}{2!} (t-t_0)^2 u_i(\mathbf{x}_0, t_0) u_j(\mathbf{x}_0, t_0) \frac{\partial^2}{\partial x_i \partial x_j} - \ldots \right] \psi(\mathbf{x}, t_0). \tag{2.11}$$

Hence, by (2.6) and (2.7),

$$G(\mathbf{x}, t \mid \mathbf{x}_0, t_0) \doteq \left[1 - (t-t_0) \langle u_i(\mathbf{x}_0, t_0) \rangle \frac{\partial}{\partial x_i} + \frac{1}{2!} (t-t_0)^2 \langle u_i(\mathbf{x}_0, t_0) u_j(\mathbf{x}_0, t_0) \rangle \frac{\partial^2}{\partial x_i \partial x_j} - \ldots \right] \delta(\mathbf{x} - \mathbf{x}_0). \tag{2.12}$$

That this is equivalent to (2.9) can most easily be seen by expressing the result in wave-vector space, writing

$$G(\mathbf{x}, t \mid \mathbf{x}_0, t_0) = \int \tilde{G}(\mathbf{k}, t \mid \mathbf{x}_0, t_0) e^{i\mathbf{k}.(\mathbf{x}-\mathbf{x}_0)} d\mathbf{k}. \tag{2.13}$$

Then (2.12) is equivalent to

$$\tilde{G}(\mathbf{k}, t \mid \mathbf{x}_0, t_0) = \frac{1}{(2\pi)^3} \left[1 - ik_i (t-t_0) \langle u_i(\mathbf{x}_0, t_0) \rangle - \frac{1}{2!} k_i k_j (t-t_0)^2 \langle u_i(\mathbf{x}_0, t_0) u_j(\mathbf{x}_0, t_0) \rangle + \ldots \right]; \tag{2.14}$$

i.e. that is

$$\tilde{G}(\mathbf{k}, t \mid \mathbf{x}_0, t_0) = \frac{1}{(2\pi)^3} \tilde{P}[\mathbf{k}(t-t_0)], \tag{2.15}$$

where

$$\tilde{P}(\boldsymbol{\eta}) = \int P[\mathbf{u}(\mathbf{x}_0, t_0)] e^{-i\boldsymbol{\eta}.\mathbf{u}} d\mathbf{u} \tag{2.16}$$

is the characteristic function for the distribution of velocity at $\mathbf{x}_0$ and t_0. Equation (2.9) is simply the inverse of (2.15).

This second method of establishing the behaviour of G at small times brings out some noteworthy features. If (2.12) is cut off after any finite number of terms, it implies that $G(\mathbf{x}, t \mid \mathbf{x}_0, t_0)$ vanishes identically for non-zero $\mathbf{x} - \mathbf{x}_0$. On the other hand, if (2.14) is cut off after a finite number of terms, the resulting expression for $\tilde{G}$ diverges for large $\mathbf{k}$, or large $t - t_0$. *One concludes that any reasonable approximate solution for the full space-function $G(\mathbf{x}, t \mid \mathbf{x}_0, t_0)$ must include terms of all orders*

of the formal expansion (2.10). Even for very short times the formal expansion is only useful because we happen to be able to sum it to all orders. However, if the moments

$$\langle \Delta x_i \rangle = \int \Delta x_i G(\mathbf{x}, t | \mathbf{x}_0, t_0)\, d\mathbf{x} = i(2\pi)^3 \left[\frac{\partial}{\partial k_i} \tilde{G}(\mathbf{k}, t \mid \mathbf{x}_0, t_0) \right]_{\mathbf{k}=0},$$

$$\langle \Delta x_i \Delta x_j \rangle = \int \Delta x_i \Delta x_j G(\mathbf{x}, t \mid \mathbf{x}_0, t_0)\, d\mathbf{x} = -(2\pi)^3 \left[\frac{\partial^2}{\partial k_i \partial k_j} \tilde{G}(\mathbf{k}, t \mid \mathbf{x}_0, t_0) \right]_{\mathbf{k}=0},$$

($\Delta \mathbf{x} = \mathbf{x} - \mathbf{x}_0$) are expanded by means of the formal solution, the resulting series appear to converge for all $t - t_0$, although the convergence is poor unless $t - t_0 \ll l/v_0$. Equation (2.14) shows that for small $t - t_0$,

$$\langle \Delta x_i \Delta x_j \rangle = U_{ij}(\mathbf{x}_0, t_0; \mathbf{x}_0, t_0)\,(t - t_0)^2, \tag{2.17}$$

where

$$U_{ij}(\mathbf{x}, t; \mathbf{x}_0, t_0) = \langle u_i(\mathbf{x}, t)\, u_j(\mathbf{x}_0, t_0) \rangle$$

is the velocity covariance. In the isotropic case, therefore,

$$\langle \Delta x_i \Delta x_j \rangle = v_1^2 \delta_{ij} (t - t_0)^2, \tag{2.18}$$

where v_1^2 is the mean square of any component of velocity at position $\mathbf{x}_0$ and time t_0.

There is fairly strong experimental evidence (see, for example, Batchelor 1953, ch. 8) that P almost always is closely Gaussian. It follows, as Batchelor (1950) has pointed out, that $G(\mathbf{x}, t \mid \mathbf{x}_0, t_0)$ must be closely Gaussian for short times. Then by (2.14) and (2.9) we have

$$\tilde{G}(\mathbf{k}, t \mid \mathbf{x}_0, t_0) = \frac{1}{(2\pi)^3} \exp\left[-\tfrac{1}{2} U_{ij}(\mathbf{x}_0, t_0; \mathbf{x}_0, t_0)\, k_i k_j (t - t_0)^2 \right], \tag{2.19}$$

and

$$G(\mathbf{x}, t \mid \mathbf{x}_0, t_0) = \frac{1}{(2\pi)^{\frac{3}{2}} (t - t_0)^3 (\det U_{ij})^{\frac{1}{2}}} \times \exp\left[-\tfrac{1}{2} u_{ij} \Delta x_i \Delta x_j (t - t_0)^{-2} \right], \tag{2.20}$$

where u_{ij} is the cofactor of $U_{ij}(\mathbf{x}_0, t_0; \mathbf{x}_0, t_0)$ and $\det U_{ij}$ denotes the determinant of these quantities. In the isotropic case,

$$\tilde{G}(\mathbf{k}, t \mid \mathbf{x}_0, t_0) = \frac{1}{(2\pi)^3} \exp\left[-\tfrac{1}{2} k^2 v_1^2 (t - t_0)^2 \right], \tag{2.21}$$

and

$$G(\mathbf{x}, t \mid \mathbf{x}_0, t_0) = \frac{1}{[2\pi v_1^2 (t - t_0)^2]^{\frac{3}{2}}} \exp\left[-(\mathbf{x} - \mathbf{x}_0)^2 / 2 v_1^2 (t - t_0)^2 \right]. \tag{2.22}$$

2.3. *An integro-differential equation for* $G(\mathbf{x}, t | \mathbf{x}_0, t_0)$

When $t - t_0$ is not small compared to l/v_0, the approximation (2.11) to the formal solution (2.10) is invalid since it is no longer legitimate to ignore the space and time variation of $u_i(\mathbf{x}, t)$. It is nevertheless possible to effect a partial summation of (2.10) which includes terms from every order in the expansion, and is such that the resulting expression for $\tilde{G}$ converges for large $\mathbf{k}$. The integral equation for this approximate form of G can be derived in two different ways. The first make suse of Kraichnan's direct interaction approximation (Kraichnan 1959).

In the second method which has been discussed elsewhere (Roberts 1960), the same result is derived by discarding or retaining terms in the formal expansion according to a certain selection criterion. The terms retained are of all order. Each of these methods supposes that the velocity field is spatially homogeneous, but this restriction can be removed by the application of a more general method due to Kraichnan (1961). The final result, for the case where the mean field $\langle \mathbf{u}(\mathbf{x}, t) \rangle$ vanishes, is the equation

$$\frac{\partial}{\partial t} G(\mathbf{x}, t \,|\, \mathbf{x}_0, t_0) = \int_{t_0}^{t} dt' \int d\mathbf{x} U_{ij}(\mathbf{x}, t; \mathbf{x}', t') \frac{\partial}{\partial x_i} G(\mathbf{x}, t \,|\, \mathbf{x}', t') \frac{\partial}{\partial x_j'} G(\mathbf{x}', t' \,|\, \mathbf{x}_0, t_0). \tag{2.23}$$

Here, as later, the fluid velocity is supposed incompressible:

$$\partial u_i(\mathbf{x}, t)/\partial x_i = 0. \tag{2.24}$$

(The compressible case can be treated by similar methods.) In the case of statistically homogeneous and stationary flows, we may write

$$\left.\begin{aligned} G(\mathbf{x}, t \,|\, \mathbf{x}_0, t_0) &= G(\mathbf{x} - \mathbf{x}_0, t - t_0), \\ U_{ij}(\mathbf{x}, t; \mathbf{x}_0, t_0) &= U_{ij}(\mathbf{x} - \mathbf{x}_0, t - t_0), \end{aligned}\right\} \tag{2.25}$$

and, upon a partial integration, (2.23) becomes

$$\frac{\partial}{\partial t} G(\mathbf{x}, t) = \frac{\partial^2}{\partial x_i \partial x_j} \int_0^t dt' \int d\mathbf{x}' U_{ij}(\mathbf{x}', t') \, G(\mathbf{x}', t') \, G(\mathbf{x} - \mathbf{x}', t - t'). \tag{2.26}$$

This result—a consequence of Kraichnan's direct interaction approximation—is the central result of this section and much of this paper. To prove it, we first notice that, when the velocity field is spacially homogeneous, the problem of diffusion from a point source, although apparently possessing only radial symmetry even in the isotropic case, can always be rephrased as a homogeneous problem. For, since the equation (2.2) is linear, the response of the system to an initial disturbance

$$\psi(\mathbf{x}, t_0) = e^{i\mathbf{k}.\mathbf{x}}, \tag{2.27}$$

is

$$\langle \psi(\mathbf{x}, t) \rangle = \int d\mathbf{x}_0 \, G(\mathbf{x}, t \,|\, \mathbf{x}_0, t_0) \, e^{i\mathbf{k}.\mathbf{x}_0}, \tag{2.28}$$

and, since for a homogeneous velocity field $G(\mathbf{x}, t \,|\, \mathbf{x}_0, t_0)$ depends on $\mathbf{x}$ and $\mathbf{x}_0$ in the combination $\mathbf{x} - \mathbf{x}_0$ only, equation (2.28) can be rewritten

$$\langle \psi(\mathbf{x}, t) \rangle = (2\pi)^3 \tilde{G}(\mathbf{k}, t \,|\, t_0) \, e^{i\mathbf{k}.\mathbf{x}}, \tag{2.29}$$

where

$$\tilde{G}(\mathbf{k}, t \,|\, t_0) = \frac{1}{(2\pi)^3} \int G(\mathbf{x} - \mathbf{x}_0, t \,|\, t_0) \, e^{-i\mathbf{k}.(\mathbf{x} - \mathbf{x}_0)} \, d(\mathbf{x} - \mathbf{x}_0) \tag{2.30}$$

is the Fourier transform of the Green's function $G(\mathbf{x}, t \,|\, \mathbf{x}_0, t_0)$. Equation (2.29) proves the average response matrix of the Fourier modes is diagonal (when the velocity field is homogeneous) and that $(2\pi)^3 \tilde{G}(\mathbf{k}, t \,|\, t_0)$ is the average response function for mode $\mathbf{k}$.

Having established this correspondence, we will now derive the approximate equation (2.26) for the response function by a method parallel to that employed

by Kraichnan (1959)† for the velocity field response function. For simplicity, we will suppose henceforth that the velocity field is also statistically stationary. The modifications necessary if the field is not stationary are easily included.

It is convenient to introduce the artifice of cyclic boundary conditions over a large cube of side L in order to expand $\psi(\mathbf{x},t)$ and $\mathbf{u}(\mathbf{x},t)$ in Fourier sums rather than Fourier integrals:

$$\psi(\mathbf{x},t) = \sum_{\mathbf{k}} \tilde{\psi}(\mathbf{k},t)\, e^{i\mathbf{k}.\mathbf{x}} \quad [\tilde{\psi}(\mathbf{k}) = \tilde{\psi}^*(-\mathbf{k})], \tag{2.31}$$

$$\mathbf{u}(\mathbf{x},t) = \sum_{\mathbf{k}} \tilde{\mathbf{u}}(\mathbf{k},t)\, e^{i\mathbf{k}.\mathbf{x}} \quad [\tilde{\mathbf{u}}(\mathbf{k}) = \tilde{\mathbf{u}}^*(-\mathbf{k})], \tag{2.32}$$

(cf. K., equation (2.1)). Equation (2.2) may be written

$$\frac{\partial \tilde{\psi}(\mathbf{k},t)}{\partial t} + ik_j \sum_{\mathbf{q}} \tilde{\mathbf{u}}_j(\mathbf{p},t)\, \tilde{\psi}(\mathbf{q},t) = 0, \tag{2.33}$$

where $\mathbf{p} = \mathbf{k} - \mathbf{q}$. The response function $\tilde{g}(\mathbf{k},t)$ for mode $\mathbf{k}$ is the solution of (2.33) under the initial conditions

$$\left.\begin{aligned} \tilde{\psi}(\mathbf{k},t) &\equiv \tilde{g}(\mathbf{k},t) = 1 \\ \tilde{\psi}(\mathbf{q},t) &\equiv \tilde{\psi}_{\mathbf{k}}(\mathbf{q},t) = 0 \quad (\mathbf{q} \neq \mathbf{k}) \end{aligned}\right\} \; t = 0, \tag{2.34}$$

(cf. §2.1). By the equation of motion $\tilde{\psi}_{\mathbf{k}}(\mathbf{q},t)$ and the direct interaction approximation, we find (cf. K., equation (2.24)) that

$$\tilde{\psi}_{\mathbf{k}}(\mathbf{q},t) = -iq_l \int_0^t \tilde{u}_l(-\mathbf{p},t')\, \tilde{g}(\mathbf{k},t')\, \tilde{g}(\mathbf{q},t-t')\, dt'. \tag{2.35}$$

Thus by (2.33) we have

$$\frac{\partial \tilde{g}(\mathbf{k},t)}{\partial t} = -\sum_{\mathbf{q}} k_i k_j \int_0^t \tilde{u}_i(\mathbf{p},t)\, \tilde{u}_j(-\mathbf{p},t')\, \tilde{g}(\mathbf{q},t-t')\, \tilde{g}(\mathbf{k},t')\, dt', \tag{2.36}$$

and, on averaging, using the principle of weak statistical dependence (cf. K., §2.2 and equation (2.25)), we find

$$\frac{\partial}{\partial t}\langle \tilde{g}(\mathbf{k},t)\rangle = -\sum_{\mathbf{q}} k_i k_j \int_0^t \langle \tilde{u}_i(\mathbf{p},t)\, \tilde{u}_j(-\mathbf{p},t')\rangle \langle \tilde{g}(\mathbf{q},t-t')\rangle \langle \tilde{g}(\mathbf{k},t')\rangle\, dt'. \tag{2.37}$$

Now let us take the limit. Make the transition $L \to \infty$. Let

$$\tilde{U}_{ij}(\mathbf{k},t-t') = \lim_{L\to\infty} \left(\frac{L}{2\pi}\right)^3 \langle \tilde{u}_i(\mathbf{k},t)\, \tilde{u}_j(-\mathbf{k},t')\rangle, \tag{2.38}$$

so that

$$U_{ij}(\mathbf{x}-\mathbf{x}',t-t') = \langle u_i(\mathbf{x},t)\, u_j(\mathbf{x}',t')\rangle = \int \tilde{U}_{ij}(\mathbf{k},t-t')\, e^{i\mathbf{k}.(\mathbf{x}-\mathbf{x}')}\, d\mathbf{k}, \tag{2.39}$$

and let

$$\tilde{G}(\mathbf{k},t) = \lim_{L\to\infty} \left(\frac{L}{2\pi}\right)^3 \langle \tilde{g}(\mathbf{k},t)\rangle \tag{2.40}$$

† This paper will be designated by 'K.' hereafter. Some differences in notation should be noted: In K., $g(\mathbf{k},t)$ refers to the velocity field (impulse) response function and not to the response function for (2.33) below. Also, in K., g refers to an averaged response while, in this paper, it does not; the average being denoted by $\langle g\rangle$. Further, the notational distinction between a quantity and its Fourier transform is different from that adopted in this paper.

so that equations (2.30), (2.31) and (2.34) are consistent (cf. K., equations (3.2), (3.3)). Then

$$\frac{\partial \tilde{G}(\mathbf{k},t)}{\partial t} = -(2\pi)^3 k_i k_j \int_0^t dt' \int d\mathbf{q} \tilde{U}_{ij}(\mathbf{p},t') \tilde{G}(\mathbf{q},t') \tilde{G}(\mathbf{k},t-t'). \tag{2.41}$$

This result can be returned to physical space by writing it as

$$\frac{\partial \tilde{G}(\mathbf{k},t)}{\partial t} = -k_i k_j \int_0^t dt' \int d\mathbf{p} \int d\mathbf{q} \int d\mathbf{x}' \, U_{ij}(\mathbf{p},t') \tilde{G}(\mathbf{q},t') \tilde{G}(\mathbf{k},t-t') \, e^{i\mathbf{x}'.(\mathbf{p}+\mathbf{q}-\mathbf{k})}; \tag{2.42}$$

that is (cf. equations (2.30), (2.39))

$$\frac{\partial \tilde{G}(\mathbf{k},t)}{\partial t} = -k_i k_j \int_0^t dt' \int d\mathbf{x}' U_{ij}(\mathbf{x}',t') \, G(\mathbf{x}',t') \, \tilde{G}(\mathbf{k},t-t') \, e^{-i\mathbf{k}.\mathbf{x}'}. \tag{2.43}$$

On using equation (2.30) again, we recover equation (2.26).

We will now investigate some elementary consequences of equation (2.26). On multiplying each side by $x_i x_j$ and integrating over all $\mathbf{x}$ and the right-hand side by parts, we find

$$\frac{\partial}{\partial t}\langle x_i x_j \rangle = \int x_i x_j \frac{\partial}{\partial t} G(\mathbf{x},t) \, d\mathbf{x} = 2 \int_0^t dt' \int d\mathbf{x}' U_{ij}(\mathbf{x}',t') \, G(\mathbf{x}',t');$$

that is

$$\langle x_i x_j \rangle = 2t\kappa_{ij}(t), \tag{2.44}$$

where $\kappa_{ij}(t)$ is defined by

$$\kappa_{ij}(t) = \frac{1}{t} \int_0^t dt'(t-t') \int d\mathbf{x}' U_{ij}(\mathbf{x}',t') \, G(\mathbf{x}',t'). \tag{2.45}$$

For short times ($t \ll l/v_0$), (2.44) and (2.45) agree with (2.17) if we assume $G(\mathbf{x}',t')$ is negligible unless $|\mathbf{x}'| \ll l$. Then,

$$\kappa_{ij} \doteq \tfrac{1}{2} t U_{ij}(0,0) \quad (t \to 0). \tag{2.46}$$

For large times ($t \gg l/v_0$),

$$\kappa_{ij} \doteq \int_0^\infty dt' \int d\mathbf{x}' U_{ij}(\mathbf{x}',t') \, G(\mathbf{x}',t') = \frac{1}{(2\pi)^3} \int_0^\infty dt' \int d\mathbf{k} \tilde{U}_{ij}(\mathbf{k},t') \, \tilde{G}(-\mathbf{k},t')$$

$$= \kappa_{ij}^\infty, \quad \text{say.} \tag{2.47}$$

Thus, for large times, $\kappa_{ij}(t)$ can be recognized as an effective 'eddy diffusivity'. Let us assume that the diffusion for time $\gtrsim l/v_0$ is dominated by the energy-containing eddies. Then it is reasonable to suppose that the integrals (2.47) should depend only on the parameters l and v_0, whence, by dimensional reasoning, we must have

$$\kappa_{ij}^\infty = \text{constant of order } l v_0.$$

In the isotropic case, we have (setting $x = |\mathbf{x}|$)

$$\kappa_{ij} = \kappa \delta_{ij}, \quad \kappa = \frac{4\pi}{3t} \int_0^t dt'(t-t') \int_0^\infty dx' x'^2 U_{ii}(x',t') \, G(x',t'), \tag{2.48}$$

and

$$\kappa_{ij}^\infty = \kappa^\infty \delta_{ij}, \quad \kappa^\infty = \frac{4\pi}{3} \int_0^\infty dt' \int_0^\infty dx' x'^2 U_{ii}(x',t') \, G(x',t'). \tag{2.49}$$

Equations (2.44) and (2.45) and their generalizations for flow which are not steady or homogeneous, imply that the Lagrangian correlation function $\langle u_i(t)\, u_j(t_0)\rangle_L = U_{Lij}(t-t_0)$ (say) is

$$U_{Lij}(t-t_0) = \int d\mathbf{x} U_{ij}(\mathbf{x}, t; \mathbf{x}_0, t_0)\, G(\mathbf{x}, t \mid \mathbf{x}_0, t_0). \tag{2.50}$$

This should be compared to the exact result

$$U_{Lij}(t-t_0) = \int d\mathbf{x} \langle u_i(\mathbf{x}, t)\, u_j(\mathbf{x}_0, t_0)\, \psi(\mathbf{x}, t \mid \mathbf{x}_0, t_0)\rangle, \tag{2.51}$$

where $\psi(\mathbf{x}, t \mid \mathbf{x}_0, t_0)$ denotes the unaveraged Green's function, i.e. the solution (2.4) of (2.2) satisfying (2.3). Equation (2.50) clearly may be obtained from (2.51) on the assumption that the ψ and $\mathbf{u}$ fields are statistically independent (see also Corrsin 1960).† However, if one decides to use an assumption of this kind, the results depend very much on what stage of the analysis is chosen for its application. For example, had we assumed that ψ and $\mathbf{u}$ are uncorrelated in (2.2), we would have obtained the absurd result $\partial\langle\psi(\mathbf{x}, t)\rangle/\partial t = 0$. Moreover, if the approximation

$$\langle u_i(\mathbf{x}, t)\, u_j(\mathbf{x}_0, t_0)\, \psi(\mathbf{x}, t \mid \mathbf{x}_0, t_0)\rangle = U_{ij}(\mathbf{x}, t; \mathbf{x}_0, t_0)\, G(\mathbf{x}, t \mid \mathbf{x}_0, t_0) \tag{2.52}$$

is used to close the hierarchy of equations which arise from (2.2) and (2.3), the result is *not* consistent with (2.50) (cf. Roberts 1957). Thus, the direct-interaction approximation is consistent with (2.52) only if (2.52) is used in a particular way. It is not clear why this should be so. However, Bourret (1960), in studying a model of turbulent diffusion due to Taylor (1922) (and which is described briefly below), has commented that, although the particle displacement cannot be Markovian, it may not be unreasonable to suppose that the particle velocity is Markovian. If this is the case, it is perhaps not altogether surprising that, when the quasi-normality approximation is applied directly to the equations for $G(\mathbf{x}, t)$, it should give worse results than when applied† to the Lagrangian velocity correlation.

Equation (2.26) is non-local in space and time, in contrast to an ordinary diffusion equation:

$$\frac{\partial G(\mathbf{x}, t)}{\partial t} = \kappa_{ij}^{\infty} \frac{\partial^2 G(\mathbf{x}, t)}{\partial x_i \partial x_j}. \tag{2.53}$$

Equation (2.53) describes molecular diffusion on time and distance scales large compared to the collision time and the mean free path, respectively. Over these large times and distances, molecular diffusion may be thought of as a random walk process for molecules. In like manner, turbulent convection may be thought of as a random walk process for fluid elements in which the effective step length is $\sim l$, and the effective velocity is $\sim v_0$. In fact, we shall see in § 2.5 that, on length and time scales large compared to l and l/v_0 respectively, (2.26) does reduce to the form (2.53). On smaller scales, however, the equation governing $G(\mathbf{x}, t)$ must reflect the persistence of correlations over finite space and time intervals.

† Saffman (1959) has used the approximate result (2.50) to derive an estimate for κ (see § 2.5 below).

Batchelor & Townsend (1956, § 2, p. 360) first suggested that this non-localness may be best expressed by an integro-differential equation. Another such equation has been derived by Bourret (1960) by generalizing a property of a simple model of turbulent diffusion due to Taylor (1922) which incorporates a persistence of velocity correlation along the path of the diffusing element, i.e. a finite Lagrangian correlation time. Taylor supposed that the fluid elements moved with velocity $\pm v$ between the equally spaced points of a lattice on the x-axis, and that the motion of an element could only be reversed at a lattice point, the probability of such an event being q. Following Goldstein (1951), who made a detailed study of Taylor's model, Bourret considered the limiting case $q \to 0$, $d \to 0$, $d/q \to l$, where d is the lattice separation. He proved that, for Taylor's model, $G(\mathbf{x}, t)$ satisfied an integro-differential equation whose generalization to three dimensions is

$$\frac{\partial G(\mathbf{x},t)}{\partial t} = \frac{\partial^2}{\partial x_i \partial x_j} \int_0^t U_{Lij}(t-t')\, G(\mathbf{x},t')\, dt'. \tag{2.54}$$

Bourret made the hypothesis that (2.54) is not a property of Taylor's model alone, but is more generally valid.

We may write (2.26) in the form

$$\frac{\partial G(\mathbf{x},t)}{\partial t} = \frac{\partial^2}{\partial x_i \partial x_j} \int_0^t dt' \int d\mathbf{x}' Q_{ij}(\mathbf{x}-\mathbf{x}', t-t')\, G(\mathbf{x}', t'), \tag{2.55}$$

where, according to our application of Kraichnan's approximation,

$$Q_{ij}(\mathbf{x},t) \doteq G(\mathbf{x},t)\, U_{ij}(\mathbf{x},t).$$

Equation (2.55) bears a strong formal resemblance to Bourett's result. Like (2.55), equation (2.54) is non-local in time but, unlike (2.55), it is local in space. This seems to imply that, although (2.54) takes into account the persistence of velocity correlation along the path of a fluid element, it does not take into account the fact that a cloud of marked particles set down at random in a turbulent flow must also display velocity correlation in space at any instant of time. The fact that it does not do so is not surprising since the model from which (2.54) was derived also does not incorporate this spatial velocity correlation. It would appear that such a correlation is contained in (2.55) through the spacial non-localness of that equation. This conclusion is supported by a study of a generalization of Taylor's model (Roberts 1961); we consider two fluid elements in motion along the lattice defined in Taylor's model, and suppose that the probability of the reversal of the velocity of either element on encountering a lattice point depends on whether the two elements were moving in the same or in opposite directions immediately before the encounter. It is found that (2.55) is obeyed and that $Q_{ij}(\mathbf{x}, t)$ is the Green function for the equation governing the diffusive flux. It is also found that (2.54) is obeyed if, and only if, the motion of the two elements is uncorrelated.

2.4. *Solution of the equation for short times*

For $t \ll l/v_0$, we may assume that the G factors in the integrand of (2.23) are negligible unless $\mathbf{x}-\mathbf{x}_0$ and $\mathbf{x}'-\mathbf{x}_0$ are both small compared with l. Thus,

$U_{ij}(\mathbf{x}', t', \mathbf{x}_0, t_0)$ in the integrand may be replaced by $U_{ij}(\mathbf{x}_0, t_0, \mathbf{x}_0, t_0)$ or, in the isotropic case, by $v_1^2 \delta_{ij}$. It follows that

$$\frac{\partial}{\partial t} G(\mathbf{x}, t) = v_1^2 \nabla^2 \int_0^t dt' \int d\mathbf{x}' G(\mathbf{x}', t') \, G(\mathbf{x} - \mathbf{x}', t - t'). \tag{2.56}$$

Taking the Fourier transform

$$G(\mathbf{x}, t) = \int \tilde{G}(\mathbf{k}, t') \, e^{i\mathbf{k}.\mathbf{x}} d\mathbf{k},$$

we find

$$\frac{\partial}{\partial t} \tilde{G}(\mathbf{k}, t) = -(2\pi)^3 v_1^2 k^2 \int_0^t dt' \, \tilde{G}(\mathbf{k}, t') \, \tilde{G}(\mathbf{k}, t - t'). \tag{2.57}$$

By taking the Laplace transform of (2.57), or by using a result of Watson (1944, § 12.2, equation (5)), we find

$$\tilde{G}(\mathbf{k}, t) = \frac{1}{(2\pi)^3} \frac{J_1(2kv_1 t)}{kv_1 t} \quad (k = |\mathbf{k}|). \tag{2.58}$$

Inverting by using a further result of Watson (1944, § 13.42, equation (4)), we find

$$G(\mathbf{x}, t) = \begin{cases} \dfrac{1}{(2\pi v_1 t)^2} [4v_1^2 t^2 - x^2]^{-\frac{1}{2}} & \text{if} \quad x < 2v_1 t, \\ 0 & \text{if} \quad x > 2v_1 t. \end{cases} \tag{2.59}$$

The corresponding probability distribution $D(x_1, t)$ for displacement along the x_1-axis (whose direction may be chosen arbitrarily) is related to $G(x, t)$ by

$$\partial D(x, t)/\partial x = -2\pi x G(x, t), \tag{2.60}$$

and so, in the present case,

$$D(x_1, t) = \begin{cases} \dfrac{1}{2\pi (v_1 t)^2} [4v_1^2 t^2 - x_1^2]^{\frac{1}{2}} & \text{if} \quad x_1 < 2v_1 t, \\ 0 & \text{if} \quad x_1 > 2v_1 t. \end{cases} \tag{2.61}$$

Both $G(x, t)$ and $D(x_1, t)$ are everywhere non-negative, but they are zero beyond a distance of $2v_1 t$ from the source. That this behaviour is not restricted to small times can be proved directly from equation (2.26) by induction. The finite maximum 'propagation speed' exhibited by equation (2.59) therefore persists for all times. This is also consistent with equation (2.9) which implies, in the present case, that the p.d.f. of velocity has a sharp cut-off at $u = 2v_1$. In fact, this p.d.f. predicted by the direct interaction approximation agrees with the actual p.d.f. of velocity only as far as the second moments.

A related unrealistic feature of (2.59) is that $G(x, t) \to \infty$ as $x \to 2v_1 t - 0$. However, the singularity is weak, since

$$\int_x^{2v_1 t + 0} 4\pi x^2 G(x, t) \, dx \doteq \frac{4}{\pi} \left(2 - \frac{x}{v_1 t}\right)^{\frac{1}{2}} \quad (x \to 2v_1 t - 0);$$

that is, the singular outgoing wave-front does not even carry a finite integrated probability. This singular type of behaviour may be attributed to the combined effects of persistence of velocity and finite maximum propagations peed. Another example is provided by Taylor's model (Taylor 1922). In this case the singular

outgoing wave-front even carries a finite integrated probability (cf. Goldstein 1951, § 8).

For a normally distributed velocity field, a comparison of equation (2.58) in the form

$$\tilde{G}(\mathbf{k},t) = \frac{1}{(2\pi)^3}\sum_0^\infty \frac{(-1)^n (kv_1 t)^{2n}}{n!(n+1)!}, \tag{2.62}$$

with the exact solution (2.21) in the form

$$\tilde{G}(\mathbf{k},t) = \frac{1}{(2\pi)^3}\sum_0^\infty \frac{(-1)^n (kv_1 t)^{2n}}{2^n n!}, \tag{2.63}$$

shows that, for short times, the direct interaction approximation gives the second moments of $G(\mathbf{x},t)$ correctly. The fractional errors in the fourth, sixth, and $2n$th moments are, respectively, $\frac{1}{3}$, $\frac{2}{3}$, and $[1-2^n/(n+1)!]$. This exhibits in another way the consequence of the effective cut-off in 'propagation speed'.

2.5. *Solution for large times*

For $t \gg l/v_0$, the diffusing particles will have suffered many displacements (statistically almost unrelated) from the energy-containing eddies, and we may expect $G(\mathbf{x},t)$ to become close to a Gaussian distribution. Batchelor & Townsend (1956, p. 358) have shown that this can be established, granted the truth of an as yet unproved extension of the central limit theorem. Alternatively, we may proceed directly by expressing the moments of the distribution of $\mathbf{x}$ as integrals over the Lagrangian velocity correlations. As Taylor (1922) has shown

$$\langle x_i x_j\rangle \to 2\kappa_{ij}^* t \quad (t\to\infty), \tag{2.64}$$

where

$$\kappa_{ij}^* = \int_0^\infty dt' U_{Lij}(t'). \tag{2.65}$$

Let us apply the argument used by Taylor to derive this result to the evaluation of a fourth moment such as $\langle x_i x_j x_k x_l\rangle$. We find

$$\langle x_i x_j x_k x_l\rangle = \int_0^t dt_1 \int_0^t dt_2 \int_0^t dt_3 \int_0^t dt_4 \langle u_i(t_1)\, u_j(t_2)\, u_k(t_3)\, u_l(t_4)\rangle_L. \tag{2.66}$$

Let τ be the Lagrangian velocity correlation time (assumed finite). It is clear that the integrand of (2.66) is negligibly small *unless*

either $\quad |t_1-t_2|<\tau \quad and \quad |t_3-t_4|<\tau,$

or $\quad |t_1-t_3|<\tau \quad and \quad |t_4-t_2|<\tau,$

or $\quad |t_1-t_4|<\tau \quad and \quad |t_2-t_3|<\tau,$

or $\quad |t_\alpha-t_\beta|<\tau, \ all\ \alpha,\beta = 1\text{–}4.$

For $t \gg \tau$, the region defined by the last of these inequalities makes a contribution to $\langle x_i x_j x_k x_l\rangle$ of the order of

$$\int_0^t dt_1 \int_{-\tau}^{\tau} ds_1 \int_{-\tau}^{\tau} ds_2 \int_{-\tau}^{\tau} ds_3 \langle u_i(t_1)\, u_j(t_1+s_1)\, u_k(t_1+s_2)\, u_l(t_1+s_3)\rangle_L.$$

The integral over s_1, s_2, s_3 is bounded and independent of t_1. Thus the contribution made by this region to $\langle x_i x_j x_k x_l\rangle$ is of order t, $t\to\infty$. However, the ranges of

t_1 to t_4 for which the first of the inequalities *alone* is satisfied, makes a contribution to $\langle x_i x_j x_k x_l \rangle$ which is of order t^2, $t \to \infty$. It is

$$\left[\int_0^t dt_1 \int_0^t dt_2 \langle u_i(t_1)\, u_j(t_2)\rangle\right]\left[\int_0^t dt_3 \int_0^t dt_4 \langle u_k(t_3)\, u_l(t_4)\rangle\right],$$

which is equal to $\langle x_i x_j \rangle \langle x_k x_l \rangle$. The regions defined by the other inequalities make similar contributions. It follows that, for $t \gg \tau$,

$$\langle x_i x_j x_k x_l \rangle = \langle x_i x_j \rangle \langle x_k x_l \rangle + \langle x_i x_k \rangle \langle x_l x_j \rangle + \langle x_i x_l \rangle \langle x_j x_k \rangle,$$

that is, the fourth cumulants are negligible if $t \gg \tau$. Similar arguments hold for moments of all orders, showing that $G(\mathbf{x}, t)$ approaches normality as $t \to \infty$.

By a proof which is an exact parallel to the above, we can show that, for $t \gg l/v_0$, the distribution satisfying (2.26) approaches normality and that the corresponding eddy diffusivity is

$$\kappa_{ij}^{\infty} = \int_0^{\infty} dt' \int d\mathbf{x}' G(\mathbf{x}', t')\, U_{ij}(\mathbf{x}', t'). \tag{2.67}$$

Consider, for example, the fourth moment $\langle x_i x_j x_k x_l \rangle$. It is easy to show from (2.26) that

$$\langle x_i x_j x_k x_l \rangle = \langle x_i x_j \rangle \langle x_k x_l \rangle + \langle x_i x_k \rangle \langle x_j x_l \rangle + \langle x_i x_l \rangle \langle x_j x_k \rangle + 2\left[\int_0^t dt'(t-t') \int d\mathbf{x}' x_i' x_j' U_{kl}(\mathbf{x}', t')\, G(\mathbf{x}', t') + 5 \text{ similar terms}\right]. \tag{2.68}$$

Assuming that expressions such as

$$\frac{1}{t}\int_0^t dt'(t-t') \int d\mathbf{x}' x_i' x_j' U_{kl}(\mathbf{x}', t')\, G(\mathbf{x}', t')$$

converge as $t \to \infty$, we see that for $t \gg l/v_0$ the first three terms on the right-hand side of (2.68) are of order $(lv_0 t)^2$ while the remainder are of order $l^3 v_0 t$ and therefore are comparatively negligible. Thus the fourth-order cumulants can be neglected if $t \gg l/v_0$. Similar arguments hold in all orders and show that G approaches normality. This result may also be established by the following alternative method.

If $t \gg l/v_0$, the mean distance $\sqrt{\langle x^2 \rangle}$ the particles will have travelled from their source and will be large compared to l so that the length and time scales of $G(\mathbf{x}, t)$ will be large compared to l and l/v_0, respectively. Under these circumstances, the only regions of integration in (2.26) for which the integrand is appreciable are those for which $G(\mathbf{x}-\mathbf{x}', t-t')$ is approximately equal to $G(\mathbf{x}, t)$. Thus, with κ_{ij}^{∞} given by (2.67), we have

$$\frac{\partial G(\mathbf{x}, t)}{\partial t} = \kappa_{ij}^{\infty} \frac{\partial^2 G(\mathbf{x}, t)}{\partial x_i \partial x_j}, \tag{2.69}$$

since for such large times it is immaterial whether the upper limit of integration in (2.26) is t or ∞. In the isotropic case (2.69) becomes

$$\frac{\partial G(\mathbf{x}, t)}{\partial t} = \kappa^{\infty} \nabla^2 G(\mathbf{x}, t), \tag{2.70}$$

where κ^{∞} is given by (2.49).

We may regard (2.69) as the first term in a series of approximations based on expanding the term $G(\mathbf{x}-\mathbf{x}', t-t')$ in the integrand of (2.26) in a Taylor series about the point $(\mathbf{x}, t)$, and we may apply an *a posteriori* check on the reasonableness of the approximation by verifying that, on substituting in the second term of this series the value of $G(\mathbf{x}, t)$ derived from (2.69), this second term is small compared to either side of (2.69). We will refrain from giving the analysis which is straightforward. It confirms that, if the relevant integrals converge, the necessary conditions for the validity of (2.69) are

$$t \gg l/v_0, \quad x \ll v_0 t. \tag{2.71}$$

The second condition arises from the finiteness of the maximum propagation velocity which, as we have already seen, gives an artificial cut-off at the distance $2v_1 t$. We may expect that for the actual case in which this cut-off is not present the second of the conditions (2.71) would be unnecessary and that the distribution of particles would be Gaussian at all distances. In any event, when the first condition is satisfied, it is clear that the fraction of particles affected by the second condition is negligibly small.

It seems extremely likely, from the exact short-time result of § 2.2 and our present results for large times, that $G(\mathbf{x}, t)$ is nearly Gaussian for all times, and that the variably diffusion coefficients defined in § 2.3 (cf. equations (2.44), (2.45) and (2.48)) will give useful estimates of the variance of the distribution at all times. On assuming a Gaussian form for $G(\mathbf{x}, t)$, we obtain from (2.45) an integral equation for $\kappa_{ij}(t)$. The approximation of (2.51) by (2.50) has been proposed independently by P. G. Saffman (unpublished) in the homogeneous case. By assuming a Gaussian form for $G(\mathbf{x}, t)$, and the isotropic form

$$\tilde{C}_{ij}(\mathbf{k}, t) = \left[\delta_{ij} - \frac{k_i k_j}{k^2}\right] \frac{v_1^2 k^2}{\pi^{\frac{3}{2}} k_0^5} \exp\left\{-\left[\frac{k^2}{k_0^2} + \tfrac{1}{2} v_1^2 k^2 t^2\right]\right\}, \tag{2.72}$$

he has obtained from the integral equation for κ_{ij} the estimate

$$\kappa^{\infty} \sim 0{\cdot}7 v_1 / k_0, \tag{2.73}$$

where $\pi^{\frac{1}{2}} k_0^{-1}$ is the longitudinal integral scale (cf. Batchelor 1953, p. 47).

3. Relative diffusion

3.1. *Formulation of problem: exact results for short times*

In this section, we study the correlation between the motion of two marked particles which are initially separated by a distance small compared to l. The choice of method is essentially that of § 2.1 and again we will adopt a formulation in terms of Eulerian moments. We introduce the passive scalar field $\psi_1(\mathbf{x}, t)$ for the first particle and $\psi_2(\mathbf{y}, s)$ for the second particle, and we require that both fields satisfy (2.2). For $\psi_1(\mathbf{x}, t)$, we take as initial condition

$$\psi_1(\mathbf{x}, t_0) = \delta(\mathbf{x} - \mathbf{x}_0), \tag{3.1}$$

and, for $\psi_2(\mathbf{x}, s)$, we take

$$\psi_2(\mathbf{y}, s_0) = \delta(\mathbf{y} - \mathbf{y}_0). \tag{3.2}$$

Let us define

$$B(\mathbf{x}, t; \mathbf{y}, s \,|\, x_0, t_0; \mathbf{y}_0, s_0) = \langle \psi_1(\mathbf{x}, t)\, \psi_2(\mathbf{y}, s) \rangle. \tag{3.3}$$

This is the joint p.d.f. of particle displacements $\mathbf{x}$ and $\mathbf{y}$ at times t and s from positions $\mathbf{x}_0$ and $\mathbf{y}_0$ at initial instants t_0 and s_0, respectively. We shall term this 'the two particle Green's function'. Clearly, since the two particles have identical properties,

$$B(\mathbf{x},t;\mathbf{y},s|\mathbf{x}_0,t_0;\mathbf{y}_0,s_0) = B(\mathbf{y},s;\mathbf{x},t|\,\mathbf{y}_0,s;\mathbf{x}_0,t_0).$$

In homogeneous steady turbulence, it depends only on difference times and difference co-ordinates. We shall then write it as

$$B(\mathbf{x}-\mathbf{x}_0,t-t_0;\mathbf{y}-\mathbf{y}_0,s-s_0\,|\,\mathbf{r}_0,\tau_0) = B(\mathbf{y}-\mathbf{y}_0,s-s_0;\mathbf{x}-\mathbf{x}_0,t-t_0\,|\,-\mathbf{r}_0,-\tau_0),$$

where $\mathbf{r}_0 = \mathbf{y}_0-\mathbf{x}_0$ and $\tau_0 = s_0-t_0$.

It is evident that if one integrates (3.3) over all $\mathbf{x}$ or all $\mathbf{y}$ the one-point Green's function of § 2 is recovered. Of more interest is the integral

$$R(\mathbf{r},t,s\,|\,\mathbf{x}_0,\mathbf{r}_0,t_0,s_0) = \int d\mathbf{x}B(\mathbf{x},t;\mathbf{x}+\mathbf{r},s\,|\,\mathbf{x}_0,t_0;\mathbf{x}_0+\mathbf{r}_0,s_0). \tag{3.4}$$

$R(\mathbf{r},t,t\,|\,\mathbf{x}_0,\mathbf{r}_0,t_0,t_0)$ is Richardson's 'distance neighbour function' (Richardson 1926). It denotes the p.d.f. at time t of separation $\mathbf{r}$ for a pair of particles which at time t_0 were situated at $\mathbf{x}_0$ and $\mathbf{x}_0+\mathbf{r}_0$. For the homogeneous and stationary flows with which we will be primarily concerned, R depends only on $\mathbf{r}_0,\tau_0,\mathbf{r}-\mathbf{r}_0,t-t_0$, and $s-s_0$ and will be written†

$$R(\mathbf{r}-\mathbf{r}_0,t-t_0,s-s_0\,|\,\mathbf{r}_0,\tau_0) = \int d\mathbf{x}B(\mathbf{x}-\mathbf{x}_0,t-t_0;(\mathbf{x}-\mathbf{x}_0)+(\mathbf{r}-\mathbf{r}_0),s-s_0\,|\,\mathbf{r}_0,\tau_0). \tag{3.5}$$

Let us now assume that the Reynolds number of the flow is sufficiently high that an inertial range of wave-numbers, or eddy sizes, exists. By this we mean that the wave-numbers which contain most of the energy are distinct from the higher wave-numbers which are responsible for most of the energy dissipation. Suppose now, that r_0 lies with this inertial range of eddy sizes. The eddies of dimension large compared to r_0 move the two marked particles together bodily without substantially altering the magnitude or direction of $\mathbf{r}_0$. In a frame of reference moving with these large-scale motions, the eddies of dimension small compared to r_0 are associated with a small r.m.s. velocity and have little effect upon $\mathbf{r}_0$. The rate of separation of the particles, in this case, is dominated by eddies of dimension $\sim r_0$, because such eddies make the principal contribution to the relative velocity of two points separated by a distance r_0 (cf. Batchelor 1953, ch. 6). These eddies disperse the particles substantially in a time of order

$$T(r_0) = r_0[v_0^2-U_{ii}(\mathbf{r}_0,0)]^{-\frac{1}{2}} \ll l/v_0. \tag{3.6}$$

For times short compared to $T(r_0)$, we may apply arguments similar to those of § 2. These show that (cf. equation (2.9))

$$B(\mathbf{x},t;\mathbf{y},s\,|\,\mathbf{x}_0,t_0;\mathbf{y}_0,s_0) = \frac{1}{(t-t_0)^3(s-s_0)^3}P\left(\frac{\mathbf{x}-\mathbf{x}_0}{t-t_0},\frac{\mathbf{y}-\mathbf{y}_0}{s-s_0}\right), \tag{3.7}$$

† A notational point must be noted here: the first argument of R in the definition (3.5) is $\mathbf{r}-\mathbf{r}_0$, the *change* in separation, and *not* $\mathbf{r}$, the separation itself.

where $P[\mathbf{u}_1(\mathbf{x}_0, t_0), \mathbf{u}_2(\mathbf{y}_0, s_0)]$ is the joint p.d.f. for velocity $\mathbf{u}_1$ at position $\mathbf{x}_0$ and time t_0 and velocity $\mathbf{u}_2$ at position $\mathbf{y}_0$ and time s_0. It follows (cf. equation (2.17)) that

$$\begin{aligned}\langle \Delta x_i \Delta y_j \rangle &= \iint \Delta x_i \Delta y_j B(\mathbf{x}, t; \mathbf{y}, s \mid \mathbf{x}_0, t_0; \mathbf{y}_0, s_0)\, d\mathbf{x}\, d\mathbf{y} \\ &= 2U_{ij}(\mathbf{x}_0, t_0; \mathbf{y}_0, s_0)\,(t-t_0)\,(s-s_0), \end{aligned} \tag{3.8}$$

where $\Delta\mathbf{x} = \mathbf{x} - \mathbf{x}_0$ and $\Delta\mathbf{y} = \mathbf{y} - \mathbf{y}_0$. Also, for these short times, (3.7) shows that Richardson's function is

$$R(\mathbf{r}, t, t \mid \mathbf{x}_0, \mathbf{r}_0, t_0, t_0) = \frac{1}{(t-t_0)^3} \mathscr{P}\left(\frac{\mathbf{r}-\mathbf{r}_0}{t-t_0}\right), \tag{3.9}$$

where $\mathscr{P}[\mathbf{V}(\mathbf{r}_0, t_0)]$ is the p.d.f. of *relative* velocity $\mathbf{V}$ between the two points $\mathbf{x}_0$ and $\mathbf{x}_0 + \mathbf{r}_0$ at time t_0. It follows from (3.9) that

$$\langle \Delta r_i \Delta r_j \rangle = \langle V_i V_j \rangle (t-t_0)^2, \tag{3.10}$$

which, for an isotropic field with r_3-axis along $\mathbf{r}_0$, gives

$$\left.\begin{aligned} \langle (\Delta r_1)^2 \rangle = \langle (\Delta r_2)^2 \rangle &= 2v_1^2[1 - g(r_0, t_0)]\,(t-t_0)^2, \\ \langle (\Delta r_3)^2 \rangle &= 2v_1^2[1 - f(r_0, t_0)]\,(t-t_0)^2, \end{aligned}\right\} \tag{3.11}$$

where $f(r,t)$ and $g(r,t) = f(r,t) + \frac{1}{2} r \partial f(r,t)/\partial r$ are respectively the longitudinal and transverse velocity correlations at time t for points separated by a distance r. Thus, Richardson's function is initially oblate spheroidal with the line joining the origin ($\mathbf{r} = 0$) to $\mathbf{r}_0$ as axis. All these results for short times are essentially due to Batchelor (1952*a*) and are included here for comparison purposes (see § 3.3).

3.2. *Integro-differential equations for* $B(\mathbf{x}, t; \mathbf{y}, s \mid \mathbf{x}_0, t_0; \mathbf{y}_0, s_0)$

When $t - t_0$ and $s - s_0$ are not small compared to $T(r_0)$, it is no longer legitimate to ignore the spatial and temporal variations of $u_i(\mathbf{x}, t)$. It is, nevertheless, possible to effect a partial summation of the formal solution for B containing terms of all orders in the expansion. Since the determination of B is a problem which is essentially inhomogeneous (even if the velocity field is homogeneous), the Fourier modes are not weakly dependent and the methods expounded by Kraichnan (1959) are not applicable. However, Kraichnan (1961) has recently generalized his methods to inhomogeneous problems, and has given an approximate equation of motion for the covariance $\langle \psi(\mathbf{x}, t)\, \psi(\mathbf{x}', t') \rangle$ of a convected passive scalar field. A straightforward generalization to our case of two scalar fields yields the result

$$\begin{aligned} \frac{\partial}{\partial t} B(\mathbf{x}, t; \mathbf{y}, s \mid \mathbf{x}_0, t_0; \mathbf{y}_0, s_0) \\ = \int_{t_0}^{t} dt' \int d\mathbf{x}'\, U_{ij}(\mathbf{x}, t; \mathbf{x}', t') \frac{\partial G(\mathbf{x}, t \mid \mathbf{x}', t')}{\partial x_i} \frac{\partial B(\mathbf{x}', t'; \mathbf{y}, s \mid \mathbf{x}_0, t_0; \mathbf{y}_0, s_0)}{\partial x_j'} \\ + \int_{s_0}^{s} ds' \int d\mathbf{y}' U_{ij}(\mathbf{x}, t; \mathbf{y}', s')\, G(\mathbf{y}, s \mid \mathbf{y}', s') \frac{\partial^2 B(\mathbf{x}, t; \mathbf{y}', s' \mid \mathbf{x}_0, t_0; \mathbf{y}_0, s_0)}{\partial x_i \partial y_j'}, \end{aligned} \tag{3.12}$$

where $G(\mathbf{x}, t \mid \mathbf{x}_0, t_0)$ is the one-point Green function of § 2. An equation similar to (3.12) holds for $\partial B/\partial s$.

The equation for $R(\mathbf{r}, t, s \mid \mathbf{x}_0, \mathbf{r}_0, t_0, s_0)$ that can be obtained from (3.12) by integration may also, in the case of homogeneous velocity fields, be derived quite easily by a device which reduces the problem to a fully homogeneous one. Instead of imagining a single pair of fluid elements placed initially (i.e. at $t = t_0$, $s = s_0$) at $\mathbf{x}_0$ and $\mathbf{y}_0$ ($\mathbf{y}_0 - \mathbf{x}_0 = \mathbf{r}_0$), we imagine an infinite number of such pairs which are statistically independent and distributed homogeneously throughout space. All these pairs have the same separation $\mathbf{r}_0$, and for each pair the signs of ψ_1 and ψ_2 are, with equal probability, either both positive or both negative; the signs assigned to different pairs are statistically independent of each other. The ψ_1 and ψ_2 fields constructed in this way are strictly homogeneous, have zero means, and are such that

$$\langle \psi_1(\mathbf{x}, t)\, \psi_2(\mathbf{x}+\mathbf{r}, s)\rangle = R(\mathbf{r}-\mathbf{r}_0, t, s \mid \mathbf{r}_0, t_0, s_0), \tag{3.13}$$

where the left-hand side refers to the homogeneous problem just constructed and the right-hand side is the Richardson function for the original inhomogeneous problem.

Having established this correspondence, we again adopt cyclic boundary conditions and expand ψ_1, ψ_2 and $\mathbf{u}$ for the homogeneous problem in the forms

$$\psi_1(\mathbf{x}, t) = \sum_{\mathbf{k}} \tilde{\psi}_1(\mathbf{k}, t)\, e^{i\mathbf{k}\cdot(\mathbf{x}-\mathbf{x}_0)}, \tag{3.14}$$

$$\psi_2(\mathbf{y}, s) = \sum_{\mathbf{k}} \tilde{\psi}_2(\mathbf{k}, s)\, e^{i\mathbf{k}\cdot(\mathbf{y}-\mathbf{y}_0)}, \tag{3.15}$$

$$\mathbf{u}(\mathbf{x}, t) = \sum_{\mathbf{k}} \tilde{\mathbf{u}}(\mathbf{k}, t)\, e^{i\mathbf{k}\cdot\mathbf{x}}, \tag{3.16}$$

(cf. K., equation (2.1) and footnote on p. 263 above). Then equation (2.2) for the ψ_1 field may be written

$$\frac{\partial \tilde{\psi}_1(\mathbf{k}, t)}{\partial t} + ik_i \sum_{\mathbf{q}} \tilde{u}_i(\mathbf{p}, t)\, e^{-i\mathbf{p}\cdot\mathbf{x}_0}\, \tilde{\psi}_1(\mathbf{q}, t) = 0, \tag{3.17}$$

and, for the ψ_2 field,

$$\frac{\partial \tilde{\psi}_2(\mathbf{k}, s)}{\partial s} + ik_i \sum_{\mathbf{q}} \tilde{u}_i(\mathbf{p}, s)\, e^{-i\mathbf{p}\cdot\mathbf{y}_0}\, \tilde{\psi}_2(\mathbf{q}, s) = 0, \tag{3.18}$$

where $\mathbf{p} = \mathbf{k} - \mathbf{q}$. By (3.17) we have (cf. K., equations (3.4) and (3.5))

$$\frac{\partial}{\partial t}\langle \tilde{\psi}_1(-\mathbf{k}, t)\, \tilde{\psi}_2(\mathbf{k}, s)\rangle = ik_i \sum_{\mathbf{q}} \langle \tilde{u}_i(-\mathbf{p}, t)\, \tilde{\psi}_1(-\mathbf{q}, t)\, \tilde{\psi}_2(\mathbf{k}, s)\rangle\, e^{i\mathbf{p}\cdot\mathbf{x}_0}. \tag{3.19}$$

Now, in the limit $L \to \infty$, the direct interaction approximation (K., § 2.4) gives

$$\begin{aligned}\langle \tilde{u}_i(-\mathbf{p}, t)\, \tilde{\psi}_1(-\mathbf{q}, t)\, \tilde{\psi}_2(\mathbf{k}, s)\rangle \\ = \langle \tilde{u}_i(-\mathbf{p}, t)\, \tilde{\psi}_{1,-\mathbf{k}}(-\mathbf{q}, t)\, \tilde{\psi}_2(\mathbf{k}, s)\rangle + \langle \tilde{u}_i(-\mathbf{p}, t)\, \tilde{\psi}_1(-\mathbf{q}, t)\, \tilde{\psi}_{2,\mathbf{q}}(\mathbf{k}, s)\rangle,\end{aligned} \tag{3.20}$$

where (cf. equation (2.35) and K., § 3)

$$\tilde{\psi}_{1,-\mathbf{k}}(-\mathbf{q}, t) = \int_{t_0}^{t} iq_j \tilde{u}_j(\mathbf{p}, t')\, \tilde{\psi}_1(-\mathbf{k}, t')\, \tilde{g}(\mathbf{q}, t-t')\, e^{-i\mathbf{p}\cdot\mathbf{x}_0}\, dt', \tag{3.21}$$

$$\tilde{\psi}_{2,\mathbf{q}}(\mathbf{k}, s) = -\int_{s_0}^{s} ik_j \tilde{u}_j(\mathbf{p}, s')\, \tilde{\psi}_2(\mathbf{q}, s')\, \tilde{g}(\mathbf{k}, s-s')\, e^{-i\mathbf{p}\cdot\mathbf{y}_0}\, ds'. \tag{3.22}$$

Thus, applying the weak statistical dependence principle (K., § 2.2), we find that, in the limit $L \to \infty$ (cf. equations (2.38) to (2.40)),

$$\frac{\partial}{\partial t}\tilde{R}(\mathbf{k},t,s\,|\,\mathbf{r}_0,\tau_0)$$
$$= -(2\pi)^3 k_i k_j \int_0^t dt' \int d\mathbf{q}\tilde{U}_{ij}(\mathbf{p},t')\,\tilde{G}(\mathbf{q},t')\,\tilde{R}(\mathbf{k},t-t',s\,|\,\mathbf{r}_0,\tau_0)$$
$$+ (2\pi)^3 k_i k_j \int_0^s ds' \int d\mathbf{q}\tilde{U}_{ij}(\mathbf{p},\tau_0-t+s-s')\,e^{i\mathbf{p}\cdot\mathbf{r}_0}\tilde{G}(\mathbf{k},s')\,\tilde{R}(\mathbf{q},t,s-s'\,|\,\mathbf{r}_0,\tau_0). \tag{3.23}$$

Returning to $\mathbf{x}$-space by the arguments of (2.41) to (2.43) this becomes

$$\frac{\partial R(\mathbf{r},t,s\,|\,\mathbf{r}_0,\tau_0)}{\partial t}$$
$$= \frac{\partial^2}{\partial r_i \partial r_j}\left[\int_0^t dt' \int d\mathbf{x}' U_{ij}(\mathbf{x}',t')\,G(\mathbf{x}',t')\,R(\mathbf{r}+\mathbf{x}',t-t',s\,|\,\mathbf{r}_0,\tau_0)\right.$$
$$\left. - \int_0^s ds' \int d\mathbf{y}' U_{ij}(\mathbf{r}_0+\mathbf{r}-\mathbf{y}',\tau_0+\tau-s')\,G(\mathbf{y}',s')\,R(\mathbf{r}-\mathbf{y}',t,s-s'\,|\,\mathbf{r}_0,\tau_0)\right]. \tag{3.24}$$

This equation may also be derived directly from (3.12) which, when the velocity field is stationary and homogeneous, may be written after a partial integration in the form

$$\frac{\partial B(\mathbf{x},t;\mathbf{y},s\,|\,\mathbf{r}_0,\tau_0)}{\partial t} = \frac{\partial^2}{\partial x_i \partial x_j}\int_0^t dt' \int d\mathbf{x}' U_{ij}(\mathbf{x}',t')\,G(\mathbf{x}',t')\,B(\mathbf{x}-\mathbf{x}',t-t';\mathbf{y},s\,|\,\mathbf{r}_0,\tau_0)$$
$$+ \frac{\partial^2}{\partial x_i \partial y_j}\int_0^s ds' \int d\mathbf{y}' U_{ij}(\mathbf{r}_0-\mathbf{x}+\mathbf{y}-\mathbf{y}',\tau_0-t+s-s')$$
$$\times G(\mathbf{y}',s')\,B(\mathbf{x},t;\mathbf{y}-\mathbf{y}',s-s'\,|\,\mathbf{r}_0,\tau_0). \tag{3.25}$$

The results (3.24) and (3.25)—consequences of Kraichnan's random coupling approximation—are the central results of this section.

We will now investigate some elementary consequences of equations (3.24) and (3.25). On multiplying each side of (3.24) by $r_i r_j$ and integrating over all $\mathbf{r}$ and the right-hand side by parts, we find

$$\frac{\partial}{\partial t}\int R(\mathbf{r},t,s\,|\,\mathbf{r}_0,\tau_0)\,r_i r_j\,d\mathbf{r} = 2\int_0^t dt' \int d\mathbf{x}' U_{ij}(\mathbf{x}',t')\,G(\mathbf{x}',t')$$
$$- 2\int_0^s ds' \int d\mathbf{r} U_{ij}(\mathbf{r}_0+\mathbf{r},\tau_0+s'-t)\,R(\mathbf{r},t,s'\,|\,\mathbf{r}_0,\tau_0). \tag{3.26}$$

By differentiating (3.26) with respect to s, we find

$$\frac{\partial^2}{\partial t\,\partial s}\int R(\mathbf{r},t,s\,|\,\mathbf{r}_0,\tau_0)\,r_i r_j\,d\mathbf{r} = -2\int d\mathbf{r} U_{ij}(\mathbf{r}_0+\mathbf{r},\tau_0+\tau)\,R(\mathbf{r},t,s\,|\,\mathbf{r}_0,\tau_0). \tag{3.27}$$

Let us take $t_0 = 0, s_0 = 0$. Then, by (3.27) and (2.50), we see that the Lagrangian correlation for relative velocity $\mathbf{V}$ between two particles which were initially separated by a distance $\mathbf{r}_0$ is

$$\langle V_i(t)\,V_j(s)\rangle_L = 2\int d\mathbf{r}\,U_{ij}(\mathbf{r},s-t)\,[G(\mathbf{r},s-t) - R(\mathbf{r}-\mathbf{r}_0,t,s\,|\,\mathbf{r}_0,0)]. \tag{3.28}$$

This result should be compared to the exact result

$$\begin{aligned}\langle V_i(t)\,V_j(s)\rangle_L = \iint d\mathbf{x}\,d\mathbf{y}[&\langle\psi_1(\mathbf{x},t)\,\psi_1(\mathbf{y},s)\,u_i(\mathbf{x},t)\,u_j(\mathbf{y},s)\rangle\\ &+\langle\psi_2(\mathbf{x},t)\,\psi_2(\mathbf{y},s)\,u_i(\mathbf{x},t)\,u_j(\mathbf{y},s)\rangle\\ &-\langle\psi_1(\mathbf{x},t)\,\psi_2(\mathbf{y},s)\,u_i(\mathbf{x},t)\,u_j(\mathbf{y},s)\rangle\\ &-\langle\psi_2(\mathbf{x},t)\,\psi_1(\mathbf{y},s)\,u_i(\mathbf{x},t)\,u_j(\mathbf{y},s)\rangle],\end{aligned}\tag{3.29}$$

where $\psi_1(\mathbf{x},t)=\psi_1(\mathbf{x},t\,|\,\mathbf{x}_0,0)$ and $\psi_2(\mathbf{y},s)=\psi_2(\mathbf{y},s\,|\,\mathbf{y}_0,0)$ denote the unaveraged Green functions. In stationary homogeneous flows, this result reduces to (3.28) on the assumption that the ψ and $\mathbf{u}$ fields are statistically independent (cf. §2.3).

Also, by adding to (3.26) the analogous equation for the derivative with respect to s, and setting $t=s$, we find

$$\begin{aligned}\frac{\partial}{\partial t}\langle r_i r_j\rangle &= \int\frac{\partial}{\partial t}R(\mathbf{r},t,t\,|\,\mathbf{r}_0,0)\,r_i r_j\,d\mathbf{r}\\ &= 4\int_0^t dt'\int d\mathbf{x}'\,U_{ij}(\mathbf{x}',t')\,G(\mathbf{x}',t')\\ &\quad -2\int_0^t dt'\int d\mathbf{r}\,U_{ij}(\mathbf{r}_0+\mathbf{r},t-t')\,[R(\mathbf{r},t,t'\,|\,\mathbf{r}_0,0)+R(\mathbf{r},t',t\,|\,\mathbf{r}_0,0)].\end{aligned}\tag{3.30}$$

For $t\ll T(r_0)$, the particles have not had time to change their separation greatly and R is negligible except near $\mathbf{r}=0$. Thus the right-hand side of (3.30) becomes $4[U_{ij}(0,0)-U_{ij}(\mathbf{r}_0,0)]t$, in agreement with (3.10). For $t\gg l/v_0$, R is appreciable even at separations r of order l. For such large separations, the second term on the right-hand side of (3.30) is quite negligible, and we find (cf. equations (2.44) and (2.45))

$$\langle r_i r_j\rangle = 2\langle x_i x_j\rangle = 2\langle y_i y_j\rangle = 4t\kappa_{ij}.\tag{3.31}$$

This is consistent with the intuitive notion that, at such large separations from their source and each other, the particles will wander independently. For intermediate ranges of t, it appears that no such definite statements can be made. However, a reasonable approximation appears to be possible and this is discussed in §3.4.

3.3 *Solution of the equations for short times*

For $t\ll T(r_0)$, we may assume that the G and B factors in the integrands of (3.25) are both negligible unless $\mathbf{x}',\mathbf{y}',\mathbf{x},\mathbf{y}$ are small compared with $\mathbf{r}_0$. Then, the U_{ij} factors in the integrands may be replaced by their values for zero $\mathbf{x}',\mathbf{y}',\mathbf{x},\mathbf{y}$ and similarly for the time arguments. Therefore, in isotropic flows, we have

$$\begin{aligned}&\frac{\partial B(\mathbf{x},t;\mathbf{y},s\,|\,\mathbf{r}_0,\tau_0)}{\partial t}\\ &\quad= v_1^2\delta_{ij}\frac{\partial^2}{\partial x_i\partial x_j}\int_0^t dt'\int d\mathbf{x}'\,G(\mathbf{x}',t')\,B(\mathbf{x}-\mathbf{x}',t-t';\mathbf{y},s\,|\,\mathbf{r}_0,\tau_0)\\ &\qquad-U_{ij}(\mathbf{r}_0,\tau_0)\frac{\partial^2}{\partial x_i\partial y_j}\int_0^s ds'\int d\mathbf{y}'G(\mathbf{y}',s')\,B(\mathbf{x},t;\mathbf{y}-\mathbf{y}',s-s'\,|\,\mathbf{r}_0,\tau_0).\end{aligned}\tag{3.32}$$

Take a combined Laplace and Fourier transform defined by

$$\tilde{B}^*(\mathbf{k},p;\mathbf{l},q\,|\,\mathbf{r}_0,\tau_0)=\frac{1}{(2\pi)^6}\int_0^\infty dt\,e^{-pt}\int_0^\infty ds\,e^{-qs}\int d\mathbf{x}\,e^{i\mathbf{k}.\mathbf{x}}\int d\mathbf{y}\,e^{i\mathbf{l}.\mathbf{y}}\,B(\mathbf{x},t;\mathbf{y},s\,|\,\mathbf{r}_0,\tau_0). \tag{3.33}$$

Then, by (3.32),

$$\begin{aligned}p\tilde{B}^*(\mathbf{k},p;\mathbf{l},q\,|\,\mathbf{r}_0,\tau_0)-\frac{1}{(2\pi)^3}\tilde{G}^*(\mathbf{l},q)\\ =-(2\pi)^3k^2v_1^2\tilde{G}^*(\mathbf{k},p)\,\tilde{B}^*(\mathbf{k},p;\mathbf{l},q\,|\,\mathbf{r}_0,\tau_0)\\ -(2\pi)^3U_{ij}(\mathbf{r}_0,\tau_0)\,k_il_j\tilde{G}^*(\mathbf{l},q)\,\tilde{B}^*(\mathbf{k},p;\mathbf{l},q\,|\,\mathbf{r}_0,\tau_0),\end{aligned} \tag{3.34}$$

where $\tilde{G}^*(\mathbf{k},p)$ is the Fourier transform with respect to $\mathbf{x}$ and the Laplace transform with respect to t of $G(\mathbf{x},t)$. By (2.57), we have

$$p+(2\pi)^3k^2v_1^2\tilde{G}^*(\mathbf{k},p)=\frac{1}{(2\pi)^3\tilde{G}^*(\mathbf{k},p)}. \tag{3.35}$$

By (3.34) and (3.35), it follows that

$$\tilde{B}^*(\mathbf{k},p;\mathbf{l},q\,|\,\mathbf{r}_0,\tau_0)=\frac{\tilde{G}^*(\mathbf{k},p)\,\tilde{G}^*(\mathbf{l},q)}{1+(2\pi)^6\,U_{ij}(\mathbf{r}_0,\tau_0)\,k_il_j\tilde{G}^*(\mathbf{k},p)\,\tilde{G}^*(\mathbf{l},s)}. \tag{3.36}$$

If we expand the denominator of (3.36), we obtain

$$\tilde{B}^*(\mathbf{k},p;\mathbf{l},q\,|\,\mathbf{r}_0,\tau_0)=\sum_0^\infty(-1)^m[(2\pi)^6U_{ij}(\mathbf{r}_0,\tau_0)\,k_il_j]^m[\tilde{G}^*(\mathbf{k},p)\,\tilde{G}^*(\mathbf{l},q)]^{m+1}. \tag{3.37}$$

Now, by (3.35)
$$\tilde{G}^*(\mathbf{k},p)=\frac{1}{4\pi^3[p+\sqrt{(p^2+4k^2v_1^2)}]}. \tag{3.38}$$

The inverse Laplace transformation of $[\tilde{G}^*(\mathbf{k},p)]^{m+1}$ is therefore (see, for example, Watson 1944, §13.2, equation (7))

$$\frac{(m+1)\,J_{m+1}(2kv_1t)}{(2\pi)^{3m+3}\,(kv_1)^{m+1}t}.$$

Thus

$$\begin{aligned}\tilde{B}(\mathbf{k},t;\mathbf{l},s\,|\,\mathbf{r}_0,\tau_0)=\frac{1}{(2\pi)^6}\sum_0^\infty(-1)^m\,(m+1)^2\left[\frac{k_il_jU_{ij}(r_0,\tau_0)}{klv_1^2}\right]^m\\ \times\frac{J_{m+1}(2kv_1t)}{kv_1t}\,\frac{J_{m+1}(2lv_is)}{lv_1s}.\end{aligned} \tag{3.39}$$

The second moments of (3.39) agree with (3.8); the higher moments are given with progressively less accuracy (cf. §2.4). Roberts (1960) has discussed the significance of (3.39) in terms of a diagram expansion. The relationship

$$\int\frac{J_{m+1}(2kv_1t)}{(kv_1t)^{m+1}}\,e^{i\mathbf{k}.\mathbf{x}}d\mathbf{X}=\begin{cases}\dfrac{2\pi m!}{(2m)!}\,\dfrac{(4v_1^2t^2-x^2)^{m-\frac{1}{2}}}{(v_1t)^{2m+2}} & \text{if}\quad x<2v_1t,\\ 0 & \text{if}\quad x>2v_1t,\end{cases}$$

can be obtained by induction from results of Watson (1944, § 13.42, equation (4), $\mu = 1$, using also § 13.24, equation (1)) or directly (Watson, § 13.14). This enables us to invert the function $\tilde{B}(\mathbf{k}, t; \mathbf{l}, s \mid \mathbf{r}_0, \tau_0)$ in the form (cf. equation (2.59))

$$B(\mathbf{x},t;\mathbf{y},s \mid \mathbf{r}_0,\tau_0) = \begin{cases} \dfrac{1}{(2\pi)^4 (v_1 t)^3 (v_1 s)^3} \displaystyle\sum_0^\infty (-1)^m \frac{[(m+1)!]^2}{[(2m)!]^2} \left[U_{ij}(\mathbf{r}_0,\tau_0) \frac{\partial^2}{\partial x_i \partial y_j} \right]^m \\ \qquad \times \left[\left(1 - \dfrac{x^2}{4v_1^2 t^2}\right) \left(1 - \dfrac{y^2}{4v_1^2 s^2}\right) \right]^{m-\frac{1}{2}} \\ \qquad \text{if} \quad x < 2v_1 t \text{ and } y < 2v_1 s, \\ 0 \qquad \text{if} \quad x > 2v_1 t \text{ or } y > 2v_1 s. \end{cases} \tag{3.40}$$

This result shows consistency with the results for one-particle diffusion as in § 2.3, the effect of the artificial cut-off $2v_1$ in the p.d.f. of velocity is apparent. It is also clear that, if $U_{ij}(\mathbf{r}_0, \tau_0)$ is small compared to v_1^2, (3.40) reduces to its first term

$$B(\mathbf{x},t;\mathbf{y},s \mid \mathbf{r}_0,\tau_0) \doteq G(\mathbf{x},t)\, G(\mathbf{y},s),$$

where the right-hand side is given by (2.59). If the initial separation of the points is so close in space and time that we can write $U_{ij}(\mathbf{r}_0, \tau_0) = v_1^2 \delta_{ij}$, equation (3.40) shows (cf. Watson, § 11.41, equation (12)) that

$$\tilde{R}(\mathbf{k},t,s \mid \mathbf{r}_0,\tau_0) = (2\pi)^3 \tilde{B}(-\mathbf{k},t;\mathbf{k},s \mid \mathbf{r}_0,\tau_0) = \frac{1}{(2\pi)^3} \frac{J_1[2kv_1(s-t)]}{kv_1(s-t)},$$

or, inverting,

$$R(\mathbf{r},t,s \mid \mathbf{r}_0,\tau_0) \to G(\mathbf{r}_0 + \mathbf{r}, s-t); \quad \mathbf{r}_0 \to 0, \quad \tau_0 \to 0. \tag{3.41}$$

This shows, as we expect, that in the limit $\mathbf{r}_0 \to 0$, $\tau_0 \to 0$, the particles are not separated by the flow and simply move together as one particle. (As a further consistency check, we note that the Lagrangian correlation (3.28) is given correctly by (3.41) in this case.)

3.4. *Solutions for large and intermediate times*

For very long times $t \gg l/v_0$, there is a high probability that the particles have separated by a distance comparable to, or greater than, l and therefore wander independently. In fact, the solution of (3.25) is exactly analogous to that of § 2.5 for the one-point Green function, and we find

$$B(\mathbf{x},t;\mathbf{y},s \mid \mathbf{r}_0,\tau_0) \to G(\mathbf{x},t)\, G(\mathbf{y},s) \quad (r \gg l), \tag{3.42}$$

where $G(\mathbf{x}, t)$ and $G(\mathbf{y}, s)$ are given, in homogeneous flows, by the appropriate solutions of (2.69). In this case we find $R(\mathbf{r}, t)$ satisfies

$$\frac{\partial R(\mathbf{r},t)}{\partial t} = 2\kappa_{ij}^\infty \frac{\partial^2 R(\mathbf{r},t)}{\partial r_i \partial r_j},$$

so that $R(\mathbf{r}, t)$ assumes a Gaussian form corresponding to a diffusivity twice that characteristic of the one particle Green function (cf. equations (2.69) and (3.31)).

Consider turbulence at the high Reynolds numbers. Since the kinetic energy density of the turbulent flow must be finite, the spectrum function $E(k)$ must satisfy

$$kE(k) \to 0, \quad k \to \infty; \quad kE(k) \to 0, \quad k \to 0.$$

Also $\int_0^k E(k)\,dk \doteq \frac{1}{2}v_0^2$ if $k \gg k_0$, $\int_k^\infty E(k)\,k^2\,dk \doteq \epsilon/2\nu$ if $k \ll k_d$,

where $k_0\,(=1/l)$ and k_d are wave-numbers characteristic of the energy-containing range and the dissipation range, respectively. (ϵ = rate of dissipation of energy per unit mass; ν = kinematical viscosity.) Thus, within the inertial range $k_0 \ll k \ll k_d$, the spectrum must be such that

$$\int_{k_0}^{k_d} E(k)\,dk \ll \tfrac{1}{2}v_0^2 \quad \text{and} \quad \int_{k_0}^{k_d} E(k)\,k^2\,dk \ll \epsilon/2\nu.$$

It follows that, if the inertial range spectrum approximates to a power law, it must be such that

$$kE(k) \to 0, \quad k \to \infty; \quad k^3E(k) \to 0, \quad k \to 0.$$

For the later developments (cf. equations (3.61) and (3.62) below), we will require the more stringent conditions

$$kE(k) \to 0, \quad k \to \infty; \quad k^2E(k) \to 0, \quad k \to 0. \tag{3.43}$$

If the initial separation satisfies

$$l \gg r_0 \gg 1/k_d, \tag{3.44}$$

we expect that, in a time large compared to $T(r_0)$ but small compared to l/v_0, $\langle(\mathbf{r}-\mathbf{r}_0)^2\rangle$ will become large compared to r_0^2 but remain small compared to l^2. For these 'intermediate times' (as we shall term them), neither the short-time solution of § 3.3 nor the long-time solution above is valid.

Consider $R(\mathbf{r}-\mathbf{r}_0, t, t+\tau \mid \mathbf{r}_0, 0)$ for $\tau > 0$. This quantity is the p.d.f. of the separation $\mathbf{r}$ of two particles (released at $t = 0$ at a separation of $\mathbf{r}_0$) one of which has been carried by the flow for a time t, and the other for a time $t+\tau$. This process may be visualized in two stages. During the first, of duration t, both particles are carried by the flow. Their separation $\mathbf{r}$ during this time is essentially unaffected by the energy-containing eddies which give nearly equal displacements to both particles. It is governed by the motions (relative to the energy-containing eddies) of dimension $\sim r$. Now, in a frame moving with the energy-containing eddies, the r.m.s. velocity associated with these small-scale motions is very small compared to v_0. Thus, the mean square separation $\langle r^2\rangle$ at the termination of the first stage is very small compared to $(v_0 t)^2$. During the second stage, of duration τ, one of the particles can be considered as fixed in space while the other is carried by the flow for a further time τ. Its motion during this time is dominated by the energy-containing motions. During the first stage the relative diffusion is given by $R(\mathbf{r}, t, t \mid \mathbf{r}_0, 0)$. During the second stage the further diffusion of the second particle should be given by $G(\mathbf{r}, \tau)$, since the energy-containing motions are almost uncorrelated with the small-scale motions. Thus, we expect

$$R(\mathbf{r}, t, t+\tau \mid \mathbf{r}_0, 0) \doteq \int R(\mathbf{r}', t, t \mid \mathbf{r}_0, 0)\,G(\mathbf{r}-\mathbf{r}', \tau)\,d\mathbf{r}'. \tag{3.45}$$

It is clear that this result is exact for $t = 0$ or $\tau = 0$. Also, the change in the mean square separation during the second stage will be of the order of $(v_0\tau)^2$. Thus,

when this is large compared to the value of $\langle r^2 \rangle$ at the end of the first stage, (3.45) becomes

$$R(\mathbf{r}, t, t+\tau \mid \mathbf{r}_0, 0) \doteq G(\mathbf{r}, \tau). \tag{3.46}$$

Consider now (3.24) and its counterpart for $\partial R/\partial s$. These show that

$$\frac{\partial R(\mathbf{r}, t, t \mid \mathbf{r}_0, 0)}{\partial t} = \frac{\partial^2}{\partial r_i \partial r_j} \left\{ \int_0^t dt' \int d\mathbf{r}' [U_{ij}(\mathbf{r}', t') - U_{ij}(\mathbf{r}_0 + \mathbf{r} - \mathbf{r}', t')] \right.$$
$$\left. \times G(\mathbf{r}', t') [R(\mathbf{r} - \mathbf{r}', t - t', t \mid \mathbf{r}_0, 0) + R(\mathbf{r} - \mathbf{r}', t, t - t' \mid \mathbf{r}_0, 0)] \right\}. \tag{3.47}$$

By the arguments above, the integrand should be dominated by contributions from small t' (because of the behaviour of R) and from small $\mathbf{r}'$ (because of the behaviour of G). We will therefore replace the R factors in the integrand by $R(\mathbf{r}, t, t \mid \mathbf{r}_0, 0)$. It seems likely from the preceding discussion that this approximation will lead to results which are at least qualitatively correct.

We now find

$$\frac{\partial R(\mathbf{r}, t, t \mid \mathbf{r}_0, 0)}{\partial t} = \frac{\partial^2}{\partial r_i \partial r_j} [K_{ij}(\mathbf{r}, t)\, R(\mathbf{r}, t, t \mid \mathbf{r}_0, 0)], \tag{3.48}$$

where

$$K_{ij}(\mathbf{r}, t) = 2 \int_0^t dt' \int d\mathbf{r}' [U_{ij}(\mathbf{r}', t') - U_{ij}(\mathbf{r}_0 + \mathbf{r} - \mathbf{r}', t')]\, G(\mathbf{r}', t'). \tag{3.49}$$

For short times $t \ll T(r_0)$, (3.49) becomes

$$K_{ij}(\mathbf{r}, t) = 2t[v_1^2 \delta_{ij} - U_{ij}(\mathbf{r}_0, 0)], \tag{3.50}$$

which, by (3.48), is in agreement with (3.10). For very large times $t \gg l/v_0$, there is a high probability that the separation of particles is $\gtrsim l$. For these separations, the second U factor in the integrand of (3.49) is negligible, and the first factor gives

$$K_{ij}(\mathbf{r}, t) = 2\kappa_{ij}, \tag{3.51}$$

in agreement with the results derived earlier (cf. equation (3.31)).

To calculate the form of $K_{ij}(\mathbf{r}, t)$ for intermediate times, we express (3.49) in the form

$$K_{ij}(\mathbf{r}, t) = 2(2\pi)^3 \int_0^t dt' \int d\mathbf{k} \, [1 - e^{i\mathbf{k}.(\mathbf{r}+\mathbf{r}_0)}] \, \tilde{U}_{ij}(\mathbf{k}, t')\, \tilde{G}(\mathbf{k}, t'). \tag{3.52}$$

Assuming isotropy, we can write

$$\tilde{U}_{ij}(\mathbf{k}, t) = \left(\delta_{ij} - \frac{k_i k_j}{k^2}\right) \frac{E(\mathbf{k}, t)}{4\pi k^2}, \tag{3.53}$$

where $E(k, 0)$ is the energy spectrum. It follows that if we adopt spherical polar co-ordinates and write

$$R(\mathbf{r} - \mathbf{r}_0, t, t \mid \mathbf{r}_0, 0) = R(r, \theta, \phi, t),$$

(3.48) has the form

$$\frac{\partial R}{\partial t} = \frac{1}{r^2} \frac{\partial}{\partial r} \left[r^2 K(r, t) \frac{\partial R}{\partial r} \right] + \frac{1}{r^2} M(r, t) \left[\frac{1}{\sin\theta} \frac{\partial}{\partial \theta} \left(\sin\theta \frac{\partial R}{\partial \theta} \right) + \frac{1}{\sin^2\theta} \frac{\partial^2 R}{\partial \phi^2} \right], \tag{3.54}$$

where, by (3.52) and (3.53),

$$K(r, t) = 4(2\pi)^3 \int_0^t dt' \int_0^\infty dk \left[\frac{1}{3} - \frac{\sin kr}{(kr)^3} + \frac{\cos kr}{(kr)^2} \right] E(k, t')\, \tilde{G}(k, t'), \tag{3.55}$$

$$M(r, t) = 2(2\pi)^3 \int_0^t dt' \int_0^\infty dk \left[\frac{2}{3} - \frac{\sin kr}{kr} + \frac{\sin kr}{(kr)^3} - \frac{\cos kr}{(kr)^2} \right] E(k, t')\, \tilde{G}(k, t'). \tag{3.56}$$

For small kr, the quantities in the square brackets [.....] in the integrands of (3.55) and (3.56) are proportional to $(kr)^2$. Also, in the inertial range, we may take (cf. equation (2.21))

$$\tilde{G}(k,t) = \frac{1}{(2\pi)^3}\exp\left[-\tfrac{1}{2}k^2v_1^2t^2\right], \tag{3.57}$$

and (cf. K., §8.4)

$$E(k,t) = E(k)\exp\left[-\tfrac{1}{2}k^2v_1^2t^2\right]. \tag{3.58}$$

Thus, since by our initial supposition (3.43), $k^2E(k) \to 0$, $k \to 0$, it follows that the integrands of (3.55) and (3.56) do not tend to infinity as rapidly as k^{-1}, $k \to 0$. Consequently the form of $E(k)$ for small k ($\sim k_0$) does not influence the values of $K(r,t)$ and $M(r,t)$ appreciably. However, these quantities do depend implicitly on the energy-containing range through the forms (3.57) and (3.58) for $\tilde{G}(k,t)$ and $E(k,t)$. We will discuss this in more detail at the conclusion of this section.

Two further approximations are clearly justified. First, since $\langle(\mathbf{r}-\mathbf{r}_0)^2\rangle$ is large compared to r_0^2 for the times under consideration, the particles have in this time lost all 'memory' of their initial separation $\mathbf{r}_0$. Thus $R(r,\theta,\phi,t)$ must be independent of r_0, θ, and ϕ, and; by equation (3.54), it must satisfy

$$\frac{\partial R(r,t)}{\partial t} = \frac{1}{r^2}\frac{\partial}{\partial r}\left[r^2K(r,t)\frac{\partial R(r,t)}{\partial r}\right]. \tag{3.59}$$

Secondly, since $\langle r^2\rangle$ is small compared to $(v_0t)^2$, the exponential factors of (3.57) and (3.58) are small at the upper limit of integration over t in (3.55) and (3.56), and we may therefore write

$$\begin{aligned} K(r,t) = K(r) &= 4\int_0^\infty dt\int_0^\infty dk\left[\frac{1}{3}-\frac{\sin kr}{(kr)^3}+\frac{\cos kr}{(kr)^2}\right]E(k)\exp\left[-\tfrac{1}{3}k^2v_0^2t^2\right] \\ &= 2\sqrt{3\pi}\int_0^\infty \frac{dk}{v_0k}\left[\frac{1}{3}-\frac{\sin kr}{(kr)^3}+\frac{\cos kr}{(kr)^2}\right]E(k). \end{aligned} \tag{3.60}$$

Equation (3.59) was proposed by Richardson (1926) for the intermediate times discussed here. To investigate further the form of the variable diffusion coefficient (3.60) we will assume that in the inertial range the spectrum is a power law† of the form (cf. equation (3.43))

$$E(k) = \beta\epsilon^{n-1}v_0^{5-3n}k^{-n} \quad (1 < n < 2), \tag{3.61}$$

† We may now take the wave-number k_d characteristic of the dissipation range to be

$$k_d = R_0^{1/(3-n)}k_0,$$

where $$k_0 \equiv 1/l = \epsilon/v_0^3, \quad R_0 = v_0^4/\epsilon\nu = v_0/k_0\nu.$$

The 'intermediate times' referred to above may now be defined more precisely by

$$T(r_0) = \left(\frac{r_0}{l}\right)^{\frac{1}{2}(3-n)}\frac{l}{v_0} \ll t \ll \frac{l}{v_0}.$$

Also, the circumstances under which (3.46) is a good approximation are

$$v_0\tau/l \gg (v_0t/l)^{1/(2-n)}.$$

Note that (3.61) may be written

$$E(k) = \beta l v_0^2(kl)^{-n}.$$

where β is a dimensionless constant of the order of unity. With this spectrum, (3.60) gives, on integrating by parts and use of results of Watson (1944, §§3.4, 13.24),

$$K(r) = \frac{\beta\pi\sqrt{6}}{n}\epsilon^{n-1}v_0^{4-3n}r^n\int_0^\infty \frac{J_{\frac{1}{2}}(x)\,dx}{x^{\frac{1}{2}(n+3)}}$$

$$= \frac{\beta\pi\sqrt{3}\;\Gamma(1-\frac{1}{2}n)}{2^{n+1}n\,\Gamma(\frac{5}{2}+\frac{1}{2}n)}\epsilon^{n-1}v_0^{4-3n}r^n \equiv \lambda r^n, \text{ (say).} \tag{3.62}$$

If we suppose that at some time $t_1 \gg T(r_0)$

$$R(r,t) = \mathscr{R}(r,t_1), \tag{3.63}$$

then at subsequent times $t(\ll l/v_0)$, (3.59) and (3.62) show that

$$R(r,t) = \tfrac{1}{2}(2-n)\,r^{-\frac{1}{2}(n+1)}\int_0^\infty \tilde{\mathscr{R}}(\xi,t_1)\,J_s(\xi r^{\frac{1}{2}(2-n)})\exp[-\tfrac{1}{4}\lambda(2-n)^2\xi^2(t-t_1)]\,\xi\,d\xi, \tag{3.64}$$

where $s = (1+n)/(2-n)$ and

$$\tilde{\mathscr{R}}(\xi,t_1) = \int_0^\infty r^{\frac{1}{2}(3-n)}\mathscr{R}(r,t_1)\,J_s(\xi r^{\frac{1}{2}(2-n)})\,dr. \tag{3.65}$$

For $t \gg t_1$, (3.64) reduces to†

$$R(r,t) = \frac{1}{(2-n)^{(4+n)/(2-n)}\,\Gamma\left(\dfrac{3}{2-n}\right)}\cdot\frac{1}{(\lambda t)^{3/(2-n)}}\exp[-r^{2-n}/(2-n)^2\lambda t], \tag{3.66}$$

so that

$$\langle r^2\rangle = (2-n)^{4/(2-n)}\frac{\Gamma\left(\dfrac{5}{2-n}\right)}{\Gamma\left(\dfrac{3}{2-n}\right)}(\lambda t)^{2/(2-n)}. \tag{3.67}$$

The behaviour of $\langle r^2\rangle$ as a function of t is extraordinarily sensitive to the value of n assumed. Two cases are worthy of notice:

$n = \frac{3}{2}$ (Kraichnan 1959)

$$K(r) \propto \epsilon^{\frac{1}{2}}r^{\frac{3}{2}}/v_0^{\frac{1}{2}}, \quad \langle r^2\rangle \propto \epsilon^2 t^4/v_0^2, \tag{3.68}$$

$n = \frac{5}{3}$ (Kolmogorov 1941)

$$K(r) \propto \epsilon^{\frac{2}{3}}r^{\frac{5}{3}}/v_0, \quad \langle r^2\rangle \propto \epsilon^4 t^6/v_0^6. \tag{3.69}$$

Neither of these agree with the form proposed by Richardson (1926, see also Batchelor 1950);

$$K(r) \propto \epsilon^{\frac{1}{3}}r^{\frac{4}{3}}, \quad \langle r^2\rangle \propto \epsilon t^3. \tag{3.70}$$

That this is so is not surprising. Kraichnan's direct interaction approximation does not give an inertial range spectrum which agrees with that derived from

† The behaviour of $R(r,t)$ and $\langle r^2\rangle$ given by (3.66) and (3.67) is almost certainly independent of the approximation

$$R(\mathbf{r}-\mathbf{r}', t-t', t \mid \mathbf{r}_0, 0) \doteqdot R(\mathbf{r}, t, t \mid \mathbf{r}_0, 0)$$

which led from (3.47) to (3.48). In fact, it can be shown that the more accurate approximation method based on (3.45) and (3.47) leads to results whose dimensional forms are identical to (3.66) and (3.67).

Kolmogorov's similarity arguments. In the same way, when this approximation is applied to turbulent diffusion, it does not give a diffusion coefficient which agrees with that derived by these similarity arguments, even if Kolmogorov's spectrum is assumed. This is because the dynamics of diffusion with a given velocity field differ on the two theories. It would seem that the behaviour of $\langle r^2 \rangle$ as a function of t might provide a sensitive test by which to confront with experiment different assumptions about the structure of the inertial range.

Kraichnan (1959) has made a detailed comparison between the direct-interaction approximation and the Kolmogorov theory. He has traced the difference in the inertial range spectra to the difference in the role played by the energy-containing eddies in the two cases. In Kolmogorov's theory these eddies merely convect the small-scale motions without influencing their dynamics, whereas in the direct-interaction approximation this is not so. In the same way, on arguments of the Kolmogorov type, the relative diffusion of particles should be independent of the energy-containing eddies. However, the application of the direct-interaction approximation has led to results which depend on the energy-containing motions. If we wish to modify our formalism in such a way that our results depend only on the small-scale motions, we would transform to a frame of reference moving with the energy-containing eddies. We would expect that results of the form (3.48), (3.49) would be qualitatively correct, provided that $\tilde{G}(k,t)$ now described one-point diffusion relative to a source moving with the energy-containing eddies. On similarity arguments of the Kolmogorov type, $\tilde{G}(k,t)$ would then depend upon $k^{\frac{2}{3}}\epsilon^{\frac{1}{3}}t$. Similarly, $E(k,t)$ would describe the structure of the small-scale eddies in a frame of reference moving with the large-scale motions, and would take the form

$$E(k,t) = E(k) f(k^{\frac{2}{3}}\epsilon^{\frac{1}{3}}t).$$

The over-all effect of these modifications would be that a quantity of the order of $[kE(k)]^{\frac{1}{2}}$ would appear in place of v_0 in the expression (3.60) for $K(r)$. Kraichnan (1959, § 9.1) has shown that this substitution resolves the conflict between the Kolmogorov theory of turbulence and the theory based on the direct-interaction approximation. The quantity $[kE(k)]^{\frac{1}{2}}$ may be considered as the r.m.s. velocity associated with the motions of wave-numbers k as they are convected by the large-scale motions. Substitution of this quantity for v_0 in (3.60) gives

$$K(r) \propto \epsilon^{\frac{1}{2}(n-1)} v_0^{\frac{1}{2}(5-3n)} r^{\frac{1}{2}(n+1)}, \tag{3.71}$$

which, taking $n = \frac{5}{3}$, leads to (3.70). With these changes in the interpretation of $\tilde{G}(k,t)$ and $E(k,t)$, the sensitivity of our results to the form of the inertial range spectrum remains.

I am extremely grateful to Dr R. H. Kraichnan for detailed discussions and helpful criticisms of the work presented in this paper.

REFERENCES

Batchelor, G. K. 1950 The application of the similarity theory of turbulence to atmospheric diffusion. *Quart. J. R. Met. Soc.* **76**, 133–46.

Batchelor, G. K. 1952*a* Diffusion in a field of homogeneous turbulence. II. The relative motion of particles. *Proc. Camb. Phil. Soc.* **48**, 345–63.

Batchelor, G. K. 1952*b* The effect of homogeneous turbulence on material lines and surfaces. *Proc. Roy. Soc.* A, **213**, 349–66.

Batchelor, G. K. 1953 *The Theory of Homogeneous Turbulence.* Cambridge University Press.

Batchelor, G. K. & Townsend, A. A. 1956 Turbulent diffusion. Article in *Surveys in Mechanics*, pp. 352–99. Ed. by G. K. Batchelor and R. M. Davies. Cambridge University Press.

Bourret, R. 1960 An hypothesis concerning turbulent diffusion. *Canad. J. Phys.* **38**, 665–76.

Corrsin, S. 1960 Progress report on some turbulent diffusion research. *Proc. Symp. on Atmospheric Diffusion and Air Pollution, Oxford* 1958, pp. 161–64. New York: Academic Press.

Goldstein, S. 1951 On diffusion by discontinuous movements and on the telegraph equation. *Quart. J. Mech. Appl. Math.* **4**, 129–56.

Kolmogorov, A. N. 1941 The local structure of turbulence in an incompressible viscous fluid for very large Reynolds numbers. *C.R. Acad. Sci. U.R.S.S.* **30**, 301.

Kraichnan, R. H. 1959 The structure of isotropic turbulence at very high Reynolds numbers. *J. Fluid Mech.* **5**, 497–543.

Kraichnan, R. H. 1961 Dynamics of non-linear stochastic systems. *J. Math. Phys.* **2**, 124–48.

Reid, W. H. 1955 On the stretching of material lines and surfaces in isotropic turbulence with zero fourth cumulants. *Proc. Camb. Phil. Soc.* **51**, 350–62.

Richardson, L. F. 1926 Atmospheric diffusion on a distance–neighbour graph. *Proc. Roy. Soc.* A, **110**, 709–37.

Roberts, P. H. 1957 On the application of a statistical approximation to the theory of turbulent diffusion. *J. Rat. Mech. Anal.* **6**, 781–800.

Roberts, P. H. 1960 Analytical theory of turbulent diffusion. *Report HSN-2, Division of Electromagnetic Research, Institute of Mathematical Sciences.* New York University.

Roberts, P. H. 1961 On Bourret's hypothesis concerning tubulent diffusion. *Canad. J. Phys.* (to appear).

Saffman, P. G. 1959 An approximate calculation of the Lagrangian correlation coefficient for turbulent diffusion. Unpublished.

Taylor, G. I. Diffusion by continuous movements. *Proc. Lond. Math. Soc.* (2), **20**, 196–212.

Watson, G. N. 1944 *A Treatise on the Theory of Bessel Functions*, 2nd ed. Cambridge University Press.

On the stability of a heterogeneous shear layer subject to a body force

By J. MENKES

Jet Propulsion Laboratory, California Institute of Technology, Pasadena

(Received 15 August 1960 and in revised form 30 March 1961)

The effects of density variation and body force on the stability of a heterogeneous horizontal shear layer are investigated. The density is assumed to decrease exponentially with height, and the body force is assumed to be derivable from a potential; the velocity distribution in the shear layer is taken to be $U(y) = \tanh y$. The method of small disturbances is employed to obtain a family of neutral stability curves depending on the choice of the Richardson number. It is demonstrated, furthermore, that the value of the critical Richardson number depends on the magnitude of the non-dimensional density gradient.

1. Introduction

It is a frequent occurrence in nature that two fluids of different densities flow one on top of the other. If the flow is predominantly horizontal, and if the density diminishes rapidly in the upward direction, then the process of turbulent mixing must cause heavier fluid elements to be moved above lighter ones and lighter fluid elements below heavier ones. Both displacements consume energy that has to be extracted from the mean flow at the expense of energy that might be available for the maintenance of turbulence.† The same considerations apply quite generally to work against any body force. The present paper, an extension of an earlier analysis (Menkes 1959), is one of a series of researches (see, for example, Prandtl 1931; Taylor 1931; Goldstein 1931; Drazin 1958) undertaken to establish the limits of stability of a shear flow in a stably stratified medium.

2. Analysis

The equations of motion governing the behaviour of an incompressible inviscid fluid under the action of a body force, $g\nabla y$, are Euler's equation,

$$\frac{D\mathbf{u}}{Dt} = -\frac{\nabla p}{\rho} - g\nabla y, \tag{1}$$

the condition of incompressibility,

$$\frac{D\rho}{Dt} = 0, \tag{2}$$

† This argument, which follows Prandtl's exposition (Prandtl, 1952, p. 131), presupposes that the total kinetic energy can be resolved into two terms: one term represents the contribution of the mean flow and the other that giving rise to the turbulent Reynolds stresses. The energy partition is assumed to be unaffected by the density stratification.

and the equation of continuity,

$$\nabla . \mathbf{u} = 0. \tag{3}$$

The velocity components $\mathbf{u}$, the pressure p, and the density ρ are assumed to consist of a time-independent part and of a perturbation. Thus we write

$$u = V[U(y) + \psi'_y(x,y,t)], \quad v = -V\psi'_x(x,y,t), \tag{4a}$$

$$p = P(y) + p'(x,y,t), \tag{4b}$$

$$\rho = \rho_0[\bar{\rho}(y) + \rho'(x,y,t)], \tag{4c}$$

$$\psi' = \psi(y)\exp[ik(x-ct)], \quad (c = c_r + ic_i). \tag{4d}$$

Here V is the velocity at $y = \pm\infty$ and ψ' is a perturbation stream function; $U(y)$, $P(y)$, and $\bar{\rho}(y)$ describe the ambient state whose stability is to be investigated; k is a wave-number and c a complex phase velocity. Also, $x = x_1/d$ and $y = y_1/d$, where x_1 and y_1 are the physical co-ordinates and d is so chosen that $dU/dy = 1$ at $y = 0$; thus d characterizes the width of the transition layer. Denoting the Froude number, V^2/gd, by F, setting $\bar{\rho} = \exp(-2Ly)$, where L is a dimensionless density gradient, and eliminating ρ' and p' from equations (1), (2), and (3) yields

$$(U-c)(\psi'' - k^2\psi) - U''\psi + (\ln\bar{\rho})'[(U-c)\psi' - (U-c)'\psi] - \frac{(\ln\bar{\rho})'}{F}\frac{\psi}{U-c} = 0, \tag{5}$$

where primes denote differentiation with respect to y.

At this point we introduce the primary velocity distribution $U(y) = \tanh y$ as the independent variable. Denoting now by primes differentiation with respect to U, and setting $\psi(y) = \phi(U)$ and $2L/F = J$, we derive the equation

$$\phi'' + a(U)\phi' + b(U)\phi = 0, \tag{6}$$

where

$$a(U) = \frac{2(U+L)}{(U+1)(U-1)}, \tag{7a}$$

$$b(U) = \frac{J}{(U-c)^2(U+1)^2(U-1)^2} - \frac{k^2}{(U+1)^2(U-1)^2} - \frac{2(U+L)}{(U-c)(U+1)(U-1)}, \tag{7b}$$

with the boundary conditions $k\phi(U) = 0$, at $U = \pm 1$. (J is the Richardson number.)

Equation (6) is of a rather simple type. Its singularities, which are located at ± 1 and c, are regular singularities. It can be demonstrated that the point at infinity is also a regular singularity. The substitution into equation (6) of

$$Z = (U-1)^{-\alpha_1}(U-c)^{-\alpha_2}(U+1)^{-\alpha_3}\phi$$

yields an equation that has at least one bounded solution at each of the singularities. The α_i are defined by

$$\alpha_1 = \frac{L}{2}\left\{\left[1 + \frac{k^2}{L^2} - \frac{2J}{L^2(1-c)^2}\right]^{\frac{1}{2}} - 1\right\}, \quad \alpha_2 = \frac{1}{2}\left\{1 - \left[1 - \frac{8J}{(1-c^2)^2}\right]^{\frac{1}{2}}\right\},$$

$$\alpha_3 = \frac{L}{2}\left\{\left[1 + \frac{k^2}{L^2} - \frac{2J}{L^2(1+c)^2}\right]^{\frac{1}{2}} - 1\right\},$$

and each represents one of the indices relative to the finite points of the singularity. After this transformation, equation (6) reads

$$Z''+\left[\frac{1-\alpha_1}{U-1}+\frac{1-\alpha_2}{U-c}+\frac{1-\alpha_3}{U+1}\right]Z'+\frac{(\sigma\tau U-r)}{(U-1)(U-c)(U+1)}Z=0, \tag{8}$$

with the boundary conditions replaced by regularity conditions on $Z(U)$ at $U=\pm 1$ and c. A sufficient condition for the existence of a trivial solution $Z=$ constant (which, of course, satisfies the boundary conditions identically) is given formally by

$$\sigma\tau=0, \tag{9}$$

$$r=0, \tag{10}$$

where σ and τ are the indices relative to the point at infinity and r is an accessory parameter (see Bieberbach 1953). After a considerable amount of tedious, but essentially straightforward, algebraic manipulation, we obtain from equations (9) and (10) the explicit relations:

$$L=-c\left[1-\frac{4J}{(1-c^2)^2}\right]-\tfrac{1}{4}(1-\mu)\left[R(1-c)(1-\xi)^{\frac{1}{2}}-R(1+c)(1-\eta)^{\frac{1}{2}}-2c\right], \tag{11}$$

and

$$R^2=\frac{R(\mu-2)\left[(1-\xi)^{\frac{1}{2}}(1-\eta)^{\frac{1}{2}}\right]+J(1-c^2)^{-2}+2(\mu+1)}{1+\left[(1-\xi)(1-\eta)\right]^{\frac{1}{2}}}, \tag{12}$$

where

$$R^2=L^2+k^2,\quad \xi=\frac{2J}{R^2(1-c)^2},\quad \eta=\frac{2J}{R^2(1+c)^2},\quad \mu=\left[1-\frac{8J}{(1-c^2)^2}\right]^{\frac{1}{2}}.$$

It is to be noted that equations (11) and (12) are not homogeneous in any of the quantities J, L, k, and c; however, there are two equations in four unknowns. It was found convenient from a computational point of view to consider L and R^2 as the primary variables, and J and c as parameters. The equations were solved numerically by an iteration technique on an IBM 704 digital computer.

3. Discussion and results

In the usual case the neutral stability curve represents possible neutral disturbances and separates the stable from the unstable ones, with no 'forbidden' disturbances present anywhere. The stability boundaries displayed in figure 1 have a meaning slightly different from that commonly accepted. A particular boundary separates unstable disturbances from stable ones *and* from those that are physically not realizable. This may be stated in a different way: as the boundary is approached from the inside along an arbitrary path one passes over possible disturbances, and the closer one gets to the boundary the smaller will be the amplification. On the other hand, when the boundary is approached from the outside one cannot be sure whether an arbitrary path consists only of permitted disturbances or not. This implies that the only statement that can be made about the attenuation is that if the path consists only of a succession of possible disturbances, then as the boundary is approached the attenuation decreases, to vanish at the boundary itself. For practical purposes, however, this distinction is immaterial since one may state without ambiguity the maximum value of k^2+L^2 that corresponds to an unstable disturbance, for a prescribed value of J.

The present analysis throws into relief the dependence of the stability on the relative magnitudes of the wave-number k and the parameter L. The governing quantity appears to be k^2+L^2. The analysis of Taylor (1931) in which the parameter L was neglected indicated that as the wave-number decreased, the instability became more pronounced. By including the effect of the density gradient, one can stabilize a disturbance that was shown, in the absence of a density gradient, to be unstable by virtue of its small wave-number. The stabilizing effect of the density gradient is thus clearly demonstrated.

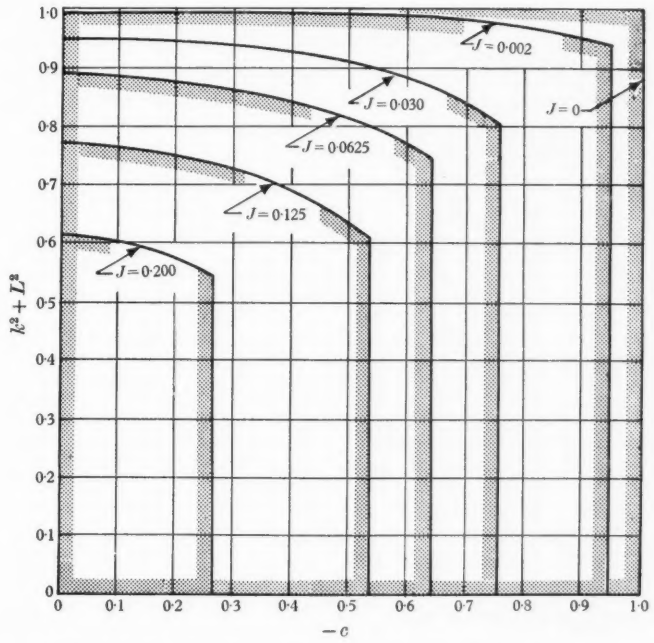

FIGURE 1. Stability map. The curves represent the boundaries between unstable disturbances (inside, shaded) and disturbances which are either damped or physically unrealizable.

The relationship that must exist between L and c, for given values of J, to obtain a neutral disturbance is displayed in figure 2. It is to be noted that the curves terminate before reaching the c-axis, thus implying that the only solution corresponding to $L = 0$ is $c = 0$, which is the one found by Drazin.

The accepted convention of referring to a critical Richardson number is unfortunate because it conjures up similarities with the critical Reynolds number of hydrodynamic stability theory to which it bears hardly any semblance. The critical Richardson number represents a number beyond which no virtual displacement† of the flow field appears possible if one forces the solution to be

† The displacement is taken to apply not only to spatial displacements but also to velocity, pressure, etc.

exponential in x as in t, and furthermore if one rules out the improper eigenfunctions associated with the continuous spectrum as demonstrated by Eliassen, Høiland & Riis (1953) and Case (1960).† In this sense, then, the flow is stable, so to say, by default. This is certainly an odd result, but one that has been obtained consistently by Taylor, Goldstein, Drazin, and the present author.

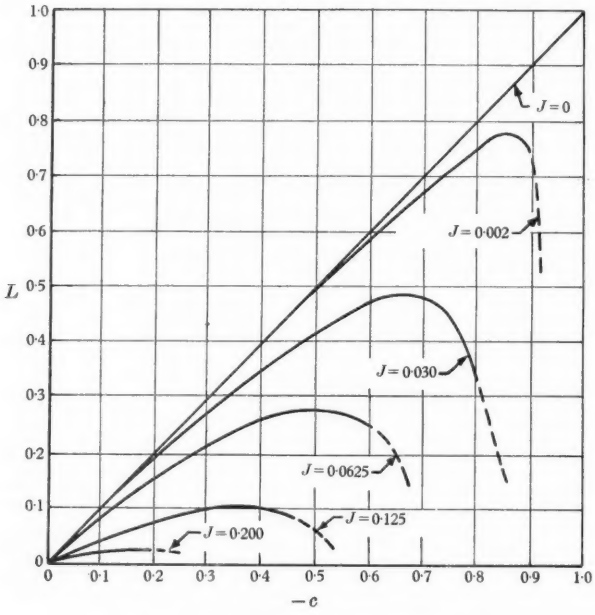

FIGURE 2. Neutral stability boundaries.

It appears to be a property of inviscid stability problems. No physical explanation can be offered, and the mathematical one provides little solace; it only states that, for $J > J_{cr}$, a physical quantity becomes imaginary when subjected to a virtual displacement (see Appendix).

The fact that the disturbance spectrum is finite, due to the presence of a cut-off wave-number, does not necessarily imply, however, that the asymptotic flow field is undetermined. It has been demonstrated by Case that, in general, the solutions associated with the continuous spectrum decay like $1/t$, while Carrier & Chang (1959) have shown that the inclusion of the continuous spectrum does not change the value of the cut-off wave-number. Thus, without solving the initial value problem in the present case, one may reason that the missing solutions will not affect the stability of the flow.

† The author is indebted to a referee for the precise formulation of the statement.

Appendix. The relationship between 'completeness' and the cut-off wave-number

The possibility that wave-like solutions to the disturbance equation may not exist can be anticipated from the following considerations. Any second-order differential equation of the type

$$Z'' + g(U)\,Z' + h(U)\,Z = 0$$

can be reduced to the canonical form

$$W'' + I(U)\,W = 0.$$

The invariant $I(U)$ is given by

$$I(U) = h - \tfrac{1}{4}g^2 - \tfrac{1}{2}g',$$

while the dependent variable is given by $W = Z\exp\frac{1}{2}\int g(U)\,dU$. When this transformation is applied to equation (8), subject to the conditions (9) and (10), we find that the invariant is given by

$$I = \frac{1}{4}\left[\frac{1-\alpha_1}{(U-1)^2} + \frac{1-\alpha_2}{(U-c)^2} + \frac{1-\alpha_3}{(U+1)^2}\right]$$
$$-\frac{1}{2}\left[\frac{(1-\alpha_1)(1-\alpha_2)}{(U-1)(U-c)} + \frac{(1-\alpha_1)(1-\alpha_3)}{(U-1)(U+1)} + \frac{(1-\alpha_2)(1-\alpha_3)}{(U-c)(U+1)}\right].$$

For the case where I is constant, it is well known that $I > 0$ corresponds to wave-like solutions and that $I < 0$ corresponds to exponential solutions. The same criterion still holds if I is a function of the independent variable (see Mott 1952, chapter 1). The form of $I(U)$ as displayed above makes it plausible that for a certain combination of values of α_i, which are functions of L, J, k and c, the magnitude of $I(U)$ will become negative. If we now try to force the solution to be wave-like, we shall find that the velocity perturbation will turn out to be a purely imaginary quantity, indicating the physical impossibility of realizing such a solution. The detailed calculations have shown that this does actually take place when $J > (k^2+L^2)(1-c)^2$, or $J > \frac{1}{4}(1-c^2)^2$, whichever is smaller. The smaller value of the Richardson number is referred to as the critical one. This simple relationship between the invariant and the cut-off wave-number has apparently not been noticed before.

This paper represents the results of one phase of research carried out at the Jet Propulsion Laboratory, California Institute of Technology, under Contract No. NASw-6, sponsored by the National Aeronautics and Space Administration. The paper was presented at the 10th International Congress of Applied Mechanics in Stresa, 31 August–7 September 1960.

The author is indebted to Dr P. Peabody for help in programming the problem for machine calculation and to Mr R. J. Mueller and Mrs M. Simes who carried out most of the calculations. The help of Mrs D. Porter in the preparation of the manuscript is gratefully acknowledged.

REFERENCES

BIEBERBACH, L. 1953 *Theorie der gewöhnlichen Differentialgleichungen, Grundleheren der mathematischen Wissenschaften*, Band LXVI. Berlin, Göttingen, Heidelberg: Springer Verlag.

CARRIER, G. F. & CHANG, C. T. 1959 On an initial value problem concerning Taylor instability of incompressible fluid. *Quart. Appl. Math.* **16**, 4.

CASE, K. M. 1960 Stability of inviscid plane Couette flow. *Phys. Fluids*, **3**, 2.

DRAZIN, P. G. 1958 The stability of a shear layer in an unbounded heterogeneous inviscid fluid. *J. Fluid Mech.* **4**, 214.

ELIASSEN, A., HØILAND, E. & RIIS, E. 1953 Two-dimensional perturbation of a flow with constant shear of a stratified fluid. *Institute for Weather and Climate Research, The Norwegian Academy of Sciences and Letters*, Publication No. 1.

GOLDSTEIN, S. 1931 On the stability of superposed streams of fluids of different densities. *Proc. Roy. Soc.* A, **132**, 524.

MENKES, J. 1959 On the stability of a shear layer. *J. Fluid Mech.* **6**, 518.

MOTT, N. F. 1952 *Elements of Wave Mechanics.* Cambridge University Press.

PRANDTL, L. 1931 *NACA Tech. Mem.* no. 625.

PRANDTL, L. 1952 *Essentials of Fluid Dynamics.* New York: Hefner.

TAYLOR, G. I. 1931 Effect of variation in density on the stability of superposed streams of fluid. *Proc. Roy. Soc.* A, **132**, 499.

Unsteady, viscous, circular flow

I. The line impulse of angular momentum

By MERWIN SIBULKIN

Convair Scientific Research Laboratory, San Diego

(Received 27 December 1960)

In this paper a study of the energy-transfer processes associated with the motion of a viscous, heat-conducting fluid is begun. The class of motions considered are unsteady, two-dimensional, vortical flows. After developing simplified equations of motion and energy appropriate to this type of flow in the low Mach-number limit, general solutions of the momentum equations are presented.

The concept of a *line impulse of angular momentum* is introduced as an example of this class of motions for which a solution of the energy field is obtainable in closed form. The solution for the line impulse can be viewed as a combination of velocity, pressure, and temperature waves concurrently radiating from the origin of the impulse and decaying with time. Particular examples of the development of the energy field of the impulse in both liquids and gases are presented for selected values of Prandtl number. The energy-transfer processes are discussed in some detail, and the resulting differences in the energy fields for liquid gases are emphasized.

---

1. Introduction

For a large class of problems in hydrodynamics and low-speed aerodynamics, it is not necessary to study the energy equation to obtain the desired solution of the flow problem. In inviscid, compressible flow the energy equation *per se* is eliminated by the use of the isentropic relationship $p/\rho^{\gamma} = \text{const}$. And, for certain viscous, compressible flow problems the energy equation is satisfied for particular values of the Prandtl number σ by a constant value of the stagnation temperature throughout the flow field, e.g. the flow over an insulated plate with $\sigma = 1$ and the flow through a shock wave with $\sigma = \frac{3}{4}$. Consequently, there have been relatively few problems in fluid dynamics in which solutions of the energy equation have been obtained compared to those in which the momentum equation has been solved.

In this investigation, interest will be focused upon the transfer of energy between fluid elements due to viscous work and to heat conduction within (but not across) the boundaries of the fluid. The particular class of problems studied are unsteady, two-dimensional flows with circular streamlines. This work was originally motivated by a desire to understand the temperature separation phenomenon exhibited by the Ranque–Hilsch vortex tube.

The investigation is divided into three parts.

In part I the energy field in an infinite fluid associated with the decay of what will be defined as a *line impulse of angular momentum* is considered. The flows of both a liquid and of a gas in the limit of Mach number equal to zero are studied, and solutions, in closed form, are obtained and compared.

The investigation will proceed as follows. First, simplified forms of the Navier–Stokes and energy equations for plane, axisymmetric flow are developed for the case where the Mach number in the flow field is everywhere much less than one. Then the general solutions for the decay of the velocity field associated with an arbitrary initial velocity distribution are given for finite and for infinite flow fields.

The particular initial velocity distribution for a *line impulse of angular momentum* is then introduced. The line impulse of angular momentum may be associated with the following physical model. If a cylindrical rod whose radius is very small compared to its length is immersed in a viscous fluid and impulsively set in rotation about its axis, the adjacent fluid will also be set in motion. The line impulse of angular momentum corresponds to the limit obtained as the radius of the rod approaches zero and the angular velocity of the rod approaches infinity in such a way that the angular momentum imparted to the fluid remains finite.

The solution obtained for the velocity field associated with the decay of the line impulse is then used to determine the energy dissipation due to viscosity. Finally, the energy fields resulting from the combined action of dissipation and heat conduction are found for both incompressible and compressible fluids.

In part II the corresponding flows in a circular cylinder of finite radius will be considered, and the energy transfer processes will be discussed in some detail. In these cases it will be necessary to resort to numerical integration to obtain the desired solutions of the energy equation.

In part III a new model for the flow in a vortex tube will be proposed. Using the methods developed in part II, velocity and energy profiles will be calculated and compared with previously published measurements. Some new experimental work based upon the proposed flow model will also be presented.

2. Notation

Because of the large number of symbols required, it has been convenient in a few instances to assign more than one meaning to a symbol where, it is hoped, no confusion should result.

The term *total* denotes the addition of the kinetic energy per unit mass to the specified quantity; the term *over-all* denotes an integrated value (e.g. of kinetic energy) for a disk of fluid of unit depth. An overbar indicates a mean value, and an asterisk indicates a non-dimensional quantity. Finally, a subscript ∞ denotes the value taken as $r \to \infty$.

3. Preliminary analysis of the conservation equations

In the present work we shall consider two idealized fluids: (i) the *perfect gas* having the equation of state $p = \rho \mathscr{R} T$ and constant values of specific heat c_p and c_v, and (ii) the *perfect liquid* having the equation of state ρ = const. and a

single, constant specific heat c. Hereafter, when the terms *gas* or *liquid* are used they will be understood to refer to the perfect fluids defined above.

In cylindical polar co-ordinates (r, θ, z) the continuity, momentum, and energy equations for two-dimensional $(\partial/\partial z = 0)$, axisymmetric $(\partial/\partial\theta = 0)$ flow are (see, for example, Pai 1956, pp. 28–44, and Howarth 1953, pp. 38–54):

$$\frac{\partial\rho}{\partial t} + \frac{1}{r}\frac{\partial}{\partial r}(r\rho u) = 0, \tag{3.1a}$$

$$\rho\left(\frac{Du}{Dt} - \frac{v^2}{r}\right) = \frac{1}{r}\frac{\partial(r\sigma_{rr})}{\partial r} - \frac{\sigma_{\theta\theta}}{r}, \tag{3.1b}$$

$$\rho\left(\frac{Dv}{Dt} + \frac{uv}{r}\right) = \frac{1}{r}\frac{\partial(r\tau_{r\theta})}{\partial r} + \frac{\tau_{r\theta}}{r}, \tag{3.1c}$$

$$\rho c_p \frac{DT}{Dt} = -\frac{T}{\rho}\left(\frac{\partial p}{\partial T}\right)_p \frac{Dp}{Dt} + \Phi + \frac{1}{r}\frac{\partial}{\partial r}\left(rk\frac{\partial T}{\partial r}\right), \tag{3.1d}$$

where t is the time, ρ is the fluid density, u the radial velocity, v the circumferential velocity, p the pressure, and T the temperature in the fluid, and where

$$\frac{D}{Dt} \equiv \frac{\partial}{\partial t} + u\frac{\partial}{\partial r}, \quad \sigma_{rr} \equiv -p + 2\mu\frac{\partial u}{\partial r} + \frac{\lambda}{r}\frac{\partial(ru)}{\partial r}, \quad \sigma_{\theta\theta} \equiv -p + 2\mu\frac{u}{r},$$

$$\tau_{r\theta} \equiv \mu\left(\frac{\partial v}{\partial r} - \frac{v}{r}\right), \quad \Phi \equiv \mu\left[2\left(\frac{\partial u}{\partial r}\right)^2 + 2\left(\frac{u}{r}\right)^2 + \left(\frac{\partial v}{\partial r} - \frac{v}{r}\right)^2\right] + \lambda\left(\frac{\partial u}{\partial r} + \frac{u}{r}\right)^2,$$

μ being the first, λ the second, coefficient of viscosity, and k being the thermal conductivity.

We now consider the relative magnitudes of u and v. For a source-free liquid, the continuity equation (3.1*a*) immediately gives $u = 0$. To study the situation for a gas we choose a characteristic radius R and velocity V and define the non-dimensional variables $s \equiv r/R$ and $\tau \equiv tV/R$. In the limit $M \to 0$ where M is the Mach number (in the sense $V \to 0$ for finite T), the changes in fluid properties will be small perturbations about the mean values $\bar{p}, \bar{\rho}, \bar{T}, \bar{\mu}$, and $\bar{k}$. The continuity equation (3.1*a*) can be formally integrated in the form

$$\frac{u}{V} = -\frac{1}{(\rho/\bar{\rho})s}\int_0^s \frac{1}{\bar{\rho}}\frac{\partial\rho}{\partial\tau}\, s'\, ds'. \tag{3.2}$$

Defining the non-dimensional variables

$$h^* \equiv \frac{h - \bar{h}}{\frac{1}{2}V^2}, \quad p^* \equiv \frac{p - \bar{p}}{\frac{1}{2}\bar{\rho}V^2}, \quad \rho^* \equiv \frac{\rho - \bar{\rho}}{\mathscr{M}\bar{\rho}}; \quad \mathscr{M} \equiv \frac{V^2}{2\bar{h}} = \frac{\gamma - 1}{2}M^2, \tag{3.3}$$

where h is the enthalpy per unit mass, and γ the ratio of the specific heats, the gas law can be written in the non-dimensional form

$$\rho^* = \{\gamma/(\gamma - 1)\}\, p^* - h^*. \tag{3.4}$$

Differentiating (3.4) and substituting the result in (3.2) gives

$$\frac{u}{V} = -\frac{\mathscr{M}}{(\rho/\bar{\rho})s}\int_0^s \left[\left(\frac{\gamma}{\gamma - 1}\right)\frac{\partial p^*}{\partial\tau} - \frac{\partial h^*}{\partial\tau}\right] s'\, ds'. \tag{3.5}$$

Since we consider only those changes in enthalpy due to viscous work (by restricting the analysis to flows with no heat transfer across the boundaries of the fluid), h^* remains finite as $\mathscr{M} \to 0$ (as, of course, does p^*), and therefore

$$\lim_{\mathscr{M}\to 0} \frac{u}{V} = 0. \tag{3.6}$$

For estimation purposes (again considering the limit $\mathscr{M} \to 0$), one may take $\mu/\bar{\mu} = h/\bar{h}$ or

$$\frac{\mu-\bar{\mu}}{\bar{\mu}} = \frac{h-\bar{h}}{\bar{h}} \doteq \frac{V^2}{2\bar{h}} \equiv \mathscr{M}.$$

Then $$\lim_{\mathscr{M}\to 0} \frac{\partial}{\partial r}\left(\mu r \frac{\partial v}{\partial r}\right) = \lim_{\mathscr{M}\to 0} \bar{\mu}\frac{\partial}{\partial r}\left\{[1+O(\mathscr{M})]\, r\frac{\partial v}{\partial r}\right\} = \bar{\mu}\frac{\partial}{\partial r}\left(r\frac{\partial v}{\partial r}\right), \tag{3.7}$$

and similarly for the heat conduction term in the energy equation.

Applying (3.6) and (3.7) to (3.1) eliminates the continuity equation and reduces the momentum and energy equations to

$$\frac{\bar{\rho}v^2}{r} = \frac{\partial p}{\partial r}, \tag{3.8a}$$

$$\bar{\rho}\frac{\partial v}{\partial t} = \frac{\bar{\mu}}{r^2}\frac{\partial}{\partial r}\left[r^2\left(\frac{\partial v}{\partial r} - \frac{v}{r}\right)\right], \tag{3.8b}$$

$$\text{(liquid)} \quad \bar{\rho}\frac{\partial e}{\partial t} = \bar{\mu}\left(\frac{\partial v}{\partial r} - \frac{v}{r}\right)^2 + \frac{\bar{k}}{r}\frac{\partial}{\partial r}\left(r\frac{\partial T}{\partial r}\right), \tag{3.8c}$$

$$\text{(gas)} \quad \bar{\rho}\frac{\partial h}{\partial t} = \frac{\partial p}{\partial t} + \bar{\mu}\left(\frac{\partial v}{\partial r} - \frac{v}{r}\right)^2 + \frac{\bar{k}}{r}\frac{\partial}{\partial r}\left(r\frac{\partial T}{\partial r}\right), \tag{3.8d}$$

where e is the internal energy per unit mass.

Comparing (3.8) to the more familiar steady, boundary-layer equations we note that the momentum equations for a liquid and for a gas become identical and are uncoupled from the energy equation as in the boundary-layer case. However, the energy equations for a liquid and for a gas differ in the unsteady terms.

The unsteady pressure term in (3.8d) can be eliminated by the use of the radial momentum equation (3.8a). After integrating (3.8a) with respect to r and differentiating with respect to t, the resulting expression in non-dimensional variables is

$$\frac{\partial p^*}{\partial \tau} = \frac{\partial p^*(a)}{\partial \tau} + 2\int_{a/R}^{s}\left(\frac{\rho}{\bar{\rho}}\frac{\partial (v^*)^2}{\partial \tau} + \mathscr{M}\frac{\partial \rho^*}{\partial \tau}\right)\frac{ds'}{s'},$$

where a is an arbitrary fixed point in the fluid. Thus

$$\lim_{\mathscr{M}\to 0}\frac{\partial p^*}{\partial \tau} = \frac{\partial p^*(a)}{\partial \tau} + 2\int_{a/R}^{s}\frac{\partial (v^*)^2}{\partial \tau}\frac{ds'}{s'} \tag{3.9}$$

and, it may be noted, $v^*(s,\tau)$ may be found from the circumferential momentum equation (3.8b) above.

The remainder of the analysis is restricted to the limit $M \to 0$; the bars over the fluid properties are no longer needed and will be omitted.

A further mathematical simplification of equations (3.8) can be achieved by employing the angular velocity ω ($= v/r$) as a dependent variable. In terms of ω we obtain

$$\rho r\omega^2 = \partial p/\partial r, \tag{3.10a}$$

$$\frac{\partial \omega}{\partial t} = \frac{\nu}{r^3}\frac{\partial}{\partial r}\left(r^3\frac{\partial \omega}{\partial r}\right), \tag{3.10b}$$

$$\rho c_p \frac{\partial T}{\partial t} = \frac{\partial p}{\partial t}\delta_{fg} + \mu r^2\left(\frac{\partial \omega}{\partial r}\right)^2 + \frac{k}{r}\frac{\partial}{\partial r}\left(r\frac{\partial T}{\partial r}\right), \tag{3.10c}$$

where ν is the kinematic viscosity and (3.8c) and (3.8d) have been combined into (3.10c), for the sake of economy, by using the 'Kronecker δ' defined below:

$$\text{for fluid = liquid,} \quad \delta_{fg} = 0, \quad c_p dT = c\,dT = de,$$

and

$$\text{for fluid = gas,} \quad \delta_{fg} = 1, \quad c_p dT = dh.$$

Finally, since we are interested in the total-energy field, we combine the momentum equation (multiplied by ω) with the energy equation to obtain the 'total-energy equation'

$$\frac{\partial \Xi}{\partial t} - \frac{\nu}{\sigma r}\frac{\partial}{\partial r}\left(r\frac{\partial \Xi}{\partial r}\right) = \frac{1}{\rho}\frac{\partial p}{\partial t}\delta_{fg} + \frac{\nu}{\sigma r}\frac{\partial}{\partial r}\left[\frac{(\sigma-1)r^3}{2}\frac{\partial \omega^2}{\partial r} - r^2\omega^2\right], \tag{3.11}$$

where, anticipating the application of (3.11) to an infinite flow field we have defined a general-purpose total energy (or enthalpy) variable Ξ by

$$\Xi \equiv c_p T + \tfrac{1}{2}v^2 - c_p T_\infty;$$

thus

$$\Xi = E - e_\infty \text{ (for a liquid)}, \quad \Xi = H - h_\infty \text{ (for a gas)}. \tag{3.11a}$$

Here E is the 'total internal energy' and H the total enthalpy, each being obtained by adding the kinetic energy to the previously defined quantities. The circumferential momentum and total-energy equations in the form (3.10b) and (3.11) form the basis of the subsequent analysis.

4. Solution of the momentum equation

4.1. *General solutions*

The boundary conditions for the circumferential momentum equation (3.10b) are determined by the requirements that $v = 0$ at $r = 0$ and, for an infinite fluid, $v = 0$ at $r = \infty$. When the fluid is bounded by a fixed cylinder of finite radius R,† $v = 0$ at $r = R$. In terms of $\omega(r, t)$, we have the relations

$$(\partial\omega/\partial r)(0, t) = 0, \tag{4.1a}$$

$$\omega(R, t) = 0 \quad \text{or} \quad \omega(\infty, t) = 0. \tag{4.1b}$$

The separation of variables technique and (4.1a) give as a solution of (3.10b)

$$\omega(r, t) = (A/r)\,e^{-\alpha t}J_1(\alpha r^2/\nu)^{\frac{1}{2}}, \tag{4.2}$$

where J_1 is the Bessel function of the first kind and A and α are constants to be determined.

† It should be clear that this use of the symbol R is not inconsistent with the use of R as a characteristic radius in § 3.

For the cylinder of finite radius, boundary condition (4.1*b*) gives $\alpha_i = \lambda_i^2 \nu / R^2$ where the λ_i are the zeros of J_1. Then, expanding an arbitrary initial condition $\omega(r, 0)$ in a Fourier–Bessel series in J_1 and combining the result with (4.2) gives the general solution (McLeod 1922)

$$v(r,t) = \sum_{i=1}^{\infty} 2R \exp\left(-\frac{\lambda_i^2 \nu t}{R^2}\right) \frac{J_1(\lambda_i s)}{[J_0(\lambda_i)]^2} \int_0^1 s^2 \omega(sR, 0)\, J_1(\lambda_i s)\, ds, \tag{4.3}$$

where $s \equiv r/R$.

For the infinite fluid, setting $k \equiv (\alpha/\nu)^{\frac{1}{2}}$ and applying the Fourier–Bessel transform to (4.2) yields

$$v(r,t) = \int_0^{\infty} \left[\int_0^{\infty} J_1(kr')\, J_1(kr)\, e^{-k^2 \nu t}\, k\, dk \right] r'^2\, \omega(r', 0)\, dr', \tag{4.4}$$

which may be integrated over k (using 4.14 (39) of Erdelyi, Magnus, Oberhettinger & Tricomi 1954), to give the general solution

$$v(r,t) = \int_0^{\infty} \frac{r'^2 \omega(r', 0)}{2\nu t} \exp\left(-\frac{r^2 + r'^2}{4\nu t}\right) I_1\left(\frac{rr'}{2\nu t}\right) dr', \tag{4.5}$$

where I_1 is the modified Bessel function of the first kind.

4.2. *Velocity field of the line impulse of angular momentum*

We define the *cylindrical impulse of angular momentum* $\Omega(r')$ as the δ-function of ω which is everywhere zero except at $r = r'$, where it tends to infinity in such a way that

$$2\pi \int_0^{\infty} \omega(r)\, r^3\, dr \equiv \Omega(r'). \tag{4.6}$$

For $r' = 0$, equation (4.6) defines the *line impulse of angular momentum* which will be designated simply by Ω.

Combining (4.6) with (4.5), the time-dependent velocity field of a cylindrical impulse occurring at $t = 0$ is given by

$$v(r, t; r') = \frac{r\Omega(r')}{8\pi\nu^2 t^2} \exp\left(-\frac{r^2 + r'^2}{4\nu t}\right) \frac{I_1(rr'/2\nu t)}{rr'/2\nu t}. \tag{4.7}$$

Since

$$\lim_{x \to 0} I_1(x)/x = \tfrac{1}{2},$$

the corresponding result for a line impulse of angular momentum is

$$v(r,t) = \frac{r\Omega}{16\pi\nu^2 t^2} \exp\left(-\frac{r^2}{4\nu t}\right). \tag{4.8}$$

A plot of (4.8) with v, r, and t made non-dimensional in an appropriate manner is given in figure 1.†

† The equation $v = (-Ar/2\nu t^2) \exp(-r^2/4\nu t)$ was first given by Taylor (1918) as a particular solution of the momentum equation (3.10*b*) which could be used to represent 'a small eddy'. Taylor then compared the decay time of this eddy with measurements of the decay of turbulence behind a grid. In the present paper, the energy field associated with this particular velocity distribution is determined.

We now consider some properties of the line impulse.†

(i) Since there are no solid boundaries, the total angular momentum of the fluid (obtained by substituting (4.8) in (4.6)) is independent of time and equal to Ω.

(ii) The over-all kinetic energy of the fluid,

$$I_k(t) \equiv 2\pi \int_0^\infty e_k r\,dr \equiv \pi\rho \int_0^\infty v^2 r\,dr, \tag{4.9}$$

is a function of time, since integrating (4.9) gives

$$I_k(t) = \rho\Omega^2/128\pi\nu^2 t^2. \tag{4.10}$$

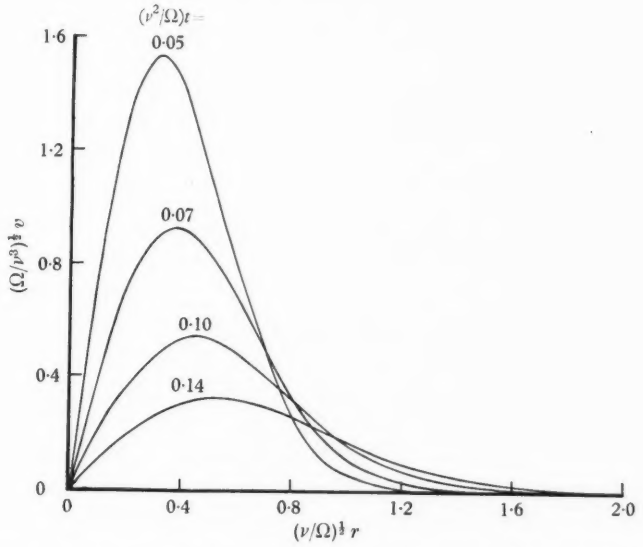

FIGURE 1. Typical profiles showing the decay and spread of the velocity field, v, of a line impulse of angular momentum created at $t = 0$.

Here e_k is the kinetic energy per unit mass. As $t \to 0$, $I_k \to \infty$, i.e. the kinetic energy of the impulse becomes infinite since the momentum remains finite as the mass of fluid in motion approaches zero at time equal to zero. This is clearly a physically unrealizable situation, and will have an important effect on the solution of the energy equation.

(iii) The viscous work, i.e. the rate of increase of energy per unit volume due to the action of shear forces, is (cf. equation (3.10c))

$$W(r,t) \equiv \frac{\partial e_k}{\partial t} + \Phi = \frac{\partial}{\partial t}\left(\frac{\rho r^2\omega^2}{2}\right) + \mu r^2\left(\frac{\partial \omega}{\partial r}\right)^2, \tag{4.11}$$

† It may be permissible to point out that (contrary to the case of line and cylindrical heat sources) the cylindrical impulse is not obtained by the superposition of a ring of line impulses since in the latter case the velocity changes direction at $r = r'$.

which for the line impulse becomes

$$W(r,t) = \frac{2\rho\Omega^2}{(16\pi)^2\nu^3t^4}\left[\left(\frac{r^2}{2\nu t}\right)^2 - 2\left(\frac{r^2}{2\nu t}\right)\right]\exp\left(-\frac{r^2}{2\nu t}\right). \tag{4.12}$$

Since this viscous work can cause only a redistribution of energy between fluid elements, we must have

$$2\pi\int_0^\infty W(r,t)\,r\,dr = 0, \tag{4.13}$$

a relationship satisfied by (4.12).

5. Solution of the energy equation for the line impulse

The handling of the unsteady pressure term in the energy equation was discussed in §3 (cf. equation (3.9)). For the velocity field of the line impulse (4.8), we set $a = \infty$ and obtain

$$\frac{1}{\rho}\frac{\partial p}{\partial t} = \frac{\Omega^2}{(16\pi)^2\nu^3t^4}\left(3 - \frac{r^2}{2\nu t}\right)\exp\left(-\frac{r^2}{2\nu t}\right). \tag{5.1}$$

Substituting (4.8) and (5.1) in (3.11) gives

$$\frac{\partial\Xi}{\partial t} - \frac{\nu}{\sigma r}\frac{\partial}{\partial r}\left(r\frac{\partial\Xi}{\partial r}\right) = \frac{\Omega^2}{(16\pi)^2\nu^3}Q(r,t;\nu,\sigma), \tag{5.2}$$

where

$$Q(r,t;\nu,\sigma) \equiv \frac{1}{t^4}\exp\left(-\frac{r^2}{2\nu t}\right)\left\{2\left(1-\frac{1}{\sigma}\right)\left(\frac{r^2}{2\nu t}\right)^2 + \left[\frac{2}{\sigma} - 4\left(1-\frac{1}{\sigma}\right)\right]\frac{r^2}{2\nu t} - \frac{2}{\sigma} + \left(3 - \frac{r^2}{2\nu t}\right)\delta_{fg}\right\}. \tag{5.2a}$$

Equation (5.2) is of the form of an inhomogeneous, unsteady diffusion equation for the total energy (enthalpy) Ξ in terms of the known distribution of total energy (enthalpy) sources Q. The variable Ξ has been defined (3.11a) such that the boundary condition at infinity is $\Xi(\infty,t) = 0$.

For the liquid case, the energy source term is due only to viscous work and, consequently, equation (5.2a) satisfies the conservation of energy relationship (cf. equation (4.13))

$$2\pi\int_0^\infty Q[\text{liquid}]\,r\,dr = 0. \tag{5.3}$$

In addition, in the absence of heat conduction ($\sigma = \infty$), equation (5.2a) reduces to (4.12), that is to

$$\{\rho\Omega^2/(16\pi)^2\nu^3\}\,Q[\text{liquid},\ \sigma = \infty] = W.$$

For the case of a gas, (5.2a) represents a total enthalpy source field and contains, in addition to the viscous-work terms, a term representing the increase in enthalpy due to fluid element contraction.The distribution of Q for liquids and gases is shown in figure 2 as a function of the similarity parameter $\theta \equiv r^2/2\nu t$, for several values of Prandtl number, σ. For a particular value of σ, the shape of $Q(\theta,t)$ is independent of time, but its magnitude at a specific value of θ decreases as t^4.

Setting

$$\Xi \equiv [\Omega^2/(16\pi)^2 \nu^3]\,(\Xi_1 + \Xi_2), \tag{5.3a}$$

a formal solution of (5.2) is given by

$$\Xi_1(r,t) = \int_\eta^t dt' \int_0^\infty Q(r',t')\, G(r,t;r',t')\, 2\pi r'\, dr', \tag{5.3b}$$

$$\Xi_2(r,t) = \int_0^\infty [\Omega^2/(16\pi)^2 \nu^3]^{-1}\, \Xi(r',\eta)\, G(r,t;r',\eta)\, 2\pi r'\, dr', \tag{5.3c}$$

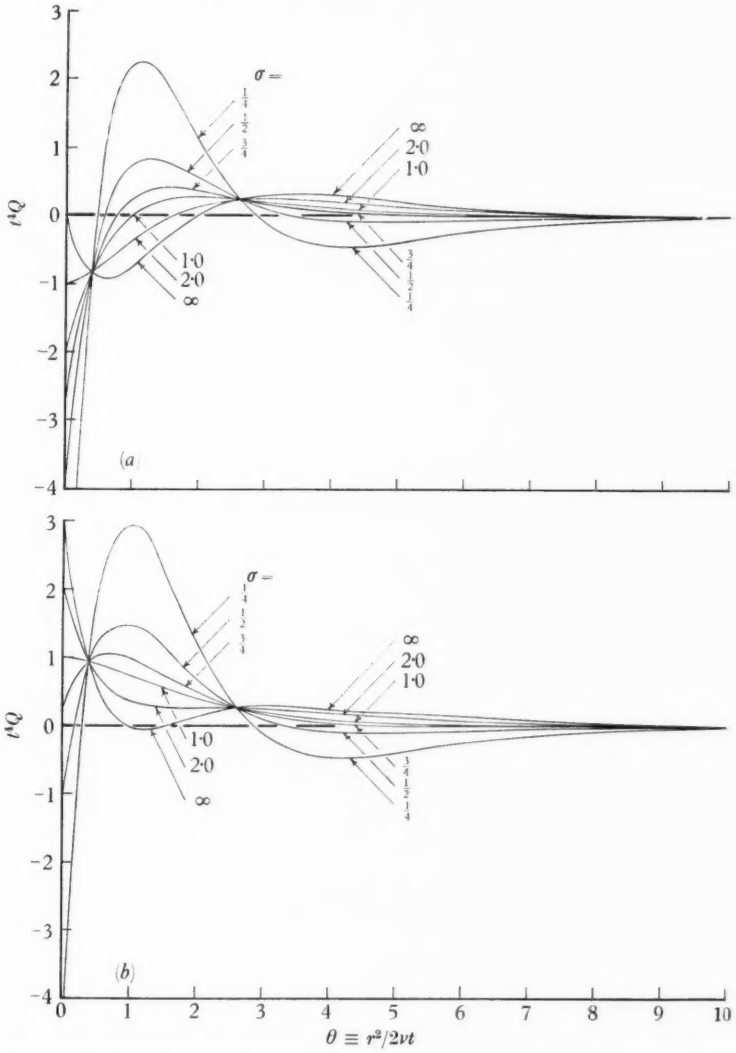

FIGURE 2. Distribution of source strength Q versus the similarity parameter θ for several values of Prandtl number σ. (*a*) Liquid, (*b*) gas.

where G is the Green's function for an instantaneous, cylindrical source (Carslaw & Jaeger 1959, p. 259) satisfying (5.2), namely

$$G(r,t;r',t') \equiv \frac{\sigma}{4\pi\nu}\exp\left[-\frac{\sigma(r^2+r'^2)}{4\nu(t-t')}\right] I_0\left[\frac{\sigma r r'}{2\nu(t-t')}\right]. \tag{5.3d}$$

In (5.3a), Ξ_1 gives the contribution to the energy field of the source distribution $Q(r,t)$, and Ξ_2 gives the contribution of the initial condition $\Xi(r,\eta)$. The singularity in Q at $t=0$ reflects the previously discussed (§4.2) singularity in the kinetic energy at $t=0$. Consequently, a parameter η (having the dimensions of time) has been introduced in (5.3b), and we will look for limiting forms of the solutions of the energy equation for $\eta/t \ll 1$.

After substituting (5.2a) and (5.3d) into (5.3b), the resulting expression for Ξ_1 may be integrated in closed form. The procedure, however, is too lengthy for presentation here; the interested reader may follow the details of the integration in Sibulkin (1960). Briefly, (5.3b) can be integrated with respect to r (using Erdelyi *et al.* 1954), in terms of a finite hypergeometric series. The remaining integration with respect to t can be carried out in terms of elementary functions and the exponential integral $\mathrm{EI}(x)$. For $x \neq 0$, $\mathrm{EI}(x)$ is defined (in terms of the Cauchy principal value) by†

$$\mathrm{EI}(x) \equiv \mathrm{P}\int_x^\infty (e^{-t}/t)\,dt, \tag{5.4a}$$

and is related to previously tabulated functions (Jahnke & Emde 1945, p. 6) by

$$\left.\begin{aligned} \mathrm{EI}(x) &= -\mathrm{Ei}(-x) \quad \text{for} \quad x>0, \\ \mathrm{EI}(x) &= -\overline{\mathrm{Ei}}(-x) \quad \text{for} \quad x<0. \end{aligned}\right\} \tag{5.4b}$$

After defining the variables

$$\theta \equiv \frac{r^2}{2\nu t}, \quad a = \frac{(\sigma-2)\,\theta}{2}, \quad \epsilon = \frac{\sigma(\sigma-2)\,\theta\eta}{2[2t+(\sigma-2)\,\eta]}, \tag{5.5}$$

the solution for the contribution of the source distribution Q to the energy field Ξ is

$$\begin{aligned} \Xi_1(r,t) = \sum_{j=0}^{3}\left[\left(\sum_{i=1}^{10}\alpha_i\beta_i\zeta_{i,j}\right)\left(\frac{2}{\sigma\theta}\right)^j \sum_{k=0}^{j}(-1)^k\frac{k!}{(j-k)!}\left(a^{j-k}e^a-\epsilon^{j-k}e^\epsilon\right)\right] \\ + \sum_{j=-3}^{-1}\left[\left(\sum_{i=1}^{10}\alpha_i\beta_i\zeta_{i,j}\right)\left(\frac{2}{\sigma\theta}\right)^j \frac{1}{(-j-1)!} \right. \\ \left. \times\left\{\mathrm{EI}(-\epsilon)-\mathrm{EI}(-a)+\sum_{k=j}^{-1}\left[(\epsilon^{k+1}-1)\,e^\epsilon-(a^{k+1}-1)\,e^a\right]\right\}\right], \end{aligned} \tag{5.6}$$

where $(\alpha\beta)_i$ and $\zeta_{i,j}$ are tabulated in the Appendix.

6. Energy field in a liquid

In §3, we defined a (perfect) liquid by $\rho = \text{const.}$ and $c = \text{const.}$ We also introduced the symbols Ξ and δ_{fg} which for a liquid have the meaning

† This definition of $\mathrm{EI}(x)$ and its relation to $\mathrm{Ei}(x)$ and $\overline{\mathrm{Ei}}(x)$ is given in an unpublished note by A. Farnell, Convair Scientific Research Laboratory, San Diego.

$\Xi = E - e_\infty$, $\delta_{fg} = 0$. As the initial condition for the line impulse in a liquid, we set the total energy E equal to a constant throughout the fluid by assuming

$$E(r, \eta) \equiv e_\infty. \tag{6.1}$$

Then $\Xi(r, \eta) = 0$ which, by (5.3*c*), makes $\Xi_2(r, t) = 0$ and reduces (5.3*a*) to

$$\Xi = [\Omega^2/(16\pi)^2 \nu^3]\, \Xi_1, \tag{6.2}$$

where the complete solution for Ξ_1 is given by (5.6) with the $(\alpha\beta)_i$ terms (cf. Appendix) evaluated for $\delta_{fg} = 0$.

At this point one must consider the significance of the time parameter η. To be precise, (6.2) is the solution for an initial energy distribution (6.1) and an initial velocity distribution given by (4.8) with $t = \eta$, i.e. an initial velocity corresponding to the velocity field of a line impulse of angular momentum at $t = \eta$. As a consequence of the singularity in the kinetic energy of the line impulse at $t = 0$ (cf. §4), one finds that setting $\eta = 0$ in (6.2) yields either $\Xi = +\infty$ or $\Xi = -\infty$ for *all* values of r and t. Consequently, we consider, in §5.1, the approximate form of (6.2) for $\eta/t \ll 1$; and, in §6.2, we investigate the development of (6.2) with η/t for the special case of $\sigma = 1$, for which the explicit expression of (6.2) is greatly simplified.

6.1. *Solution for* $\eta/t \ll 1$

For $\eta/t \ll 1$, the dominant terms in the solution for Ξ_1, (5.6), are those in the series $\sum_{k=j}^{-1} (\epsilon^{k+1} - 1)\, e^\epsilon$. For a liquid, $\sum_{i=1}^{10} \alpha_i \beta_i \zeta_{i,-3} = 0$, and the approximate solution for Ξ_1 is given by

$$\Xi_1 \approx \left(\sum_{i=1}^{10} \alpha_i \beta_i \zeta_{i,-2} \right) (\tfrac{1}{2}\sigma\theta)^2 e^{-1} e^\epsilon. \tag{6.3}$$

Carrying out the evaluation of (6.3) for $\eta/t \ll 1$, and using (6.2), yields the energy distribution

$$E(r, t; \eta) - e_\infty \approx \frac{\Omega^2}{2(16\pi)^2 \nu^3} \frac{\sigma(1-2\sigma)\,(1-\frac{1}{2}\sigma\theta)}{\eta t^2}\, e^{-\frac{1}{2}\sigma\theta}, \tag{6.4}$$

and defining the non-dimensional variables

$$E^* \equiv \Omega(E - e_\infty)/\nu^3 \quad \text{and} \quad t^* \equiv \nu^2 t/\Omega \tag{6.5}$$

gives the energy distribution in the non-dimensional form

$$E^*(r, t; \eta) \approx \frac{\sigma(1-2\sigma)\,(1-\frac{1}{2}\sigma\theta)}{2(16\pi)^2 \eta^* (t^*)^2}\, e^{-\frac{1}{2}\sigma\theta}. \tag{6.4a}$$

In order to eliminate the dependence of E upon η, we define $\bar{e}_k$ (a mean kinetic energy per unit mass at $t = \eta$) by

$$\rho L^2 \bar{e}_k(\eta) \equiv I_k(\eta), \quad L \equiv (\Omega/\nu)^{\frac{1}{2}}, \tag{6.6}$$

where L is a characteristic length. Applying (4.10) and (6.5) to (6.6) yields

$$\bar{e}_k^* = [128\pi(\eta^*)^2]^{-1}. \tag{6.7}$$

Comparing (6.4*a*) and (6.7) one notes that, at a given position in space and time, the total energy increases as the square root of the initial kinetic energy; thus, for $(\eta/t) \to 0$,

$$\frac{E^*}{(\bar{e}_k^*)^{\frac{1}{2}}} \approx \frac{\sigma(1-2\sigma)\,(1-\frac{1}{2}\sigma\theta)}{32\sqrt{2}\,\pi^{\frac{3}{2}}(t^*)^2}\, e^{-\frac{1}{2}\sigma\theta}. \tag{6.8}$$

Equation (6.8) constitutes the solution for the energy field of a line impulse of angular momentum in a liquid. It is interesting to note that, although the shape of the energy input distribution Q is a function of σ (cf. figure 2a), only the amplitude of the energy distribution E^* is dependent upon σ while its shape is similar to that of Q for $\sigma = 1$. Since, by (5.3), the over-all rate of energy input into the liquid is zero (relative to the energy level at infinity), the energy distribution (6.8) should, and does, satisfy the condition

$$2\pi \int_0^\infty E^*(r,t)\, r\, dr = 0. \tag{6.9}$$

6.2. *Solution for $\sigma = 1$*

When $\sigma = 1$, the Appendix shows that $\alpha_i = 0$ for $i = 6$ to 10. (This simplification is related to the corresponding simplification for $\sigma = 1$ in the basic energy equation (3.11).) Evaluating the remaining terms in (5.6) from the Appendix for $\sigma = 1$, and making use of (5.4b), (6.2), (6.5), and (6.7), gives

$$\frac{E^*(r,t)}{(\bar{e}_k^*)^{\frac{1}{2}}} = \frac{(\eta/t)}{64\sqrt{2}\pi^{\frac{3}{2}}(t^*)^2}\left\{(2-2\theta+\tfrac{1}{4}\theta^2)\left[\mathrm{Ei}\left(-\frac{\frac{1}{2}\theta}{[2t/\eta]-1}\right)-\mathrm{Ei}(-\tfrac{1}{2}\theta)\right]e^{-\frac{1}{2}\theta}\right.$$

$$\left.+\left[\frac{1}{(2t/\eta)-1}+3-\left(\frac{2t}{\eta}-1\right)(1-\tfrac{1}{2}\theta)\right]\exp\left[-\frac{\frac{1}{2}\theta}{1-(\eta/2t)}\right]-(3+\tfrac{1}{2}\theta)\,e^{-\theta}\right\}. \tag{6.10}$$

To find E^* for $r = 0$ ($\theta = 0$), we use the series expansion (Jahnke & Emde 1945, pp. 1, 2)

$$\mathrm{Ei}(-x) = 0{\cdot}5772 + \ln x + O(x)$$

to obtain

$$\frac{E^*(0,t)}{(\bar{e}_k^*)^{\frac{1}{2}}} = \frac{1}{32\sqrt{2}\pi^{\frac{3}{2}}(t^*)^2}\left[\frac{\eta}{t}\ln\frac{1}{(2t/\eta)-1}-\frac{1-(\eta/t)}{1-(\eta/2t)}\right]. \tag{6.10a}$$

(As a check on the analysis, one can obtain (6.10a) directly by setting $r = 0$ and $\sigma = 1$ in (5.4) and integrating the reduced equation for Ξ_1.) The development of E^* as η/t varies from 1 to 0 is shown in figure 3. The result for $\eta/t = 0$ from (6.10) is, of course, identical to (6.8) for $\sigma = 1$.

7. Energy field in a gas

7.1. *Analysis of initial conditions*

In §3 we defined a (perfect) gas by $\rho = p/\mathscr{R}T$ and $c_p = \text{const}$. We also introduced the symbols Ξ and δ_{fg} which for a gas have the meaning $\Xi = H - h_\infty$, $\delta_{fg} = 1$. Once the Ξ field for a gas-flow problem has been determined, the energy field is found from the relationship

$$E = \{H + \tfrac{1}{2}(\gamma-1)\, v^2\}/\gamma. \tag{7.1}$$

It will be assumed that $\gamma > 1$.

As the initial condition for the line impulse in a gas, we again set the energy E equal to a constant throughout the fluid by assuming

$$E(r,\eta) \equiv e_\infty. \tag{7.2}$$

Combining (4.8), (7.1), and (7.2) gives the initial enthalpy distribution

$$\frac{\Xi(r,\eta)}{\Omega^2/(16\pi)^2\nu^3} = -\frac{(\gamma-1)}{\eta^3}\left(\frac{r^2}{2\nu\eta}\right)\exp\left(-\frac{r^2}{2\nu\eta}\right). \tag{7.3}$$

After substituting (7.3) into (5.3*c*), the resulting equation for Ξ_2 can be integrated (Sibulkin 1960) to obtain

$$\Xi_2 = \frac{2(\gamma-1)\sigma}{\eta^2}\left\{\frac{(t-\eta)[2t+(\sigma-2)\eta]+\sigma^2\eta r^2/4\nu}{[2t+(\sigma-2)\eta]^3}\right\}\exp\left\{-\frac{\sigma r^2}{2\nu}\frac{1}{[2t+(\sigma-2)\eta]}\right\}, \tag{7.4}$$

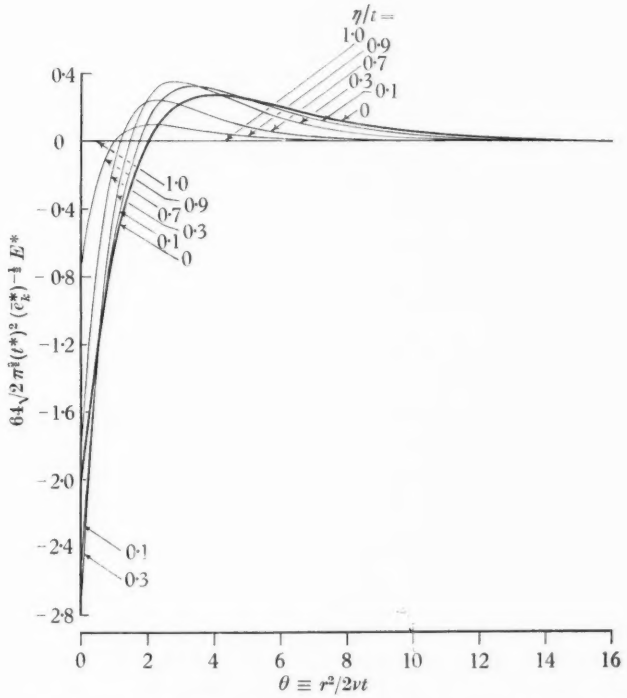

FIGURE 3. Development of the energy field, E^*, in a liquid having a Prandtl number $\sigma = 1$ as a function of the parameter η/t. For fixed time t, the portion of the ordinate in brackets is constant; the solution for the line impulse is the curve at the limit $\eta/t = 0$.

which, when combined with (5.6) in (5.3*a*), gives the general solution for the total enthalpy field, Ξ ($= H - h_\infty$), in a gas. The approximate form of the solution for $\eta/t \ll 1$ and the solution for $\sigma = 1$ will be considered in §§ 7.2 and 7.3.

For either a liquid or a gas, (7.2) sets the initial local-energy-perturbation, $(E - e_\infty)$, equal to zero. In addition, for a liquid, since $\rho = \text{const.}$, condition (7.2) is sufficient to make the initial over-all energy-perturbation,

$$I_T = 2\pi\int_0^\infty (\rho E - \rho_\infty e_\infty)\, r\, dr,$$

equal to zero; thereafter, conservation of energy requires that I_T remain equal to zero (cf. (6.9)). The corresponding situation for a gas is more complicated.

Returning, for a moment, to the non-dimensional variables (3.3) used in the preliminary analysis of §3, and defining

$$I_T^*(t) \equiv 2\pi \int_0^\infty \frac{(\rho E - \overline{\rho e})}{\mathscr{M}\overline{\rho e}} r\,dr \quad \text{and} \quad E^{**} \equiv \frac{E-\bar{e}}{\frac{1}{2}V^2}, \tag{7.5}$$

we derive the result

$$I_T^* = 2\pi \int_0^\infty (\gamma E^{**} + \rho^* + \gamma \mathscr{M} \rho^* E^{**})\, r\,dr. \tag{7.6}$$

Consistent with our previous restriction to gas flows in the limit $M \to 0$, (7.6) reduces to

$$I_T^* = \gamma I_E^* + I_\rho^*, \tag{7.7a}$$

after defining

$$I_E^*(t) \equiv 2\pi \int_0^\infty E^{**}(r,t)\, r\,dr \quad \text{and} \quad I_\rho^*(t) \equiv 2\pi \int_0^\infty \rho^*(r,t)\, r\,dr, \tag{7.7b}$$

where I_ρ^* is the over-all mass-perturbation. Applying the first law of thermodynamics, between time $t' = \eta$ and $t' = t$, to an open system bounded by radius R (see, for example, Keenan 1941, pp. 32ff.) gives

$$2\pi \int_0^R \rho(r,t)\, E(r,t)\, r\,dr = 2\pi \int_0^R \rho(r,\eta)\, E(r,\eta)\, r\,dr + 2\pi \int_\eta^t \left[E(R,t') + \frac{p(R,t')}{\rho(R,t')}\right] \int_0^R \frac{\partial \rho(r,t')}{\partial t'} r\,dr\,dt'. \tag{7.8}$$

The last term in (7.8) expresses the change in energy of the fluid within R due to the energy content of the fluid crossing the boundary R and to the work done on the system in moving this fluid across R. Now if we let $R \to \infty$ and use the integrals defined in (7.5) and (7.7*b*), (7.8) reduces to

$$I_T^*(t) = I_T^*(\eta) + \gamma[I_\rho^*(t) - I_\rho^*(\eta)]. \tag{7.9}$$

Thus, for a gas, in contrast to the situation for a liquid, the total-energy integral I_T^* is not necessarily constant with time, but depends upon the variation with time of the mass integral I_ρ^*. This is due to the possibility, for a gas, of the fluid 'at infinity' exchanging energy with the interior fluid. In order to apply (7.9) to the solution obtained in the next section, the initial values of I_T^* and I_ρ^* must be determined. However, since (7·2) makes $I_E^*(\eta)$ identically equal to zero, $I_T^*(\eta) = I_\rho^*(\eta)$, and the problem is reduced to the determination of the initial density distribution $\rho^*(r,\eta)$.

The density distribution $\rho^*(r,\eta)$ is given in terms of $p^*(r,\eta)$ and $h^*(r,\eta)$ by the perfect gas law (3.4). If we identify the mean fluid properties, $(\bar{\ })$, used in the general analysis of §3 with the fluid properties at infinity, $(\ )_\infty$, in the case of the line impulse, $p^*(r,\eta)$ can be found by integrating the radial momentum equation (3.8*a*) for the velocity distribution (4.8); $h^*(r,\eta)$ follows directly from (7.1) and (7.2). The combined result is

$$\rho^*(r,\eta) = \frac{2\gamma}{V^2} \frac{\Omega^2}{(16\pi)^2 \nu^3 \eta^3} \left(\theta - \frac{1}{\gamma - 1}\right) e^{-\theta}, \tag{7.10}$$

which, when integrated, gives for the initial value of the mass integral the result

$$I^*_\rho(\eta) = \frac{4\pi\gamma(\gamma-2)}{V^2(\gamma-1)}\frac{\Omega^2}{(16\pi)^2\nu^2\eta^2}. \tag{7.11}$$

7.2. *Solution for* $\eta/t \ll 1$

As in the liquid case (cf. §6.1), the dominant terms in (5.6) for $\eta/t \ll 1$ are those in the series $\sum_{k=j}^{-1}(e^{k+1}-1)e^e$. For a gas, however, $\sum_{i=1}^{10}\alpha_i\beta_i\zeta_{i,-3} \neq 0$, and, keeping terms of $O(\eta^{-1})$, the approximate solution for Ξ_1 is

$$\Xi_1 \approx \tfrac{1}{2}\sigma\left\{\frac{1}{\eta^2 t}+\frac{1}{\eta t^2}\left[-\tfrac{5}{2}\sigma+3+\sigma(\sigma-1)\theta\right]\right\}e^{-\frac{1}{2}\sigma\theta}. \tag{7.12}$$

To the same order of magnitude, the approximate form of (7.4) is

$$\Xi_2 \approx \tfrac{1}{2}(\gamma-1)\,\sigma\left\{\frac{1}{\eta^2 t}+\frac{1}{\eta t^2}\left[-\sigma+1+\tfrac{1}{4}\sigma^2\theta\right]\right\}e^{-\frac{1}{2}\sigma\theta}. \tag{7.13}$$

Comparing the magnitude of $H-h_\infty$ given by (7.12) and (7.13) with the magnitude of v^2 given by (4.8) shows that the corresponding approximate form of (7.1) is

$$E-e_\infty \approx (H-h_\infty)/\gamma; \tag{7.14}$$

that is, for $\eta/t \ll 1$, the kinetic energy is much less than the induced increment of thermal energy. Substituting (7.12) and (7.13) into (5.3a) and applying (7.14) gives, for $\gamma \neq 2$,

$$E-e_\infty \approx -\left(\frac{\gamma-2}{\gamma}\right)\frac{\sigma\Omega^2}{2(16\pi)^2\nu^3\eta^2 t}e^{-\frac{1}{2}\sigma\theta}. \tag{7.15a}$$

For $\gamma = 2$, the terms of $O(\eta^{-2})$ cancel identically and, using (6.5) and (6.7), the non-dimensional energy distribution is

$$\frac{E^*}{(\bar{e}^*_k)^{\frac{1}{2}}} \approx \frac{\sigma(1-\frac{3}{4}\sigma)(1-\frac{1}{2}\sigma\theta)}{32\sqrt{2}\pi^{\frac{3}{2}}(t^*)^2}e^{-\frac{1}{2}\sigma\theta}. \tag{7.15b}$$

Equations (7.15) constitute the solution for the energy field of a line impulse of angular momentum in a gas. As such they must satisfy the energy relationships derived in §7.1. Applying the same considerations that led to (7.14), one can show, for $\eta/t \ll 1$, that $e-e_\infty \approx E-e_\infty$ and that $p^* \ll h^*$, which reduces the gas law (3.4) to $\rho^* \approx -\gamma e^*$. Consequently, the mass integral $I^*_\rho(t)$ may be obtained by integrating (7.15a); the result is

$$I^*_\rho(t) = -\gamma I^*_E(t) = \frac{4\pi(\gamma-2)}{V^2}\frac{\Omega^2}{(16\pi)^2\nu^2\eta^2}. \tag{7.16}$$

Combining (7.9), (7.11), and (7.16) gives

$$I^*_\rho(t)-I^*_\rho(\eta) = -(1/\gamma)\,I^*_\rho(\eta) \quad \text{and} \quad I^*_T(t)-I^*_T(\eta) = -I^*_\rho(\eta),\dagger \tag{7.17}$$

which shows that,

$$\left.\begin{aligned} &\text{for } \gamma < 2, && I^*_\rho(t) > I^*_\rho(\eta) \quad \text{and} \quad I^*_T(t) > I^*_T(\eta);\\ &\text{for } \gamma = 2, && I^*_\rho(t) = I^*_\rho(\eta) \quad \text{and} \quad I^*_T(t) = I^*_T(\eta);\\ &\text{for } \gamma > 2, && I^*_\rho(t) < I^*_\rho(\eta) \quad \text{and} \quad I^*_T(t) < I^*_T(\eta). \end{aligned}\right\} \tag{7.18}$$

† Since $I^*_T(t) = 0$ and $I^*_T(\eta) = I^*_\rho(\eta)$, this equation also shows that the solution for the energy field for $\eta/t \ll 1$, (7.15), satisfies the first law of thermodynamics expressed in the form (7.9).

That is, for $\gamma < 2$, there is a net compression of the fluid set in motion by the line impulse, and the work accompanying this compression causes the total energy of the line impulse to increase with time. For $\gamma > 2$, the opposite occurs; for $\gamma = 2$, the energy of the line impulse remains constant, and this is the physical explanation for the cancellation of the higher-order terms in (7.12) and (7.13) for $\gamma = 2$.

Since the net effect of compression is zero for the $\gamma = 2$ gas, it is not surprising that the energy field of the line impulse in that case, (7.15*b*), has the same form as the energy field for the line impulse in a liquid, (6.8). However, although the *net* effect of compression is zero for the $\gamma = 2$ gas, there is still a *local* increase in enthalpy due to compression (cf. equation (5.1)) for $\theta < 3$ and a corresponding decrease for $\theta > 3$. To show the effect of the local density changes more fully, the development of the energy field in a $\sigma = 1, \gamma = 2$ gas will be considered in the next section.

7.3. *Solution for* $\sigma = 1, \gamma = 2$

As was the case for the liquid (cf. §6.2), the evaluation of (5.6) is considerably simpler when the Prandtl number $\sigma = 1$. The result is (Sibulkin 1960)

$$\frac{E^*}{(\bar{e}_k^*)^{\frac{1}{2}}} = \frac{1}{64\sqrt{2}\pi^{\frac{3}{2}}(t^*)^2}\left\{\frac{1}{2}\left[1-\tfrac{1}{2}\theta+\frac{(8-6\theta)(\eta/t)-(6-3\theta)(\eta/t)^2+(1-\frac{1}{2}\theta)(\eta/t)^3}{[2-(\eta/t)]^3}\right]\right.$$
$$\left.\times\exp\left[-\frac{\frac{1}{2}\theta}{1-(\eta/2t)}\right]+\frac{2\eta}{t}(\theta-1)e^{-\theta}\right\}. \quad (7.19)$$

The development of E^* as η/t varies from 1 to 0 is shown in figure 4. The result for $\eta/t = 0$ from (7.19) is, of course, identical to (7.15*b*) for $\sigma = 1$. Comparing figures 3 and 4, it can be seen that, during the early stages of development of the line impulse, say for $\eta/t > 0{\cdot}5$, the energy distributions are not too different in that E^* is negative at $\theta = 0$ for both the liquid and the gas. Later on, as $\eta/t \to 0$ however, the local effects of compressibility (as discussed in §7.2) cause E^* to become positive at $\theta = 0$ and continue to cause E^* to be negative at values of $\theta > 3$.

7.4. *Discussion of results*

The results obtained in the preceding sections lead to the following qualitative description of the history of what we have defined as a *line impulse of angular momentum*, (4.6).

At the time the line impulse originates, $t = \eta$, the fluid is nearly at rest except in a region near the axis where, for $r^2/2\nu\eta < O(10)$, the circumferential velocity v rises sharply to a maximum before returning to zero at the axis. Corresponding to this velocity maximum, there is a temperature minimum (relative to the temperature of the fluid at infinity) such that the total energy—kinetic plus thermal —is constant throughout the fluid. And, as a consequence of the velocity field, there is a pressure minimum at the axis.†

† It is suggested that the interested reader sketch the profiles at $t = \eta$ for reference during the remainder of this discussion.

As the line impulse decays for $t > \eta$, a 'shear wave' radiates from the axis in the sense that the radius of the velocity maximum increases with time while its magnitude decreases (figure 1). Simultaneously, a 'thermal wave' and a 'pressure wave' propagate radially. If we fix our attention on a fluid element initially at rest at a radius r' (which in the limit $\eta \to 0$ includes all fluid elements), the passage of the shear wave sets the fluid elements into circular† motion about the axis of the line impulse with a velocity which rises to a maximum and then

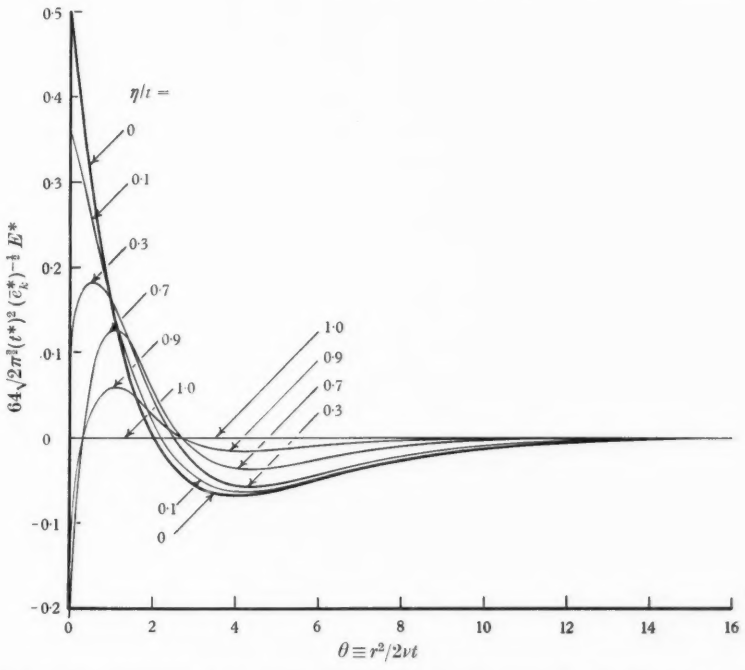

FIGURE 4. Development of the energy field E^* in a gas having a Prandtl number $\sigma = 1$ and a ratio of specific heats $\gamma = 2$ as a function of the parameter η/t. For a fixed time t, the portion of the ordinate in brackets is constant; the solution for the line impulse is the curve at the limit $\eta/t = 0$.

decays to zero as $t \to \infty$. Thus the initial tendency of the shear wave is to increase the energy of the element by increasing its kinetic energy. On the other hand, the passage of the thermal wave tends to decrease the energy of the element. For Prandtl numbers σ greater than one, the kinematic viscosity is greater than the thermal diffusivity and the shear wave spreads more rapidly than the thermal wave causing the total energy of the element at r' to increase at first; for $\sigma < 1$, the reverse occurs. These effects can be traced on figure 2 by noting that, at a fixed radius $r = r'$, θ decreases as t increases.

† For a liquid the streamlines are circles; for a gas, subject to the limitation $M \ll 1$ assumed in this paper, the streamlines are perturbed circles in that $r(t) \to r'$ as $M \to 0$, as a consequence of (3.6).

In addition to the effects of shear and heat conduction described above, the passage of the pressure wave causes the pressure at r' to decrease at first and then tends to return the pressure to its initial value; and, for a gas, the work of compression accompanying this pressure variation first decreases and then increases the energy of the element. The over-all effect of compressibility depends upon the value of γ for the gas (as discussed in §7.1) in such a way that the total energy of the fluid set in motion by the line impulse increases with time for $\gamma < 2$ and decreases for $\gamma > 2$ (7.15*a*). For $\gamma = 2$, the total energy of the gas remains constant, and the solution for the energy field in this case, (7.15*b*), has the same form as the solution for the liquid (6.8). These solutions show that for $t/\eta \gg 1$, $E^* - e_\infty \approx 0$ throughout the fluid for $\sigma = \frac{1}{2}$ in the case of a liquid and for $\sigma = \frac{4}{3}$ in the case of the gas. The differences between the liquid and the $\gamma = 2$ gas are due to the local effects of compressibility, and are further illustrated by the differences in the development of the line impulse with η/t as shown in figures 3 and 4 and discussed in §7.3.

Appendix

The values of $(\alpha\beta)_i$ and $\zeta_{i,j}$ are tabulated below.

			$\zeta_{i,j}$						
	$(\alpha\beta)_i . 4\sigma\theta t^3 \exp(\frac{1}{2}\sigma\theta)$	$j =$	-3	-2	-1	0	1	2	3
$i = 1$	$(-2+3\sigma\delta_{fg})\,(\sigma-2)^2$	$i = 1$	1	-2	1	0	0	0	0
2	$2[1-2(\sigma-1)-\frac{1}{2}\sigma\delta_{fg}]\,(\sigma-2)^2$	2	1	-3	$+3$	-1	0	0	0
3	$-4[1-2(\sigma-1)-\frac{1}{2}\sigma\delta_{fg}]\,(\sigma-2)$	3	0	1	-2	1	0	0	0
4	$[1-2(\sigma-1)-\frac{1}{2}\sigma\delta_{fg}]\,\sigma^2(\sigma-2)\,\theta$	4	0	1	-3	$+3$	-1	0	0
5	$4(\sigma-1)\,(\sigma-2)^2$	5	1	-4	$+6$	-4	$+1$	0	0
6	$-16(\sigma-1)\,(\sigma-2)$	6	0	1	-3	$+3$	-1	0	0
7	$16(\sigma-1)$	7	0	0	1	-2	1	0	0
8	$4\sigma^2(\sigma-1)\,(\sigma-2)$	8	0	1	-4	$+6$	-4	1	0
9	$-8\sigma^2(\sigma-1)\,\theta$	9	0	0	1	-3	$+3$	-1	0
10	$\frac{1}{2}\sigma^4(\sigma-1)\,\theta^2$	10	0	0	1	-4	$+6$	-4	1

REFERENCES

Carslaw, H. S. & Jaeger, J. C. 1959 *Conduction of Heat in Solids*, 2nd edn. Oxford University Press.

Erdelyi, A., Magnus, W., Oberhettinger, F. & Tricomi, F. G. 1954 *Tables of Integral Transforms*, Vol. 1. New York: McGraw-Hill.

Howarth, L. (ed.) 1953 *Modern Developments in Fluid Dynamics, High Speed Flow*, Vol. 1. Oxford University Press.

Jahnke, E. & Emde, F. 1945 *Tables of Functions*. New York: Dover.

Keenan, J. H. 1941 *Thermodynamics*. New York: John Wiley.

McLeod, A. R. 1922 The unsteady motion produced in a uniformly rotating cylinder of water by a sudden change in the angular velocity of the boundary. *Phil. Mag.* **44**, 1–14.

Pai, S-I. 1956 *Viscous Flow Theory*. I. *Laminar Flow*. Princeton: Van Nostrand.

Sibulkin, M. 1960 Unsteady, viscous, circular flow. Part I. The line impulse of angular momentum. *Convair Sci. Res. Lab., San Diego, Res. Note* no. 39.

Taylor, G. I. 1918 On the dissipation of eddies. *Adv. Comm. Aero., Lond., Rep. and Mem.* no. 598. (Available in Batchelor, G. K. (ed.) 1960, *The Scientific Papers of G. I. Taylor*, Vol. II, p. 96. Cambridge University Press.)

The boundary layer on a flat plate in a stream with uniform shear

By J. D. MURRAY*

Mathematics Department, University College London

(Received 13 March 1961)

The incompressible laminar boundary layer on a semi-infinite flat plate is considered, when the main stream has uniform shear. A solution is obtained for the first two terms of an asymptotic solution for small viscosity. It is shown that one of the principal effects of free-stream vorticity is to introduce a modified pressure field outside the boundary-layer region.

1. Introduction

The region behind a bow shock wave is associated with an inviscid rotational flow. This vorticity in the inviscid flow will in some way affect the boundary layer on the body. To provide some understanding of the effects on the viscous boundary layer of a free-stream vorticity, the laminar boundary layer in a two-dimensional incompressible fluid of constant properties on a semi-infinite flat plate is studied, when the main stream has uniform shear.

Li (1955, 1956) and Yen (1955) have considered this problem. Li (1955) obtained a solution on the assumption that there is no pressure gradient as $y/\nu^{\frac{1}{2}} \to \infty$, where y is the Cartesian co-ordinate measured from the plate, taken as the x-axis, and ν is the kinematic viscosity. Yen used the same boundary condition but employed a Polhausen technique on the velocity profile in the boundary layer at different stations on the plate, and showed that a form factor is required, which depends on the boundary-layer thickness. Li (1956) retracted his first solution and included in his boundary conditions a pressure gradient at the edge of the boundary layer. Glauert (1957) used the same equations and, in effect, the same boundary conditions as Li (1955). He stated that the pressure gradient at the edge of the boundary layer must be zero. This pressure-gradient condition is considered below.

In this note a solution is obtained for the first two terms in an asymptotic solution for small viscosity. The effect of the shear on the boundary layer is $O(\nu^{\frac{1}{2}})$, which may be deduced from the introduction of a vorticity number—the ratio of the main-stream vorticity to the average vorticity in the boundary layer—or from perturbation considerations on the Navier–Stokes equation. Accordingly, the correction to the Blasius solution for a uniform main stream must be included to $O(\nu^{\frac{1}{2}})$. From consideration of the various boundary conditions and a study of the pressure gradient over the complete field of flow, a solution is obtained which is correct to $O(\nu^{\frac{1}{2}})$ everywhere in the field of flow. The solution

* Now at Hertford College, Oxford.

being the first two terms of an *asymptotic* expansion, terms of $O(\nu)$ must be considered if they arise. The term of $O(\nu)$ which does appear is shown to be consistent with the modified definition of the displacement thickness which is necessary when the main-stream shear is present.

The difference in the following solution consists mathematically in the different treatment of the boundary conditions as $y/\nu^{\frac{1}{2}} \to \infty$ and in the method of solution.

2. Basic equations and solution

Let (x_2, y_2) be the rectangular Cartesian co-ordinates, with the origin at the leading edge, the x_2-axis along the plate and y_2 perpendicular to it. The velocity in the main stream is taken as $U_2 = U_0 + \Omega_0 y_2$. Take any length l as reference length. (Alternatively ν/U_0 or U_0/Ω_0 may be used.) Use non-dimensional co-ordinates and velocities denoted by subscripts 1 by taking all lengths as multiples of l, and velocities as multiples of U_0. From the continuity equation there is a non-dimensional stream-function ψ_1, such that $u_1 = \partial\psi_1/\partial y_1$, $v_1 = -\partial\psi_1/\partial x_1$. The dimensional stream-function is $U_0 l\psi_1$. The non-dimensional free-stream velocity is

$$U_1 = 1 + N y_1, \quad N = \Omega_0 l/U_0. \tag{1a,b}$$

The usual boundary-layer transformation is to stretch the y_1 co-ordinate by $y = R^{\frac{1}{2}} y_1$, and to use

$$\chi = R^{\frac{1}{2}}\psi_1 \tag{2}$$

as dependent variable, where R is the Reynolds number $U_0 l/\nu$. However, for a uniform main stream, the flow along the plate is obtained correctly to $O(R^{-\frac{1}{2}})$ for both the boundary-layer flow and the external stream if parabolic co-ordinates (ξ_1, η_1) are used. (For a discussion of optimal co-ordinates in general, see Kaplun (1954).) We therefore use parabolic co-ordinates here defined by

$$(\xi_1 + i\eta_1)^2 = x_1 + iy_1 \quad (\eta_1 \geqslant 0)$$

in the whole (x_1, y_1)-plane, with $\eta_1 = 0$ on the plate, $\xi_1 > 0$ on the upper half plane and $\xi_1 < 0$ on the lower half plane. We then stretch the η_1 co-ordinate by writing $\eta = R^{\frac{1}{2}}\eta_1$, and transform the stream-function by (2) as before. We also drop the subscript 1 from ξ_1. All the derivatives of χ with respect to ξ and η are bounded as $R \to \infty$, and correctly to $O(R^{-\frac{1}{2}})$ the equation for χ (boundary-layer equation) is

$$\frac{\partial}{\partial\eta}\left[\xi\left(\frac{\partial^3\chi}{\partial\eta^3} + \frac{\partial\chi}{\partial\xi}\frac{\partial^2\chi}{\partial\eta^2} - \frac{\partial\chi}{\partial\eta}\frac{\partial^2\chi}{\partial\xi\partial\eta}\right) + \left(\frac{\partial\chi}{\partial\eta}\right)^2\right] = 0. \tag{3}$$

For a uniform main stream, we have $N = 0$, and the solution in parabolic co-ordinates is then known to be

$$\chi = \xi f_0(\eta), \tag{4}$$

where f_0 is the Blasius solution.

For a given non-zero N it appears that the simplest asymptotic expansion for χ will commence with the terms

$$\chi = \xi f_0(\eta) + \frac{4N}{R^{\frac{1}{2}}}\xi^2 f_1(\eta) + \ldots, \tag{5}$$

the rotational contribution being necessarily even in ξ. Substituting into (3) and equating coefficients of ξ^2 and ξ^3, we get

$$\frac{\partial}{\partial\eta}(f_0''' + f_0 f_0'') = 0, \tag{6a}$$

and

$$\frac{\partial}{\partial\eta}(f_1''' + f_0 f_1'' - f_0' f_1' + 2 f_0'' f_1) = 0, \tag{6b}$$

where the prime denotes differentation with respect to η. On the plate $u = v = 0$, and so $f_0(0) = f_0'(0) = 0, f_1(0) = f_1'(0) = 0$. Also, as $\eta \to \infty, f_0' \to 2$. The boundary condition on f_1 as $\eta \to \infty$ will be discussed later.

Integration of (6*a*) with the given boundary condition at infinity yields the Blasius equation. Equation (6*b*) is

$$f_1^{(4)} + f_0 f_1''' + f_0'' f_1' + 2 f_0''' f_1 = 0, \tag{7}$$

which on integration gives

$$f_1''' + f_0 f_1'' - f_0' f_1' + 2 f_0'' f_1 = A_1, \tag{8}$$

where A_1 is a constant. Note that f_1 above is the particular case $n = -1$ in the general consideration of uniform flow along a flat plate made by Goldstein (1960).

As regards the condition on f_1 as $\eta \to \infty$, what we require is that the vorticity ω should asymptotically differ from the vorticity Ω_0 of the given main stream by an exponentially small amount, and that (with this exponentially small change of vorticity neglected) the difference in the irrotational flow obtained from the asymptotic form of the boundary-layer flow and that from the given main stream should itself tend to zero as the unstretched co-ordinate $\eta_1 \to \infty$. (Note that $\eta_1 \to \infty$ at every point whose distance from the nearest point of the plate $\to \infty$.)

By this means we satisfy (i) the physical condition that the diffusion of vorticity produced at the solid surface should contribute only an exponentially small vorticity outside the boundary layer, (ii) the condition that the boundary-layer flow should merge smoothly into the main-stream flow which itself satisfies (i), and (iii) the condition that the perturbation of the main stream, due to such effects as the displacement thickness, should vanish at an infinite distance. As shown below, these conditions are sufficient (as in the uniform flow case) for a solution to be defined. It is, of course, necessary that (iv) any induced pressure gradient in the region outside must be bounded; but when (iii) is satisfied, so is (iv).

For small η, we have

$$f_0(\eta) = \frac{\alpha\eta^2}{2!} - \frac{\alpha^2\eta^5}{5!} + \ldots, \tag{9}$$

and, for large η,

$$f_0(\eta) \sim 2\eta - \beta, \quad f_0''(\eta) \sim \gamma e^{-\lambda^2} \quad (\lambda = \eta - \tfrac{1}{2}\beta), \tag{10}$$

where γ, α (= 1·3282) and β (= 1·7208) are constants.

The two solutions of (7) with double zeros at the origin are given by

$$\left.\begin{aligned} y_2(\eta) &= \frac{\alpha\eta^2}{2!} - \frac{\alpha^2\eta^5}{5!} + 23\frac{\alpha^3\eta^8}{8!} + \ldots, \\ y_3(\eta) &= \frac{\alpha\eta^3}{3!} - 2\frac{\alpha^2\eta^6}{6!} + 9\frac{\alpha^3\eta^9}{9!} + \ldots, \end{aligned}\right\} \tag{11}$$

for small enough η, of which y_2 is a complementary function of (8) and y_3 a particular integral of (8) with $A_1 = \alpha$. When η (or λ) is large, asymptotic approximations to complementary functions of (8) are (i) constant, (ii) $E_{-1}(\eta)$, (iii) $H_{-1}(\eta)$, where E_{-1} and H_{-1} are related to the cylindrical parabolic functions (Whittaker & Watson 1927) and

$$\left.\begin{aligned} &E_{-1}(\eta) = \lambda^2(1+\tfrac{1}{2}\lambda^{-2}) = \eta^2 - \beta\eta + \tfrac{1}{2}(1+\tfrac{1}{2}\beta^2) \\ \text{and} \quad &H_{-1}(\eta) \sim e^{-\lambda^2}\lambda^{-3}(1-3\lambda^{-2}+\ldots). \end{aligned}\right\} \tag{12}$$

A fourth complementary function of (7), which is a particular integral of (8) with $A_1 = \alpha$, is asymptotically equal to $-\frac{1}{2}\alpha\eta$. Consequently, there must be constants $a_2, b_2, c_2, a_3, b_3, c_3$ such that

$$\left.\begin{aligned} &y_2 \sim a_2 + b_2 E_{-1} + c_2 H_{-1} \\ \text{and} \quad &y_3 \sim -\tfrac{1}{2}\alpha\eta + a_3 + b_3 E_{-1} + c_3 H_{-1}. \end{aligned}\right\} \tag{13}$$

These equations were solved on a Univac machine and the constants evaluated, the result being

$$a_2 = 1{\cdot}0315, \quad b_2 = 0{\cdot}8354, \quad a_3 = 0{\cdot}96530, \quad b_3 = 1{\cdot}13165.$$

A solution of (8) for $f_1(\eta)$ may be taken in the form $Ay_2 + By_3$, where A and B are constants to be determined. Thus,

$$\begin{aligned} f_1(\eta) &= Ay_2 + By_3 \\ &\sim (Aa_2 + Ba_3) - \tfrac{1}{2}B\alpha\eta + (Ab_2 + Bb_3)E_{-1} + (Ac_2 + Bc_3)O(e^{-\lambda^2}) \\ &= [(Aa_2 + Ba_3) + \tfrac{1}{2}(Ab_2 + Bb_3)(1+\tfrac{1}{2}\beta^2)] \\ &\quad - [(Ab_2 + Bb_3)\beta + \tfrac{1}{2}B\alpha]\eta + (Ab_2 + Bb_3)\eta^2 \\ &\quad + (Ac_2 + Bc_3)O(e^{-\lambda^2}), \end{aligned}$$

and

$$f_0(\eta) \sim 2\eta - \beta.$$

From (1) we have, in the main stream,

$$\chi = 2\xi_1\eta + \frac{2N}{R_1^{\frac{1}{2}}}\xi_1^2\eta^2, \tag{14}$$

and so A and B must be chosen to make the coefficient of η^2 have the value $\frac{1}{2}$, that is,

$$Ab_2 + Bb_3 = \tfrac{1}{2}. \tag{15}$$

From (5) we have, for large η,

$$\chi \sim (2\eta - \beta) + \frac{4N}{R_1^{\frac{1}{2}}}\xi^2(\tfrac{1}{2}\eta^2 + C\eta + D),$$

neglecting exponentially small terms, where

$$C = -\tfrac{1}{2}(\alpha B + \beta), \quad D = (Aa_2 + Ba_3) + \tfrac{1}{8}(2+\beta^2).$$

Hence $$\psi_1 \sim (2\xi_1\eta_1 + 2N\xi_1^2\eta_1^2) - \frac{\beta\xi_1}{R^{\frac{1}{2}}} + \frac{4NC}{R^{\frac{1}{2}}}\xi_1^2\eta_1 + \frac{4ND}{R}\xi_1^2.$$

This is now the boundary condition for small η_1 of the inviscid flow problem (that is the solution of $\nabla^2\psi_1 = N$), which must merge smoothly into the main-stream flow with the diffusion of vorticity produced at the plate exponentially small. With these boundary conditions the solution is

$$\psi_1 = (2\xi_1\eta_1 + 2N\xi_1^2\eta_1^2) - \frac{\beta\xi_1}{R^{\frac{1}{2}}} + \frac{4NC}{R^{\frac{1}{2}}}\left(\xi_1^2\eta_1 - \frac{\eta_1^3}{3}\right) + \frac{4ND}{R}(\xi_1^2 - \eta_1^2). \tag{16}$$

This stream-function satisfies conditions (i), (ii) for *any* C and D. A and B are undetermined and may still be chosen to make C *or* D equal to zero.

η	$f_1(\eta)$	$f_1'(\eta)$	η	$f_1(\eta)$	$f_1'(\eta)$
0	0	0	2·4	4·62326	2·57583
0·2	0·06021	0·59050	2·6	5·15005	2·69786
0·4	0·23139	1·10870	2·8	5·70444	2·85023
0·6	0·49837	1·54698	3·0	6·29155	3·02377
0·8	0·84423	1·89611	3·2	6·91480	3·21037
1·0	1·25044	2·14999	3·4	7·57617	3·40417
1·2	1·69800	2·31087	3·6	8·27670	3·60154
1·4	2·16951	2·39299	3·8	9·01689	3·80052
1·6	2·65164	2·42199	4·0	9·79695	4·00015
1·8	3·13689	2·42963	4·2	10·61697	4·20004
2·0	3·62408	2·44577	4·4	11·47697	4·40000
2·2	4·11712	2·49144	4·5	11·92197	4·50000

TABLE 1

Since $$u_1 = \frac{1}{2(\xi_1^2+\eta_1^2)^{\frac{1}{2}}}\frac{\partial\psi_1}{\partial\eta_1}, \quad v_1 = \frac{-1}{2(\xi_1^2+\eta_1^2)^{\frac{1}{2}}}\frac{\partial\psi_1}{\partial\xi_1},$$

u_1, with ψ_1 given by (16), tends to infinity with η_1 unless $C = 0$. With this value of C and equation (15), we get

$$B = -\beta/\alpha, \quad A = (1 + 2(\beta/\alpha)b_3)/2b_2, \tag{17a}$$

and $$C = 0, \quad D = a_2(1 + 2(\beta/\alpha)b_3)/2b_2 - (\beta/\alpha)a_3 + \tfrac{1}{8}(2+\beta^2). \tag{17b}$$

With these relations, $A = 2{\cdot}3534$, $B = -1{\cdot}2955$ and $f_1(\eta)$ and $f_1'(\eta)$ are as shown in table 1, and figure 1 below. With C and D from (17*a*, *b*), condition (iii) is satisfied. Denoting the pressure gradient in the extended boundary-layer flow by $(P_1, P_2, 0)$, we have

$$P_1 = -\frac{1}{2(\xi_1^2+\eta_1^2)^{\frac{1}{2}}}\left(u_1\frac{\partial u_1}{\partial\xi_1} + v_1\frac{\partial v_1}{\partial\xi_1}\right) - Nv_1,$$

and $$P_2 = -\frac{1}{2(\xi_1^2+\eta_1^2)^{\frac{1}{2}}}\left(u_1\frac{\partial u_1}{\partial\eta_1} + v_1\frac{\partial v_1}{\partial\eta_1}\right) + Nu_1,$$

with u_1, v_1 from above. If C were not equal to zero, for large ξ_1 and η_1 respectively, we would have

$$\left.\begin{aligned} P_1 &\sim \frac{4N^2D}{R}, \quad P_2 \sim 0, \\ P_1 &\sim 0, \qquad P_2 \sim -2(N^2C/R^{\frac{1}{2}})\,\eta_1, \end{aligned}\right\} \tag{18}$$

and, for ξ_1 not small and small η_1 (i.e. at the edge of the boundary layer),

$$\left.\begin{aligned} P_1 &\to -\frac{N}{2R^{\frac{1}{2}}}(2C+\beta)\frac{1}{\xi_1} + \frac{2N^2(2D-C^2)}{R} + O(R^{-\frac{3}{2}}), \\ P_2 &\to O(R^{-\frac{3}{2}}). \end{aligned}\right\} \tag{19}$$

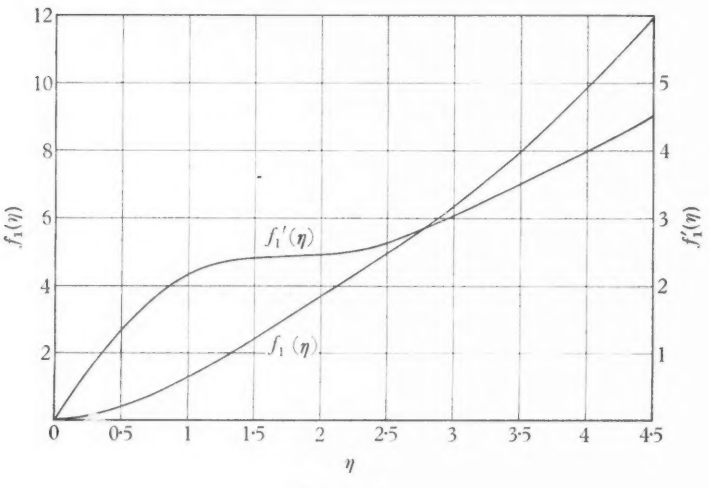

FIGURE 1

It may have been thought, from a consideration of the problem only as far from the plate as the edge of the boundary layer, that the pressure gradient (19) should be zero to $O(R^{-\frac{1}{2}})$, in which case C would be equal to $-\frac{1}{2}\beta$ (Glauert 1957). However, from (18), this would result in an unbounded pressure gradient in the free stream as $\eta_1 \to \infty$, which seems improbable from physical considerations. Therefore with $C = -\frac{1}{2}\beta$, although from (19) the pressure gradient is zero to $O(R^{-\frac{1}{2}})$, there is a pressure gradient growth as η_1 increases as in (18).

Thus, unless $C = 0$, condition (iii) (and (iv)) is violated. With C and D from (17*b*), equation (16) becomes

$$\psi_1 = (2\xi_{\mathrm{S}1}\eta_1 + 2N\xi_{\mathrm{S}1}^2\eta_1^2) - \frac{\beta\xi_{\mathrm{S}1}}{R^{\frac{1}{2}}} + \frac{4ND}{R}(\xi_{\mathrm{S}1}^2 - \eta_1^2). \tag{20}$$

The solution given by (5), and that for the inviscid region outside the boundary layer (that is, where the vorticity created at the plate is exponentially small) given by (20), then satisfies conditions (i) to (iii), and also (iv), to $O(R^{-\frac{1}{2}})$. From (19), with C and D from (17*b*), there is therefore an induced pressure gradient of $O(R^{-\frac{1}{2}})$ and equal to $-N\beta/2R^{\frac{1}{2}}\xi_{\mathrm{S}1}$ at the edge of the boundary layer.

The complete solution to the flow problem is given by (5) with A and B from (17a). The inviscid flow is given by (20) which gives the known Blasius solution for $N = 0$. Since we are seeking a solution, correct to $O(R^{-\frac{1}{2}})$, the term in (20) of $O(R^{-1})$ could perhaps be omitted. However, this term must be considered in relation to any continuation to $O(R^{-1})$ of the series solution. This term represents an outflow as $\eta_1 \to \infty$, which is consistent with the revised definition of the displacement thickness δ_1 when there is a main-stream shear present. (This has also been discussed by Curle (1957).) For ease of physical interpretation, we consider the definition in Cartesian co-ordinates in the form

$$\int_0^{y_1} (1+Ny_1)\,dy_1 = \int_0^{y_1+\delta_1} u_1 dy_1, \tag{21}$$

where y_1 is the distance (outside the boundary layer) from the plate of the position at which the displacement thickness δ_1 is measured. This is the classical definition when $N = 0$. From (21), with u_1 obtained from (5) and (20), we get

$$\delta_1 = -\frac{1}{N}(1+Ny_1) + \frac{1}{N}\left[(1+Ny_1)^2 + 2N\left(\frac{\beta x_1^{\frac{1}{2}}}{R^{\frac{1}{2}}} - \frac{4ND}{R}x_1\right)\right]^{\frac{1}{2}}, \tag{22}$$

from which $\delta_1 \to 0$ as $y_1 \to \infty$, as it must since any finite displacement of the stream lines at infinity would correspond to an infinite increase in mass flow. In the case of uniform main-stream flow ($N = 0$), the inviscid-flow solution gives the displacement–thickness profile as the solid body for which it is the potential flow solution. From (21), if $y_1 = 0$ in the limits of the integrals in (22), we get at the edge of the boundary layer,

$$\delta_1 = -\frac{1}{N} + \frac{1}{N}\left[1 + 2N\left(\frac{\beta x_1^{\frac{1}{2}}}{R^{\frac{1}{2}}} - \frac{4ND}{R}x_1\right)\right]^{\frac{1}{2}}, \tag{23}$$

defined in terms of the defect of mass flux in the boundary layer, which is consistent with our definition. With δ_1 obtained from (23) as the profile of an equivalent body, equation (20) gives the inviscid flow past it, as in the case of a uniform main-stream flow. Care must be exercised in interpreting the result given by (23), since the correct defect of mass flux to $O(R^{-1})$ is not known completely until further terms are obtained in the asymptotic solution (5). It does, however, illustrate the consistency of the above solution and the definition of the displacement thickness. It is at this stage that a mathematical limitation on N is imposed, namely,

$$N < R^{\frac{1}{2}}/4Dx_1^{\frac{1}{2}}.$$

The shearing stress is given by $\tau_2 = \mu\,\partial u_2/\partial y_2$, and the contribution due to the free-stream vorticity is easily calculated from (5). In particular, according to (5), the skin friction on the plate is given in non-dimensional form by

$$\tau_0 = \left[\frac{\tau_2}{\rho U_0^2}\right]_{y_2=0} = \frac{f_0''(0)}{4R^{\frac{1}{2}}\xi_1} + \frac{Nf_1''(0)}{R} + \ldots, \tag{24}$$

where ρ is the density, and $\xi_1 = x_1^{\frac{1}{2}}$ on the plate. The second term in (24) gives the increase in the skin friction due to the main-stream vorticity. It is interesting to

note that this contribution does not depend on the position ξ_1 on the plate. From (17*a*, *b*) and table 1, we get

$$\tau_0 = \frac{1}{R^{\frac{1}{2}} x_1^{\frac{1}{2}}} 0{\cdot}33206 + \frac{N}{R} 3{\cdot}1259 + \ldots . \tag{25}$$

Since $\xi_1 = x_1^{\frac{1}{2}}$ on the plate, outside the boundary layer, $\tau = N/R$, and so, from (23), the presence of the boundary layer increases the effect on the plate of the vorticity in the main stream. The variation with η of $f_1(\eta)$, $f_1'(\eta)$ is shown in figure 1.

In conclusion, it may be said that one of the principal effects of free-stream vorticity is to introduce a modified pressure field outside the boundary-layer region. As a result, the skin friction, boundary-layer separation, and stability will all be affected. These effects are important when the displacement effects become significant. It should be noted that the displacement effect due to the free-stream vorticity is of $O(R^{-1})$.

The author would like to thank Professor Sydney Goldstein of Harvard University for many helpful discussions during this investigation. This research was supported in part by the U.S. Office of Naval Research under Contract Nonr-1866 (34) at Harvard University.

REFERENCES

Curle, N. 1957 *Aero. Res. Counc., Lond., Rep.* no. 19024.
Glauert, M. B. 1957 *J. Aero. Sci.* **24**, 848.
Goldstein, S. 1960 *Lectures on Fluid Dynamics*, Ch. 8. New York: Interscience.
Kaplun, S. 1954 *Z. angew. Math. Phys.* **5**, 111.
Li, T. Y. 1955 *J. Aero. Sci.* **22**, 651.
Li, T. Y. 1956 *J. Aero. Sci.* **23**, 1128.
Whittaker, E. T. & Watson, N. 1927 *Modern Analysis*. Cambridge University Press.
Yen, K. T. 1955 *J. Aero. Sci.* **22**, 728.

REVIEWS

Hydrodynamics of Oceans and Atmospheres. By CARL ECKART. London: Pergamon Press, 1960. 290 pp. 63*s*.

From the title of this book, a prospective reader might expect a direct physical attack on the finite-amplitude turbulent convective circulations of the atmosphere and oceans, which would be intimately connected with observation and would suggest new types of physical measurement to decide such critical hypothetical elements as might occur in the theoretical development. Probably the word 'hydrodynamics' conveys some more restricted and formal meaning to the author than it does to the reviewers, because this book is principally a systematic study of wave motions of infinitesimal amplitude in an inviscid compressible stratified fluid on an infinite plane or on a sphere, with and without rotation. Starting with a concise and rather interesting discussion of the relevant thermodynamic concepts, the author formulates the basic problem of the book as the study of the hydrodynamic equations by the methods of perturbation theory. In this he takes the zero-order state to be one of no motion, which is regarded as given, and attention is thereafter essentially restricted to the first-order perturbations. Chapter III presents some discussion of steady solutions to the perturbation equations, and points out that the second-order equations cannot be completely neglected even in a first-order theory, since in some cases they imply relations among the first-order quantities which are not consequences of the first-order equations. Apparently the analogy of this with the process of 'suppression of secular terms' leads to these relations being called 'secular equations' by the author—a terminology which seems somewhat unfortunate because of the extensive use of this term as a synonym for 'eigenvalue equation'. Indeed, the widespread use of such special terms and symbols makes the book somewhat difficult to use for reference purposes, though it must be admitted that the author often has good reasons for his usage. When Chapter VIII is reached, a set of variables convenient for the study of waves has been introduced, the equations have been put into a standard form and their mathematical properties discussed briefly, and we are ready to attack some specific problems. The remainder of the book discusses such problems—basically the free waves of various systems with plane and spherical level surfaces, with and without rotation. Here we find a number of interesting things—a unified discussion of acoustic and gravity waves, a very thoroughgoing presentation and use of the ray theory, a clear discussion of the significance of the 'unlimited' (i.e. not square integrable) eigenfunctions in unbounded atmospheres, illustration of the applications of the WKB approximation, and some general results obtainable by the use of comparison and oscillation theorems. The principal limitation in this study of waves is that only the simplest types of boundary conditions have been considered—the upper and lower boundaries are always level surfaces, and the lateral boundaries are mostly not present at all; the case of vertical lateral boundaries is discussed only briefly in the simplest possible cases, without rotation. Thus

edge waves and Kelvin waves are not mentioned. In addition, there is essentially no discussion of the excitation of waves by external influences, which is a pity since there are many important questions in this area which are accessible and of which a discussion within the author's general framework would have been most interesting. The only approach to such questions is in Chapter VI, 'General Theorems Concerning the Field Equations', where it is simply pointed out that in principle the solutions to the equations with forcing terms can be found once the eigen-solutions are known. But even here the emphasis on free waves has led the author to the assertion that for a finite volume of fluid the eigen-solutions are denumerable, and every regular (i.e. C^1) solution of the time-dependent first-order equations is expressible in the form

$$\mathbf{U} = \Sigma_n A_n(t)\, \mathbf{U}_n(x, y, z), \quad \text{etc.}$$

Counter-examples to this statement have already been given in Chapter III on 'Steady Motions'—the eigenvalue zero is always non-denumerably infinitely degenerate; even in its linearized version, hydrodynamics is not as simple as quantum mechanics. In this connexion, the author notes (p. 37) that with spherical level surfaces and rotation the only steady motions are the zonal geostrophic flows, i.e. the infinite degeneracy of the eigenvalue zero is partially split by the effects of rotation and spherical level surfaces; but his assertion that this effect of rotation has been overlooked in the past is unwarranted (see, for instance, Lamb's *Hydrodynamics*, §§206, 212, 223). In general, the properties of waves in rotating systems are much more widely known than is suggested by the limited bibliographic references; another example is the relation between Rossby waves and tidal oscillations of the second kind (mentioned on the dust jacket as an example of the unification brought about by the use of modern methods of atomic theory). This was pointed out by Haurwitz in 1940.

As is evident from the above sketch of the contents of the book, there are many parts of the hydrodynamics of oceans and atmospheres having considerable physical interest which are not discussed: the stability of waves on baroclinic currents in the atmosphere, the general circulation of the ocean, exchange processes across the sea–air interface, everything related to viscosity or turbulence, all problems related to heat transfer, such as the oceanic thermocline, all problems related to water vapour in the air, such as clouds, all problems related to radiation, such as the mean stability of the atmosphere. But the author states clearly at the beginning that such problems will not be discussed, and he can only be criticized for choosing an all-inclusive title. From the physical point of view, however, there is one fundamental objection to a basic feature of the perturbation-theory approach used. This is that the basic state (zero-order solution) may be regarded as given, and not subject to friction and heating. There are phenomena in the atmosphere and ocean for which this procedure is satisfactory, and for which the linearized perturbation equations then yield very useful information. Examples of such phenomena are tidal motions, refraction of sound and of surface waves, lee waves, tsunamis, and seiches. However, it is important to realize *that these are all phenomena which have little or no effect on the basic state*. A much more difficult problem is encountered in studying those

phenomena in which the basic state is itself greatly influenced by the non-steady motions. Indeed, it is the explanation of the basic or average state that is frequently the most interesting and challenging aspect of the problems, and it is here that the fundamental physical questions of oceanographic and meteorological hydrodynamics, more often than not, lie. Under these conditions, it is certainly not permissible to disregard the effects of friction and heating on the zero-order solution. This is not to say that the perturbation technique is then worthless, but only that the mathematical difficulties become much more extreme than those treated elegantly by Dr Eckart, and that other techniques may be more productive.

Chapter III, on 'Steady Motions', if it is to be taken as some sort of a model of the real atmosphere, furnishes several examples of the dangers involved in applying the perturbation approach without a knowledge of the actual orders of magnitude involved. Friction is neglected even in the first-order equations, and the horizontal winds are therefore geostrophic. As a result, the author is forced to require that the horizontal pressure gradient vanish at the equator—in spite of observational evidence to the contrary. One of the more frustrating problems in meteorology is thereby denied existence. The author also uses the horizontal divergence of the geostrophic wind to deduce that air rises and is heated where the average surface pressure increases from west to east, and sinks and is cooled where the pressure decreases from west to east. This is not in agreement with observational evidence. Furthermore, the same relationship leads to the absurd result that the heating must vanish when averaged along any latitude circle! These difficulties are of course traceable to the author's choice of a basic state, and the neglect of friction, and should not be interpreted as a failure of the perturbation method *per se*. A much more fundamental error is the neglect of the now well-established *observational* evidence that the 'friction' and 'heating' which determine the average large-scale motions of the atmosphere are to a great extent a result of the non-steady motions. One questions then the physical relevance of a procedure which enables the steady-state solution to 'be considered independently of the components that change with time' (p. 22).

L. N. Howard, N. Phillips and H. Stommel

Lectures on Fluid Mechanics. By S. Goldstein, with J. M. Burgers. New York: Interscience, 1961. 309 pp. $ 6.60 or 50*s*.

From 23 June to 19 July 1957, the American Mathematical Society held a Summer Seminar in Applied Mathematics at Boulder, Colorado, to indoctrinate a general mathematical audience in four broad regions of applied mathematics. Each of the four groups of lectures has since appeared as a book, including the present volume on Fluid Mechanics, with 274 pages by S. Goldstein and 29 pages by J. M. Burgers.

One of the pleasures of reading a book of this kind is in seeing an author's personality shine through the printed page much as it must have done in the lecture room. This is not least so in Prof. Goldstein's preface, where he explains that he

has attempted to offer only an enticing taste of fluid mechanics; that, clearly, no sort of completeness was possible; and that he has included, in the main, topics that have interested him. Incidentally, he gives later enough brief mention, with references, to the major branches of fluid mechanics which are not otherwise treated to avoid the well known dangers of innocent readers ignoring their existence!

The earlier chapters will give the connoisseur of Sydney Goldstein's Cambridge and Manchester lectures on hydrodynamics many a happy moment of recollection. To this classical material has been added an account of the elements of compressible flow, including boundary-layer aspects, as well as of the foundations of continuum magnetohydrodynamics.

The more advanced material includes a sketch of our knowledge of the exact two-dimensional incompressible flow past a semi-infinite plate. At a distance x behind the leading edge that is large compared with ν/U (where ν is kinematic viscosity, and U mainstream velocity), the flow is asymptotically determinate, as the Blasius solution within the boundary layer, merging outside it into the potential flow around the parabolic displacement-thickness contour. Early writers thought that higher approximations for large Ux/ν would also be determinate, and calculable by expansion in descending powers of Ux/ν. It now appears that the expansion must include logarithmic terms, and also arbitrary constants. The need for the latter is at once evident when we consider that the equations determining the asymptotic expansion would be unaffected by the presence of a bulbous rim along the leading edge, which, nevertheless, would cause an alteration to the boundary layer that would only gradually attenuate as Ux/ν increased. In fact, these constants can be determined only by joining the asymptotic solution on to a suitable numerical solution in the neighbourhood of the leading edge.

The book ends with some plasma dynamics. The calculation of electrostatic wave motions, derived by perturbing the collision-free Boltzmann equation for the electron velocity distribution about a Maxwellian distribution, is given, with some discussion of Landau damping. In addition, Dr Burgers makes a contribution that includes his calculation of the effects of a shock wave passing through fluid of large conductivity in the field of a magnetic dipole.

One's only regret, in a book like this aimed at giving a first taste of fluid mechanics, is the paucity of figures (seventeen altogether). Even though it may have been necessary to accept what it is not surprising to find the famous editor of *Modern Developments in Fluid Mechanics* calling 'one glaring and horrible omission—the omission of any comparison of theoretical with experimental results', nevertheless some diagrammatic representations of even calculated flow fields would have helped readers, unfamiliar with the subject's flavour, to appreciate that spicy component imparted to it by retinal reception of flow figuration.

M. James Lighthill

JOURNAL OF FLUID MECHANICS

Volume 11, Part 2 September 1961

CONTENTS

The motion of a thin oil sheet under the steady boundary layer on a body
by L. C. SQUIRE *page* 161

The motion of a shock-wave through a region of non-uniform density
by G. A. BIRD 180

Cavity flow past a slender pointed hydrofoil
by E. CUMBERBATCH and T. Y. WU 187

A theory for the core of a leading-edge vortex
by M. G. HALL 209

Ship waves in a stratified ocean
by ALBERT A. HUDIMAC 229

An experimental investigation of the oscillating lift and drag of a circular cylinder shedding turbulent vortices
by J. H. GERRARD 244

Analytical theory of turbulent diffusion
by P. H. ROBERTS 257

On the stability of a heterogeneous shear layer subject to a body force
by J. MENKES 284

Unsteady, viscous, circular flow. I. The line impulse of angular momentum
by MERWIN SIBULKIN 291

The boundary layer on a flat plate in a stream with uniform shear
by J. D. MURRAY 309

REVIEWS
Hydrodynamics of Oceans and Atmospheres 317
Lectures on Fluid Mechanics 319

Printed in Great Britain at the University Press, Cambridge
(Brooke Crutchley, University Printer)